5-2019

Assessing Paleoenvironmental and Geomorphic Variability in Relationship to Paleoindian Site Burial; Centennial Valley, Montana

Hillary A. Jones
Utah State University

ASSESSING PALEOENVIRONMENTAL AND GEOMORPHIC VARIABILITY IN RELATIONSHIP TO PALEOINDIAN SITE BURIAL; CENTENNIAL VALLEY, MONTANA

by

Hillary A. Jones

A thesis submitted in partial fulfillment
of the requirements for the degree

of

MASTER OF SCIENCE

in

Archeology and Cultural Resource Management

(Geoarcheology)

Approved:

_____	_____
Judson Byrd Finley, Ph.D. Major Professor	Tammy M. Rittenour, Ph.D. Major Professor
_____	_____
Kenneth P. Cannon, Ph.D. Committee Member	Richard S. Inouye, Ph.D. Vice Provost for Graduate Studies

UTAH STATE UNIVERSITY

Logan, Utah
2019

ABSTRACT

Assessing Paleoenvironmental and Geomorphic Variability in Relationship to Paleoindian Site Burial; Centennial Valley, Montana

by

Hillary A. Jones, Master of Science

Utah State University, 2019

Major Professor: Dr. Judson B. Finley
Department: Sociology, Social Work, and Anthropology

Wave action along the shores of Lima Reservoir in Centennial Valley, Montana is actively eroding the southern margins of three neighboring Paleoindian sites. Despite ostensible similarity among the sites, major taphonomic differences are apparent in exposed sediments. Shoreline cutbank exposures one-to-five meters high connect the sites and reveal a complicated geomorphic history. Although each site contains artifact evidence of terminal Pleistocene-early Holocene occupations, Paleoindian components at these three localities occur in very different contexts: one is buried while the other two are apparent surface scatters. These discrepancies raise the question of what geomorphic variables caused differences among late Quaternary sediment sequences in the area encompassing the three sites. Furthermore, as burial promotes site structure preservation and is a key consideration for assessing NRHP significance, these differences prompt the management question of which other landforms in the valley could contain buried cultural material and which preclude the possibility. In order to answer these questions, I used a multi-pronged approach including optically stimulated luminescence dating,

granulometry, stratigraphic profiling and facies analysis. I accomplished two nested objectives with this research. First, I reconstructed the last 60,000 years of geomorphic events for the area surrounding the three sites in order to determine what conditions resulted in site burial. Second, I used those findings to outline criteria for differentiating occupation-age and pre-occupation-age sediment packages in Centennial Valley. I determined, in part, that cultural age deposits are present at both high and low elevations and that they may be marked by a stacked paleosol sequence. The oldest packages, far pre-dating human occupation, are deep lacustrine and high energy alluvial sediments that may be recognized by redoximorphic color alteration and thick pedogenic gypsum horizons.

(232 pages)

PUBLIC ABSTRACT

Assessing Paleoenvironmental and Geomorphic Variability in Relationship to Paleoindian Site Burial; Centennial Valley, Montana

Hillary A. Jones, Master of Science

Wave action along the shores of Lima Reservoir in Centennial Valley, Montana is actively eroding the southern margins of three neighboring Paleoindian sites. Despite ostensible similarity among the sites, major site formation differences are apparent in exposed sediments. Shoreline cutbank exposures one-to-five meters high connect the sites and reveal a complicated geomorphic history. Although each site contains artifact evidence of terminal Pleistocene-early Holocene occupations, Paleoindian components at these three localities occur in very different contexts: one is buried, while the other two are apparent surface scatters. This raise the question of why sites of the same age are in both buried and exposed contexts. Moreover, buried sites are more likely to have preserved spatial layout and sites with buried components are more likely to be considered significant under National Register of Historic Places criteria. These factors therefore prompt the management question of where might other buried sites be located in the valley? In order to answer these questions, I used a multi-pronged approach including optically stimulated luminescence dating, sediment grain size analysis, stratigraphic profiling and sediment facies analysis. I accomplished two nested objectives with this research. First, I reconstructed the last 60,000 years of geomorphic events for the area surrounding the three sites in order to determine what conditions resulted in site burial. Second, I used those findings to outline criteria for differentiating occupation-age

and pre-occupation-age stratigraphic layers in Centennial Valley. I determined, in part, that cultural-age deposits are present at both high and low elevations and that they may be marked by a specific soil sequence. The oldest packages, far pre-dating potential human occupation, are deep lake and high energy stream sediments that may be recognized by soil color alteration and thick gypsum horizons.

ACKNOWLEDGMENTS

This thesis was a labor of love that I would not have been able to accomplish without the help of many individuals. I first wish to thank my committee; Judson Finley, Tammy Rittenour, and Kenneth Cannon. I came to Utah State expressly to study geoarcheology under Dr. Finley and I can't over-emphasize how much I owe to his tutelage and mentoring over the years. Dr. Rittenour taught me all of what I know about OSL and granulometry and our many office visits were invaluable in helping me tease out a very complicated geomorphic picture in my study area. Dr. Cannon is the reason I had this thesis project in the first place and he freely shared his knowledge and research of the area with me. I am very grateful to Kevin O'Dell of ACR Consultants for his support, backing, and confidence while I pursued this extended journey, it's good to be back. Thanks to William Eckerle, he and his wife Margo camped at my study area and spent an entire day investigating the site with me. Bill's help and insights were invaluable for this project. I wish to thank Molly Boeka Cannon who helped me countless times with thesis questions despite not being on my committee. Thanks to Janis Boettinger, who taught me the language of soils. Thanks to Geoffrey Smith for letting me try my hand at geoarcheology in Nevada. Thanks to Chris Finley who took a chance on me and gave me my professional start in archeology. He is one of the main reasons I took this direction.

Thank you to my cohort; Elizabeth Hora-Cook and Anastasia Lugo Mendez. I couldn't have gotten through without you and I hope the three of us can collaborate again. Thank you to my adopted cohort; Carlie, Diana, Kirk, Maureen, Bessy, Drew, Caleb, and Jonathan. Our talks, camp-outs and meals in the Barn, Vet Sci and around Logan are some of my fondest memories.

Finally, I am deeply grateful to my ever-supportive, actively engaged, and loving

family. Thanks to Helen Fellows (Gram), Alicia and John, Daisy, Neil, and the rest of my extended family for your support, encouragement, interest in my research and willingness to hear about sediment through this long process. Thanks especially to my parents Kerry and Mark Anderson. Thanks Ma and Mark for always having my back, reading my entire thesis cover to cover, taking time off work to travel to Utah and see my thesis defense, cook food for the party and for designing and sewing my defense shirt. Finally, thank you to my soon-to-be husband Sam for giving me a chance after our confrontational start in Theory class. Thank you for getting me through completing my thesis and helping heal my neck and back after I did. You and me-- who could have predicted this?

Hillary Ann Jones

CONTENTS

Page

LIST OF TABLES

LIST OF FIGURES

CHAPTER 1:

INTRODUCTION

Lima Reservoir, the impounded reach of the Red Rock River, has occupied southwest Montana's Centennial Valley for over a century (Figures 1 and 2) (Bureau of Reclamation (BOR) 2004). Erosion and archeological site damage along the reservoir's banks has been ongoing since its impoundment (Figure 3). In the valley, the Bureau of Land Management (BLM) faces the problem of identifying significant and/or buried archeological sites adjacent to the reservoir, as well as the question of how to allocate limited financial resources in their detection and management (Peart et al. 2012). While bank erosion exacerbates management issues, it also prompts research questions regarding why buried artifacts are present in some exposures but not others and where other buried sites may be located.

Three National Register of Historic Places (NRHP) eligible sites (24BE43, 24BE46, and 24BE52) lie along a roughly three km (1.9 miles) stretch of the north shore of Lima Reservoir (Figure 4). Wave action is actively eroding the lakeside southern margins of the sites, exposing subsurface stratigraphy (Peart et al. 2012). Despite ostensible similarity between the sites, major differences are apparent in exposed sediments. Shoreline cutbank exposures one-to-five meters high connect the three sites and reveal a complicated geomorphic history. Although each site contains terminal Pleistocene-early Holocene occupations, Paleoindian deposits at these three localities occur in very different contexts: one is buried while the other two appear to be surface artifact scatters. This raises the question of what geomorphic variables caused differences among late Quaternary sediment sequences in the area encompassing the three sites.

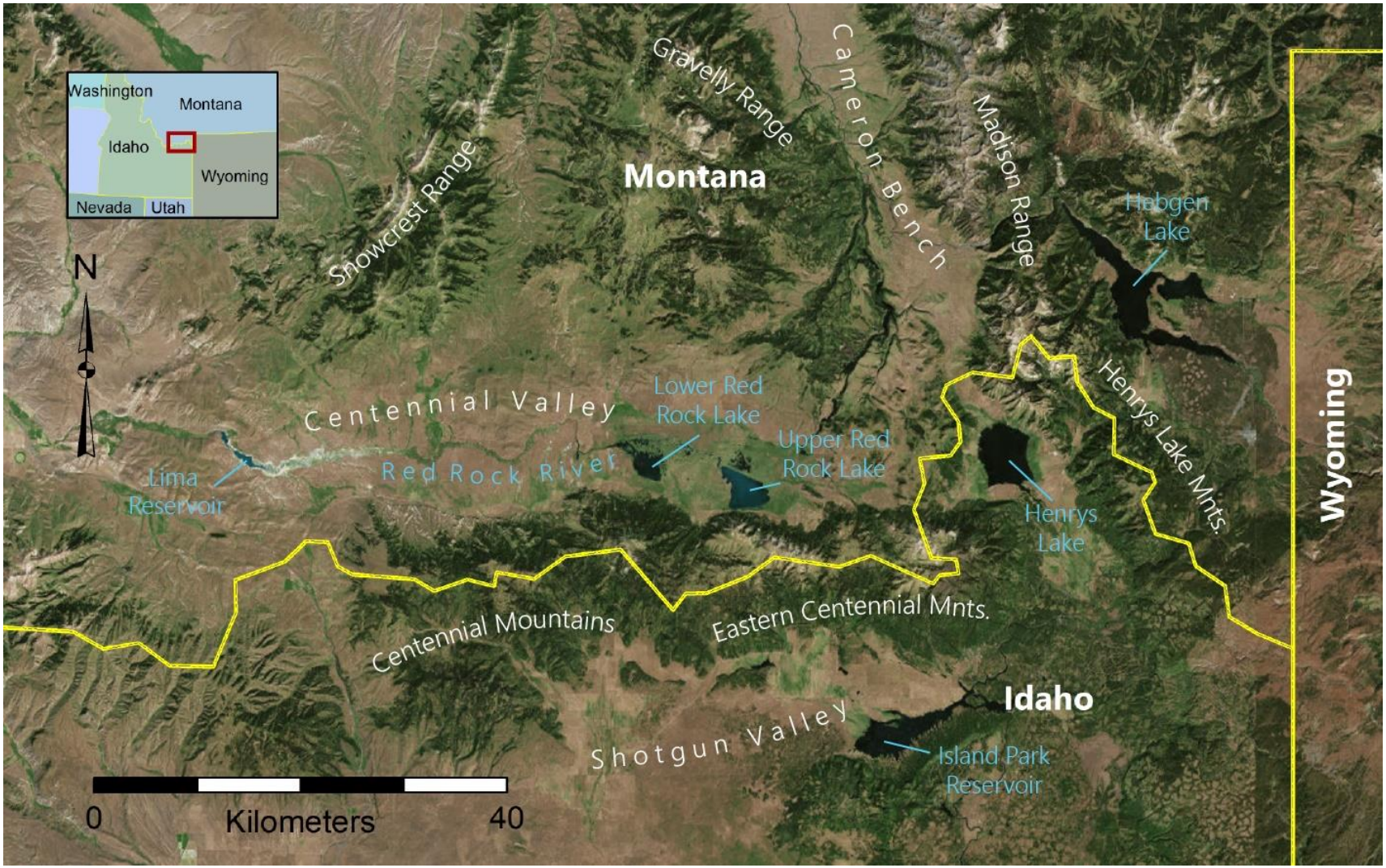

Figure 1. Regional overview of Centennial Valley and Lima Reservoir.

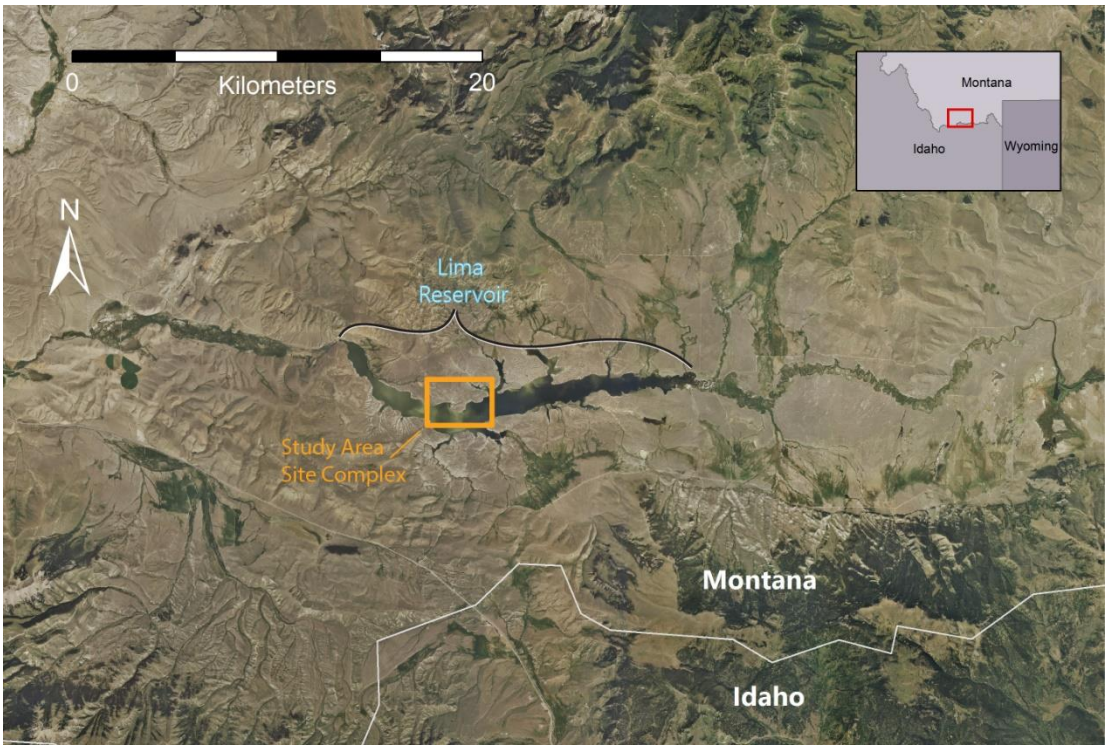

Figure 2. Detail view of Lima Reservoir within Centennial Valley with study area indicated.

Furthermore, as burial is advantageous for preserving site structure (Ebert 1992) and a key consideration in assessing NRHP significance (King 2013), it also prompts the management question of what other landforms in the valley could contain buried archeological material.

This research accomplishes two objectives; it reconstructs the study area's geomorphic history (emphasizing what geomorphic conditions resulted in site burial), and it outlines defining characteristics of occupation-age exposures to help orient future investigations. I used a multi-pronged approach to determining sediment package depositional environment and spatial extent, chronology of geomorphic events, and effects of post-depositional disturbances. My methods included aerial photograph examination, GPS landform mapping, stratigraphic profiling, optically stimulated

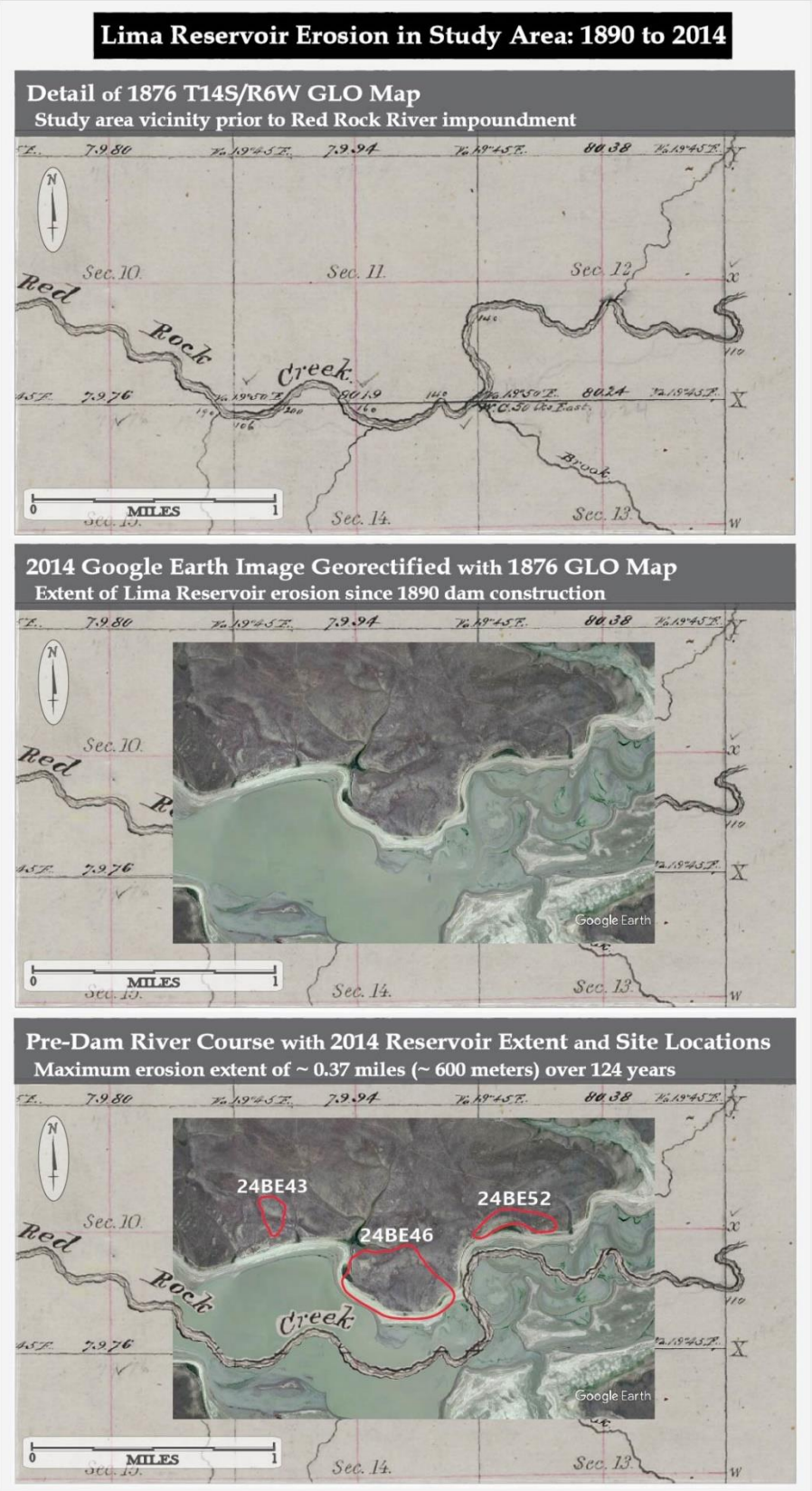

Figure 3. Erosional progression in study area; pre-dam to 2014.

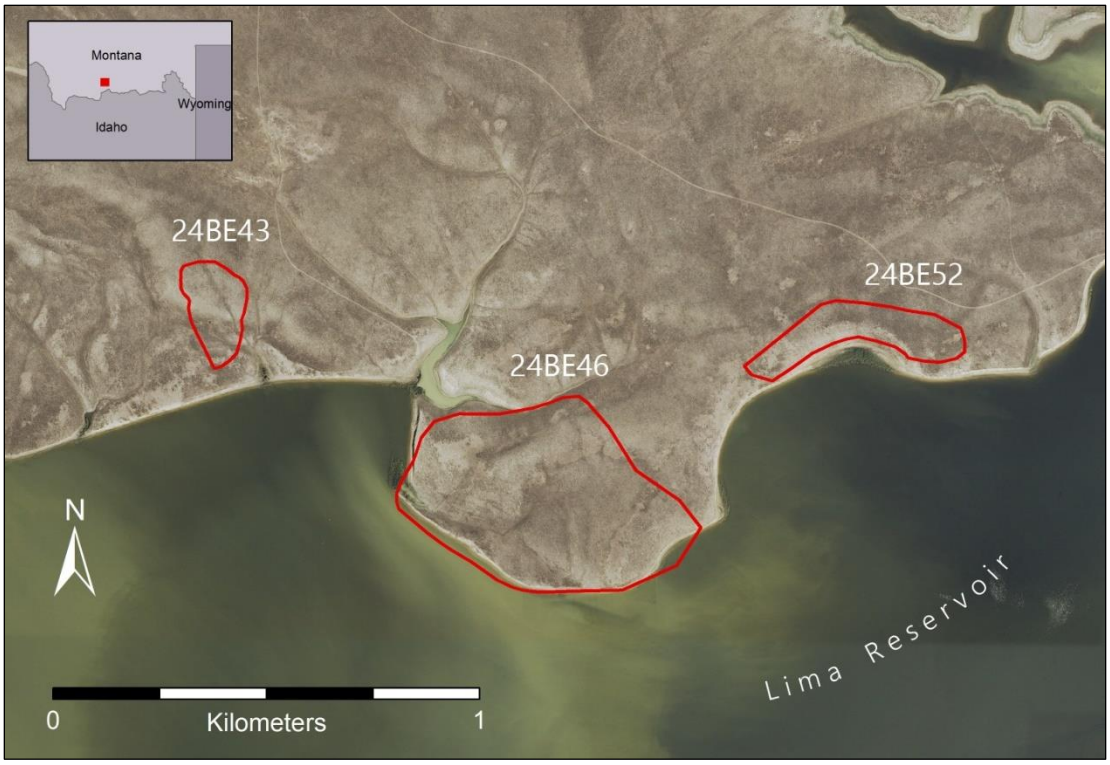

Figure 4. Close-up of study area showing Paleoindian site locations.

luminescence (OSL) dating, granulometry, and comparison of stratigraphy to facies models.

Reconstructing the area's geomorphic history first required establishing the relative sequence of erosional and aggradation events in the study area. I began by examining the stratigraphy, sedimentology, soil formation, and geochronology of geological outcrops in and around the three archaeological sites. My focus was determining the local effects of erosion, intersecting sediment sources and paleotopography on site burial during the Pleistocene-Holocene transition. I speculated what erosive factors may have created accommodation space in underlying sediments such as stream avulsion, fault throw or blowout and compared bounding surfaces with stratigraphic and facies models (Miall 2000). More importantly, I pieced together the

timing of aggradation events and determined whether sediment packages derived from lacustrine, alluvial, eolian or other depositional environments. Identifying when sediments were deposited and recognizing what time periods unconformities or diastems represent is key to understanding what climatic or autogenic controls drove system changes and how archeological

sites were affected. Finally, using a combination of chronometric age controls and principles of cross-cutting relationships I established which exposures and sediment packages in the study area are young enough to contain buried archeology.

The second objective was applying my geomorphic sequence interpretations to address the management issue of how researchers can recognize landforms with archeological burial potential. Based on qualitative and quantitative comparisons between pre- and post-occupation age sediment packages in the study area, I compiled a list of outcrop characteristics correlating with occupation-age and pre-occupation outcrops. For instance, in a portion of 24BE46's cutbank, a conspicuous pair of buried paleosols signals a mid-to-late Holocene sediment sequence. I intend for this list to help BLM and other archeologists select study locations for research aimed at discovering buried sites in the valley.

This research lays the groundwork for locating buried sites not only in Centennial Valley, but in other Rocky Mountain valleys with similar Quaternary geomorphic histories. Buried archeological components are important because sites covered soon after occupations generally maintain vertical and horizontal artifact spatial relationships better than exposed sites (Ebert 1992; Schiffer 1987). Furthermore, this research increases our understanding of how sites become buried in these environments and how

complex sedimentological systems influence site taphonomy (Bettis and Hajic 1995; Blum et al. 1992). A need exists for a comprehensive method to identify landforms with potential to contain subsurface sites and to increase our understanding of how sites become buried in the first place. This need is both to identify potentially data-rich sites for future investigation as well as for helping land managers avoid inadvertent damage to such localities.

CHAPTER 2:

BACKGROUND

The study area lies in southwest Montana's Centennial Valley (Figures 1 and 2). The Centennial Valley is a structural basin (graben) extending approximately 68 km (42 miles) east to west (Hill 2005:39). It is bounded by the Centennial Mountains to the south, the Snowcrest and Gravelly Ranges to the north and the Henrys Lake Mountains to the east (Lonn et al. 2000). The Lima Dam, built in 1890, sits at a natural constriction near the valley's west end, impounding the west-flowing Red Rock River and creating Lima Reservoir (Albanese 2005; BOR 2004). The study area is situated on the reservoir's north shore approximately three miles east-southeast of Lima Dam. The study area is approximately three kilometers square and encompasses sites 24BE43, 24BE46, and 24BE52 (Figure 4). The landforms and stratigraphy of the study area and surrounding valley floor are complex, having been shaped by recent tectonics, volcanic activity, and a combination of geomorphic processes.

Geologic and Environmental Setting

The Centennial Valley's geologic structure results from Laramide orogenic compression, Basin and Range style extension, and Yellowstone hotspot volcanism, all of which contribute to the area's seismic instability (Alden 1953:37; Honkala 1960; Majerowicz et al. 2010). Following late Cretaceous Laramide crustal thickening and folding, the area underwent extensional block faulting, which uplifted the Centennial Mountains and down-dropped the Centennial Valley floor (Pierce and Morgan 1992).

Antecedent Sevier-Laramide contractional structures apparently dictated the geometry and locations of some valley fault systems (Anastasio et al. 2010:197; Myers and Hamilton 1964:86). Simultaneously, the Yellowstone hotspot tracked across southern Idaho, creating the Snake River Plain (SRP) and separating the so-called 'Montana-Idaho Basin and Range' (MIBAR) segment from the central Basin and Range province (Stickney and Bartholomew 1987). Just north of the SRP, the Centennial Valley lies within the overlap of two tectonic regions; the Centennial Tectonic Belt, which is associated with the MIBAR and the Centennial Shear Zone, associated with the SRP (Payne et al. 2008; Stickney and Bartholomew 1987) (Figure 5). The Centennial Tectonic Belt is the most tectonically active region of the MIBAR and is characterized by numerous northwest-trending normal faults (Stickney and Bartholomew 1987:1608). To the south, the Centennial Shear Zone accommodates the MIBAR's rapid extension against the slowly expanding Snake River Plain with dextral (right-lateral) fault slip. Situated in the overlap of these tectonic zones, the frequency of ground-rupturing faulting in Centennial Valley has apparently increased through the Pleistocene and Holocene (Anastasio et al. 2010:2006). Movement on the valley's major fault systems has averaged approximately .3 mm per year since the latest Pinedale glaciation (Sonderegger et al 1982:11). Historically, earthquakes in the area have produced ground deformation, kilometers-long fault scarps, changes in ground altitude up to 6.7 meters, and numerous landslides (Myers and Hamilton 1964; Nolan 1964). Given the area's level of seismic activity, consideration of tectonic factors is critical when interpreting late Quaternary geomorphology. This includes determining the genesis of unconformities, extrapolating the positions of target-age sediment units between landforms, and assessing post-

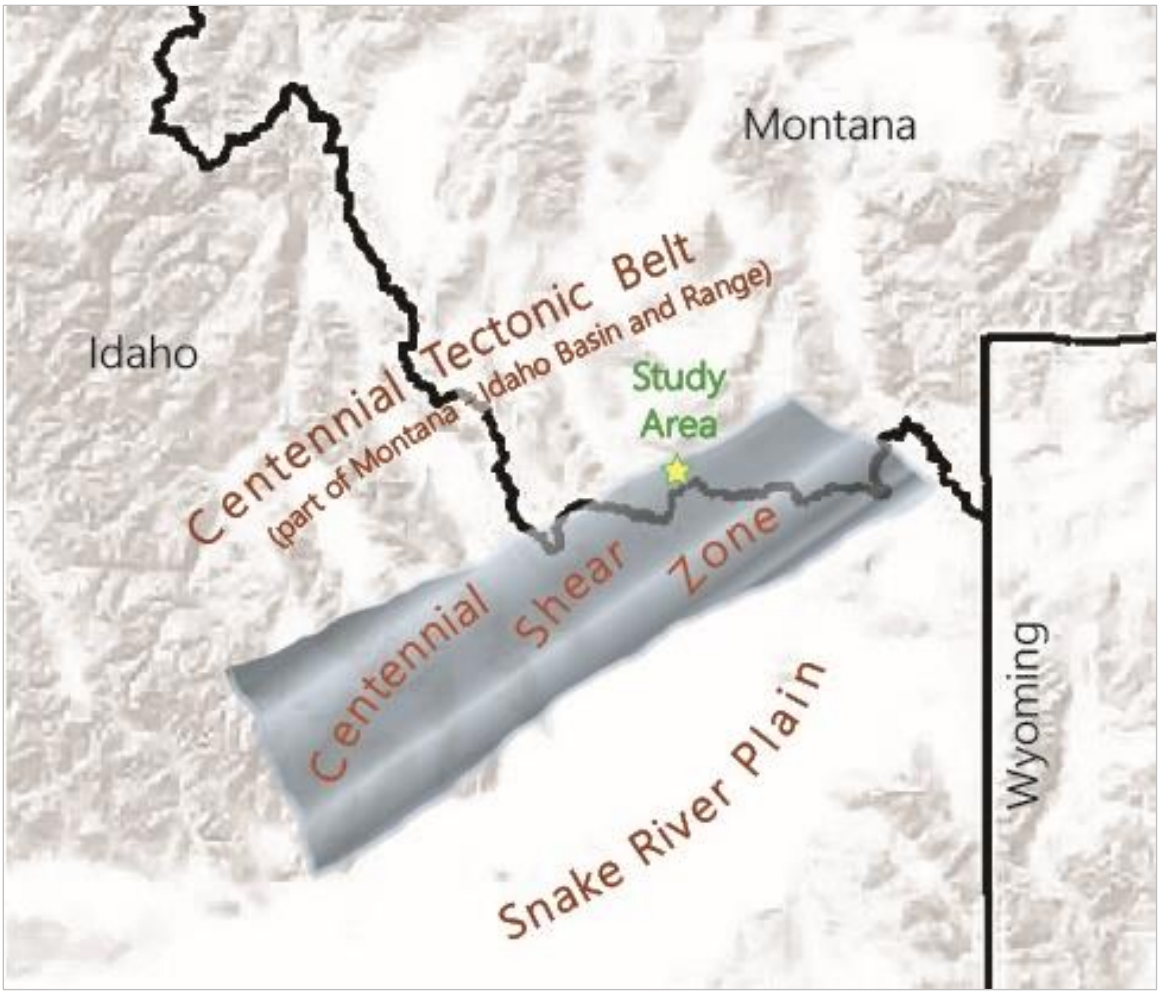

Figure 5. Location relative to Centennial Shear Zone, Centennial Tectonic Belt, and the Snake River Plain.Modified from Payne et al. (2008:Figure 1) and Stickney and Bartholomew 1987.

occupation disturbances.

Understanding the potential range of late Quaternary sediment variability requires establishing what rock types are available for weathering and transport in the valley. The preserved rock record in the Centennial Valley includes all major eras of the Phanerozoic eon as well as Proterozoic basement rocks (Hill 2005). Precambrian metamorphosed sedimentary and igneous intrusions are exposed in the valley's far eastern end (Witkind 1972), and Precambrian gneiss and schist are present on the valley's northern edge (Alden 1953:39). Paleozoic and Mesozoic formations consist largely of carbonates, shales,

siltstones, sandstones, and some coal beds (Hill 2005:39). Following the Laramide orogeny, Cretaceous and Tertiary erosion of the newly uplifted mountains created clastic formations in the valley. The Cretaceous Frontier and overlying Tertiary/Cretaceous Beaverhead Group dominate west Centennial Valley's slopes and uplands (Dyman et al. 2008). The Frontier Formation consists largely of conglomerate, sandstone, siltstone, and mudstone; the Beaverhead is somewhat coarser and dominated by quartzite and limestone conglomerates and some sandstone (Ryder and Scholten 1973). Late Quaternary deposits include indurated rhyolite and ash flows on the valley margins (Sonderegger et al. 1982). However, Holocene deposits mostly consist of unconsolidated alluvial fan, lacustrine, colluvium, stream alluvium and dune sediments (Lonn et al. 2000; Ryder and Scholten 1973). Having derived largely from fine to medium-grained sedimentary rocks, recent deposits are generally fine. Near my study area along the valley axis, mapped deposits consist primarily of stream alluvium, lacustrine, and eolian sediments (Lonn et al. 2000, Majerowicz et al. 2010; Scholten et al. 1955). Characterizing when, how, and where these three depositional environments interacted was therefore a key component of my investigation.

Researchers have conducted numerous paleoenvironmental studies that determined climate cyclicity drives much, but not all, recent geomorphic change in Centennial Valley. Paleolakeshores and invertebrate fossils suggest the presence of multiple lakes in Centennial Valley, but the timing of their creation and lateral extents are not precisely understood (Honkala 1949; Sonderegger et al. 1982). Moraine fronts overlapping lacustrine material suggest that some paleolakes pre-date the last glacial maximum (LGM) approximately 18.8 to 16.5 ka (Licciardi and Pierce 2008; Meyers and

Hamilton 1964). Following deglaciation, cool and more mesic conditions contributed to filling the valley to a level of 2099 meters (6,888 ft.) above sea level. Mumma et al. (2012) used Lower Red Rock Lake sediment cores to reconstruct paleoclimatic shifts in the eastern Centennial Valley and found that post-LGM deglaciation coincided with an abrupt lacustrine facies change from near-shore sands to overlying deep-water clays. The Younger Dryas occurred between approximately 12,900 and 11,600 (Alley 2000) making the climate abruptly colder and drier. These conditions likely contributed to lake recession, which exposed lacustrine silts to northwest winds and resulted in the formation of loess barchan dunes (Honkala 1949:129). Dune fields halted or altered small drainages in the valley and diverted the Red Rock River up to 3 km (~ 2 miles) in one location. However, remaining water bodies may have arrested dune progression in other areas (Honkala 1949:130). Small lakes occupied Centennial Valley during the Holocene, possibly as late as 3800 cal BP (Meyers and Hamilton 1964:93). Honkala (1949) interprets late Pleistocene and Holocene sediment facies as interfingering terrestrial and lacustrine deposits formed as alluvial fans spread into rising and falling lake margins. Faulting and warping associated with major earthquakes likely played a role in emptying the last large lakes. This is evidenced by a fault-broken mid-Holocene shoreline warped more than 18 meters (Myers and Hamilton 1964:93). The Upper and Lower Red Rock Lakes represent the mid-Holocene lakes' modern remnants.

The Red Rock River has alternately incised, aggraded, and avulsed through the late Pleistocene and Holocene (Honkala 1949). Many of these adjustments result from stream competency and capacity measures, which are related to upland-contributed sediment load, water availability and ultimately climatic circumstances (Bull 2008).

However, climate forcing is not the only important factor driving river behavior in the Centennial Valley (Hill 2005:45). Late Quaternary river incision exceeding 15 meters is likely connected to fault uplift in the seismically active valley (Honkala 1949:124; Meyers and Hamilton 1964). Furthermore, major shift in river course, as well as lake development, have been directly linked to volcanic lahar deposition and seismic-associated mass-wasting. During the late Pleistocene, most of Centennial Valley drained east-northeast through an outlet linked to Madison Valley (Myers and Hamilton 1964:95). Meanwhile, the west-flowing ancestral Red Rock River had its headwaters at the west end of the valley. Around the time of the Pleistocene-Holocene transition, tectonic downwarping of Centennial Valley's west end lowered the base level of the ancestral Red Rock and intensified head-cutting eastward through Centennial Valley. Concurrently, glacial damming (Honkala 1949:127) and quake-triggered landslide damming obstructed the valley's northeastern outlet (Myers and Hamilton 1964). These conditions resulted in eventual stream piracy by the west-flowing river and reversal of drainage flow for Centennial Valley.

Climatic conditions, tectonic events, and volcanism shaped Centennial Valley's late Quaternary geomorphic landscape and sedimentologic records (Hill 2005:45). Geomorphic processes related to these controls established antecedent landforms that people occupied in the Centennial Valley. These geomorphic processes continued to interact with cultural material left by those people and played a key role in the character of archeological site formation.

Previous Archeological Research

Archeological research in Centennial Valley spans the 1970s through present but includes few formal excavations (Hill and Davis 2005; Murray 1977; Peart et al. 2012, 2013, 2014; Schuster 2005). Archeological study began in 1974 with the University of Montana's (UM) Lima Reservoir's shoreline surveys (Murry et al. 1977). Three sites identified during that investigation (24BE43, 24BE46, and 24BE46) are the focus of this research. USUAS re-recorded and expanded these sites' boundaries in 2011 (Peart et al. 2012). Although archeologists have excavated relatively few areas in Centennial Valley, the Tree Frog and Merrell Locality make notable exceptions (Hill and Davis 2005; Schuster 2005; Vanwert 2000). UM excavated two localities of the Shoshone Tree Frog site (Schuster 2005; Vanwert 2000). The single-component locality contains a diverse protohistoric artifact assemblage including Intermountain Tradition pottery sherds and horse bones. Unfortunately, the shallow site lacks components old enough to overlap substantially with cultural material in my study area.

The Merrell Locality is a late Quaternary paleontological/archeological site situated on Lima Reservoir's south shore just east of the dam (Hill and Davis 2005). The locality contains a rich record of Pleistocene fauna including mammoth, camel, and scimitar cat remains dating to ca. 49,000 cal BP (Hill 2005:52). Merrell Locality strata exhibit facies consistent with lacustrine, marsh, colluvial, and alluvial environments. In addition to paleontological remains, the Merrell Locality contains a sparse surface and subsurface artifact assemblage including a possible Middle to Late Archaic projectile point fragment. All subsurface artifacts occur within the one-meter-thick uppermost colluvial stratum. Overall, the archeological assemblage lacks primary context and there

appears to be no affiliation between cultural material and underlying Pleistocene faunal remains. Merrell Locality sediment package ages overlap with those in my project area and some similarities between soil sequences and sediment facies are apparent.

Study Sites

The three sites in my study area (24BE43, 24BE46, and 24BE52) share artifact composition and landscape position similarities. However, dissimilar stratigraphic profiles prompt questions regarding the geomorphic site formation history of each locality. Site 24BE43 sits at the far western end of the study area on a dissected terrace overlooking Lima Reservoir to the south (Figures 4 and 6). The site includes two artifact concentrations extending above and below a possible ancient lake terrace incised by a shallow drainage (Figure 6) (Peart et al. 2011a, 2012). USUAS noted a diverse assemblage at 24BE43, including two Frederick (Late Paleoindian) (Kornfeld et al. 2010) and two unidentifiable Paleoindian projectile point fragments, multiple groundstone pieces, scattered fire-cracked rock, and abundant debitage. Surveyors located all artifacts on the ground surface (Peart et al. 2012).

Site 24BE46 is situated near the study area center and presents the most complex stratigraphy, largest artifact assemblage, and widest cultural time span of the three sites (Figures 4 and 7) (Peart et al. 2011b, 2012). Projectile point styles include Agate Basin (early Paleoindian), unidentifiable Paleoindian/Early Archaic, Hanna (Middle Archaic), unidentified corner-notched, and unknown side-notched (Late Prehistoric). In 2011, USUAS identified two artifact concentrations on the terrace top and one stretching along the shoreline at the site's southern margin (Peart et al. 2011b, 2012). Densely

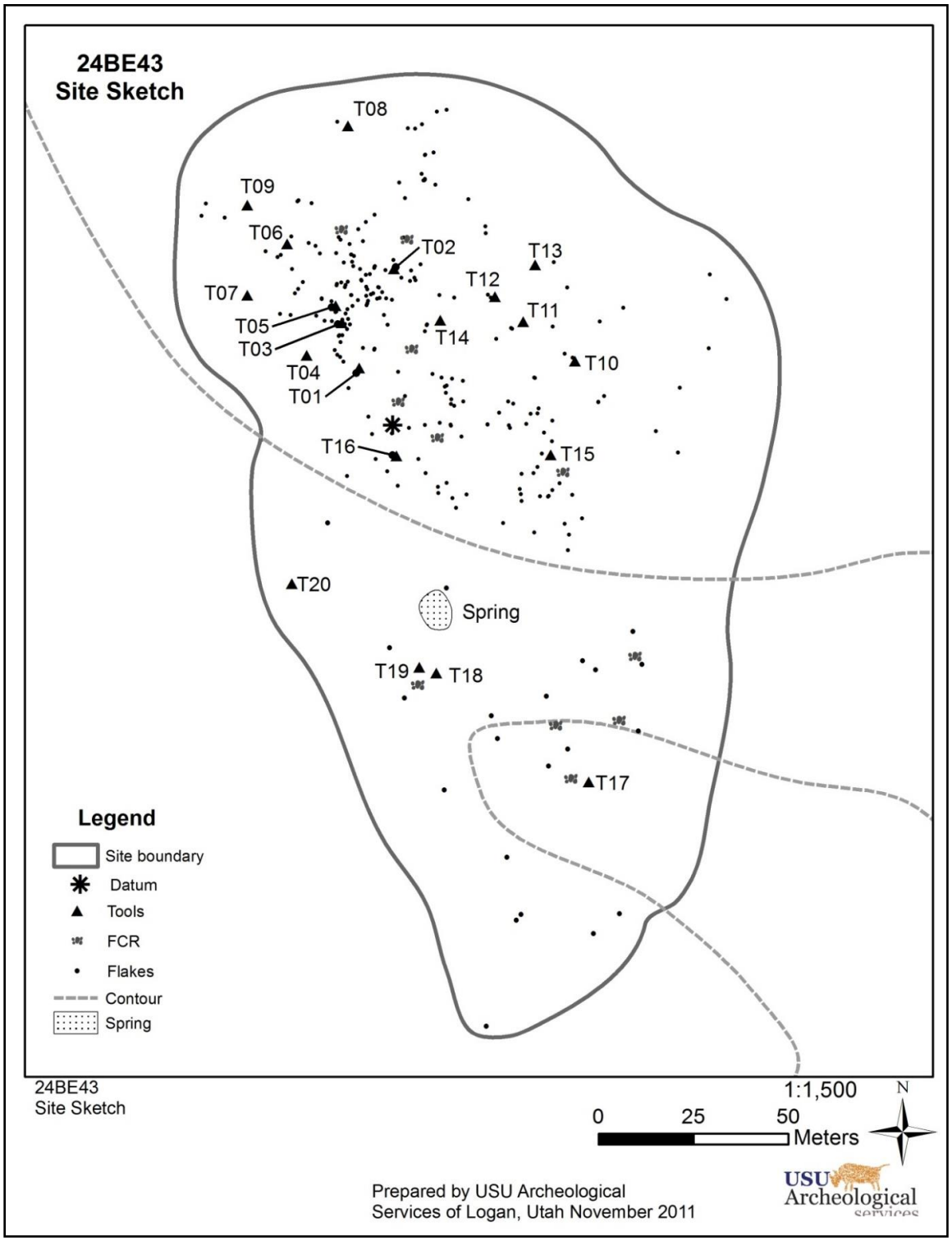

Figure 6. Planview map of site 24BE43.Reproduced from Peart et al. (2012:Figure 28).

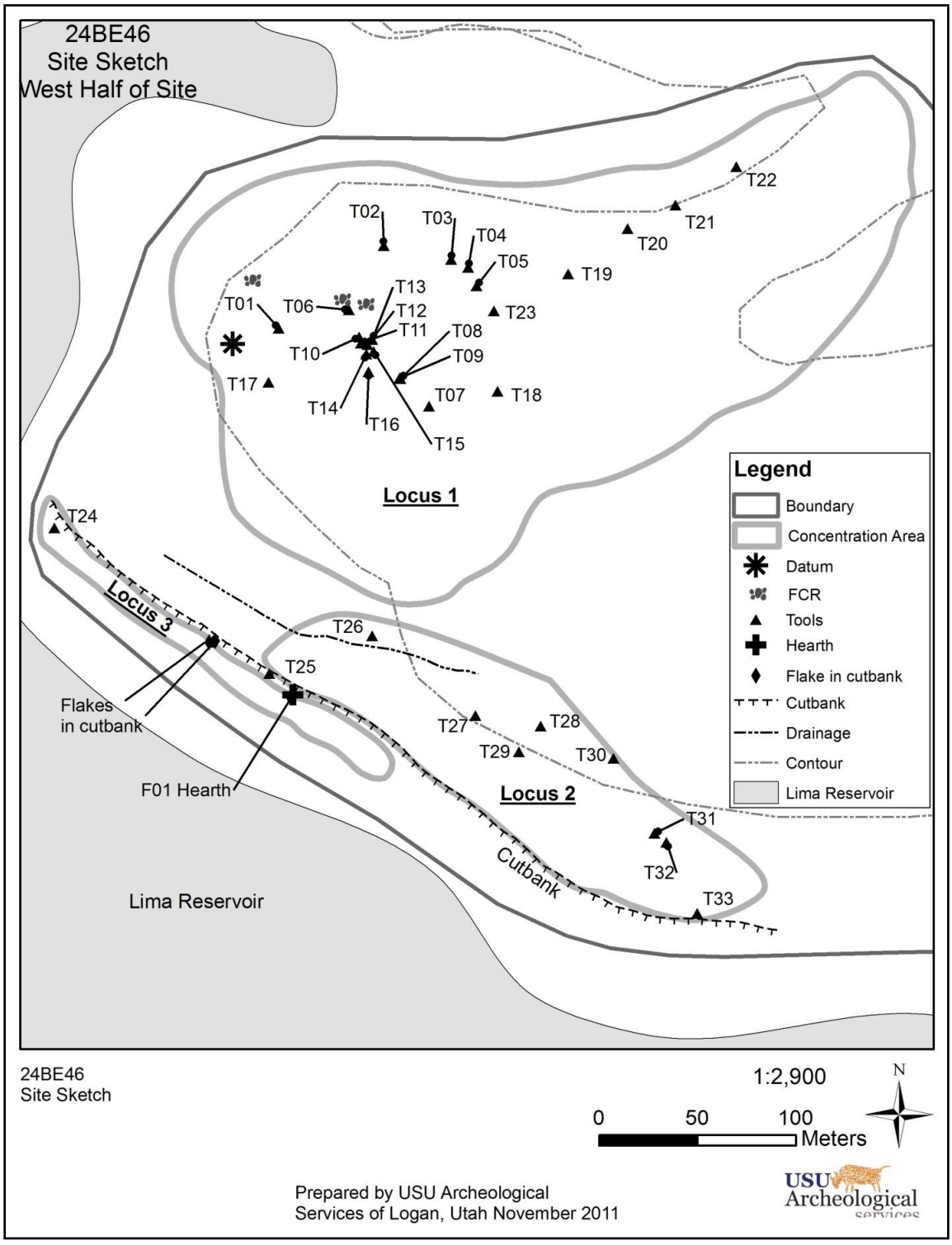

Figure 7. Planview map of site 24BE46. Reproduced from Peart et al. (2012:Figure 34).

concentrated artifacts on this section of beach indicate artifact displacement from either the terrace surface or previously buried contexts within the landform. In addition to locating redeposited artifacts on the beach below the site's cutbank, Peart et al. (2011b) discovered a hearth and associated debitage eroding out of the site's southern exposure (Figures 8 and 9). Researchers collected three charcoal samples for radiocarbon dating. The hearth was 55 cm below the modern surface and about 10 cm beneath a buried paleosol. Although the wall collapsed some time before May 2014, destroying the hearth, I observed numerous artifacts (n ~ 30) present in the cutbank face at maximum depths of about 70 cmbs. USUAS interpreted 24BE46 as situated on and within Pleistocene and Holocene lacustrine sediments with good potential for containing significant buried cultural material (Peart et al. 2012).

Site 24BE52, the eastern-most site, contains the fewest artifacts, least diverse assemblage, and lacks an apparent subsurface component (Peart et al. 2012). The site is situated on a high terrace, which rises approximately eight meters above the present Lima Reservoir shoreline (Figures 4 and 10) (Peart et al. 2011c, 2012). The locality is a sparse lithic scatter with scant debitage and few tools. Diagnostic artifacts consist of two Agate Basin (early Paleoindian) projectile point fragments. USUAS did not note any features or artifact concentrations when they re-recorded the locality in 2011. All artifacts were observed on top of the terrace and none were in the cutbank or along the beach below it. However, Peart et al. (2011c) concluded that intact portions of 24BE52 likely have good burial potential.

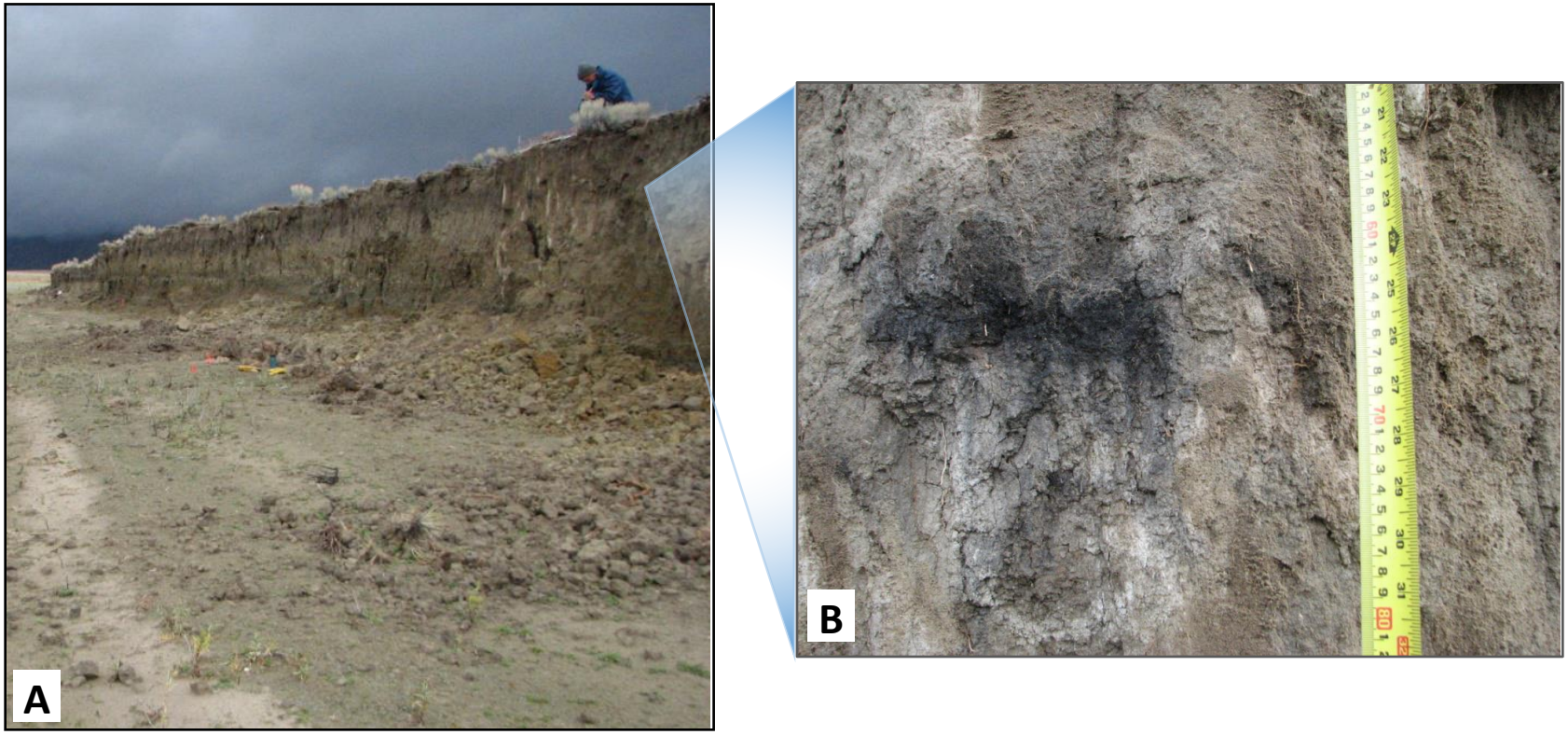

Figure 8. Cutbank exposed hearth (Feature 1) in 24BE46, overview to the west-northwest (A) and closeup facing north (B). Modified from Peart et al. (2012:Figures 37 and 38).

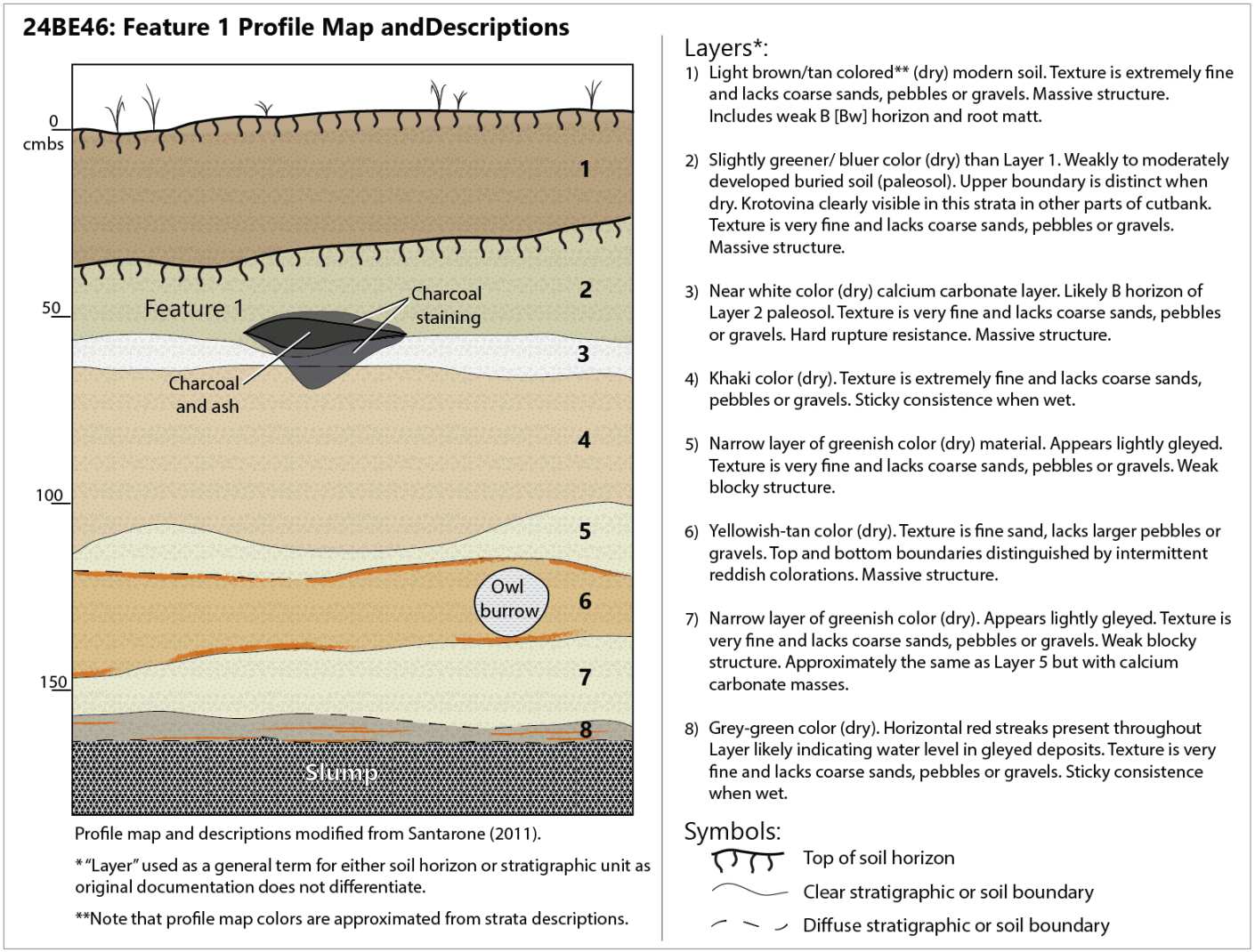

Figure 9. 24BE46 Feature 1, profile map and descriptions. Modified from Santarone (2011) field notes.

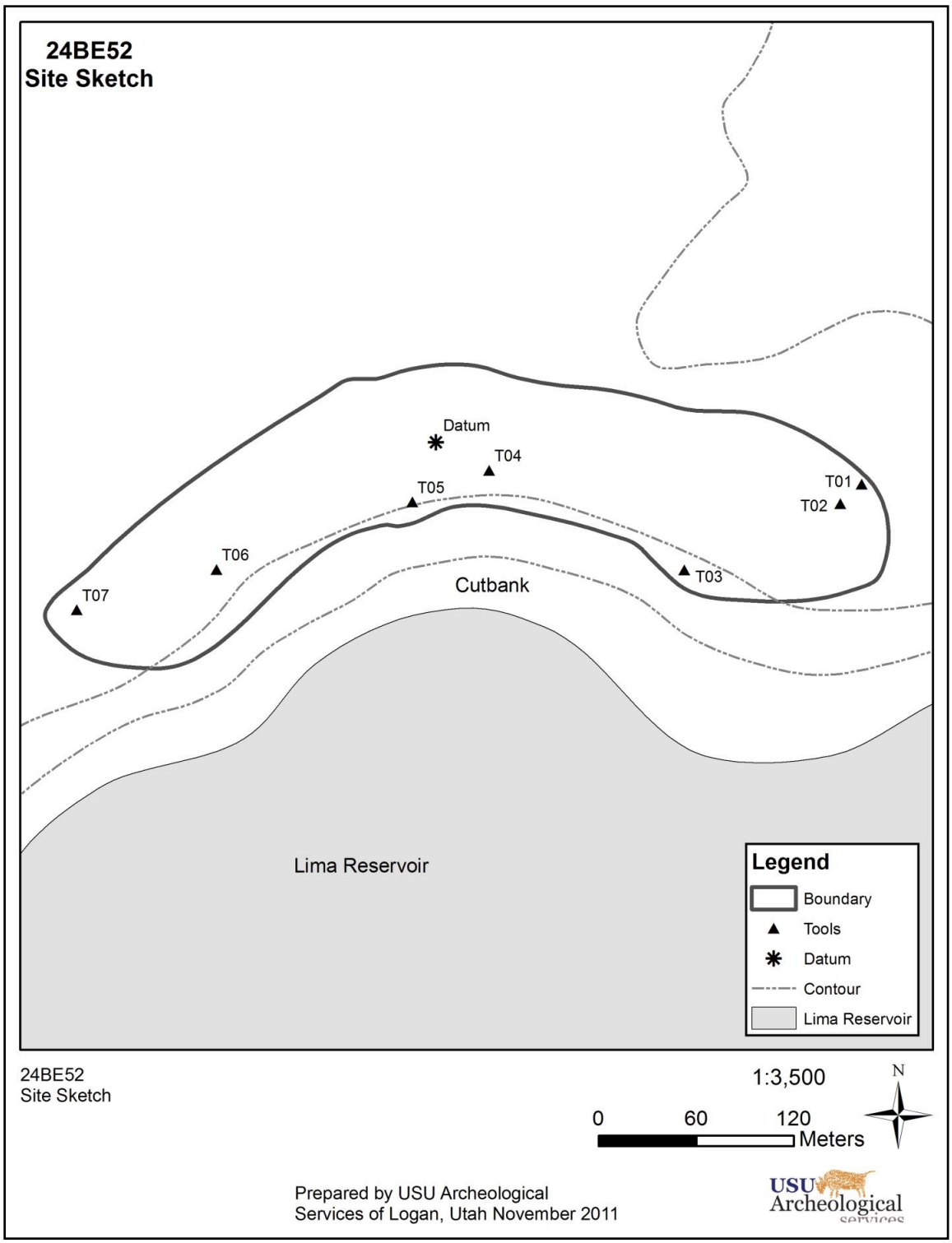

Figure 10. Planview map of site 24BE52. Reproduced from Peart et al. (2012:Figure 47).

Local Geologic Interpretations

My research seeks to understand the cause of depositional variability among the three sites, and although previous geologic mapping near Lima Reservoir provides some insight, it presents three subtle but importantly different interpretations (Figure 11; Lonn et al. 2000; Majerowicz et al. 2010; Scholten et al. 1955). The area surrounding the sites has been variously interpreted as exclusively Quaternary alluvium (Lonn et al. 2000), undifferentiated Quaternary lake deposits (Scholten et al. 1955), or differentiated Quaternary lake deposits (Majerowicz et al. 2010). Majerowicz et al. (2010) interpret the older package as Middle Pleistocene lake sediments, while the younger deposit dates to the late Holocene. The primary difference between the two deposits is that eolian sediment caps the older lacustrine material. Not only do these geologic interpretations disagree in significant ways, none are mapped at scales useful to site-specific archaeological interpretations. Therefore, a major problem for geoarchaeological analysis is a local understanding of the stratigraphy and facies associations for the three sites at finer scales than presently mapped.

Centennial Valley's complex geomorphic history and observed discrepancies in site stratigraphy pose two nested questions. First, why do the site formation histories of these three neighboring sites differ so greatly and, more specifically why do two sites appear to lack subsurface archeology while one contains a verified buried component? Second, how can other landforms with post-occupation age deposits be identified? These questions are not answerable with existing research. Addressing these problems therefore hinges on defining, correlating, and interpreting stratigraphic units and their boundaries at a scale useful to archeological interpretation.

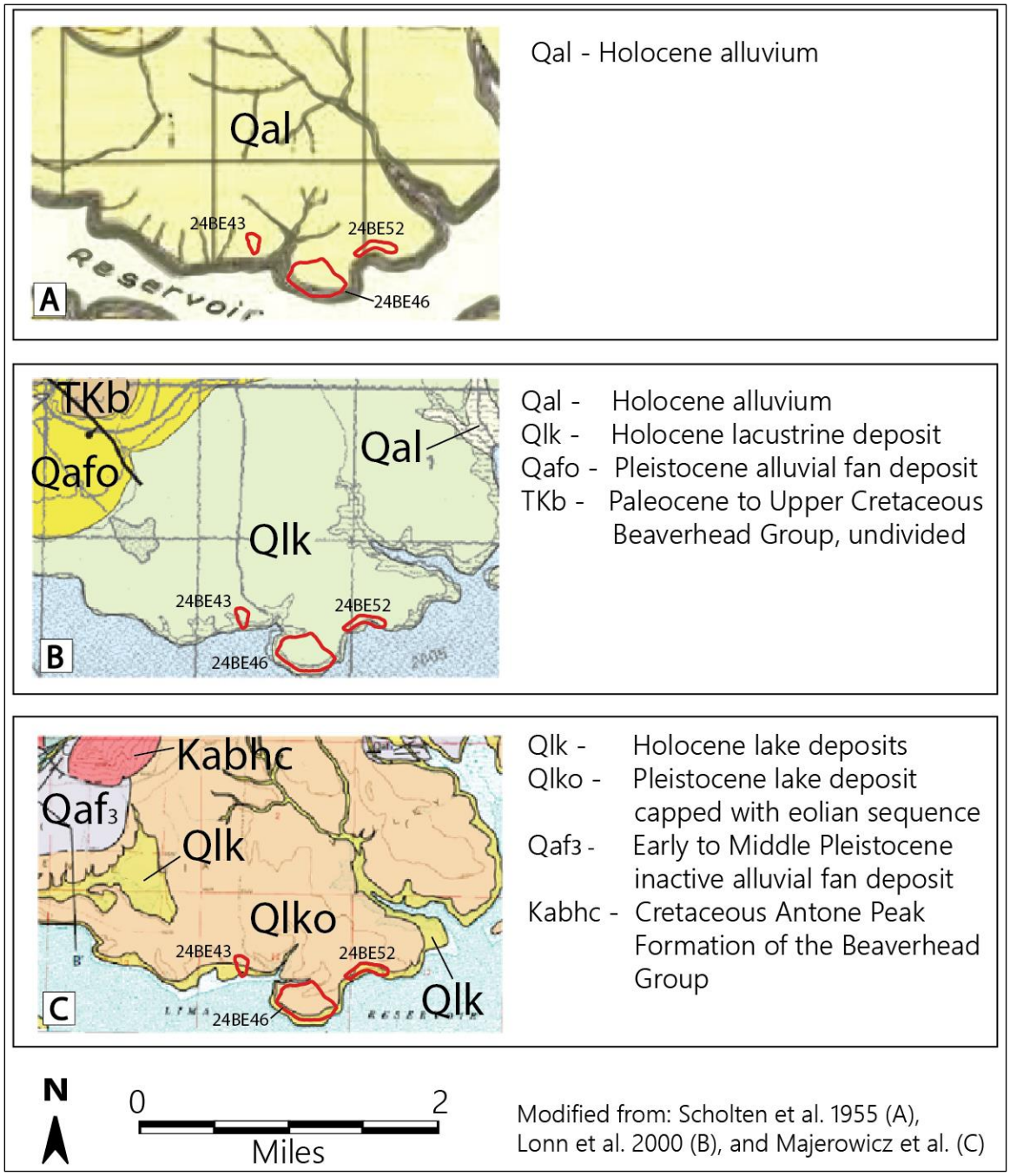

Figure 11. Representative previous geologic mapping of study area. Modified from Scholten et al. 1955 (a) Lonn et al. 2000 (b) Majerowicz et al. 2010 (c)

My overarching objective was to reconstruct the study area's recent geomorphic history, determine what conditions led to site burial and describe characteristics of occupation-age sediment packages. To that end, three investigation methods constituted the backbone of my research: stratigraphic profiling to establish event sequences, granulometric analysis to interpret depositional environments, and OSL dating to provide age control. The following chapter describes how I applied these techniques to my research questions, my specific lab and field protocols, and my how my methods evolved with increasing understanding of the area.

CHAPTER THREE:

METHODS

My research objectives were determining how sites were buried in the study area and distilling what characteristics signal occupation-age sediments in Centennial Valley. I used three primary methods to address these questions; stratigraphic description, granulometry, and OSL dating. Resolving my research questions required first establishing a relative geomorphic event sequence in the study area, then fixing these events to a chronometric timeline (Waters 2000) and determining what processes were responsible for observed sediment packages and (if possible) unit boundaries. My last step involved summarizing distinguishing characteristics of pre- and post-occupation age sediments so as to model areas more and less likely to contain buried archeological material in Centennial Valley. I employed coarse- and fine-scale stratigraphic description to establish relative event sequences, granulometric analysis to infer depositional environments, and OSL dating to provide age control. I augmented these methods as necessary with evidence from GPS landform mapping, aerial photographs examination, accelerator mass spectrometry (AMS) radiocarbon dating, and X-ray powder diffraction (XRD) mineral analysis. The following sections summarize my field, granulometric and OSL methods and how I used them to address my research questions.

Fieldwork and Stratigraphic Description

My first step was reconstructing a relative sequence of events based on coarse- and fine-scale stratigraphic description of the study area's cutbank exposures. Shoreline

cutbank faces are largely vertical and range from approximately one to nine meters high. An important aspect of my initial fieldwork was examining the roughly 3.5 km long undulating cutbank adjacent to the reservoir edge (Figure 4). Along the face, I noted general similarities and differences between exposures in terms of sediment facies structure, bed tilt (strike and dip measured with clinometer), apparent soil sequences, color, redoximorphic and carbonate feature development and texture. I recorded each observation point's location with either a Trimble GeoXT GPS (sub 1-meter accuracy) or Garmin Rino handheld GPS (sub 3-meter accuracy) and took photographs using a Kodak DX6490 4.0 megapixel digital camera. I also traced laterally continuous beds and tephra layers, identified apparent unconformities and noted relative elevation relationships between landforms. While cutbank visibility was generally good, talus, wall slump, ephemeral drainage incision, vegetation and walls exceeding ladder height of 4 m (13 ft.) obscured strata visibility in some areas. I compensated by excavating windows through overlying sediments, extrapolating contiguous beds from adjacent exposures, and following high strata to ladder-accessible areas where possible.

In addition to broad-scale cutbank observation and recording, I selected ten locations for detailed stratigraphic description within the west, central and east sub-areas of the study area (Figure 12). I chose stratigraphic profile locations based on two criteria: representing maximum stratigraphic variability among outcrops and describing outcrops with post-occupation age sediment packages. I recognized post-occupation age units by either identifying in situ artifacts or relationship to preliminarily OSL-dated sediment packages. Given that my fieldwork spanned two years, my description and sampling procedures evolved as my knowledge of sedimentology and soil formation increased.

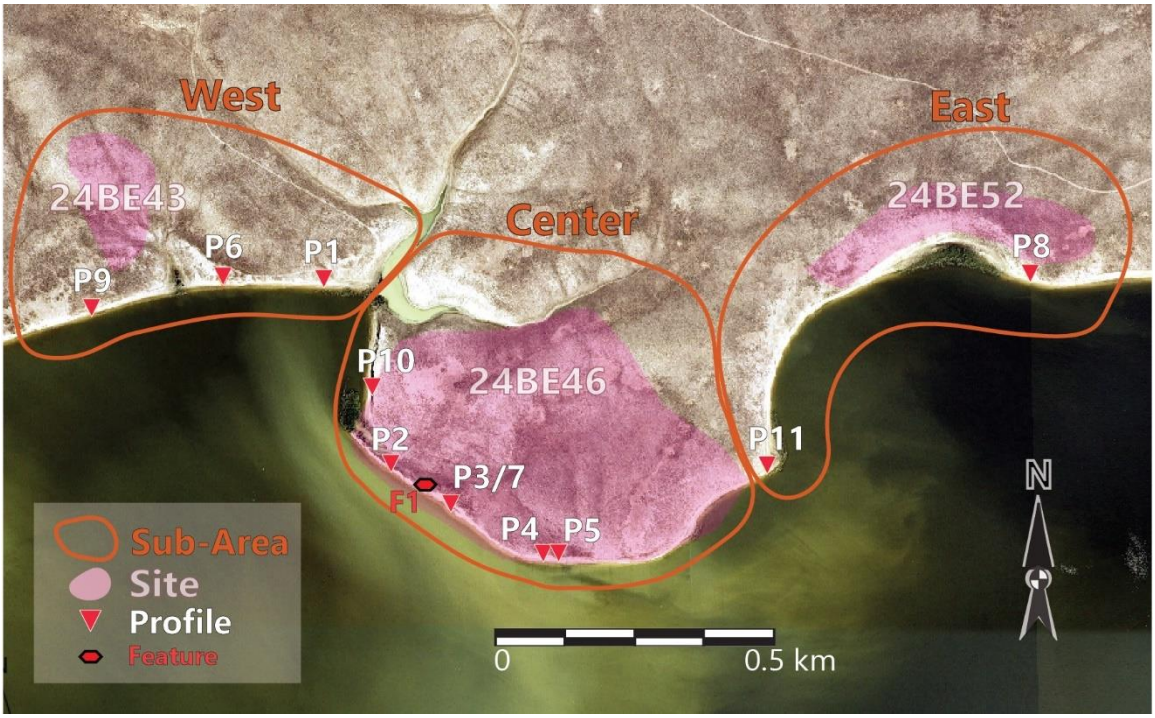

Figure 12. Study area plan map showing locations of west, central and east sub-areas, sites (24BE43, 24BE46, and 24BE52), stratigraphic profiles (P1-P11), and Feature 1.

Consequently, some stratigraphic descriptions are more detailed than others. I re-profiled four of the ten stratigraphic sections to mitigate data discrepancies.

My methods for describing stratigraphic profiles involved wall facing, sediment units and soil horizon boundary identification, strata description, and OSL and granulometric sample collection. Stratigraphic profiles averaged one meter wide and ranged from approximately two to five meters tall. After selecting a stratigraphic location for detailed description, I first cleaned and faced the wall to remove overwash deposits, better expose color variations between strata[1], and observe natural failure along pedologic and sedimentologic cleavage structures. Furthermore, if the profile wall was high (3+ meters) or appeared unstable, I stepped back the top of the profile to decrease the risk of

[1] Note that I use "strata" as an umbrella term encompassing both sediment units and soil horizons

the wall collapsing. In these instances, I maintained depth control by extending a tape measure (plumb) from the end of a pole at the top of the wall. I then measured strata depth by holding a rod level between plumb measuring tape and profile feature of interest. I GPS recorded the location of each stratigraphic profile, took digital photographs of the cleaned face, closeups of notable strata, and overviews of the profile position along the cutbank wall.

After facing the profile location, I determined sediment unit upper and lower boundaries and further subdivided these into soil horizons if pedologic development was present. Two important considerations in stratigraphic description were deciding whether to 'lump' or 'split' sediment packages (possibly representing overlapping scales of environmental cyclicity) into single or multiple units and determining whether observed stratigraphic differences result from depositional conditions or succeeding pedologic development (Holliday 2004:8; Miall 2000; Waters 2000). In my project area, the issues of designating appropriate-scale unit divisions and recognizing pedogenic versus sedimentologic horizonation were complex given that study area sediment packages derive from intermingling processes. Buried paleosols and welded soils are common in the area but often subtle in appearance (Lonn et al. 2000; Majerowicz et al. 2010; Peart et al. 2012; Scholten et al. 1955). Furthermore, inundation from both the modern reservoir and intermittent Pleistocene and Holocene lakes has altered sediment matrix color with bands of redoximorphic staining, complicating sediment package differentiation. I therefore used a combination of sedimentology and soil description techniques to define units and differentiate between sediment and soil horizonation (Midwest Geoscience Group (MGG) 2015; North American Commission on Stratigraphic Nomenclature

(NACSTRAT) 1983; Schoeneberger et al. 2012). To establish stratigraphic boundaries, I first identified unconformities and sediment package boundaries in the profile. These are often signaled by buried A Horizon diastems or abrupt texture or structure changes. I generally relied little on color for differentiating units because post-depositional processes (such as gleying and gypsum development) have altered parent material hue in many places. In areas exhibiting thinly bedded (apparently cyclic) variation, I grouped strata consisting of fine-scale repeating patterns while making note of minor intra-unit variation (rather than separating each lens into a separate unit). If pedogenic alteration was present, I subdivided each unit into soil horizons within the unit boundaries.

Following boundary differentiation, I labeled and described the morphology of each sediment unit and soil horizon. I numbered and described units sequentially from bottom (oldest) to top. If a unit exhibited soil development, I first recorded the horizon's morphologic characteristics and then assigned appropriate master and suffix designations per NRCS naming conventions (Schoeneberger et al. 2012). I sketched a scaled profile map of the profile and recorded numerous qualitative characteristics for each unit and horizon. These included stratum depth, dry Munsell color and code, texture (following Folk 1954), structure type (including ped size and grade if applicable), consistence, effervescence (using 10% concentration hydrochloric acid), and lower boundary topography and distinctness. I recorded other notable attributes such as carbonate mass development, redoximorphic features, bioturbation, organic content, and original bedding structure details if present. If applicable, I also noted variations within strata such as bed grading, color mottling, contrasting sediment lenses, and macrofossils.

While the shoreline cutbank provides a stratigraphic picture of the study area's

southern margin, the area's interior is obscured, complicating three-dimensional sequence stratigraphy reconstruction. To facilitate stratigraphic extrapolation into the project area's interior, I described two profiles on the west and east-facing walls of the central study area's south-extending terrace (SL10 and SL11, respectively) (Figure 12). Profile extrapolation between these stratigraphic windows aided my interpretations of events for the interior of the south-extending terrace. In addition, I studied aerial photographs of the project area prior to fieldwork, outlining what appeared to be distinct landforms (such as possible oxbows or terrace tops). I ground-truthed these interpretations with field observation. Finally, I recorded Trimble GeoXT (sub 1-meter accuracy following post-processing) GPS shapefiles demarcating prominent and subtle landform features across several kilometers. For instance, I mapped the current cutbank foot and crest edges, swales denoting apparent abandoned meander channels, ephemeral drainage cuts and other topographic breaks. As vegetation and recent sediments obscured the ground surface, I based my landform distinctions primarily on subtle topographic aspect changes and to some extent vegetation differences. Finally, I used these mapped features (including profile locations), aerial and ground photos, profile sketches and descriptions, and outcrop observations to construct an ArcMap document of feature positions, tables of qualitative stratigraphic profile descriptions, and detailed panel figures for each locality (see Chapter 4: Results). These data enabled me to reconstruct a relative sequence of geomorphic events for the project area. After constructing the relative event sequence, I fixed stratigraphic units in a chronometric framework using OSL dating.

Optically Stimulated Luminescence (OSL) Dating

OSL dating depends on the ability of quartz grains to accumulate a luminescence signal based on environmental radiation intensity and burial duration. Given a known level of environmental radiation, this characteristic allows estimation of time elapsed since grains were last exposed to sunlight (Aitken 1998:6). In natural settings, sun-exposed sediments are constantly 'zeroed' of luminescence signal. The last time a sand grain is exposed to sunlight before burial is known as the ‘bleaching event,’ and this brings the grain’s radiation-acquired signal to essentially zero (Godfrey-Smith et al. 1988). Following burial, the grain begins to amass signal which is essentially the accumulation of radiation-stimulated electrons that have fallen into traps, or defects, in the mineral's crystal lattice (Nelson et al. 2015). The strength of the signal results from two factors: the flux of environmental ionizing radiation (emitted from the radioactive decay of ^{238}U, ^{235}U, ^{232}Th, ^{87}Rb, ^{40}K and cosmic rays) and time elapsed since the bleaching event (Aitken 1998; Galbraith and Roberts 2012). The combined intensity of radioactive materials over a period of time constitutes the environmental dose rate (D_R) of a particular location. The D_R is determined through chemical analysis of constituent minerals in the direct vicinity (approximately 15cm radius) of the extracted OSL sample (Nelson et al. 2015). The D_R accumulated since burial is known as the 'natural signal'. Following burial, the natural signal within a grain accumulates until the electron-holding traps in its crystal lattice become saturated. At low radiation levels, saturation occurs after approximately 200,000 years, marking the upper limit of the effectiveness for the technique (Aitken 1992:129).

I used Murray and Wintle's (2000) single-aliquot regenerative-dose (SAR) OSL

protocol for determining grains' burial-event age. For this technique, a light-shielded OSL sediment sample is first brought into a dark lab (see below for my specific sampling and processing techniques). Following target grain extraction and preparation, small aliquots of quartz sand are exposed to a laser. The light-stimulated grains emit a photon signal (the natural signal) which is captured and recorded by a photomultiplier instrument. The zero-signal grains are then exposed to a known 'regenerative dose' of radiation. The regenerative dose is much higher than expected in natural settings to produce a similar level of signal in the grains over a very short period of time. Following dosing, the aliquot is again exposed to laser light and the resulting signal captured. These steps are repeated multiple times at varying regenerative dose levels. The dose levels are calibrated to produce regenerative signals higher and lower than the original natural signal. The resulting regenerative signals are then graphed to create a saturating exponential growth curve with artificial signals bracketing the natural signal (Murray and Wintle 2000:60; Wintle and Murry 2006). Where the natural signal falls on this curve is known as the equivalent dose (D_E). The D_E estimates how much radiation exposure (in Gy) is necessary to produce a comparative signal from the same aliquot. Therefore, knowing how much radiation a location emits in a year, it is possible to estimate the length of time since the bleaching event. In the simplest terms, deposit age (or the number of years since grain burial) is calculated by dividing the equivalent dose (D_E) by the environmental dose rate (D_R) (Galbraith and Roberts 2012; Nelson et al. 2015):

$$age = \frac{equivalent\ dose}{environmental\ dose\ rate} \qquad \text{or} \qquad Age\ (ka) = \frac{D_E\ (Gy)}{D_R\ (Gy\ ka^{-1})}$$

OSL Field Sampling and Laboratory Analysis Procedures.

I collected OSL samples from selected strata within my profiles in order to provide age control, using protocol recommended by Nelson et al. (2015). After facing and describing a profile, I identified one or more units for OSL dating. I collected the sample by pounding an approximately 5 cm (2 in.) diameter, 25 cm (10.5 in.) long metal pipe into the freshly exposed cutbank wall. Given that near-surface sediments are vulnerable to pedoturbation and bioturbation-caused sediment mixing, I sought to sample strata one meter or more below surface and evincing minimal pedogenesis (Bateman et al. 2003). Unfortunately, given the shallow nature of buried sites in my study area, this was rarely possible and sediment mixing may have affected some samples. After extracting the pipe and capping both ends, I collected sediment (~500 ml) from a 15 cm radius surrounding the OSL sample location. This was for the purpose of determining environmental D_R through chemical composition analysis. I also collected a small sample of sediment (~50 ml) in an airtight container for determining local moisture content. Finally, I recorded necessary information for estimating cosmic dose contribution including sample depth below ground surface, GPS location and elevation.

I collected 19 OSL samples. Among those, I determined which samples were the most critical and ultimately chose 14 samples for laboratory analysis. I processed OSL samples in Utah State University's Luminescence Laboratory in Logan following Rittenour's (2012) protocol for SAR technique preparation. In the dark lab, I discarded light-exposed sediment from the pipe ends and wet-sieved the remaining portion to a target size range. Target grain size fractions were as fine as 63-150 μm and as coarse as 180-250 μm. Following chemical treatment to remove carbonates and organics (using

10% hydrochloric acid and bleach, respectively), quartz and feldspar grains were extracted using sodium polytungstate (2.7 g/cm^3) heavy mineral flotation. Following separation, the sand was rinsed, dried, treated with hydrofluoric acid (47% concentration) to remove feldspar and hydrochloric acid (30%). Finally, the quartz was dried, sieved and ready for analysis. Based on Murray and Wintle's (2000) SAR protocol, 1 mm-sized aliquots of quartz sand were exposed to blue or green laser light under controlled conditions on a Risø TL/OSL reader. For each of my samples, approximately 30 aliquots were analyzed and of these, about 15 were used for age calculation. Regenerative dose curves were created for each aliquot and a D_E estimate made for the natural signal's position on that curve. The resulting D_E scatters were analyzed using either Galbraith et al.'s (1999) minimum age model (MAM) or Galbraith and Roberts' (2012) central age model (CAM) as appropriate for scatter skew and dispersion (Tammy Rittenour, personal communication 2016). Generally, the CAM is used for D_E scatters exhibiting symmetrical overdispersion. Alternately, MAM calculation is preferred in situations where sediment mixing or incomplete bleaching is suspected (Galbraith and Roberts 2012:16). Pertinent to my study area, samples from archeological contexts, soils, and water-lain deposits are prone to these complications.

After using OSL dating to establish chronometric age control for my stratigraphic event sequence, I ascertained what geomorphic processes were likely responsible for observed sediment packages. I used granulometry augmented with facies analysis and qualitative field data to make these determinations.

Granulometric Analysis

Determining what depositional process buried archeological remains and how quickly is key to my research implications because low-energy burial immediately following occupation is most conducive to artifact spatial preservation (Dincauze 2000; Ebert 1992). Establishing the depositional environment of individual sediment packages requires multiple lines of evidence and comparison to modern analogs (James and Dalrymple 2010). I built my depositional environment interpretations on evidence including facies description, consistence, color, and other qualitative measures. These data augmented my granulometric, or particle size analysis (PSA), as my primary means of determining sediment package depositional environment.

Granulometry involves determining the proportional contribution of different-sized particles in a sediment sample, and it is an established method for inferring depositional mechanism and environment (Pye 1987; Flemming 2000; Folk 1954, 1966; Friedman 1961, 1971; Krumbein and Pettijohn 1938; Sahu 1964; Thomas 1987). However, Gale and Hoare (1991:68) provide an alternative perspective. A relationship exists between sediment texture and depositional processes given that air and water flow competency and suspended particle concentration partially dictate particle size proportions in terminal depositional environments (Sahu 1964; Singh et al. 2015). While the relationship between geomorphic process and size-frequency distribution is complex, previous researchers have used statistical methods including simple descriptive statistics, factor analysis, and moment measures to infer depositional environment (Friedman 1979; Schleyer 1987).

Sample Collection, Preparation, and Analysis.

I collected 96 sediment samples from 10 stratigraphic profiles in the study area. After facing a profile and identifying unit and sub-unit horizon boundaries I collected sediment samples from the wall in plastic specimen bags, labeling each according to profile number, unit/horizon designation, depth and date. For most profiles, I collected samples according to a 'horizon sampling' (Schoeneberger et al. 2012) strategy, gathering approximately equal volumes of sediment from the stratum's top to bottom boundary. The NRCS describes this method as the most effective and efficient approach and the most useful for identifying inter-horizon (and inter-unit) distinctions (Schoeneberger et al. 2012:8-1). Per NRCS protocol, I collected samples from the smallest identified strata subdivisions, providing the horizon was less than 50cm thick. For example, if a sediment unit exhibited three horizons of soil development, I sampled each horizon within that unit separately. If a unit showed no horizonation, I sampled the entire unit column as one specimen. In cases where stratigraphy was extremely complex or I returned to sample a profile I had not previously sampled, I used incremental or fixed-depth sampling techniques (Schoeneberger et al. 2012:8-2). In one case (profile 10), time constraints necessitated both attenuated profile description and fixed-depth sampling method. In this instance, I collected a ~5 cm tall sediment column from the top of each strata.

Preparing sediment samples for granulometry required disaggregation of indurated clay peds (using mortar and pestle) and separating the > 1mm coarse fraction from < 1mm fine fraction using a 1.00 mm Fisherbrand Test Sieve. I weighed the fine and coarse fractions separately, to a precision of .01 grams. Determining what proportion the fine fraction makes up of each sample's total weight allowed me to normalize the

outputs when I analyzed the fine fraction using laser diffraction. I passed all fine fractions through a sediment splitter in order to ensure even mixing of component grain sizes.

I conducted granulometric analysis of my samples using a Malvern Masterizer 2000 laser diffraction instrument (Malvern) at Utah State University's Geochemistry Lab. Laser diffraction particle size analysis is based on the premise that larger particles deflect a beam of light at a wider angle than smaller particles (McCave et al. 1986). The Malvern passes a sediment sample diluted in deionized (DI) water past a laser beam and captures the resulting diffracted light scatter on a receiver. I used a standard operating procedure for the instrument customized for high clay content samples (Tammy Rittenour, personal communication 2016). Following laser obscuration calibration with DI water, I added a small amount of sediment (~1 g) to one liter of water under constant agitation. This solution was sonicated for 60 seconds to dissolve clay peds. The subsample was then passed through the laser beam with a target obscuration between 5% and 15%. I processed three aliquots per sample and each subsample was analyzed three times to ensure reproducibility of results (nine total per sample). The analysis output consisted of a percentage contribution for each of the 67 binned grain size categories.

I used the laser diffraction data to compute comparative and descriptive statistics for each sample. After averaging the results of the nine sample aliquots, I normalized these results by multiplying each category with the fine fraction proportion of the sample total. For instance, if the fine fraction constituted 90% of sample weight and coarse fraction constituted 10%, I multiplied each binned grain size category by 90%. Using these corrected data, I then produced grain-size frequency curves for each sample and calculated median, skewness, kurtosis, and sorting (standard deviation) following Folk

and Ward (1957). I also compared known-environment control samples to unknown study area samples using factor analysis, principal component analysis and method of moments (Friedman 1979). Control sample comparisons were a key factor in determining sediments' depositional environments. General descriptions of my control sample and selection criteria are given below.

Control Samples

In order to use granulometry as a line of evidence for determining depositional environments, I compared study area sediment sample particle size distributions to comparative samples from known environments. I selected control samples based on two criteria: similarity to the study area's likely depositional environments and comparability of control samples' pedogenic alteration with Centennial Valley unknowns. Study area sediment packages likely developed in either lacustrine, alluvial or eolian settings (Lonn et al. 2000; Majerowicz et al. 2010; Scholten et al. 1955). I therefore selected control samples from sediment packages formed in similar settings and with similar time spans since deposition. I obtained comparative samples from stratigraphic study locations in three regions; northern Utah’s Cache Valley, northeastern Idaho’s Snake River Plain, and southern Utah (near Kanab). The Cache Valley study locations represent four depositional environments: shallow lacustrine, deep lacustrine, alluvial terrace (stream channel), and alluvial floodplain. The Snake River Plain and southern Utah samples represent eolian loess and eolian sand dune sediments, respectively. Among potential strata samples from these locations, I chose strata representing the greatest range of pedogenic alteration for each sediment package.

Pedogenesis alters the particle size distribution (PSD) of the parent material and should be accounted for when interpreting a deposit's textural makeup (Reading 1986:451). Soil forming processes such as chemical weathering transformation and eluvial translocation result in shifting fine fraction proportions in the pedon through time (Simonson 1959). Gale and Hoare (1991) argue that lessivage (clay translocation) has the greatest impact on soil texture of any pedogenic process. In extreme cases, introduced (translocated) clay may constitute up to 30% of a soil body (Avery 1980). Finally, argilliturbation and cryoturbation in soils with vertic and gelic properties may move large clasts upward through the pedon resulting in displacement of coarse, as well as fine fraction sediments (Birkeland 1999:161). Given the impact of soil formation on sediment package texture, I selected control samples with broad ranges of soil development in an effort to capture minimum and maximum pedogenic alteration of parent material.

Unknown sediment samples in the study area exhibit wide ranges of soil development stages and pedogenesis has apparently altered PSD to varying degrees. Approximately 20% of study area strata exhibit a high degree of soil formation alteration such as clay skin development or angular blocky structure. Another ~50% show some pedogenic alteration and the remaining ~30% exhibit little or no soil development. I therefore included samples exhibiting the most extreme degrees of pedogenic alteration degree so as to increase comparability with unknowns. At minimum, I processed one sample from the bottom of each sediment package (unit) at each study location. This position in the soil profile should theoretically evince the least amount of pedogenic alteration. Additionally, I identified Horizons with eluvial and illuvial properties and processed control samples from strata exhibiting clay loss or accumulation.

I processed 21 control samples including four each from stream channel, overbank flood, deep lacustrine, shoreline lacustrine and proglacial eolian loess deposits. Additionally, I processed one sample of eolian dune sand derived from weathered and reworked Jurassic Navajo Formation sandstone (composed primarily of fossilized eolian dunes). I did not anticipate any of my unknown samples to originate from a similar environment but this sample served as a comparative example of an extremely well-sorted, mature, eolian deposit. Full descriptions of control samples are presented in the Results.

Using stratigraphic description, OSL dating and granulometry, I modeled a basic stratigraphic event sequence for the study area, tied these strata to a chronometric timeline, and interpreted geomorphic processes responsible for observed strata. The outcomes of my field and lab analyses are described in the following Results chapter.

CHAPTER FOUR:

RESULTS

This chapter presents OSL dating, granulometry, and stratigraphic mapping results centered largely on detailed studies of ten stratigraphic profile locations. I begin with a brief overview of OSL age results and which samples produced dates within a cultural time frame. General trends in granulometry data are presented next. I then provide stratigraphic descriptions of the ten profile locations and relevant observation points along the cutbank. The profile descriptions and observation points are grouped into three sub-regions (west, central, and east) which correspond to areas with similar topography and stratigraphy (Figure 12). Profile figures incorporate OSL age and granulometry plots in order to better illustrate stratigraphic changes. Finally, I provide descriptions and frequency graphs of granulometry control samples. I compare these to study area samples to help infer the depositional environments of study area sediments.

Optically Stimulated Luminescence Dating

A total of 14 OSL samples taken in 2014 and 2015 from eight profile locations were analyzed (Table 1). Depth ranged from 23 to 130 cm below surface. Most sample ages were calculated using the Central Age Model (CAM) (Galbraith and Roberts 2012). However, ages for samples USU-1700 and USU-1701 were calculated using the Minimum Age Model (MAM) due to D_E overdispersion exceeding 25% (Appendix A).

Three samples (USU-1704, USU-2187, and USU-2188) are well outside a cultural time frame (> 14,000 cal BP; Kornfeld et al. 2010), dating to 36 ka or older. A fourth

sample, USU-2050, pre-dates human occupation by about 5,000 years, roughly coinciding with the LGM. The ten remaining samples produced ages within the range of human occupation in the valley. These samples are USU-1700, USU-1701, USU-1702, USU-1703, USU-1705, USU-1834, USU-1835, USU-2049, USU-2185, and USU-2186. With the exception of USU-2049, all cultural-age samples were collected in the central study area, within or near site 24BE46. Sample USU-2049 is from Profile 8 in the eastern study area, near site 24BE56. The western sub-area produced no occupation-age OSL samples (Table 1). Consideration of stratigraphic context and qualitative data is important for choosing an appropriate OSL age model as well as interpreting the meaning and reliability of results in a geomorphic setting (Galbraith et al. 2005). Accordingly, I appraised OSL results in the context of granulometry texture data and qualitative field observations.

Granulometry Results

I analyzed a total of 79 granulometry samples from nearly every strata at the ten profile locations. Particle size distributions of these samples were statistically analyzed in order to characterize USDA texture class, central tendency, cumulative percentile, and modality (Appendix B). Texture classifications include broad categories of clay, silt, sand, and gravels, as well as ratios including fine to coarse fractions. Measures of central tendency consist of median, mean, sorting (standard deviation), skewness and kurtosis. Cumulative percentile statistics and graphs aid in visualizing relative contributions of binned clast sizes and are useful for comparing differences in grain size dispersion. Finally, because central tendency can mask differences between normally and

Table 1. Finalized OSL age data.

USU OSL Lab ID #	Profile #	Unit / Horizon	Depth (cm)	Approx. sample elevation (m AMSL)	OD (%)[a]	Number of aliquots[b]	Dose rate (Gy/Ka)	Equivalent dose ± 2σ (Gy)	OSL age ± 2σ (ka)	Age model[c]	Within cultural time range?[d]
USU-1700[e]	P2	Unit 4 / 3C	130	1997.10	42.1 ± 8.1	17 (33)	2.18 ± 0.14	26.16 ± 7.794	13.37 ± 3.83	MAM	Yes
USU-1701[e]	P2	Unit 4 / 3C	100	1997.40	37.7 ± 7.1	20 (40)	2.37 ± 0.12	28.96 ± 5.114	12.20 ± 2.45	MAM	Yes
USU-1702[e]	P3	Unit 2 / 2Bkb	50	1998.74	0.0	12 (28)	2.99 ± 0.16	7.47 ± 0.67	2.50 ± 0.33	CAM	Yes
USU-1703[e]	P3	Unit 3 / C	48	1998.76	10.0 ± 5.0	13 (27)	2.95 ± 0.16	7.75 ± 0.72	2.62 ± 0.36	CAM	Yes
USU-1704[e]	P4	Unit 2 / 3C2	95	1997.91	23.6 ± 5.2	18 (31)	1.75 ± 0.10	63.37 ± 8.16	36.23 ± 5.89	CAM	No
USU-1705[e]	P5	Unit 1 / 3ABkb	110	1997.26	15.2 ± 5.1	13 (29)	2.31 ± 0.16	29.44 ± 3.36	12.74 ± 1.99	CAM	Yes
USU-1834[e]	P3	Unit 3 / C	50	1998.74	14.5 ± 5.2	14 (32)	2.99 ± 0.16	9.06 ± 1.01	3.03 ± 0.45	CAM	Yes
USU-1835[e]	P7	Unit 1 / 3ABkb	77	1998.04	5.8 ± 4.5	19 (28)	2.96 ± 0.16	26.33 ± 1.62	8.91 ± 1.04	CAM	Yes
USU-2049[f]	P8	Unit 7 / Bw	136	2004.95	14.8 ± 4.6	18 (29)	3.39 ± 0.19	48.67 ± 4.74	14.35 ± 2.01	CAM	Yes
USU-2050[f]	P9	Unit 5 / Bw	76	2001.33	26.4 ± 6.1	15 (27)	2.84 ± 0.16	55.98 ± 8.65	19.73 ± 3.64	CAM	No
USU-2185[f]	P2	Unit 6 / Bw	23	1998.17	24.1 ± 8.6	17 (51)	2.96 ± 0.15	2.23 ± 0.42	0.75 ± 0.16	CAM	Yes
USU-2186[f]	P5	Unit 2 / 2C	36	1998.00	28.1 ± 6.9	20 (57)	2.48 ± 0.14	9.13 ± 1.48	3.68 ± 0.70	CAM	Yes
USU-2187[f]	P10	Unit 7 / C	60	2001.28	20.3 ± 5.3	13 (30)	3.30 ± 0.26	199.6 ± 26.09	60.39 ± 10.48	CAM	No
USU-2188[f]	P11	Unit 2 / 4C3	73	2004.68	19.0 ± 5.2	14 (20)	4.24 ± 0.32	220.2 ± 27.61	51.90 ± 8.75	CAM	No

[a] OD is overdispersion of D_E values, calculated per Galbraith et al. (1999). OD exceeding 25% is significant
[b] Indicates number of aliquots used for age calculation with total number processed in parentheses
[c] Calculations per Galbraith and Roberts (2012) Central Age Model (CAM) or Minimum Age Model (MAM)
[d] Approximately 14,000 cal BP and later per Kornfeld et al. (2010); [e] Samples collected in 2014, [f] Samples collected in 2015

non-normally distributed clast size distributions, modality measures help identify differences among heterogenous sediment bodies (Schleyer 1986). Modality measures are especially important for characterizing mixed sediments and those affected by pedogenesis (Yong et al. 2017). I used these data to help categorize the depositional environments of study area strata through comparison to published data and control samples (Friedman 1961; Pye 1987; Singh et al. 2015; Smith and Rogers 1999).

Researchers employ various methods for quantifying sediment size frequency and dispersion (Sahu 1964; Weltje and Prins 2007). Each technique presents trade-offs and multi-modal distributions, in particular, pose problems for characterization and comparability (Yong et al. 2017:106). Given that many (49 out of 79) study area samples exhibited polymodal distributions, I chose statistical methods suited to characterizing mixed sediment bodies. Based on Blott and Pye's (2001:1237) recommendations, I used Folk and Ward's (1957) measures expressed in metric units (Appendix B).

General tendencies were noted among granulometry samples. With the exception of Profile 10 strata, sediments in the study area are dominated by fine fractions (<1mm clast sizes). Very few strata contained more than 1% granules (1mm-2mm) or gravels (>2mm). The majority of samples are classified as silt or silt loam based on NRCS texture classifications (Schoeneberger et al. 2012). Almost all sediments from profile locations in the study area west end (Profiles 9, 6, and 1 west to east) have unimodal frequency distributions. Central tendency for these strata is generally medium to coarse silt, but many include peaks in the fine silt and clay categories. In contrast to the west end, central area sediments (Profiles 10, 2, 3/7, 4, and 5 from west to east) exhibit much more heterogenous distributions. Nearly all strata in the central sub-area are very poorly

sorted (Folk and Ward 1957). Many are bimodally distributed and a few exhibit three or even four modality peaks. Finally, in the study area east end, Profiles 11 and 8 (west to east) have higher clay fractions relative to the central and west areas. This is especially true for Profile 11 strata, which on average contain the highest percentages of clay (~15-20%) in the study area. These sediments are somewhat better sorted as well, with 5 out of 6 Profile 11 strata being *poorly sorted* as opposed to the generally *very poorly sorted* central area sediments. At the far east end of the study area, Profile 8 strata have heterogenous size frequencies, with an equal number of bimodal and unimodal distributions. In contrast the majority of study area layers, units 2 and 4 in Profile 8, contain substantial sand fractions (42% and 49%, respectively). Having outlined trends in the raw data, the following section synthesizes OSL and granulometry results in the context of stratigraphic field descriptions in the study area.

Stratigraphic Profiling and Field Observations

This section provides a west-to-east account of stratigraphic profiles and relevant observation points. These pinpointed exposure descriptions provide a framework for weaving together stratigraphy, OSL, and granulometry datasets into a coherent picture of geomorphic change across the landscape and through time. I mapped a total of ten stratigraphic profiles on cutbank faces within the project area (Figure 12). Profile locations were selected following initial broad-scale stratigraphic observations of the roughly 3 km (1.9 miles) long shoreline exposure. The primary criteria for selecting profile locations were capturing maximum stratigraphic variability and describing areas with verified subsurface cultural material. Additionally, I profiled areas overlapping or on

opposite sides of suspected unconformities in order to determine age relationships among different depositional environments. Profile locations were numbered sequentially as I selected them for study, in no particular geographic order. However, this section presents profile location narratives and selected observation point descriptions from west to east along the shoreline face without regard to profile numbering. Study location descriptions are divided into three sub-areas: west end, central, and east end. Each sub-area exhibits general internal consistency in terms of elevation, topographic relief and, to a lesser extent, sequence stratigraphy. Conveniently, each sub-area also roughly coincides with one of the three archeological sites. This organization helps structure a synthetic analysis of topographic and stratigraphic trends in the following Discussion chapter.

Each of the following profile summaries provides stratigraphic descriptions, grain-size frequency graphs and OSL dating results. Additionally, cumulative frequency particle size graphs (in green) are added for notable or representative strata. All color and consistence data are for dry material unless otherwise noted. Effervescence class is based on application of 10% concentration (1N) hydrochloric acid (HCl). Strata names follow NRCS soil and lithostratigraphic description conventions (Boggs 1995; Schoeneberger et al. 2012; Soil Survey Staff 2014). Sediment and soil textures are based on Folk (1954) and USDA (Schoeneberger et al. 2012) systems. I used field texturing methods to estimate soil texture during profiling. For this data summary, however, the more precise granulometry texture data are given. I used Folk's (1954) sediment naming convention (also based on granulometry data) to provide a more nuanced description of particle size-ranges and relative contributions but supplemental NRCS texture classifications are included in Appendix B. Finally, each sediment package and soil layer has both sediment

unit and soil horizon designations. For brevity, however, and to emphasize distinctions between pedogenically altered and non-altered sediment packages, strata are only referred to by either the unit or horizon name in the text. If units are split into multiple soils, I use soil horizon designations; if not, I refer to unit numbers.

Study Area West End

The study area west end is approximately 0.37 km^2 and encompasses site 23BE43 and Profiles 9, 6, and 1 (west to east, respectively) (Figure 13). Elevations in the area range from approximately 1996 m (6548 ft.) AMSL at shoreline level to 2011 m (6597 ft) near the northern, interior extent of 24BE43. Elevations are based on Trimble GPS data. Topographically, the west end upland is rolling but relatively flat (Figure 14). It is incised by two shallow ephemeral stream drainages and contains an intermittent spring within the boundary of site 24BE43. The west end cutbank face is moderately high with vertical faces averaging about 3 m above 1-2 m high talus slopes. Stratigraphically, the area is characterized by medium thickness (~40 cm) gently undulating beds of medium to coarse silt-dominated sediment packages. Two strata are notable in this area. The first is a bright white, finely laminated silt bed with abrupt upper and lower boundaries. It is consistently ~25 cm thick and present in Profile 9 (unit 2) and Profile 6 (unit 3). The second notable stratum is a gypsum-rich soil horizon of variable thickness (~40-50 cm) situated above the laminated silt bed. It is present in the east half of the sub-area and mapped as By and 2By in Profile 6 and Bty in Profile 1. Finally, the west end exhibits apparent tectonic off-set in at least two locations (Observation Points A and B). Profile and observation point data are provided below, described from west to east.

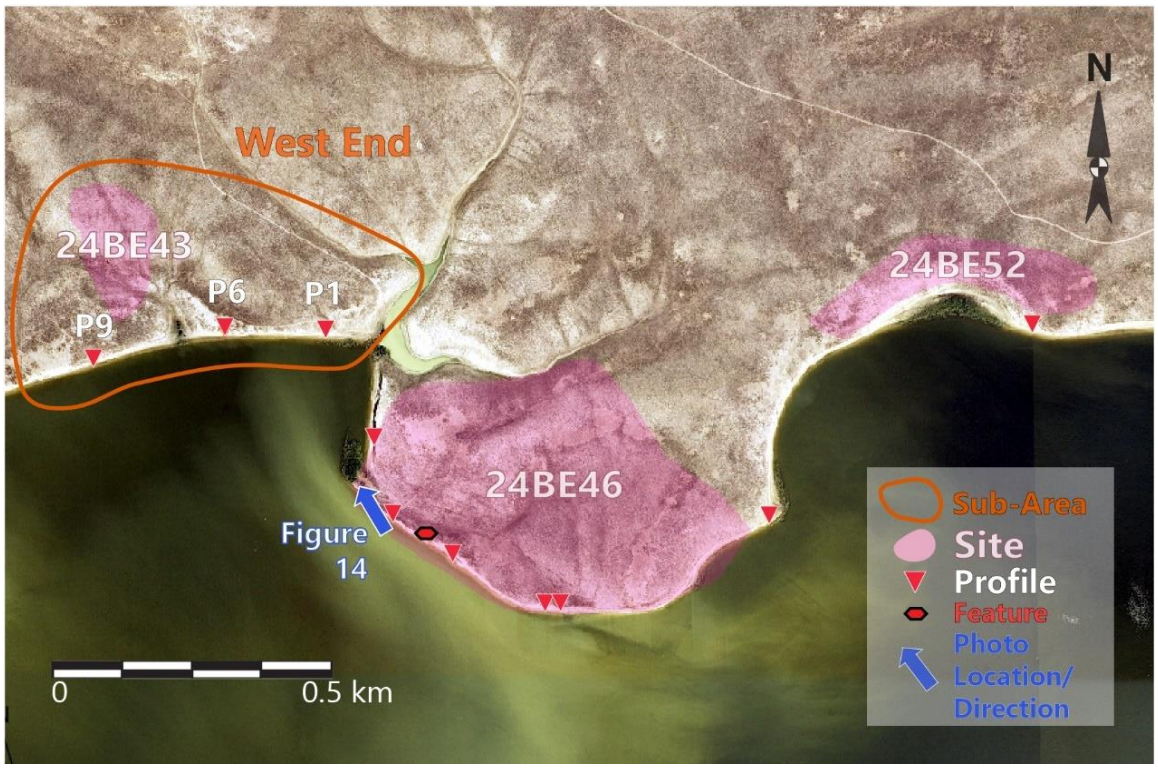

Figure 13. Study area west end map with Profiles 9, 6, and 1 and overview photo (Figure 14) location indicted.

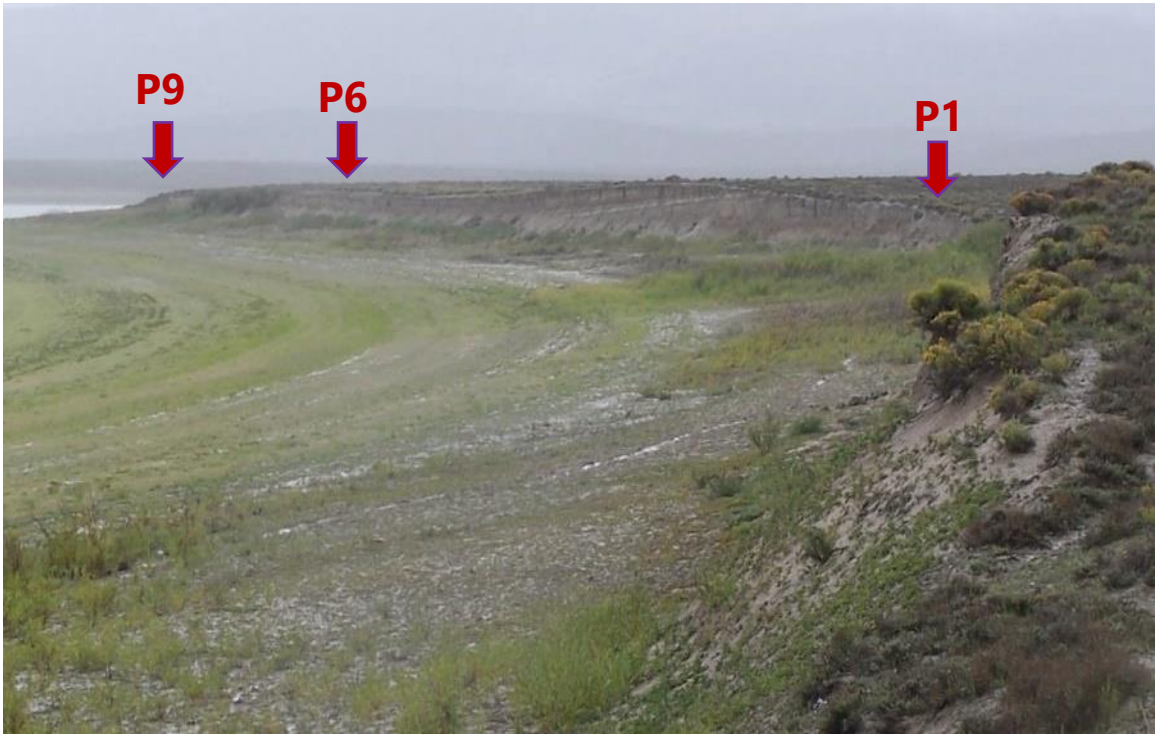

Figure 14. Overview of west end with profile locations marked. View northwest.

Profile 9

Profile 9 is located at the far west end of the study area and has a top elevation of 2002.09 m (6568 ft) AMSL. The cutbank exposure in this area averages two to three meters high (Figure 15). Profile 9 is the closest stratigraphic study location to site 24BE43, although recoded site boundaries do not extend to the cutbank face. Profile 9

Figure 15. Overview of Profile 9, view north.

reveals five sediment packages; units 1 through 5 from bottom to top (Figure 16). The uppermost package, unit 5, produced an OSL age of 19.73 ± 3.64 ka at 76 cmbs (USU-2050) indicating all units predate human occupation. This exposure is therefore a record of pre-cultural conditions.

The lowest three packages of Profile 9 (units 1, 2, and 3) exhibit striking color and structure differences but are similar in terms of package thickness, boundary morphology and internal bedding plane orientation. Units 1-3 average ~20 cm thick,

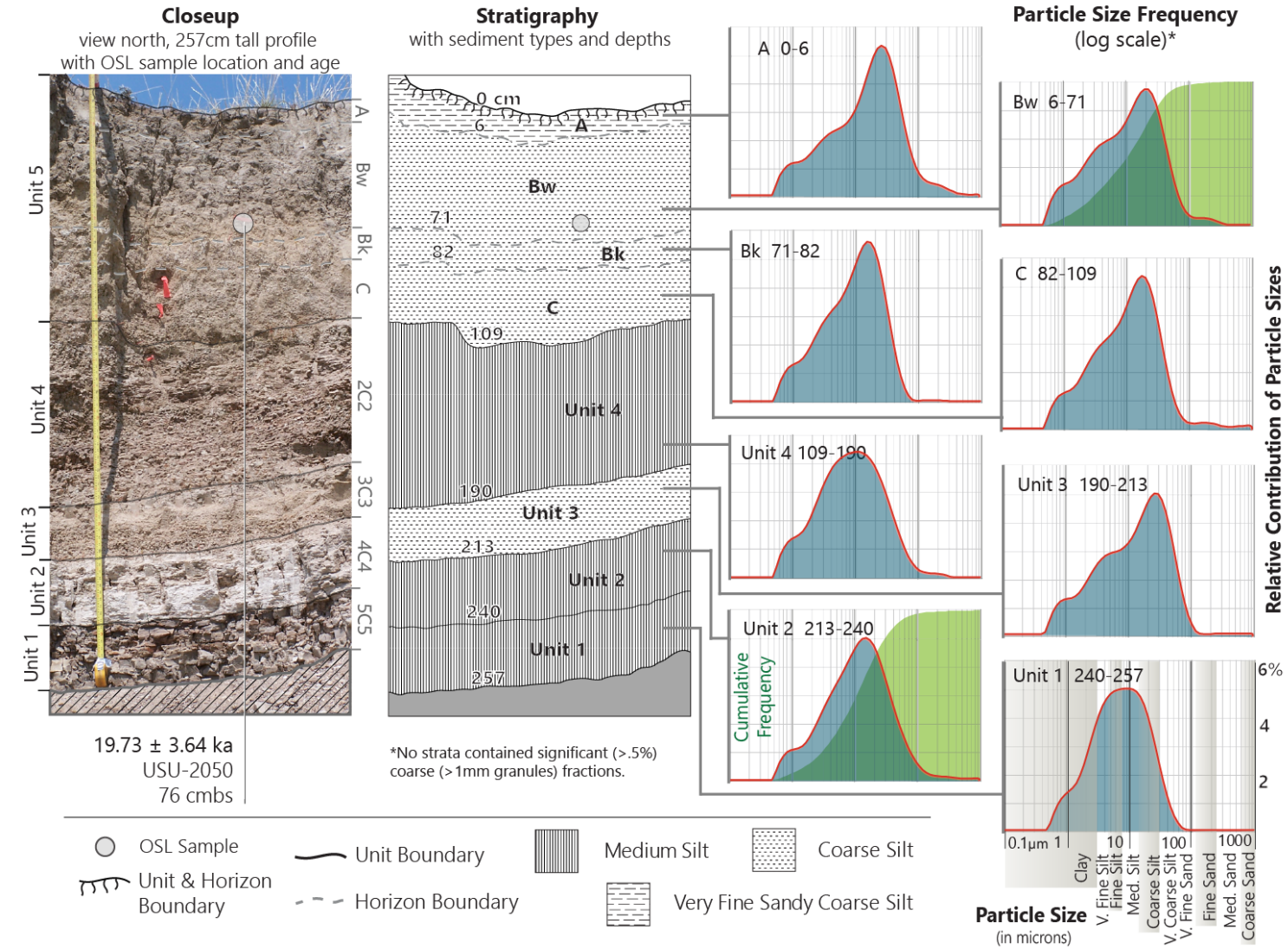

Figure 16. Profile 9 detail with stratigraphy, OSL, and granulometry data. All graphs have same vertical and horizontal scales

Table 2. Profile 9 stratigraphic descriptions.

Unit	Horizon	Depth (cmbs)	Description
Unit 5	A	0-6	Very fine sandy coarse silt. 10YR5/2 (grayish brown). Very fine granular structure, very soft consistence, ~20% organic content. Strongly effervescent. Diffuse wavy boundary.
	Bw	6-71	Coarse silt. 10YR 6/3 (pale brown). Very fine subangular blocky structure, hard consistence. Strongly effervescent. Clear smooth boundary.
	Bk	71-82	Coarse silt. 2.5Y 6/3 (light yellowish brown). Very fine subangular blocky structure, moderately hard consistence. Violently effervescent with ~5% fine threads of $CaCO_3$. Diffuse smooth boundary.
	C	82-109	Coarse silt. 2.5Y 6/3 (light yellowish brown). Thin platy structure, slightly hard consistence. Structures fine toward top. Strongly effervescent. Slight redoximorphic staining throughout. Diffuse smooth boundary.
Unit 4	2C2	109-190	Medium silt. 10YR 6/3 (pale brown - outside ped), 5Y 7/2 (light gray - inside ped). Medium subangular blocky parting to medium platy structure, soft consistence. Top ~30 cm of unit is dominantly platy structure. Slightly effervescent overall, but strongly effervescent at ~138 cmbs. Abrupt smooth boundary.
Unit 3	3C3	190-213	Coarse silt. 2.5Y 7/3 (pale brown). Fine subangular blocky structure, slightly hard consistence. Structures fine upward, becoming very fine subangular blocky near top. Strongly effervescent. Slight redoximorphic staining throughout. Abrupt smooth lower boundary.
Unit 2	4C4	213-240	Medium silt. 5Y 8/1 (white). Finely parallel laminated structure (depositional), slightly hard consistence. Strongly effervescent. Very abrupt smooth boundary.
Unit 1	5C5	240-257	Medium silt. 5Y7/2 (light gray). Coarse angular blocky structure, firm consistence (moist). Strongly effervescent. Redoximorphic reddening from ~240-253 (upper two-thirds) of strata. Abrupt smooth lower boundary (profile mapped to unit base).

exhibit parallel (slightly convex upward) internal bedding planes and are delineated by abrupt smooth boundaries. Grain size distributions (GSD) are unimodal and dominated by medium and coarse silt (Table 2, Figure 16). These strata have proportionally high

clay fractions, averaging near 10%. Clay fractions are illustrated by GSD plateaus at approximately 1.0 µm. Overlying these strata, unit 4 is a much thicker package (~81 cm) which has a less distinct upper boundary. However, the GSD, internal bedding planes, and lower boundary shape of unit 4 are similar to lower packages. Finally, units 1 through 4 appear conformable given their smooth boundary shapes, consistent lateral package thickness and parallel orientation of boundaries with internal bedding.

Unit 2 in Profile 9 is the prominent, finely laminated white silt bed noted earlier. In this vicinity, unit 2 and strata directly above and below, exhibit gently rolling topography (Figure 15). However, it is not known whether the bed orientations result from deposition over a paleotopographic surface or from subsequent (tectonic or subsidence-triggered) displacement.

At Profile 9, soil development is only present in the uppermost sediment package (unit 5). Pedogenic development consists of a A-Bw-Bk-C sequence. The soil contained a thin (11 cm thick) white layer that appeared to be calcium carbonate ($CaCO_3$). The presence of calcium carbonate versus more rapidly developing but similar-looking minerals could possibly indicate advanced age. X-ray diffraction (XRD) analysis of the white mineral layer from a depth of ~71-82 cmbs in unit 5 confirmed the presence of $CaCO_3$ and the absence of a similar-looking and more rapidly developed mineral, gypsum ($CaSO_4 \cdot 2H_2O$) (Table 3). These data suggest that, given similar environmental conditions, the presence of $CaCO_3$ development similar to that observed in the Profile 9 Bk horizon in other sediment packages may signal deposition around the time of the LGM (19.73 ± 3.64 ka, UDU-2050).

Table 3. XRD chemical composition results for Profile 9, 71-82 cmbs.

Sample # SL9_Bk_71-82*

Compound Name	Score	Scale Factor	Chemical Formula
Calcite	54	0.816	$CaCO_3$
Quartz	41	0.971	SiO_2
Nontronite	18	0.094	$Na_{0.33}Fe_2^{+3}(Si, Al)4O_{10}(OH)_2 \cdot H_2O$
Aluminum	16	0.035	Al

*XRD analysis conducted at Utah State University Geochemistry Lab in Logan, Utah

Observation Point A

Observation point A (OP-A) lies approximately 50 meters east-northeast of Profile 9 (Figure 17). OP-A shows evidence of tectonic movement along two primary fault lines (Figure 18). Although OP-A lies between Profiles 9 and 6, the prominent white silt bed (unit 2 in Profiles 9 and 6, respectively) is absent in this location. However, by extrapolating trends of the white bed across the exposure face, it appears that the stratum once overlaid OP-A sediments but has since been removed (Figure 17). OP-A strata therefore pre-date both the white bed and a cultural timeframe, although it is unclear how long after deposition tectonic deformation of those sediments occurred. One indication of

Figure 17. Panorama overview of OP-A location in relation to Profiles 9, 6 and white silt stratum (dotted white line). Note that dotted line indicates full visible extent of stratum.

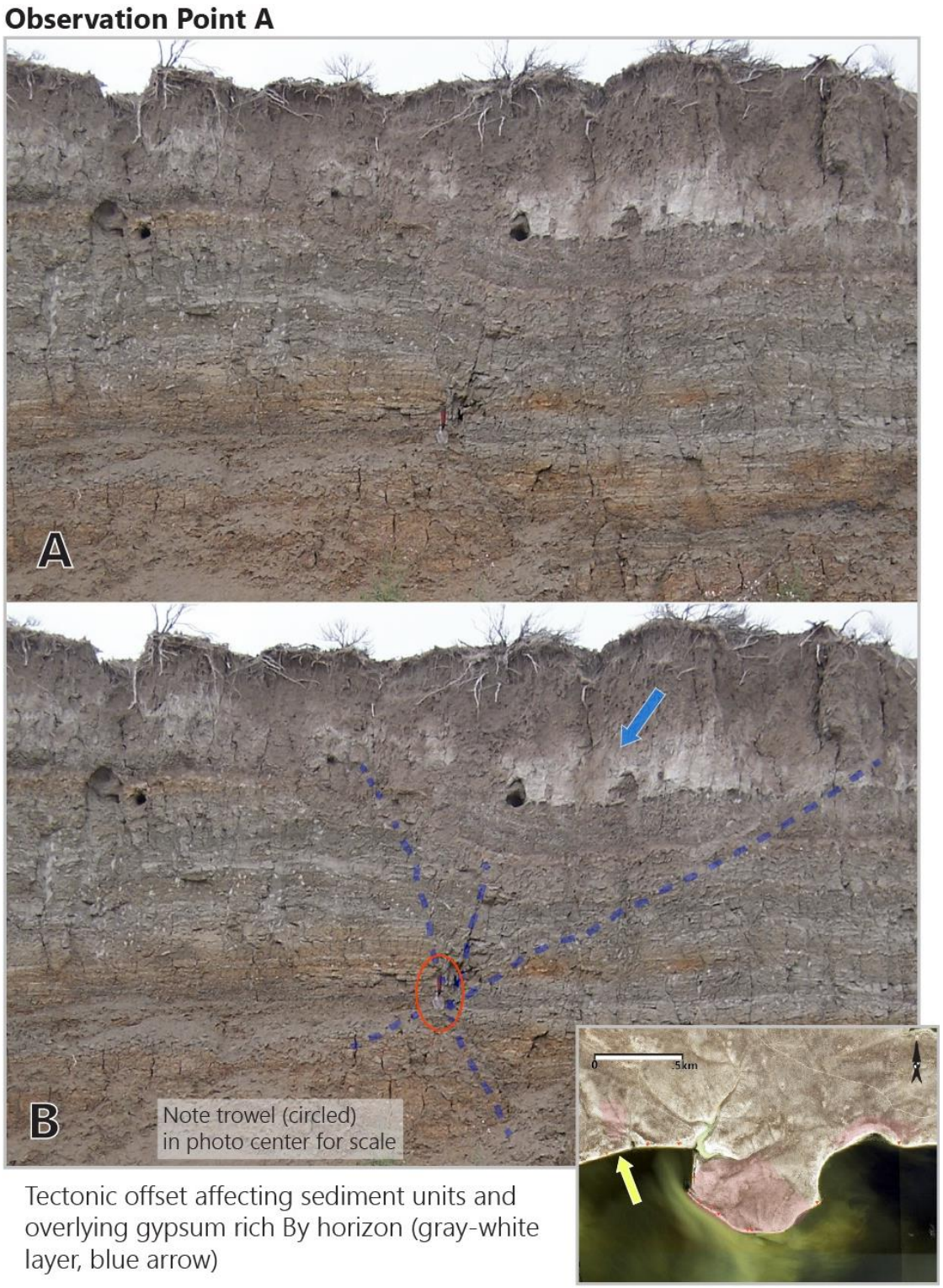

Figure 18. Observation Point A (OP-A) showing apparent tectonic offset. Photo (A) is unmodified exposure photo. Photo (B) highlights fault line positions with notations. Note that the grayish-white gypsum-rich soil horizon near the wall top (blue arrow) undulates in accordance with underlying deformed beds.fault movement age is displacement of a

gypsum rich soil horizon near the top of the exposure. The gypsum horizon continues to the east and is evident as horizons By and 2By2 in Profile 6 and Bty in Profile 1.

Profile 6

Profile 6 is situated east of OP-A and lies approximately 150 m southeast of site 24BE43. The exposure has a top elevation of 2000.55 m (6563 ft) AMSL. Vertical wall height in this vicinity averages about three to four meters (Figure 19). Similarly to Profile 9, the Profile 6 exposure shows five sediment packages (Figure 20). Units 2, 3, and 4 of Profile 6 are analogous to units 1, 2, and 3 at Profile 9. Sediment textures are dominated by coarse silt, and extant depositional bedding structures are parallel laminated (Table 4). No OSL samples provide age control for this location.

Figure 19. Overview of Profile 6, view north.

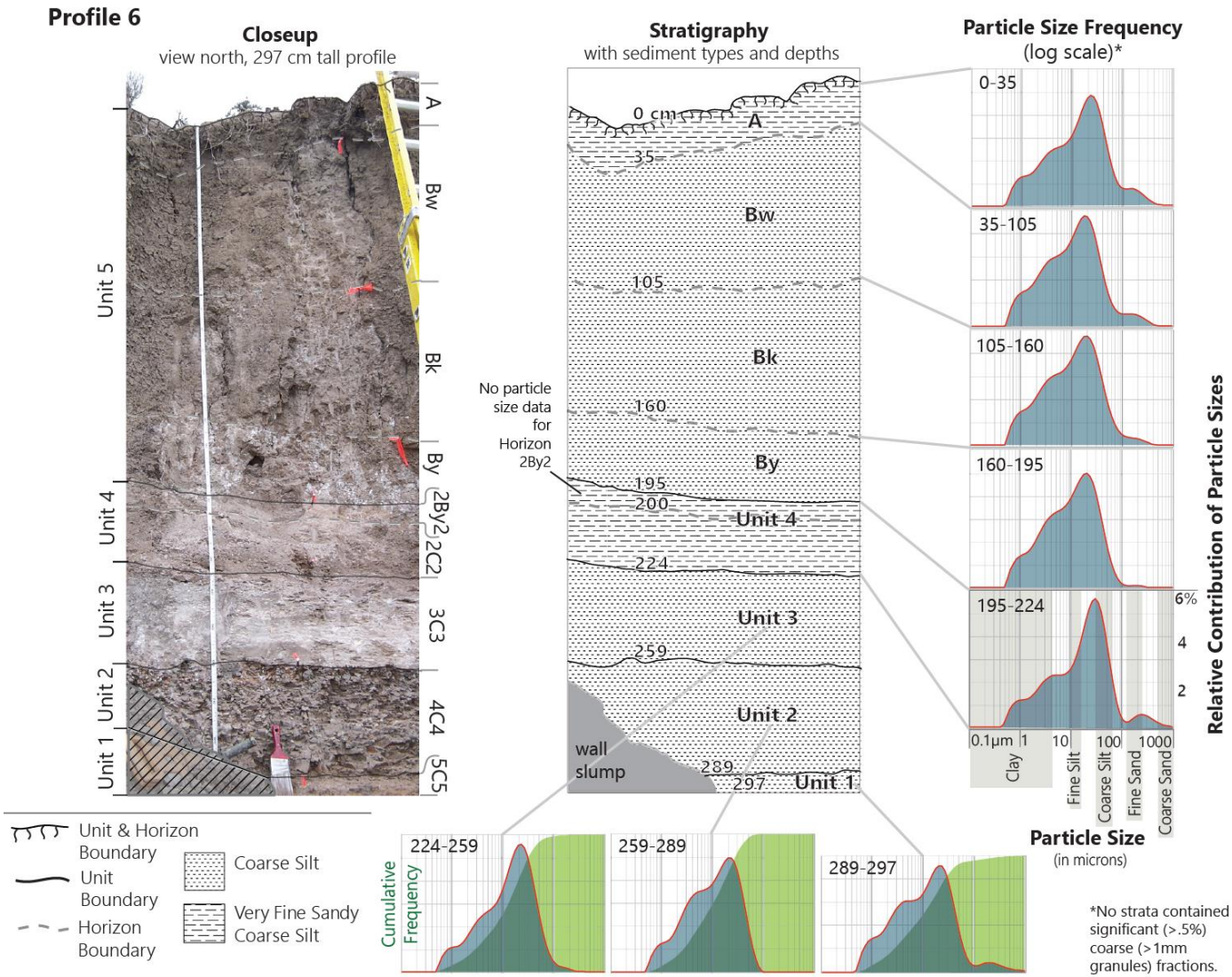

Figure 20. Profile 6 detail including stratigraphy and granulometry data.

Table 4. Profile 6 stratigraphic descriptions.

Unit	Horizon	Depth (cmbs)	Description
Unit 5	A	0-35	Very fine sandy coarse silt. 10YR 5/3 (brown) Very fine granular structure. Strongly effervescent. Few krotovina and many fine rootlets. Diffuse wavy boundary.
	Bw	35-105	Coarse silt. 2.5Y 7/2 (light gray). Weak coarse subangular blocky structure. Strongly effervescent. Few fine to medium roots. Diffuse wavy boundary.
	Bk	105-160	Coarse silt. 2.5Y 2/6 (light brownish gray). Weak coarse subangular blocky structure. Strongly effervescent with 5% diffuse $CaCO_3$ masses throughout. Clear wavy boundary.
	By	160-195	Coarse silt. 2.5Y 5/3 (light olive brown). Weak coarse subangular blocky structure. Strongly effervescent. Abundant (~40%) gypsum masses throughout. Diffuse wavy boundary.
Unit 4	2By2	195-200	No specific data was gathered for this horizon. 2By2 is a continuation of By soil formation into underlying Unit 4.
	2C2	200-224	Very fine sandy coarse silt. 2.5Y 6/3 (light yellowish brown silt). Weak medium blocky structure, slightly hard consistence. Strongly effervescent. Clear smooth boundary.
Unit 3	3C3	224-259	Coarse silt. 2.5Y 7/2 (light gray). Parallel planar laminated structure (depositional), slightly hard consistence. Strongly effervescent. Very minimal (~2% of area) redoximorphic striations throughout. Abrupt smooth boundary.
Unit 2	4C4	259-289	Coarse silt. 5Y 6/2 (light olive gray). Medium to coarse angular blocky structure, very hard consistence. Peds fine upward from ~4 cm at unit bottom to 1.5 cm at top. Slightly effervescent. Redoximorphic concentrations (reddish-black ferro manganese oxide staining) on ped faces. Clear smooth boundary.
Unit 1	5C5	289-297	Coarse silt. 10 YR 5/6 (yellowish brown). Parallel laminated structure (depositional), very friable consistence (moist). Strongly effervescent with horizontal calcite streaks throughout. No lower boundary.

Profile 6 shows a similar soil development sequence in the uppermost package as Profile 9, with the addition of a gypsum horizon. Profile 6 is the only study location that contains both the white finely laminated silt bed (unit 3) and the overlying gypsum soil horizon, making it a key exposure for understanding sequence stratigraphy in the western sub-area. The gypsum horizon begins in bottom 35 cm of unit 5 (as horizon By) and extends into the top of unit 4 (as horizon 2By2).

Observation Point B

Similar to OP-A, OP-B exhibits apparent tectonic offset of redoximorphically stained sediment packages (Figure 21). It lies between Profile 6 to the west and Profile 1 to the east. The gypsum-rich horizon (By and 2By2 at Profile 6) is present at the OP-B location. However, the gypsum horizon overlaps deformed beds and does not appear altered by tectonic action.. Note that in Figure 20, the By horizon appears to undulate. However, this is only a visual effect of wall curvature at the location and the horizon is in fact flat-lying. If the By horizons at OP-B and OP-A are conformable (and they appear to be), tectonic movement at OP-B predates offset at OP-A farther to the west.

Profile 1

Profile 1 lies at the east edge of the western sub-area (Figure 22). It is situated on a short wall (~2m high) of coarse and fine silt beds at an elevation of 2001.39 m (6566 ft) AMSL. The profile is approximately equidistant between sites 24BE43 and 24BE46 near the west edge of a large ephemeral drainage. Profile 1 exposes four distinct sediment packages; units 1 to 4 from lowest to highest (Figure 23). Given the irregular undulations, abrupt contact distinctiveness, and structural dissimilarities all contacts between units may represent erosional unconformities. No OSL samples provide age control at this

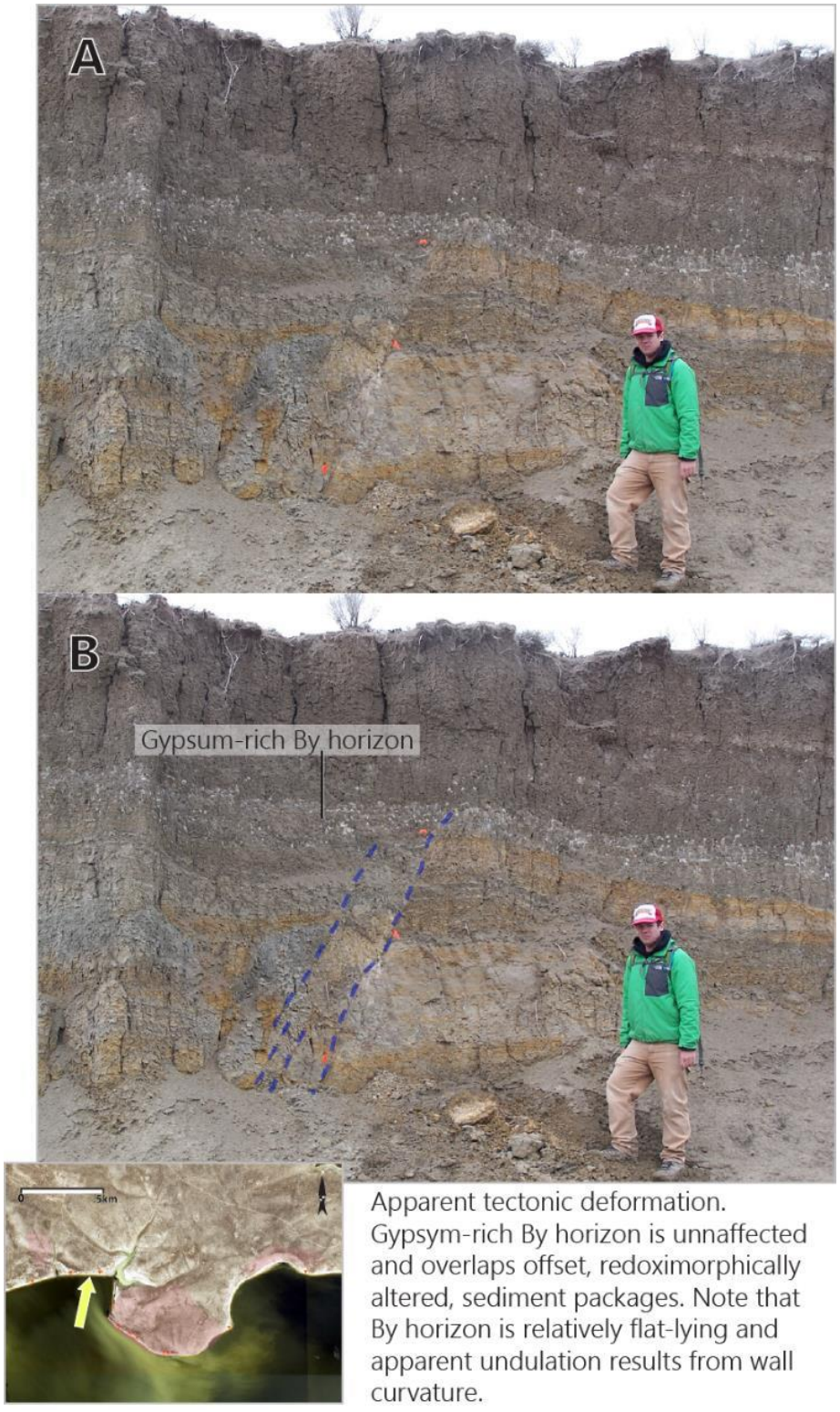

Figure 21. Observation Point B (OP-B). Photo (A) shows fault segment marked by pin flags. Photo (B) highlights fault contacts with dotted lines. Note overlapping By horizon.

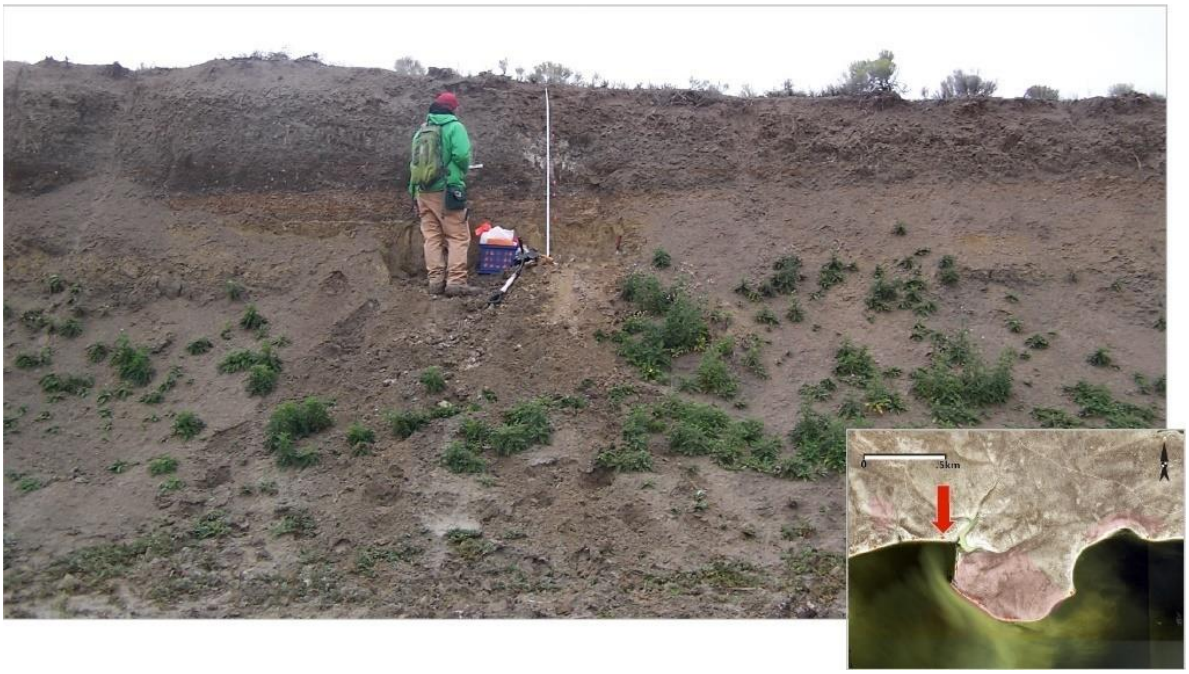

Figure 22. Overview of Profile 1, view north

profile location.

Clast size distributions are unimodal among all sediment packages and dominated by fine to coarse silt (Table 5). Additionally, units 1, 2, and 3 also contain significant clay fractions of approximately 21%, 14%, and 15%, respectively (Appendix B). Similar to Profiles 9 and 6, Profile 1 only shows pedogenic alteration in the uppermost unit. Unlike Profiles 9 and 6, however, Profile 1 has deeply formed soils in the upper package (Figure 23). Horizon A is about 70 cm thick and the underlying Bty soil averages ~50cm. The thick, prominent Bty horizon appears conformable with By horizons present in OP-B, Profile 6, and OP-A to the west. XRD analysis of a sediment sample from the Bty horizon confirms the presence of gypsum ($CaSO_4 \cdot 2H_2O$) with no significant amount of $CaCO_3$ (Table 6). As noted earlier, gypsum may form relatively rapidly versus calcium carbonate. In relation to Profile 9, XRD results (and soil development generally) indicate

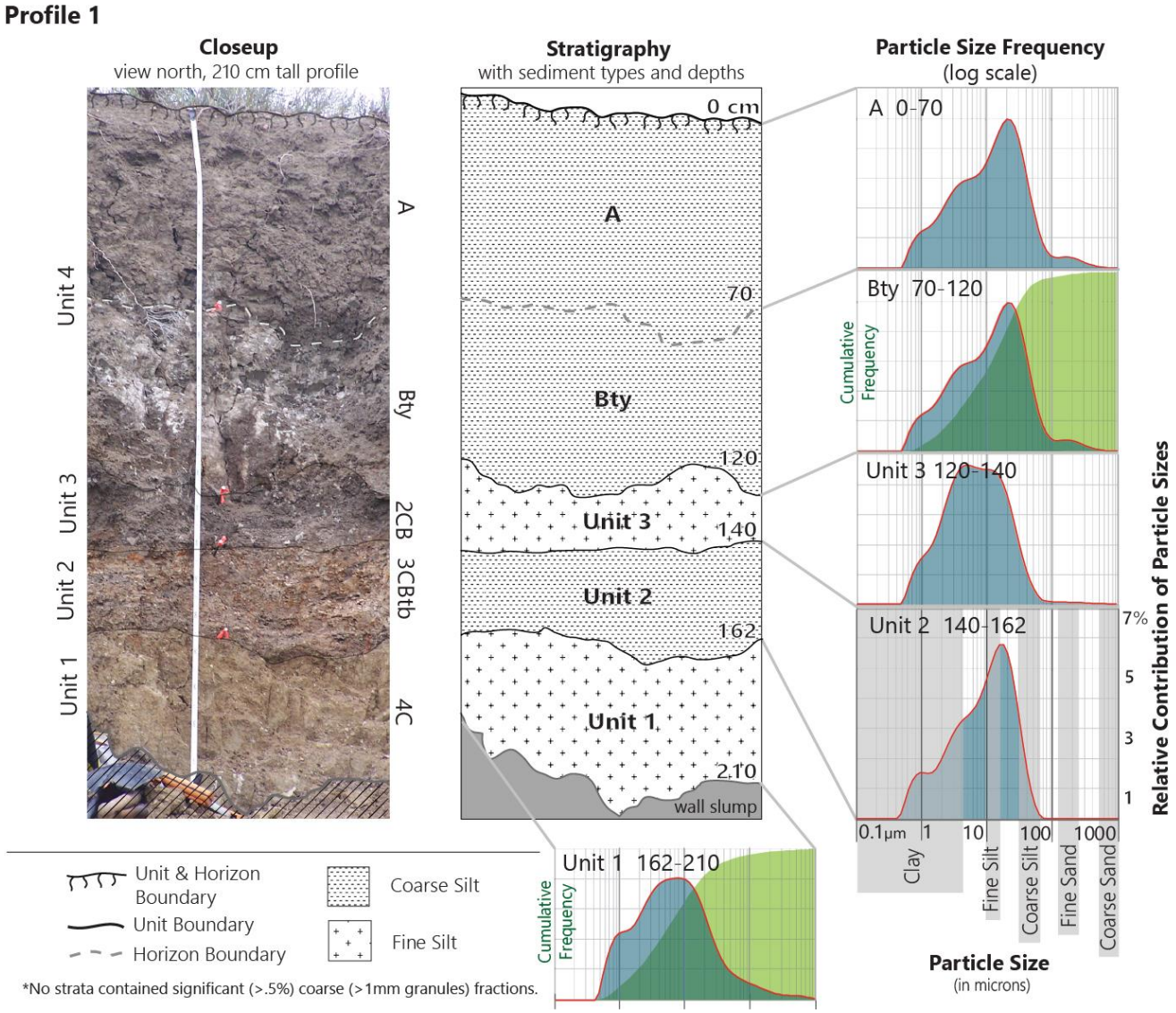

Figure 23. Profile 1 detail including stratigraphy and granulometry data.

Table 5. Profile 1 stratigraphic descriptions.

Unit	Horizon	Depth (cmbs)	Description
Unit 4	A	0-70	Coarse silt. 2.5Y 6/2 (light brownish gray silt). Coarse subangular blocky structure, hard consistence. Ped size increases with depth. Strongly effervescent. Abrupt wavy lower boundary.
	Bty	70-120	Coarse silt. 2.5Y 4/1 (dark grey). Coarse angular blocky structure, hard consistence. Strongly effervescent. Gypsum masses coat ped faces throughout horizon. Abrupt wavy boundary.
Unit 3	C	120-140	Fine silt. 5Y 4/2 (olive green). Fine parting to very fine angular blocky structure, hard consistence. Strongly effervescent. Redoximorphic features ($Fe2O_3$ masses) concentrated in upper 5 cm of horizon (~40% mottles by area). Abrupt smooth boundary.
Unit 2	2CBtb	140-162	Coarse silt. 2.5Y 5/4 (light olive brown) silt loam. Medium parting to fine angular blocky structure, hard consistence. Strongly effervescent. Redoximorphic features ($Fe2O_3$ masses) cover ~10% of area. Visible clay skins coat ped surfaces. Clear wavy lower boundary.
Unit 1	3C	162-210	Fine silt. 5Y 5/4 (olive). Structureless (massive), soft consistence. Strongly effervescent. No lower boundary.

Table 6. XRD chemical composition results for Profile 1, Bty horizon.

Sample # SC1_Bty_70-120*			
Compound Name	**Score**	**Scale Factor**	**Chemical Formula**
Quartz, syn	50	0.629	SiO_2
Gypsum	43	0.640	$CaSO_4 \cdot 2H_2O$
Nontronite	23	0.111	$Na_{0.33}Fe_2^{+3}(Si, Al)4O_{10}(OH)_2 \cdot H_2O$
Sapphirine-1A	21	0.069	$(Al_5Mg_3)(Al_4Si_2)O_{20}$

*XRD analysis conducted at Utah State University Geochemistry Lab in Logan, Utah

that the upper unit of Profile 1 (P1-U4) may have been deposited more recently than the upper unit of Profile 9 (P9-U5).

Overall, western sub-area sediment packages tend to exhibit gently undulating

topography, are silt and clay-dominated and unimodally distributed. Soils are present only in the uppermost units at each profile location. Moving to the east, central area strata generally exhibit more heterogenous textures, show evidence of several cut and fill sequences, and have pedogenic alteration in multiple subsurface units. Central area units also tend to have coarser sediment modes and are more sand-dominated. The following section summarizes stratigraphic profiling results for the central sub-area.

Central Study Area

The central study area is approximately 0.30 km^2 and encompasses a more varied stratigraphic record than the east or west sub-areas. It contains most of site 24BE46 and includes five profile locations; 10, 2, 3/7, 4, and 5 (west to east) (Figures 24 and 25).

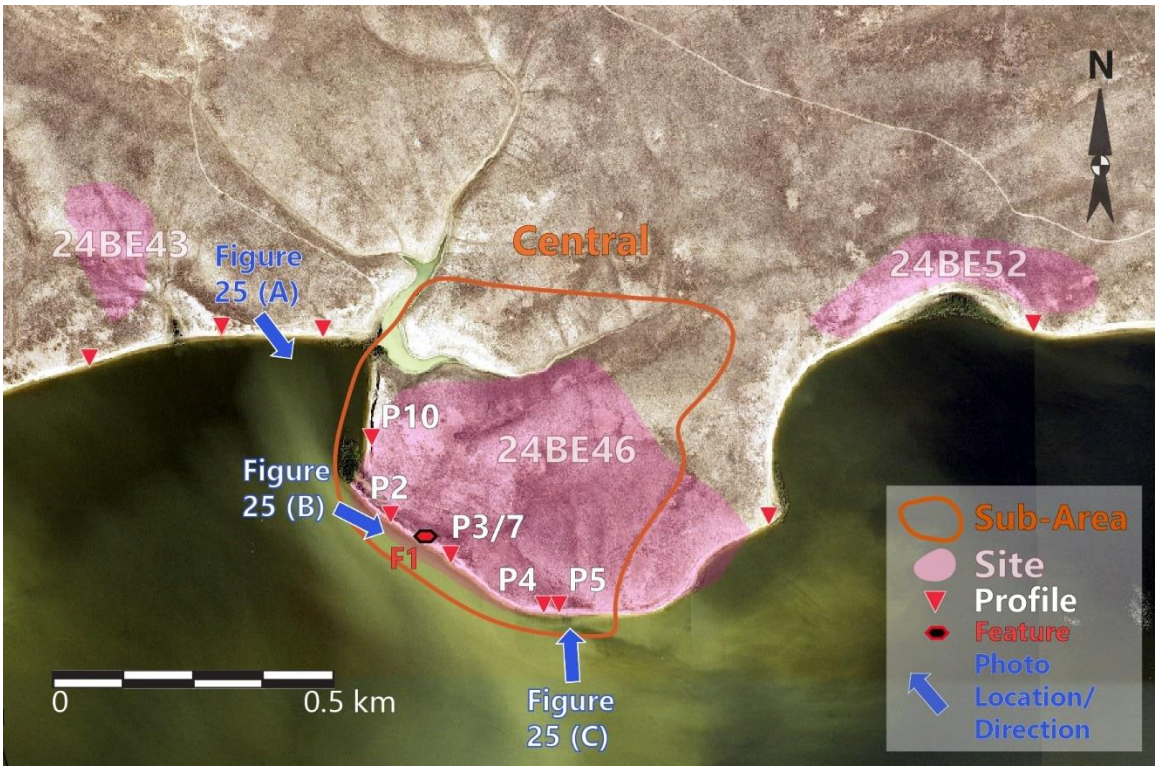

Figure 24. Central study areaindicating profile, feature and overview photo locations.

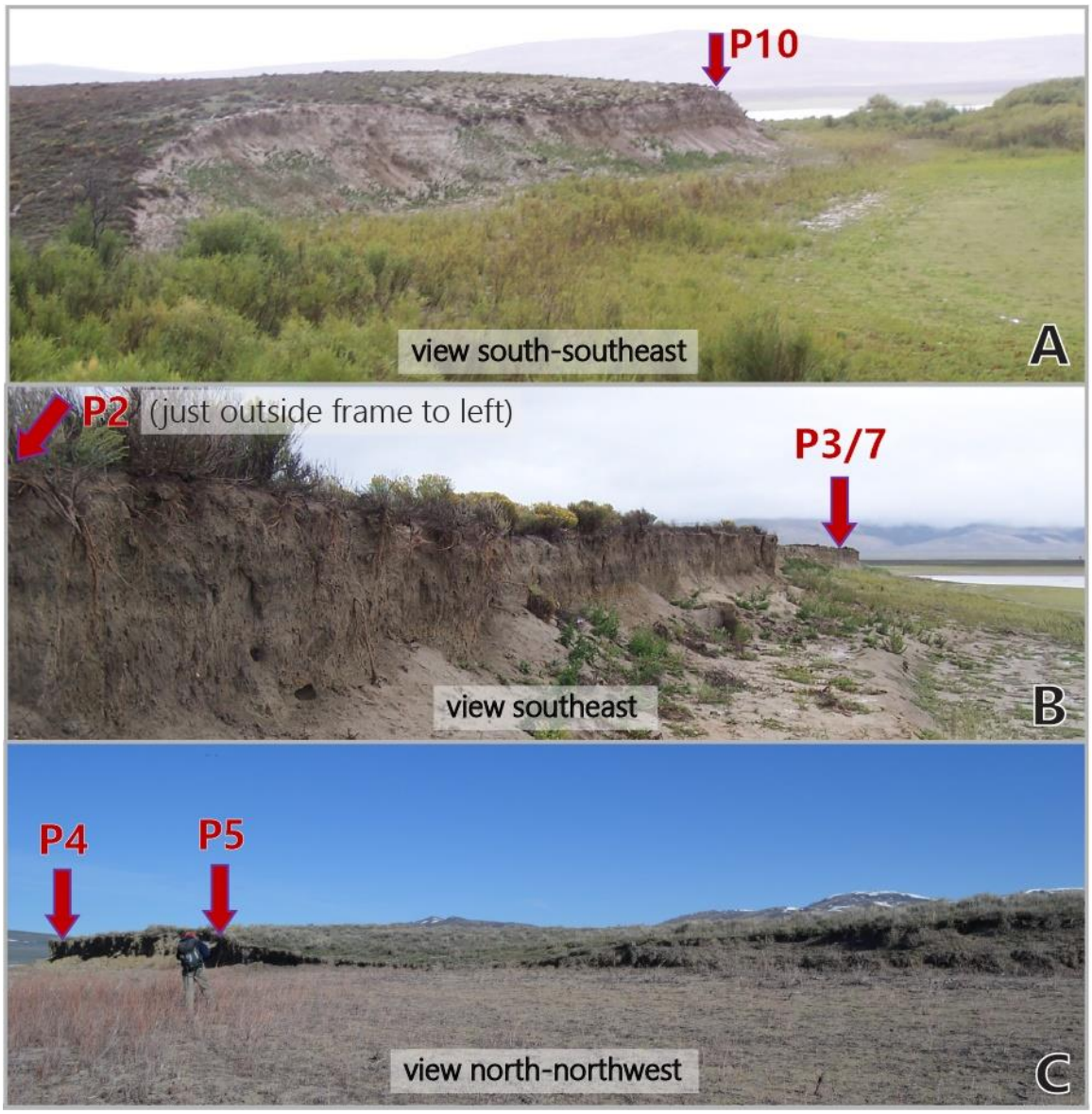

Figure 25. Overviews of central study area with profile locations indicated. Photo locations shown on Figure 24 map.

Elevations in the central area range from approximately 1996 m (6548 ft) AMSL (the lowest in the study area) to 2007 m (6584 ft). Inland of the shoreline, topography and elevation changes are more irregular than the east and west sub-regions. Aerial photographs and Trimble landform mapping reveal abrupt (but relatively low relief) dip-degree changes in upland slopes. Stratigraphically, many sediment packages are laterally discontinuous. Among the five profile locations, only strata between Profiles 2 and 3/7

are traceable. Erosion episodes and diastems are indicated by at least one buttress unconformity and two buried paleosols. The central sub-region includes both the youngest (0.75 ± 0.16 ka, USU-2185 at 23 cmbs) and oldest (60.39 ± 10.48, USU-2187 at 60 cmbs) OSL ages in the study area. However, no straightforward relationship is apparent between sample age and either depth or elevation.

Central area deposits generally have higher proportions of sand and coarse material (Figure 26), are more poorly sorted and exhibit more multi-modal grain distributions than sediments in the west and east (Appendix B). Grain size distributions are 83% very poorly or extremely poorly sorted (Folk and Ward 1957) within the central sub-area. In contrast, only 5% and 43% of west and east end strata (respectively) are very poorly sorted and none are extremely poorly sorted. Higher proportions of coarse material indicate central area sediments derive from higher energy environments and, or,

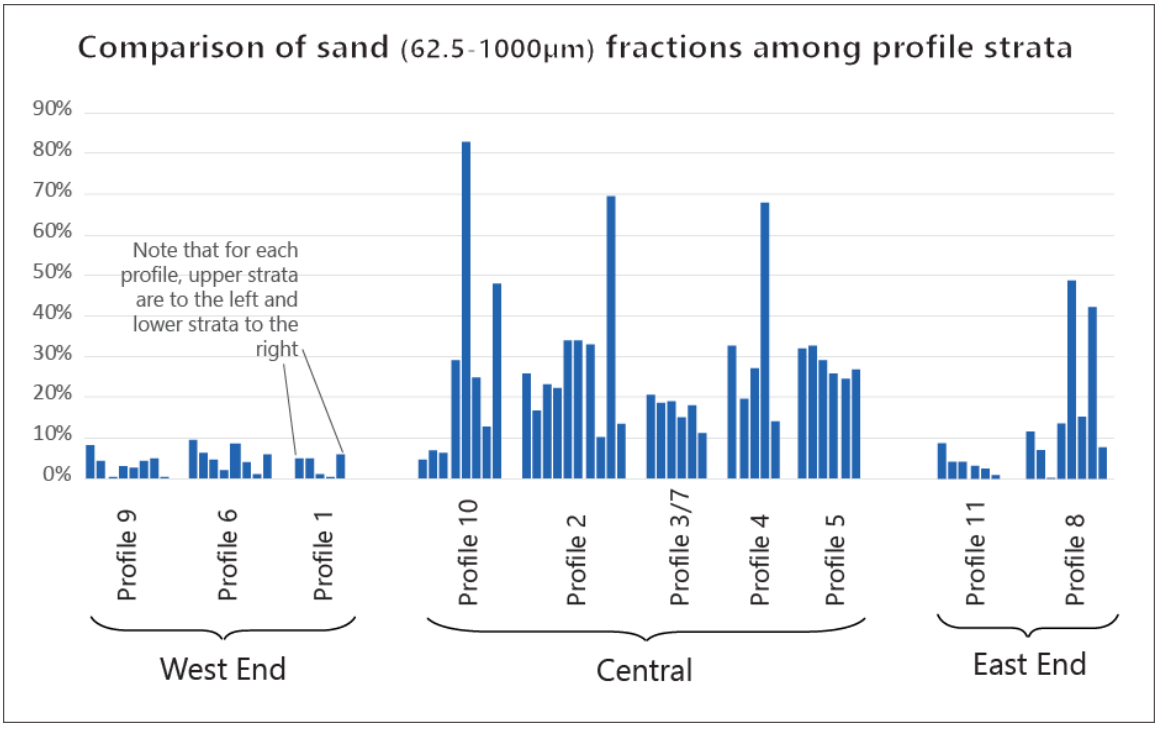

Figure 26. Relative sand contributions for west, central, and east sub-area strata.

had coarser material available for deposit than those in the east and west. Wider grain size ranges may indicate input from multiple depositional mechanisms or post-depositional sediment mixing.

Soil sequences in the central sub-region are highly variable with some areas exhibiting only surface pedogenesis and others showing multiple buried epipedons. A conspicuous paleosol pair is present along about 0.25 km of the south margin. The paleosols are present in Profiles 2 and 3/7 and may relate to soils in Profile 5. Significantly, these paleosols are associated with in situ artifacts (obsidian flakes) observed in the cutbank wall. Furthermore, paleosol depths bracket the position of a subsurface feature (F1) identified by USUAS in 2011.

Abrupt upland slope intersections, discontinuous strata and OSL age ranges spanning tens of thousands of years with no clear age-to-depth association suggest complex cut and fill mechanisms have affected the central sub-region for much of the late Quaternary. Variable soil sequences and buried epipedons support this assumption. Based on previous research and initial observations, incision and deposition may have resulted from a combination of river meander erosion, oxbow lake filling, low-angle alluvial fan aggradation or other geomorphic factors including lake inundation or dune migration. Results of central area strata description and analysis are detailed below.

Profile 10

Profile 10 is situated on the west margin of site 24BE43 with a top elevation of 2001.88 m (6568 ft) AMSL (Figure 27). All Profile 10 strata ages far exceed archeological timespans (Figure 28). An OSL sample at the base of unit 7, the uppermost unit (60 cmbs), returned an age of 60 ± 10.48 ka (USU-2187). While Profile 10 strata

Figure 27. Overview of Profile 10 location. View east-northeast.

substantially pre-date human occupation, quantifying depositional conditions for these units is nonetheless important for defining sediment sequences too old for cultural association in the area.

Profile 10 strata are highly variable in terms of texture and sorting (Table 7, Figure 28). Unit 5 in this profile is composed of the coarsest sediments in the study area (fine silty medium gravel). The GSD of this sediment package is multimodal exhibiting four peaks in the medium gravel, fine gravel, fine sand and clay categories (Figure 28). Unsurprisingly, it is classified as extremely poorly sorted (Folk and Ward 1957). At the opposite extreme, unit 4 (directly below unit 5) shows an extremely leptokurtic distribution profile, dominated by nearly 14% fine sand (138 to 240 µm). GSD analysis throughout the study area revealed that most binned clast size categories contribute

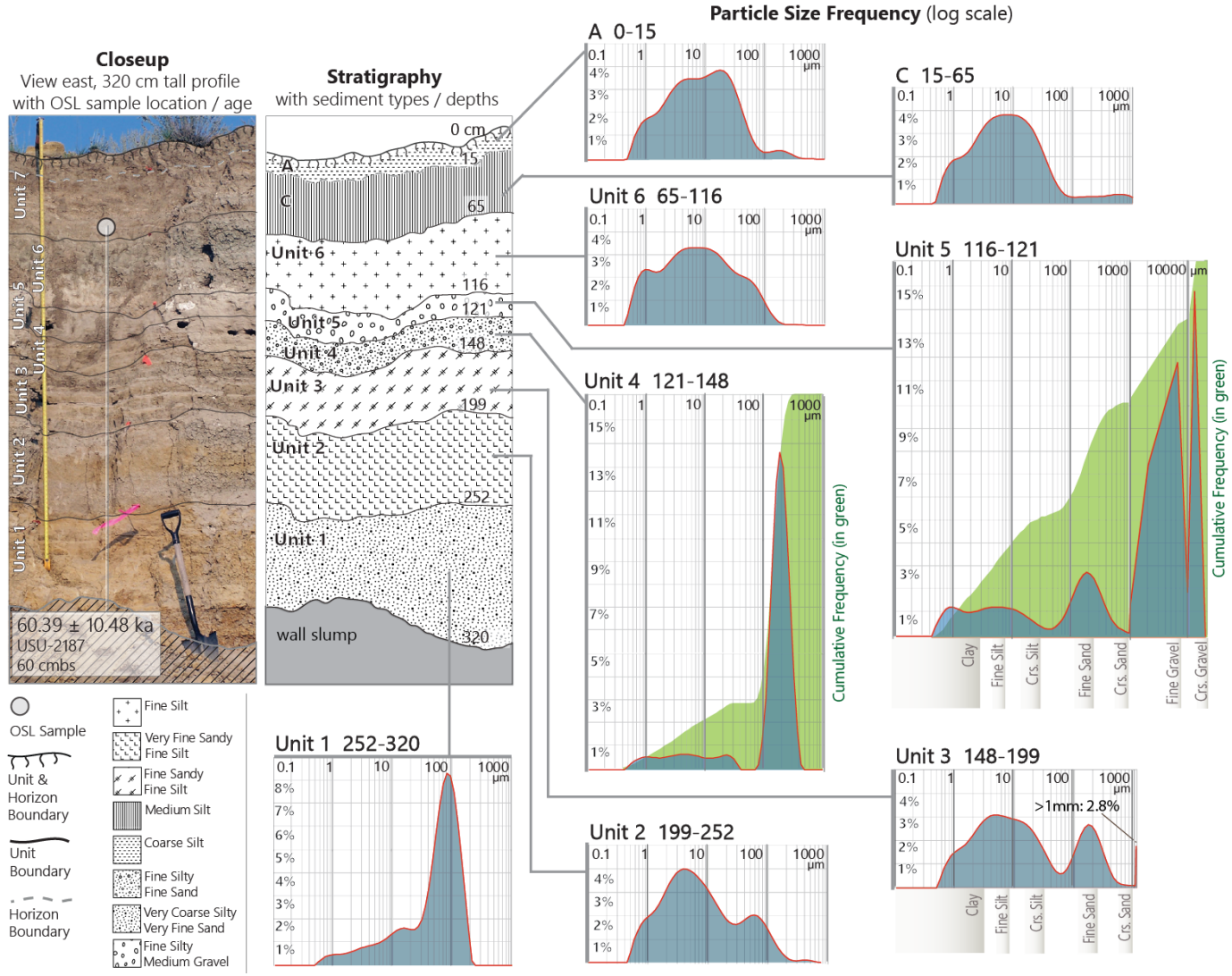

Figure 28. Profile 10 detail including stratigraphy, OSL, and granulometry data.

Table 7. Profile 10 stratigraphic descriptions.

Unit	Horizon	Depth (cmbs)	Description
Unit 7	A	0-15	Coarse silt. 2.5Y 5/2 (grayish brown).
	C	15-65	Medium silt. 2.5Y 5/3 (light olive brown).
Unit 6	2C2	65-116	Fine silt. 5Y 7/1 (light gray).
Unit 5	3C3	116-121	Fine silty medium gravel. 2.5Y 7/1 (light gray).
Unit 4	4C4	121-148	Fine silty fine sand. 2.5Y 6/2 (light brownish gray).
Unit 3	5C5	148-199	Fine sandy fine silt. 5Y7/2 (light gray).
Unit 2	6C6	199-252	Very fine sandy fine silt. 2.5Y 7/2 (light gray).
Unit 1	7C7	252-320	Very coarse silty very fine sand. 2.5Y 7/6 (yellow sandy loam).

relatively slightly to total study area sediment bodies (usually < 6% of total). Unit 4, with 14% of total being fine sand, exhibits a significantly higher degree of sorting than most other sediment packages in the study area.

Observation Point C

Observation point C (OP-C) is the location of soft sediment deformation structures approximately 50 m south-southeast of Profile 10 (Figure 29). The structures lie approximately 2.5 m below ground surface. The formations occur in a package contiguous with unit 2 of Profile 10. The structures are therefore stratigraphically below OSL sample USU-2187 (60.39 ± 10.48 ka) at Profile 10 and were formed well before human occupation. However, they indicate antecedent conditions in which sediment loading or tectonic action may have caused mixing of saturated materials from different

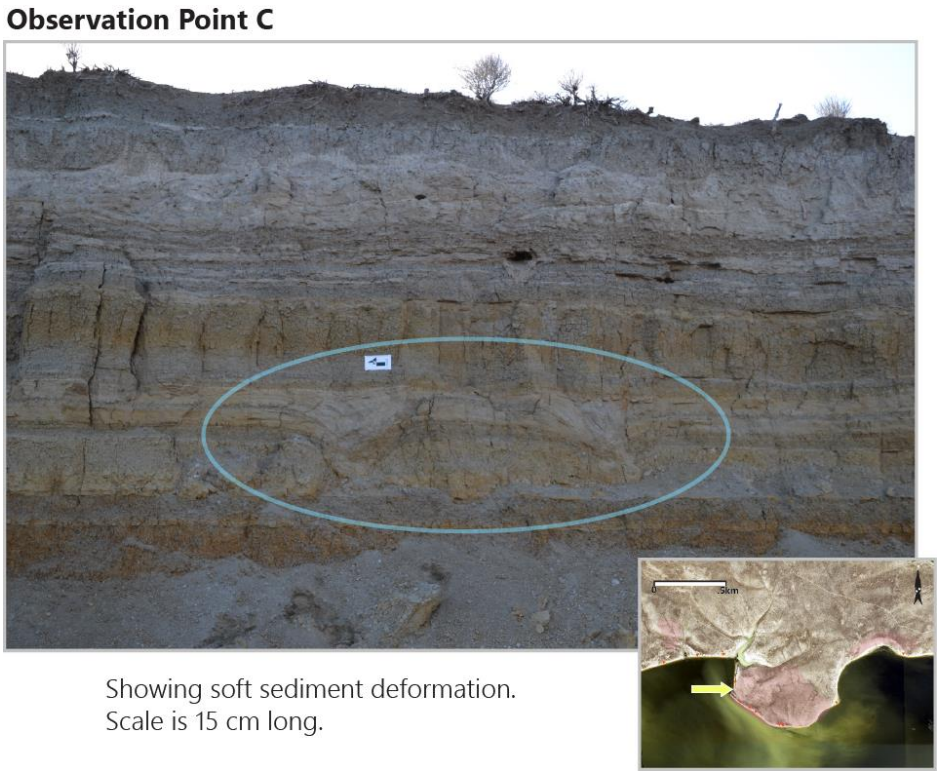

Figure 29. Observation point C (OP-C). Soft sediment deformation structures.

strata. It is unknown if similar conditions occurred during the Holocene.

Profile 2

Profile 2 has a top elevation of 1998.40 m (6556 ft) AMSL and a wall height of 1.6 m (Figure 30). The exposure includes six sediment packages (units 1 through 6) (Figure 31). Based on OSL samples and associated artifacts, the upper three units are cultural age (Table 1). Obsidian flakes were noted in the wall exposure in and around the Profile 2 location (Figure 31, b). Profile 2 captures a buttress unconformity in which the oldest units (1, 2, and 3 from bottom to top), are incised and overlain by younger packages 4, 5, and 6. The architecture of this cut and fill sequence (Figure 32) provides evidence for determining what erosive processes were responsible for creating an accommodation space in the central study area, and when and by what means it was

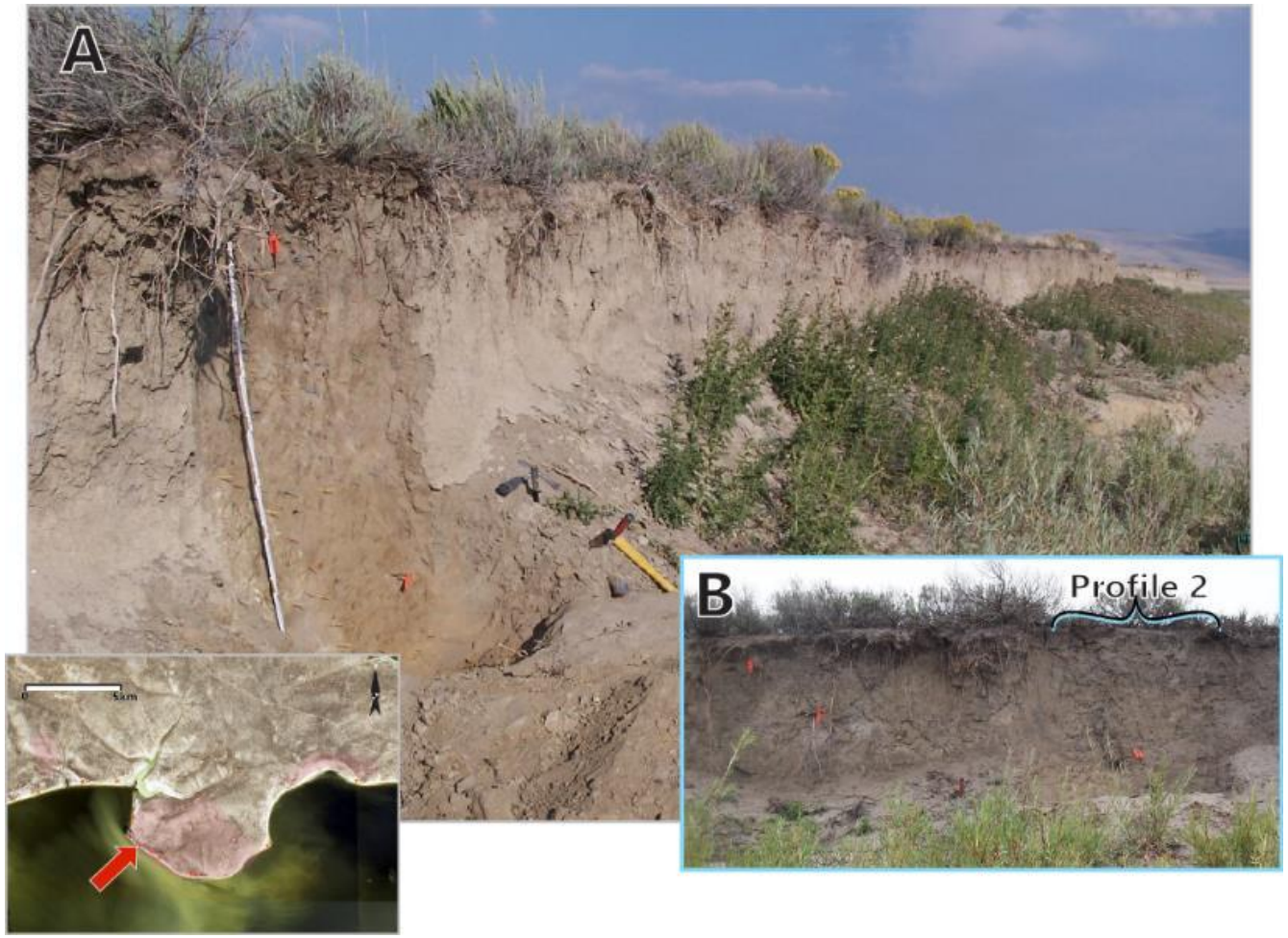

Figure 30. Overview of Profile 2 location.(A) View southeast from profile 2. (B) View northeast showing in situ flakes marked by flagging tape.

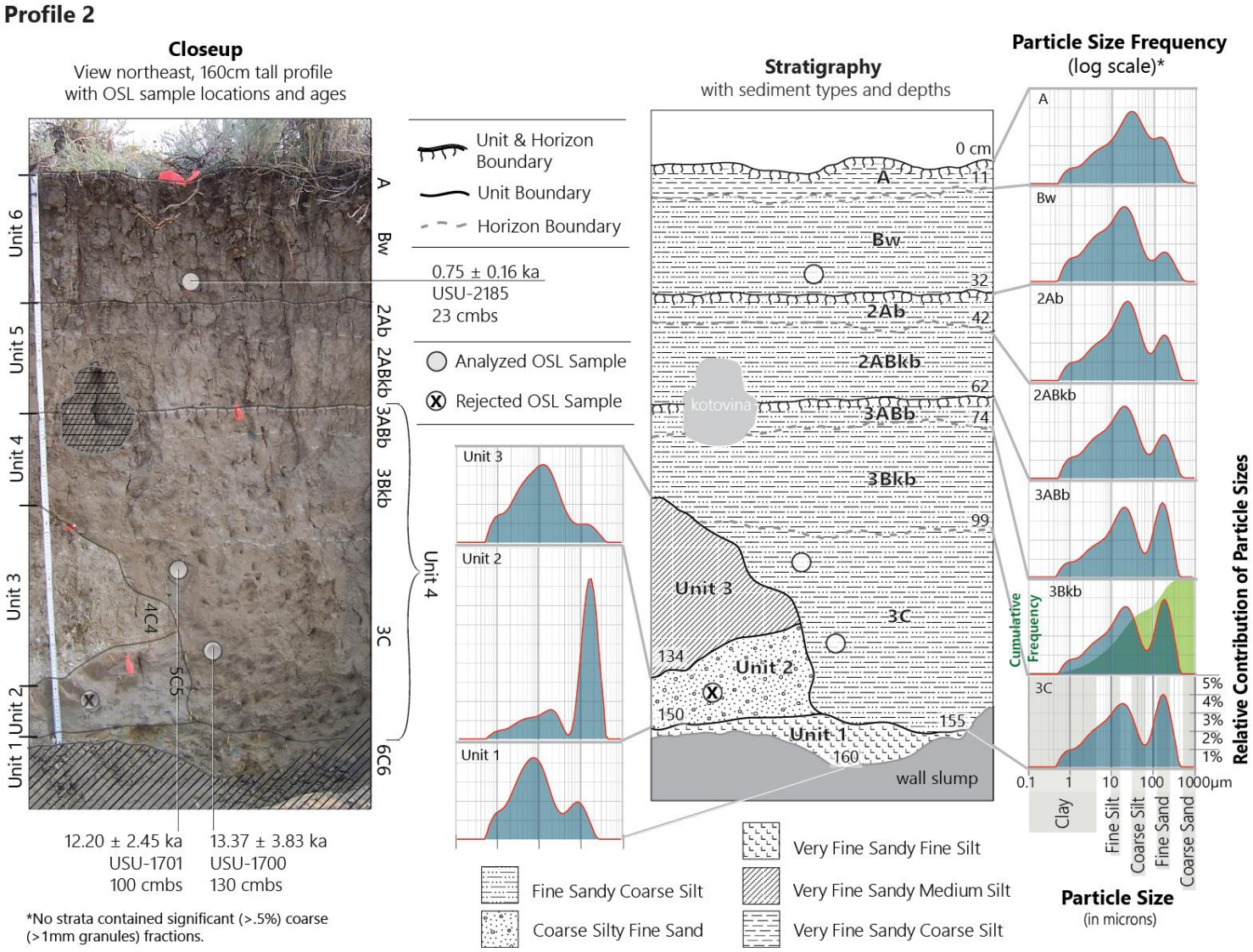

Figure 31. Profile 2 detail including stratigraphy, OSL, and granulometry data.

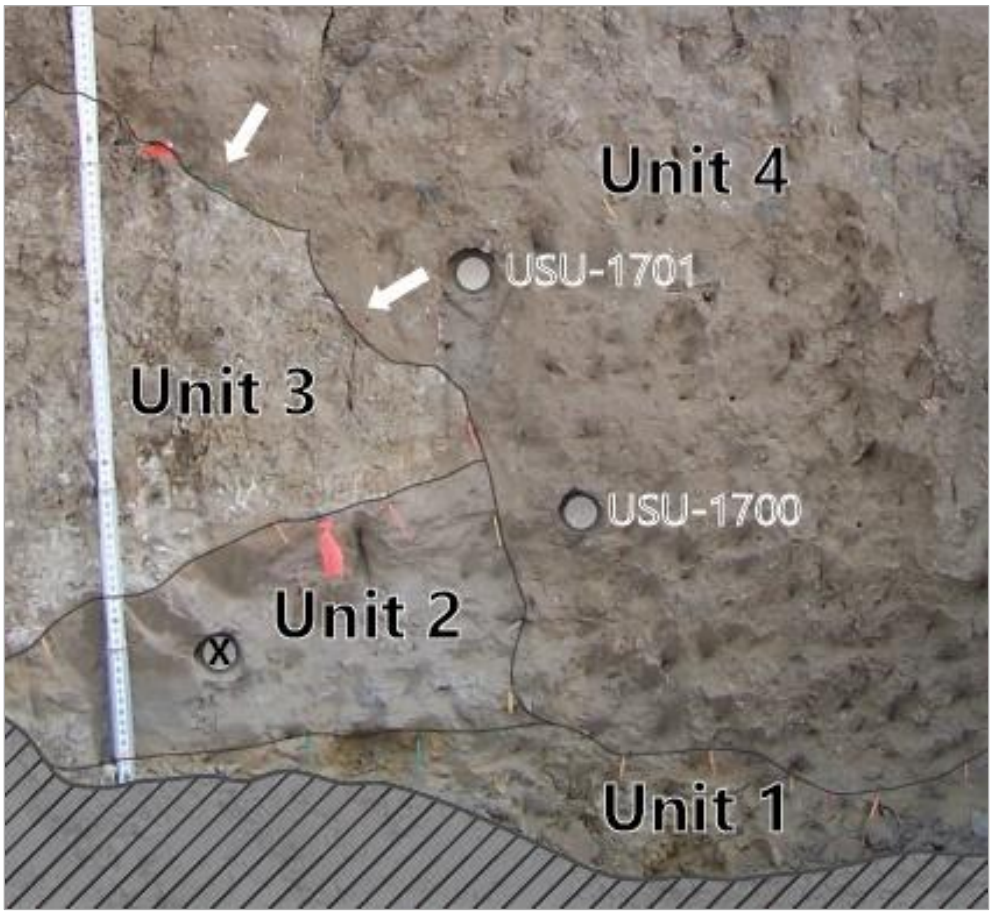

Figure 32. Closeup of Profile 2 showing buttress unconformity. White arrows indicate convex-shaped cuts into unit 3 along contact.

filled. The contact between unit 4 and the underlying units 1, 2, and 3 is very abrupt. The angle of the contact varies from nearly horizontal at the bottom to roughly vertical in the middle and about 45° at the top. The contact shape is wavy with at least two distinct convex troughs cut into the older sediments.

The area in and around Profile 2 is notable as obsidian flakes (n ~10) are exposed at depths (up to 77 cmbs) in the cutbank wall. The artifacts appear to be in situ as I did not observe flakes near krotovina or other post-depositional disturbances. Moreover, dated artifact-containing strata all produced ages within a cultural time-frame. Unit 4 produced OSL ages of 13.37 ± 3.83 ka at 130 cmbs (USU-1700) and 12.20 ± 2.45 ka at

100 cmbs (USU-1701). The uppermost package, unit 6, was OSL dated as 0.75 ± 0.16 ka at 23 cmbs. OSL ages generally increase with depth as would be expected with undisturbed sediments. However, the 2σ standard error margins for the lowest two samples (USU-1700 and USU-1701) overlap in age (Figure 33). Therefore, it is not known whether unit 4 accumulated incrementally or during a single event.

Profile 2 sediments are dominated by sand and silt (Table 8). All strata have bimodal grain size distributions. Modal peaks for the upper three units are each centered at ~21-28 µm (coarse silt) and ~195 µm (fine sand) (Appendix B). Unit 4 has the second

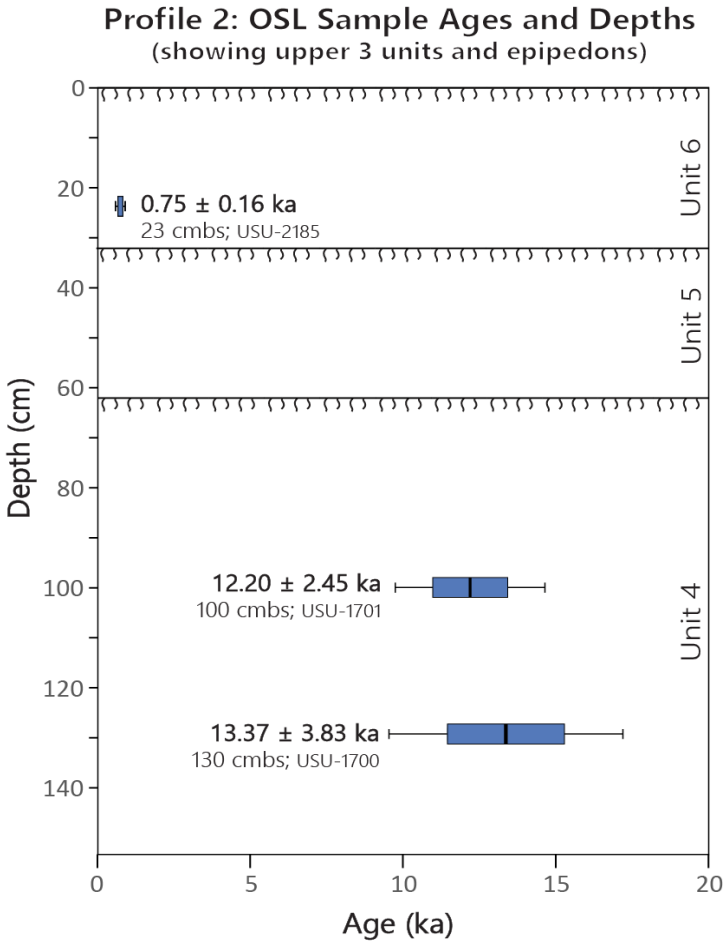

Figure 33. Relationship of Profile 2 OSL ages and depth. Note soil formation (indicating depositional hiatus) at the tops of units 4, 5, and 6.

Table 8. Profile 2 stratigraphic descriptions.

Unit	Horizon	Depth (cmbs)	Description
Unit 6	A	0-11	Very fine sandy coarse silt. 10YR 5/2 (grayish brown) Soft consistence, medium subangular blocky structure. Slightly effervescent. ~25% organic content. Gradual wavy boundary.
	Bw	11-32	Fine sandy coarse silt. 10YR 7/2 (light gray). Fine to medium columnar structure, hard consistence. Strongly effervescent, few (~1%) fine $CaCO_3$ flecks throughout. Clear smooth boundary.
Unit 5	2Ab	32-42	Fine sandy coarse silt. 10YR 6/2 (light grayish brown). Medium columnar structure, hard consistence. Strongly effervescent. Clear smooth boundary.
	2ABkb	42-62	Fine sandy coarse silt. 2.5Y 6/2 (light brownish gray). Medium columnar structure, hard consistence. Strongly effervescent. Gradual smooth boundary. *Note*: The base of this unit/horizon includes a fine gravel stone line approximately 3.5 cm long by 1.5cm high. The contact possibly represents a ravinement surface.
Unit 4	3ABb	62-74	Fine sandy coarse silt. 10YR 5/3 (brown silt loam). Medium columnar structure, hard consistence. Strongly effervescent, few (~2%) fine $CaCO_3$ threads throughout. Diffuse smooth boundary.
	3Bkb	74-99	Fine sandy coarse silt. 2.5Y 6/2 (light brownish gray). Structureless (massive), moderately hard consistence. Strongly effervescent, common (~10%) medium $CaCO_3$ threads throughout. Clear wavy boundary.
	3C	92-155	Fine sandy coarse silt. 2.5Y 6/3 (light yellowish brown). Structureless (massive), hard consistence. Strongly effervescent, few (~2%) fine $CaCO_3$ masses throughout. Abrupt irregular boundary.
Unit 3	4C4	92-134	Very fine sandy medium silt. 2.5Y 7/3 (pale brown). Fine blocky structure, moderately hard. Strongly effervescent. Common medium gypsum crystals in lower ~10 cm. Abrupt irregular boundary.
Unit 2	5C5	134-150	Coarse silty fine sand. 2.5 Y 7/2 (light gray). Finely parallel laminated structure (depositional), slightly hard consistence. Strongly effervescent, finely disseminated carbonates throughout. Very abrupt smooth boundary.
Unit 1	6C6	155-160	Very fine sandy fine silt. 10YR 5/4 (yellowish brown). Very fine blocky structure, moderately hard. Strongly effervescent. No lower boundary. *Note*: A distinct redoximorphic concentration stain (10YR 6/6 brownish yellow) occurs at 150-155 cmbs.

highest sand fraction in the profile and is coarser than the packages immediately above and below it. Unit 4 directly overlies the previously noted buttress unconformity. If unit 4 was deposited in conjunction with the incision episode, both the cutting and filling processes may be connected to a higher energy process or event such as a flash flood or stream avulsion.

Soil development at Profile 2 consists of a modern surface soil overlying two buried paleosols (Figure 31). The surface soil alters unit 6, the upper paleosol is formed into unit 5 and the lower paleosol alters unit 4. The surface soil is approximately 0.75 ± 0.16 ka (USU-2185) and consists of an 11 cm thick A horizon overlying a 22cm Bw. Below, the upper paleosol is formed into unit 5 and includes a 20 cm thick carbonate horizon (2ABkb). The boundary between unit 5 (above) and 4 (below) may represent a ravinement surface as it incorporates a fine gravel stone line approximately 3.5 cm long by 1.5 cm high which rests on the lower unit 4 paleosol (Table 8). Furthermore, the top horizon of the lower paleosol (3ABb) shares both A and B horizon properties indicating the original pedon may have been truncated prior to deposition of Unit 5. Alternately, the 3ABb horizon could represent a welded soil in which the A horizon inherited B horizon properties post-burial.

Horizon A at Profile 2 had the highest observed organic content of any study area strata. The majority of study area sediments contained little to no organic matter. For study area sediments with organic content, I removed as much visible plant matter as possible before conducting granulometry analysis. However, I did not know whether various organic removal techniques would produce significant differences in grain-size distribution results. I therefore used Profile 2, A horizon material (with the highest

observed organic content) to test whether removal method affected grain size distribution (Appendix C). I used an analysis of variance (ANOVA) statistical test to quantify GSD differences among subsamples subjected to mechanical (tweezers), H_2O_2 saturation, or water flotation organic removal. I found that removal methods produce significant differences among distributions at the 10 (D_{10}), 50 (the median, D_{50}) and 90 (D_{90}) cumulative percentiles. Appendix C provides full details of the experiment including subsample preparation details, significance values, and boxplot graphs of D_{10}, D_{50}, D_{90} distributions for the three methods.

Profile 3/7

Profile 3/7 is located approximately 130 m southeast of Profile 2 on a slightly taller exposure (178 cm) with a top elevation of 1999.81 m (6561 ft) AMSL. The buried paleosol pair present at Profile 2 is also visible in Profile 3/7 (Figures 34 and 35). All OSL ages from this profile (maximum depth of 77 cmbs) are within an archeological timeframe.

Reconstructing the chronology of the area between Profile 2 and Profile 3/7 is key to understanding archeological burial in the study area. Profile 3/7 is associated with buried debitage and is the profile nearest the former location of Feature 1; the radiocarbon-dated hearth. Profile 3/7 lies approximately 54 meters southeast of feature F1, identified by USUAS (Peart et al. 2012:50). In October 2011, USUAS mapped F1 in the cutbank of site 24BE46 and collected feature fill for radiocarbon dating (Figures 8 and 9). The feature consisted of a shallow basin-shaped hearth measuring 30 cm wide with ash and charcoal staining extending from about 55 to 80 cm below surface. Santarone (2011) noted that the feature was situated just below the upper boundary of a

Figure 34. Overview of Profile 3/7 location, view northwest. Prior to wall-facing.

prominent buried paleosol. Feature F1 was destroyed by wall slump some time prior to May 2014 when I revisited the site. However, I submitted two of USUAS's feature fill samples for AMS radiocarbon dating and determined that F1 dates between 9560-8500 (sample # 147407) and 8430-8100 cal BP (sample # 147408) (Table 9). These ages are consistent with a Late Paleoindian site occupation, as indicated by Frederick tradition projectile points (~9500 cal BP) found at the site (Peart et al. 2012; Kornfeld et al 2010).

Profile 3/7, as illustrated in Figure 35, represents the combination of two adjacent stratigraphic locations (Profiles 3 and 7) made before and after a major wall slump destroyed the first profiled location. In May 2014, I mapped the stratigraphy of Profile 3

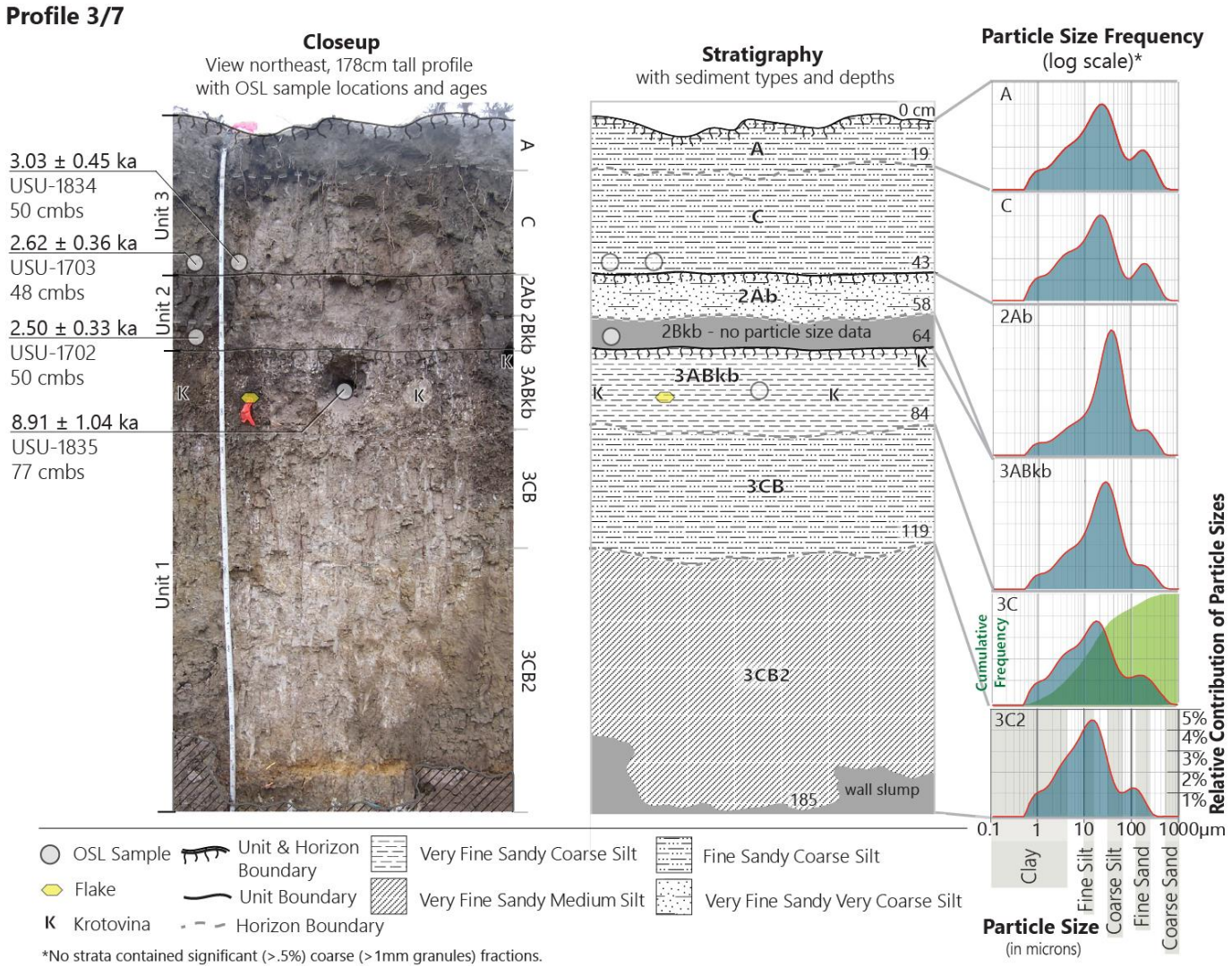

Figure 35. Profile 3/7 detail including stratigraphy, OSL, and granulometry data.See text for explanation of OSL depth discrepancies.

Table 9. Radiocarbon results for feature F1 at site 24BE46.

Sample #	^{14}C age year BP	95.4% (2σ) cal age ranges (2014)*	Relative area under distribution	Sample substance
147407**	8080 ± 240	9560-8500 cal BP	1.0	Ashy sediment and charcoal from hearth (darkest sediments sampled)
147408**	7390 ± 80	8430-8100 cal BP	1.0	Ashy sediment and charcoal from hearth (alternate sample)

* based on Reimer et al. 2004, rounded to nearest decade
** samples processed at Keck Carbon Cycle AMS Facility at University of California (UC) Irvine's Earth System Science Department.

and collected two OSL samples (USU-1702 and USU-1703). I returned to the location in August 2014 to collect two additional OSL samples. This decision was due to preliminary OSL age estimates being significantly younger than Feature 1 radiocarbon dates, despite having been collected from analogous depths. Unfortunately, between May and August 2014, the Profile 3 location collapsed, destroying the mapped exposure. A previously undetected vertical wall fissure (later the site of wall failure) may have introduced light-contaminated quartz into my original samples, thus artificially raising their ages. I therefore faced the cutbank directly behind the original profile and collected an additional OSL sample (USU-1834) at the same depth as USU-1703. I then mapped another profile (Profile 7) on a more stable wall face approximately four meters west of Profile 3 and collected an additional OSL sample (USU-1835) from below the lowest paleosol.

The apparent OSL sample depth discrepancies in Figure 30 are due to combining information from Profiles 3 and 7. The photograph in Figure 30 is of the more recent Profile 7 location. Consequently, only USU-1835 is shown in its actual location. USU-

1702, USU-1703, and USU-1834 from P3 are shown in their relative stratigraphic positions. Undulating surface topography resulted in overlapping below-surface depths for samples collected from different absolute elevations and strata.

The Profile 3/7 exposure consists of three sediment packages (Units 1-3). Sediments at Profile 3/7 are all variations of sandy silt (Table 10). Textures are somewhat similar to the upper three units of Profile 2, but with higher silt ratios (Appendix B). All but one stratum (3ABkb) exhibits bimodal distributions. Modal peaks of Profile 3/7 strata are centered at ~20-30 µm (coarse silt) and 170-200 µm (fine sand). Soil formation is

Table 10. Profile 3/7 stratigraphic descriptions.

Unit	Horizon	Depth (cmbs)	Description
Unit 3	A	0-19	Fine sandy coarse silt 2.5Y 6/2 (light brownish gray). Fine granular structure.
	C	19-43	Fine sandy coarse silt. 2.5 Y7/2 (light gray).
Unit 2	2Ab	43-58	very fine sandy very coarse silt. 2.5Y 5/2 (grayish brown.
	2Bkb	58-64	[No Data]
Unit 1	3ABkb	64-84	Very fine sandy coarse silt. 2.5Y 6/3 (light yellowish brown). Very fine subangular blocky structure. Common (~ 20%) medium (avg. 4 mm) CaCO3 masses.
	3CB	84-119	Fine sandy coarse silt. 2.5Y 7/3 (pale brown). Moderate grade fine prismatic structure. Few medium CaCO3 masses.
	3CB2	119-185	Very fine sandy medium silt. 5Y 7/3 (pale yellow). Weak grade medium prismatic structure. Few fine CaCO3 masses extending from horizon top to ~ 137 cmbs. *Note:* This horizon includes a distinct band of redoximorphic staining (2.5Y 7/6; yellow) near the bottom, from 170 to 175 cmbs. This band appears similar to the redoximorphic concentration layer at 150-155 in Unit 1 of Profile 2.

evident in all three units, with the lowest package (unit 1) showing the thickest soil sequence (121 cm).

Profile 4

Profiles 4 and 5 are located 220 m and 250 m (respectively) southeast of Profile 3/7 at the southern tip of site 24BE46 (Figure 36). To the northwest, Profile 4 is a 1.3 m high exposure with a top elevation of 1998.86 m (6558 ft) AMSL (Figure 37). The profile consists of four sediment packages, with soil development present only in the upper unit. An OSL sample from unit 2 (USU-1704, 95 cmbs) produced an age of 36.23 ± 5.89 ka, substantially pre-dating human presence. This unit was selected for OSL sampling because it consists of laminated fine sand with good potential for complete bleaching. It is unknown whether the overlying units 3 and 4 were deposited in a cultural timeframe. Profile 4 sediments are silt and sand dominated and all strata show bimodal distributions (Table 11, Appendix B). Modal peaks are less uniform than at Profiles 2 and 3/7, with concentrations at ~5-7 µm (fine silt), 19-28 µm (coarse silt), 112 µm (very fine sand), and 170 µm and 195 µm (fine sand). Unit 2 consists of fine parallel laminated fine sand. Directly below and above, units 1 and 3 are structureless (massive). Only the uppermost package (unit 4) shows pedogenic alteration other than redoximorphic staining. The epipedon of unit 4 (A horizon) exhibits slight darkening due to organic accumulation and weak prismatic structure. Redoximorphic concentrations are present in units 1 and 3. These concentrations are well-developed enough to have partially cemented unit 3.

Figure 36. Panoramic composite of Profiles 4, 5, and surrounding topography. View (left to right) north-northwest to north-northeast.

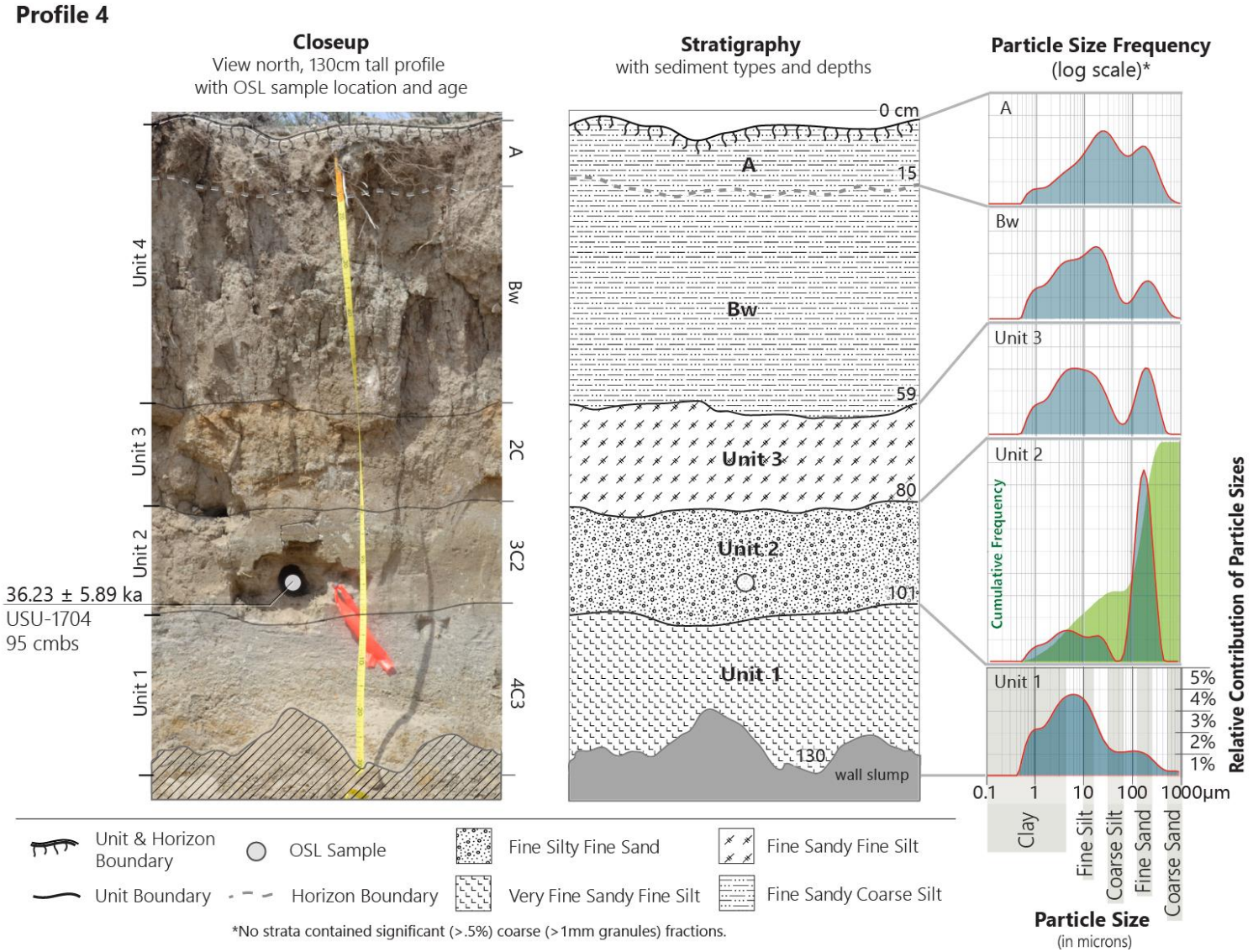

Figure 37. Profile 4 detail including stratigraphy, OSL, and granulometry data.

Table 11. Profile 4 stratigraphic descriptions.

Unit	Horizon	Depth (cmbs)	Description
Unit 4	A	0-15	Fine sandy coarse silt. 10YR 5/2 (grayish brown).
	Bw	15-59	Fine sandy coarse silt. 2.5Y 6/2 (light brownish gray). Weak fine prismatic structure.
Unit 3	2C	59-80	Fine sandy fine silt. 2.5Y 7/4 (pale brown). Structureless (massive). Redoximorphic staining throughout unit. *Note*: This unit appears to have more resistant weathering properties compared to Unit 4, above. This is possibly due to redoximorphic concentrations having hardened parts of this sediment package. Redoximorphic cementation is indicated by small fractures separating Units 3 and 4. The fractures are most abundant where redoximorphic color is most saturated.
Unit 2	3C2	80-101	Fine silty fine sand. 2.5Y 6/3 (light yellowish brown). Finely horizontally laminated structure (depositional).
Unit 1	4C3	101-130	Very fine sandy fine silt. 5Y 7/1 (light gray). Structureless (massive). Faint redoximorphic concentrations in lower half of unit. No lower boundary.

Profile 5

Profile 5 is located about 25 m southeast of Profile 4. It is situated on a gentle southeast facing slope at the west margin of a shallow, south-draining swale. The profile has a wall height of 123 cm and a top elevation of 1998.36 m (6556 ft) AMSL (Figure 38). Beyond Profile 5 to the east, the sloping cutbank pinches out to approximately shoreline level forming a low swale. (Figure 37). About 130 m farther east, the cutbank wall rises again, revealing horizontal red and white sand and clay beds markedly different from Profile 5 strata. It appears that an unconformity is located somewhere in the low

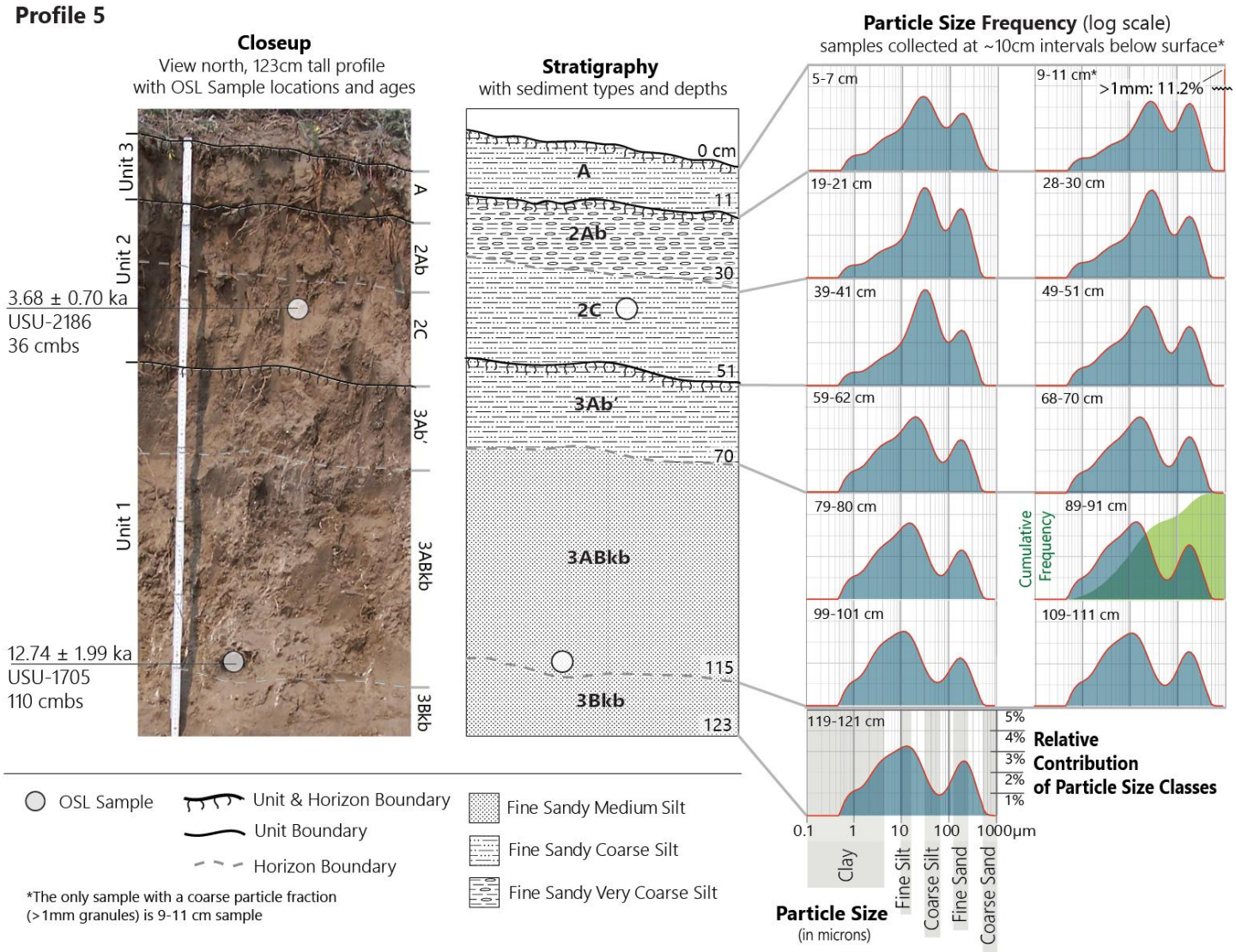

Figure 38. Profile 5 detail including stratigraphy, OSL, and granulometry data.

swale between Profile 5 and the higher cutbank wall about 130m east. The two OSL samples at Profile 5 are both within cultural timeframes. The OSL sample from unit 2 yielded an age of 3.68 ± 0.70 ka (USU-2186) at 36 cmbs. The lower sample from unit 1 dated to 12.74 ±1.99 ka (USU-1705) at 110 cmbs.

Profile 5 consists of three sediment packages (Table 12) with soil development

Table 12. Profile 5 stratigraphic descriptions.

Unit	Horizon	Depth (cmbs)	Description
Unit 3	A	0-11	Fine sandy coarse silt. 10YR 6/3 (pale brown). Structureless (massive), soft consistence. Strongly effervescent. Clear smooth boundary.
Unit 2	2Ab	11-30	Fine sandy very coarse silt. 10YR 5/3 (brown). Weak very fine prismatic structure, hard consistence. Strongly effervescent. Gradual smooth boundary.
	2C	30-51	Fine sandy coarse silt. 10YR 6/2 (light brownish grey). Structureless (massive), soft consistence. Strongly effervescent. Clear smooth boundary.
Unit 1	3Ab'	51-70	Fine sandy coarse silt. 10YR 3/2 (very dark grayish brown). Structureless (massive), slightly hard consistence. Strongly effervescent, few (~ 2%) fine CaCO3 threads throughout. Clear smooth boundary. *Note*: This horizon exhibits faint color mottling and infrequent rodent krotovinas indicating slight bioturbation throughout.
	3ABkb	70-115	Fine sandy medium silt. 10YR 4/1 (dark gray). Weak very fine columnar parting to structureless (massive), moderately hard consistence. Strongly effervescent, common (~10%) medium CaCO3 threads. Common krotovina. Diffuse smooth boundary.
	3Bkb	115-123	Fine sandy medium silt. 10YR 4/3 (brown). Medium subangular blocky structure, moderately hard consistence. Violently effervescent, common (~ 5%) medium CaCO3 threads. No lower boundary.

present in all units. Sediments at Profile 5 are dominated by bimodally distributed sandy silts. Profile 5 includes two buried paleosols in addition to a weakly developed surface soil. The upper unit (3) shows only an A horizon. Below, the paleosol formed into unit 2 has an A-C sequence. However, the lowest unit (1) exhibits a more well-developed soil sequence with a 20 cm thick upper horizon (3Ab') capping two calcic horizons (3ABkb and 3Bkb).

Study Area East End

The study area east end is approximately 0.32 km^2 and encompasses the eastern edge of site 24BE46 and all of site 24BE52 (Figure 39). It also includes Profiles 11 and 8 (from east to west), and observation points D and E. This sub-area includes the highest elevations in the study area, averaging around 2006 m (6,581 ft.) AMSL. Upland topography is relatively flat-lying with low relief. Three characteristics of the eastern study area are notable. First, cutbank walls in the area are generally very high (average 5-8 m above shoreline) with nearly vertical faces (Figure 40; a - f). Second, exposed stratigraphy is horizontal and contiguous through most of the area. An exception to this generalization is that strata near Profile 8 at the east edge of 24BE52 (just east of a broad south-sloping swale (Figure 40; c and d) are strikingly dissimilar from other east-end beds in terms of color, package thickness, and texture (Figure 40; e and f). Finally, at the west edge of the eastern sub-area, two thin tephra layers are visible within the stratigraphic sequence.

High vertical walls in the center of the east sub-region (Figure 40; b and d) prevented me from safely accessing this area for stratigraphic profiling. Fortunately, I

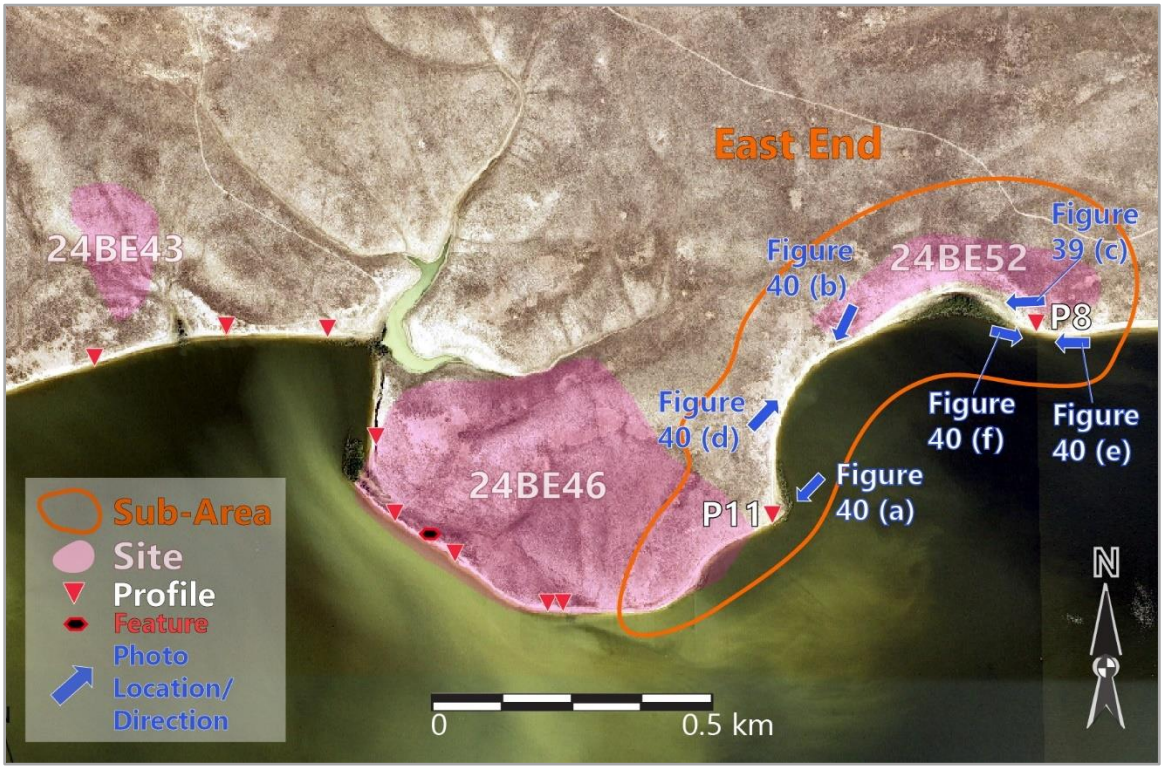

Figure 39. Study area east end.Showing locations of Profiles 11 and 8 and Figure 39 overview photo positions.

was able to trace contiguous strata northeast from Profile 11, where a high talus slope and eroded upland surface made the exposure top accessible. Consequently, my interpretations for much east-end stratigraphy rely on extrapolations from Profile 11. Additionally, the inaccessible beds appear conformable with lower strata described in Observation Points D and E. I therefore base interpretations on these locations as well. Profile and observation point descriptions are given below, from west to east.

Observation Point D

Observation point D (OP-D) marks the location of two buried tephra layers separated by approximately 2 m of vertical stratigraphy (Figure 41). The upper tephra lens is approximately 4 cm thick and the lower about 2 cm. Due to talus cover, I could

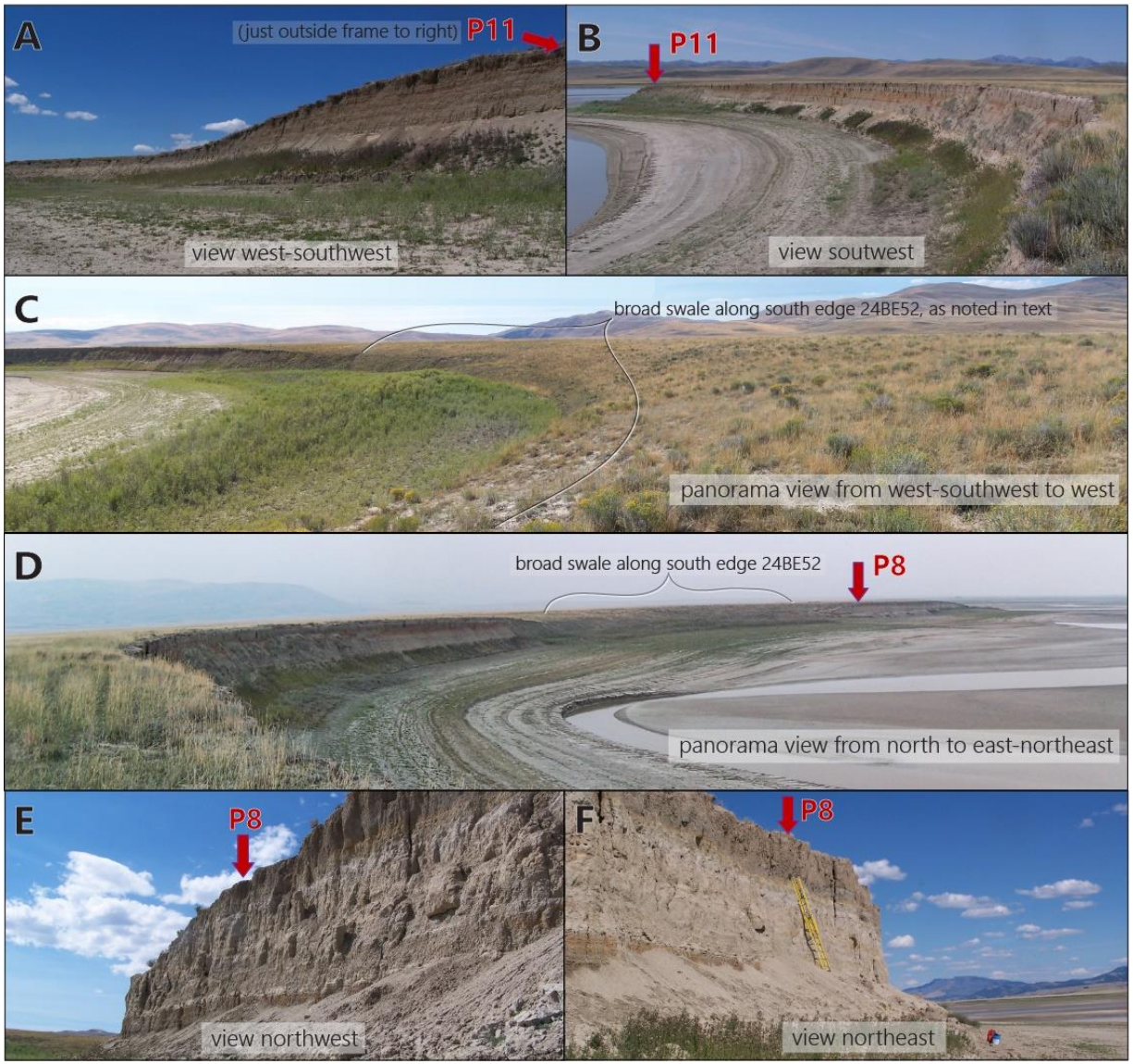

Figure 40. Overviews of study area east end with profile locations indicated. Photo locations shown on Figure 38 map.

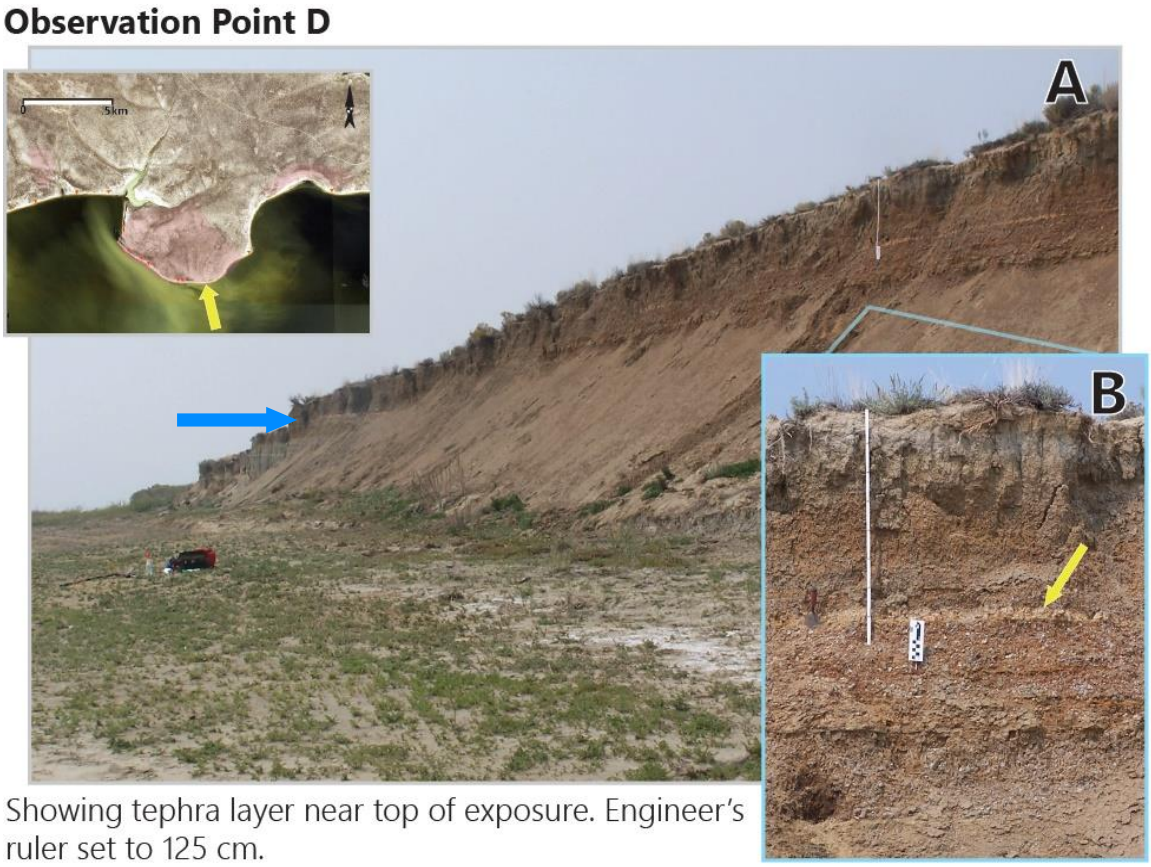

Figure 41. Observation Point D (OP-D) showing two buried tephra layers, view west (a) and northwest (b). Blue arrow (background) shows approximate location of lower tephra exposure. Yellow arrow (inset b) shows upper tephra visible in foreground.

not identify a single vertical section exposing both the upper and lower tephra layers. However, by tracing the intervening horizontal, contiguous strata, I conclude that they are likely part of a conformable sequence.

Profile 11

Profile 11 is about 280 m northeast of OP-D (Figure 42). It is located on a short vertical wall (average > 2 m high) situated at the top of a high talus slope which extends approximately 6 m above shoreline level. The profile top stands at 2005.41 m (6579 ft) AMSL. Profile 11 consists of five units, all medium or fine silt (Figure 43, Table 13). Sediments are overall very fine textured with high clay fractions ranging from 14-21%

Figure 42. Profile 11 overview, view northwest.

clay. Profile 11 strata all rank within the top 20th percentile of clay proportions for study area sediments (Appendix B). Soil development is weak and limited to the surface horizon. Given high clay contents and parallel horizontal bedding, it is assumed Profile 11 strata were deposited in one of the lowest energy depositional environments represented in the study area.

An OSL sample from 73 cmbs in unit 2 produced an age of 51.90 ± 8.75 (USU-2188), much older than cultural occupation. It is unknown whether overlying units 3, 4, and 5 could be occupation age. However, given similarities in color, texture, structure, redoximorphic alteration and boundary orientation among the five units (Table 13), the packages appear conformable and to have developed in similar environments. It is therefore unlikely that the upper units formed within a cultural timeframe.

Profile 11

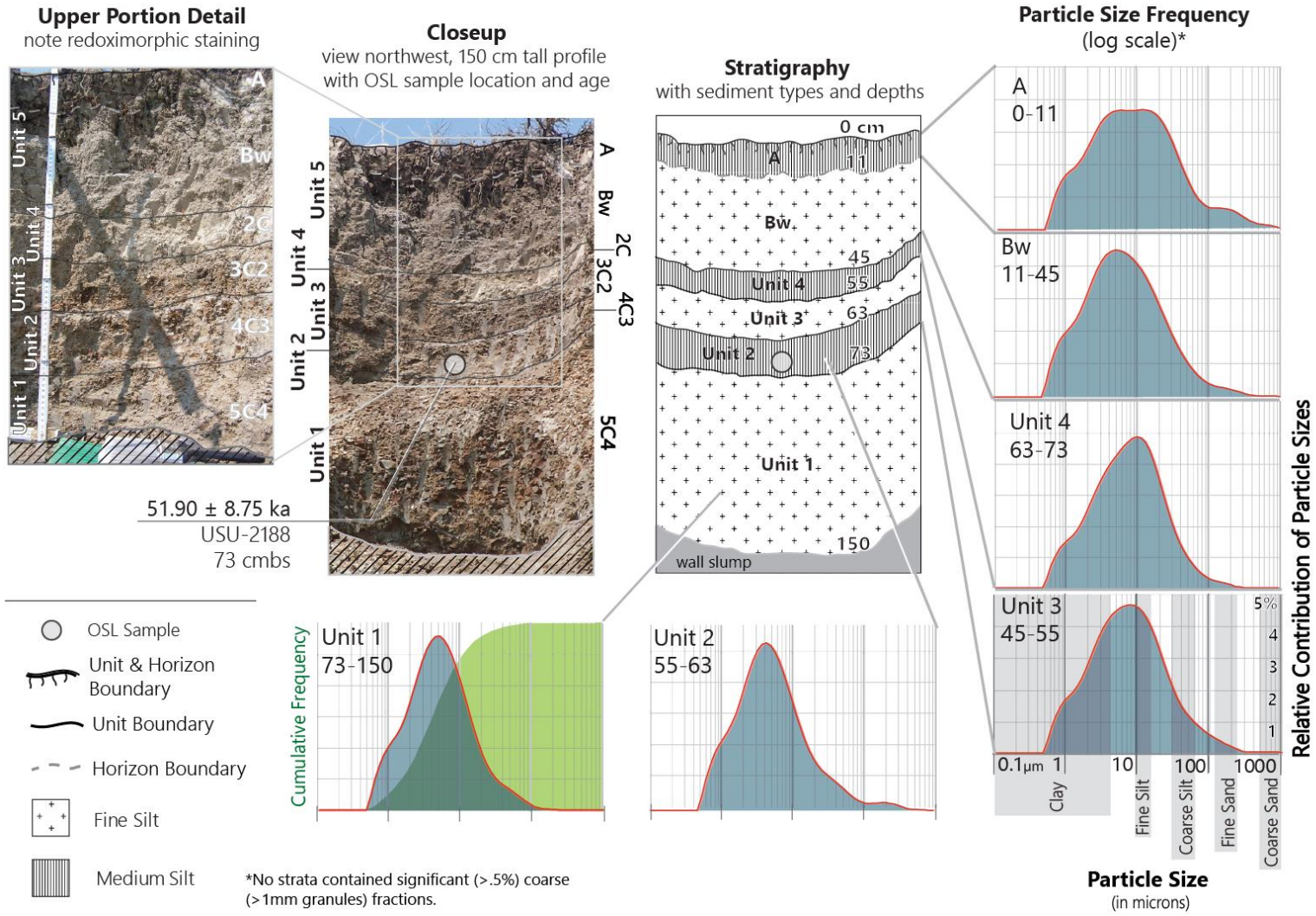

Figure 43. Profile 11 detail including stratigraphy, OSL, and granulometry data.

Table 13. Profile 11 stratigraphic descriptions.

Unit	Horizon	Depth (cmbs)	Description
Unit 5	A	0-11	Medium silt. 10YR 4/2 (dark grayish brown). Medium subangular blocky structure, soft consistence. Strongly effervescent. Approximately 15% organic content. Gradual wavy boundary.
	Bw	11-45	Fine silt. 5Y 7/1 (light gray). Coarse subangular blocky structure, hard consistence. Strongly effervescent. Clear smooth boundary.
Unit 4	2C	45-55	Medium silt. 2.5Y 6/6 (olive yellow, ped outsides) 5Y 8/2 (pale yellow, ped insides). Fine angular blocky structure, moderately hard consistence. Slightly effervescent. Clear smooth boundary.
Unit 3	3C2	55-63	Fine silt. 7.5YR 5/4 (brown, ped outsides), 5Y 6/3 (pale olive, ped insides). Fine angular blocky structure, moderately hard consistence. Very slightly effervescent. Prominent redoximorphic concentrations cover 100% of ped surfaces. Abrupt smooth boundary. *Note*: This unit is very similar to Unit 1, but with finer ped structures. Unit 3 also appears more red when naturally weathered (not freshly faced).
Unit 2	4C3	63-73	Medium silt. 10YR 6/4 (light yellowish brown, ped outsides), 5Y 7/1 (light gray, ped insides). Medium angular blocky structure, moderately firm consistence for individual peds (but unit is friable overall). Slightly effervescent. Few (~ 1%) fine gypsum masses throughout with higher gypsum concentration in top 1 cm of unit. Abrupt smooth boundary. *Note*: Bed appears lighter (more buff colored) when weathered.
Unit 1	5C4	73-150	Fine silt. 5YR 4/4 (reddish brown, ped outside), 5Y 5/2 (olive gray, ped inside). Medium angular blocky structure, hard consistence. Very slightly effervescent. Few (~1%) fine gypsum masses throughout. Prominent redoximorphic concentrations on 100% of ped surfaces. No lower boundary. *Note*: This unit appears strikingly red when weathered.

Profile 11 strata have a markedly 'striped' appearance with texture and color alternating between units (Figure 43). In terms of texture, unit 1, unit 3, and horizon Bw (from bottom to top) are composed of fine silt. In comparison, unit 2, unit 4, and horizon A consist of medium silt (Table 13). Strata color alternates between darker shades of reddish or olive brown (associated with fine silt packages) and lighter hues of light yellow or gray (associated with medium silt units). Color variation between ped faces and ped insides indicates redoximorphic oxidation is at least partially responsible for strata hues. However, it is not known whether, for instance, fine silt and dark red colors correlate because different sediment bodies react disparately to saturation conditions or because strata were deposited in dissimilar conditions. Regardless, these distinct bed sets provide a clear visual indicator for identifying strata in the field that substantially pre-date human occupation. This is especially true given that color variations are more pronounced in weathered exposures than in freshly faced sediments. These characteristics, easily visible from a distance, could potentially provide a useful marker of pre-occupation deposits in the valley.

Observation Point E

Observation Point E (OP-E) is located approximately 70 m north of Profile 11. It shows variable sequence stratigraphy and facies transitions through time (Figure 44). Although isolated wall slumps prevent certainty, strata in the upper ~ 1.5 m of the OP-E exposure (a) appear contiguous with Profile 11 units. Similarities include alternating dark (red) and light redoximorphic color variations concordant with texture changes. Field texturing reveals these beds are silt-dominated but clay-rich. Below these bed sets, lower strata (Figure 44, b) exhibit sand-dominated crossbedding, including flaser structures. Such

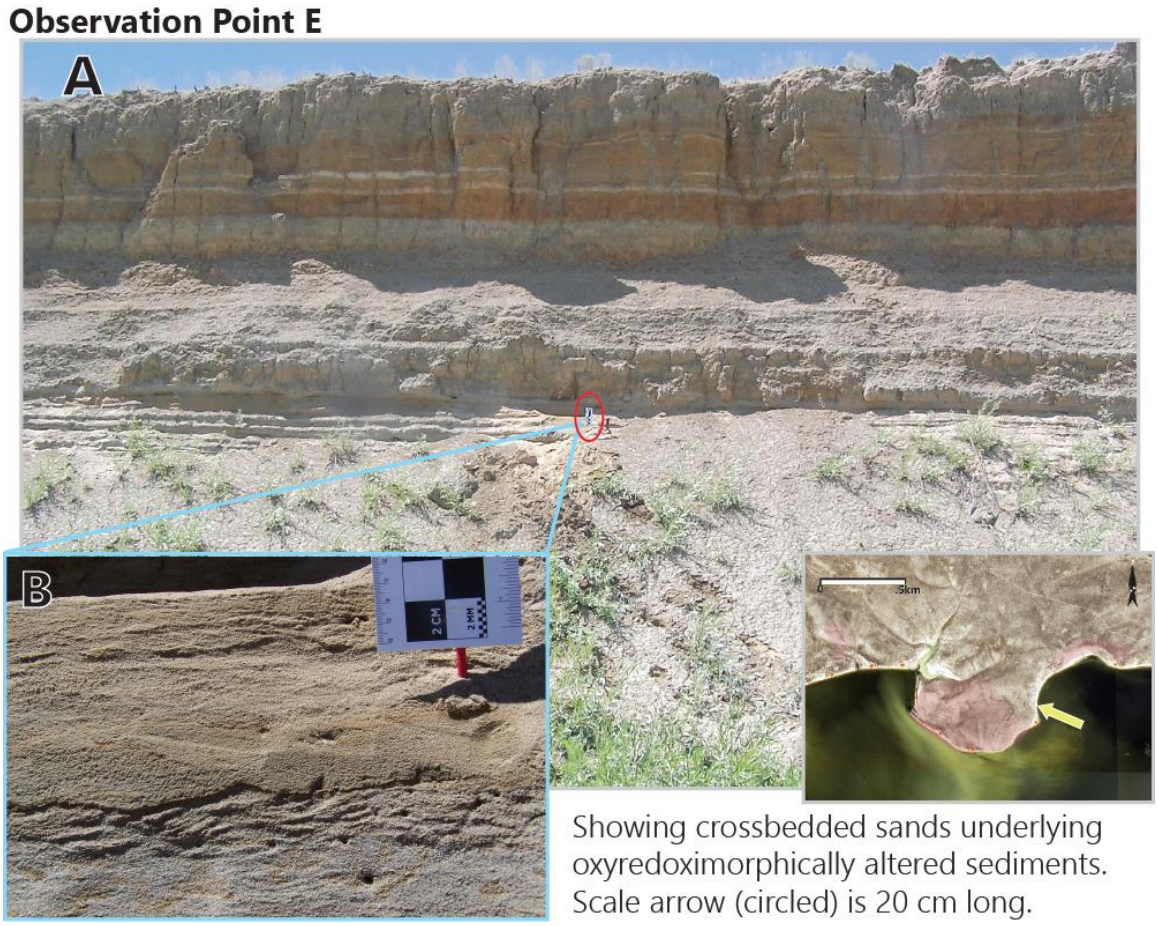

Figure 44. Observation Point E (OP-E) showing upper silt beds contiguous with Profile 11 over crossbedded sands.

facies transitions could signal a change from shallow to deep water at this location. Assuming continuity between upper OP-E and Profile 11 strata, this transition would have taken place prior to ~ 52,000 years ago.

Profile 8

Profile 8 is located at the far east end of the study area, within site 24BE52 (Figure 45). The profile is situated on an approximately 5 m high exposure with a top elevation of 2006.31 m (6582 ft). Profile 8 consists of seven units and soil development is present only in the uppermost unit 7 (Figure 46, Table 14). An OSL sample (USU-2049)

Figure 45. Overview of Profile 8, view north-northeast.Ladder is 3.9 m (13 ft) for scale.

collected from near the base of unit 7 (at 136 cmbs) yielded an age of 14.35 ± 2.01 ka, within a cultural timeframe. This is the only OSL sample outside of the central sub-area to produce an occupation-age date. Notably, unit 7 is occupation-age but lies approximately 6 to 8 m (20 to 26 ft) higher in elevation other early cultural time frame packages in the study area. This outlier cultural-age stratum may provide clues regarding the late Pleistocene geomorphic history of the study area and its significance is examined more fully in the following Discussion chapter.

Profile 8 sediments are dominated by coarse and medium silts but also include fine sand (Table 14). Package structures are dominantly depositional with little to no pedogenic alteration except in the uppermost unit. Previous inundation is indicated by redoximorphic staining in units 1, 2, 3, and 5 (from bottom to top). Additionally, unit 4

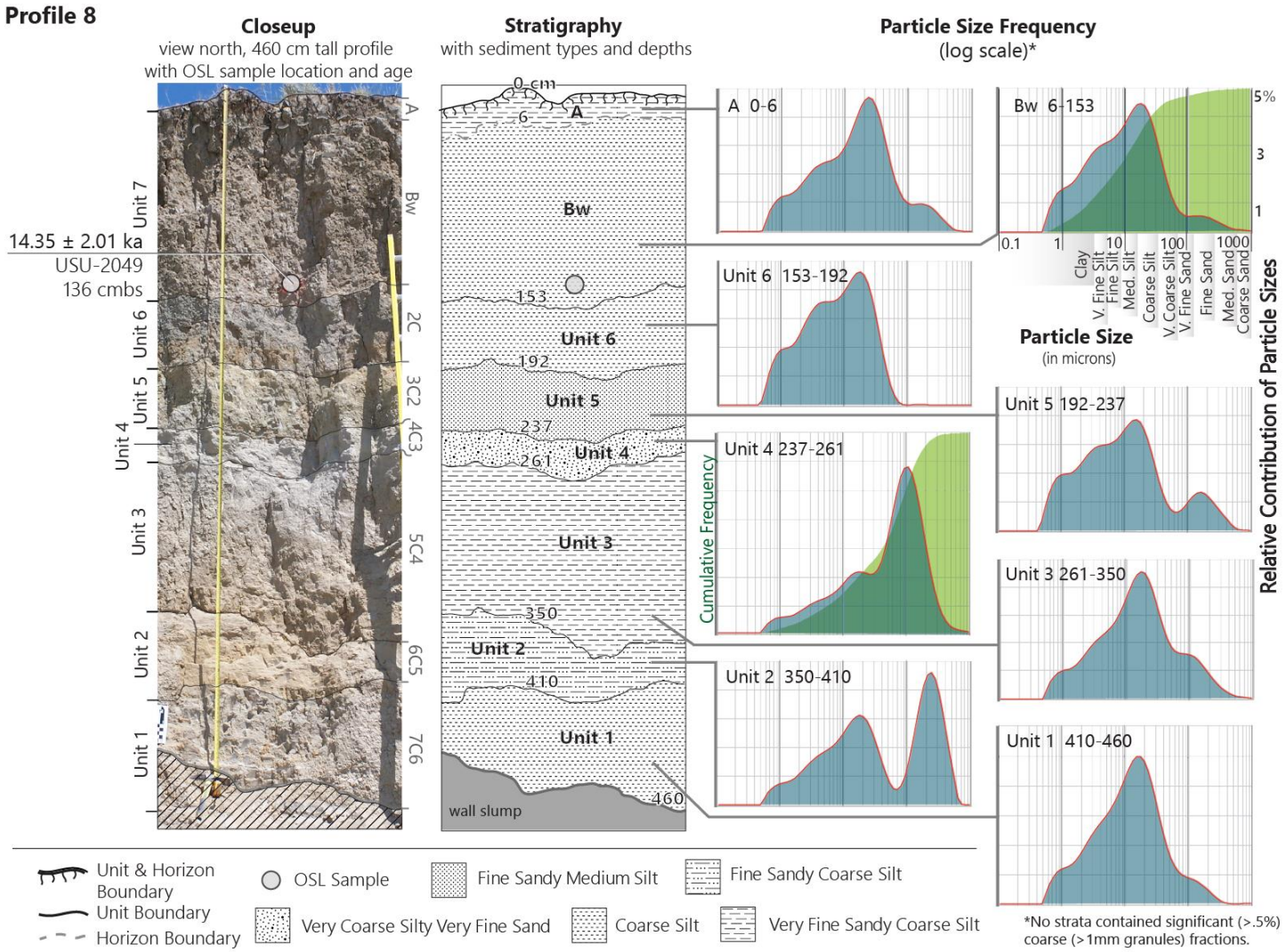

Figure 46. Profile 8 stratigraphy, OSL sample location and particle size distribution metrics. Note that particle frequency diagrams are presented at equivalent scales but with differing vertical extents.

Table 14. Profile 8 stratigraphic descriptions.

Unit	Horizon	Depth (cmbs)	Description
Unit 7	A	0-6	Very fine sandy coarse silt. 10YR 5/2 (grayish brown). Fine granular structure, soft consistence. Violently effervescent. Diffuse wavy boundary.
	Bw	6-153	Coarse silt. 2.5Y 6/2 (light brownish gray). Medium prismatic parting to medium angular blocky structure, hard consistence. Strongly effervescent. Clear wavy boundary.
Unit 6	2C	153-192	Coarse silt. 5Y 7/3 (pale yellow). Structureless (single grain), moderately hard consistence. Strongly effervescent. Clear wavy boundary. *Note*: Clasts are small (~2-4mm) aggregates of weakly cemented fine sediment, similar to rip-up clasts.
Unit 5	3C2	192-237	Fine sandy medium silt. 5Y 6/3 (pale olive) with faint redoximorphic yellowing at unit top. Cross-stratified structure, moderately hard consistence. Strongly effervescent. Clear smooth boundary. *Note*: Clasts are small (~1-2mm) aggregates of weakly cemented fine sediment. Unit 5 also includes thin lenses of contrasting finer and coarser sediments.
Unit 4	4C3	237-261	Very coarse silty very fine sand. 5Y 7/1 (gray). Cross-stratified structure, slightly hard consistence. Strongly effervescent. Clear smooth boundary. *Note*: Small (~ 3 mm) bivalve mollusk macrofossils present throughout.
Unit 3	5C4	261-350	Very fine sandy coarse silt. 5Y 7/2 (light gray), with increased redoximorphic reddening toward bottom. Structureless (massive) in upper 2/3, transitioning to parallel laminated, moderately hard consistence. Strongly effervescent. Clear smooth boundary. *Note*: Unit 3 is composed of thin repeating sediment lenses.
Unit 2	6C5	350-410	Fine sandy coarse silt. 5Y6/2 (light olive gray) with faint redoximorphic staining in unit interior. Moderately hard consistence, cross-stratified structure. Strongly effervescent. Diffuse wavy boundary. Sand is sub-rounded spherical.
Unit 1	7C6	410-460	Coarse silt. 5Y 7/2 (light gray, matrix color). Matrix color is mottled with ~ 50% 10YR 6/6 (brownish yellow) redoximorphic concentration masses. Fine subangular blocky structure, moderately hard consistence. Strongly effervescent. No lower boundary.

includes small (~3 mm) bivalve mollusk macrofossils. Such macrofossils are possibly indicative of a lacustrine depositional environment (James and Dalrymple 2010).

Granulometric Comparison of Study Area and Control Sediment Samples

Reconstructing the area's geomorphic history first required stratigraphic profiling and establishing age control to identify occupation age sediment packages. My next step was determining what geologic processes deposited cultural age sediments to outline criteria for identifying target units in the field. I was also interested in determining the depositional circumstances of high energy and pre-occupation packages in order to recognize 'fatally flawed' units. I established likely depositional mechanisms using both qualitative (i.e. stratigraphic description and landform mapping), and quantitative approaches. A key quantitative approach for assessing depositional environment was granulometric analysis and comparison of study area sediments with known-origin control samples.

The typically complex histories of sediment bodies and variability in factors such as source material lithology, deposit reworking, and transport medium velocity and turbidity demonstrates that no simple relationship exists between depositional environment and particle size distribution (Gale and Hoare 1991, Tanner 1991). Particle characteristics such as sorting, texture range, and modality can vary widely for a given transport process and considerable overlap may occur, especially at the interface between depositional environments. Moreover, pedogenic processes (particularly lessivage) and other forms of post-depositional disturbance serve to further muddle interpretations. While acknowledging these limitations, generalizations can be made regarding how grain

size distributions typically relate with environment and granulometry therefore provides another line of evidence for discerning depositional mechanism (Gale and Hoare 1991:68).

In order to use granulometric data to help infer depositional environment, I statistically compared sediment samples from the 79 study area strata with 21 control samples collected from known environments. Study area deposits likely formed in late Quaternary eolian, alluvial, or lacustrine contexts (Lonn et al. 2000, Majerowicz et al. 2010; Scholten et al. 1955) and I selected comparative samples accordingly. As much as possible, I chose comparative samples with age and climate histories analogous to the study area. Although many variables were beyond my control, I sought deposits laid down in the late Quaternary in valleys flanking the western edge of the northern Rocky Mountains. With one exception, my control samples come from valleys, which had supported, at varying times; pluvial lakes, glacial melt-fed streams and deflated lake and river terrace deposits which in turn left fine sediments available for wind transport.

I obtained five eolian sediment control samples; three dune sand and two proximal loess (Figure 47). The loess specimens and two of the dune samples were collected in the St. Anthony dune field of eastern Idaho, approximately 80 kilometers southeast of Centennial Valley. The proximal loess samples (#s PL-RF7-60 and PL-MO4-100) date between about 8,000 and 3,000 cal B.P. (Rich et al. 2015; Tammy Rittenour personal communication April 12, 2017). The specimens were collected from eolian deposits close to deflated Snake River Plain sediment sources and thus have substantial fractions of both silt (44% and 62%, respectively) and sand (52% and 35%) (Figure 47; a, Appendix B). Unlike more distal loess deposits, proximal eolian sediments

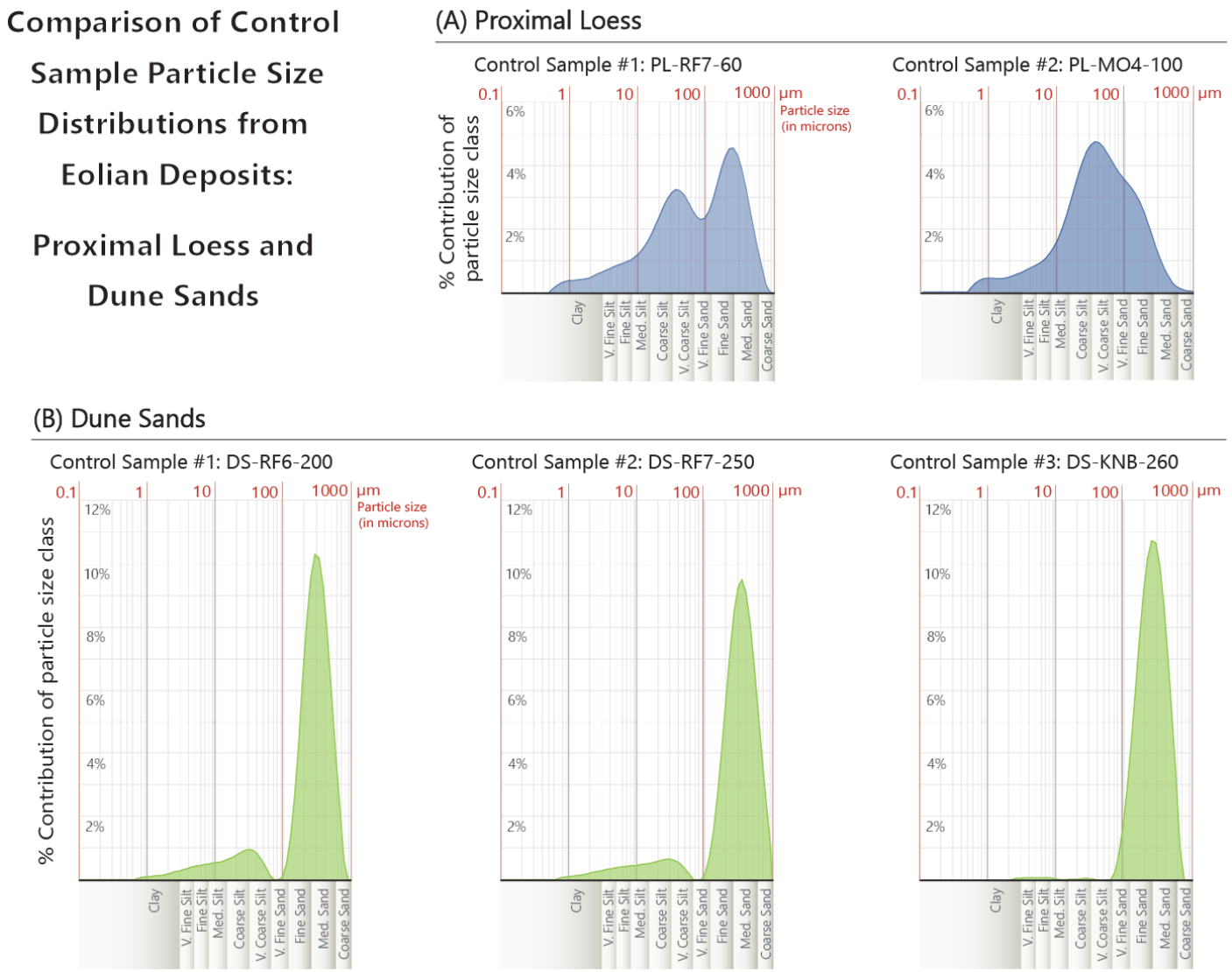

Figure 47. Eolian (proximal loess and dune sands) control sample comparisons.

are often poorly sorted because clast transport results from a combination of suspension, saltation, and creep (Pye 1987:121). Overall, mean grain size decreases linearly according to increased distance from source but overlapping or variable depositional mechanisms tend to produce multimodal size distributions as is evident for sample PL-RF7-60 (Bagnold 2005:118 [1954]) (Figure 47; a).

The two Idaho dune samples (#s DS-RF6-200 and DS-RF7-250) also date within the range of about 8,000 and 3,000 cal B.P. These sediments were taken from more highly winnowed barchan dunes formed farther from the Snake River's previous course. The Idaho dune sand samples are therefore more well-sorted and contain much higher sand (85% and 88%, respectively) versus silt (14% and 11%) fractions (Figure 47; b, Appendix B). The third dune sample (DS-KNB-260) is from about 13 kilometers northwest of Kanab, in southern Utah. It was collected from mid-Holocene dunes composed of weathered and reworked Navajo sandstone; a Jurassic formation consisting of fossilized eolian sand dunes (Fillmore 2000). Although this control sample is not directly analogous to my expectations for Centennial Valley's previous climate and available sediment sources, I included it as an extreme comparative example of well-sorted eolian dune sands. The sample is composed of 99% sand, 46% of which is medium sand.

I obtained all of the lacustrine and alluvial control sample sediments during fieldwork for USU's Soil Genesis, Morphology, and Classification course in the fall of 2015. The deep and shallow lacustrine and higher energy alluvial samples were collected from the walls of mechanically excavated pits while the lower energy alluvial sediments were obtained using a manual sediment corer. All samples are from Cache Valley, Utah

locations. The four shallow lacustrine control samples (sample #s SL-PRS-11, SL-PRS-73, SL-PRS-135, and SL-PRS-166) come from the east margin of Cache Valley, just north of the Blacksmith Fork River, near Millville (Figure 48; a, Appendix B). Samples were collected from three sediment packages of shallow lake sediments likely deposited during, and just prior to, Lake Bonneville's highstand around 18.5 ka (Benson et al. 2011; Evans et al. 1996; Janecke and Oaks 2011). The upper three samples (SL-PRS-11, SL-PRS-73, and SL-PRS-135) were likely deposited during the highstand, while the lowest package (SL-PRS-166) was deposited earlier. The upper three samples exhibit similar grain size distributions and are dominated by coarse and very coarse silt (ranging from ~18% to 28%) with sand making up about 9% to 16%. The lowest, oldest sample is considerably coarser and contains approximately 59% sand. If this package was deposited just prior to the highstand, it would have been laid down in shallower water and therefore more influenced by Blacksmith Fork River prodelta coarse sediment influxes.

The four deep lacustrine samples (#s DL-EFA-21, DL-EFA-52, DL-EFA-88, DL-EFA-146) were collected about 1.5 km southwest of Providence and about 4 km from the east edge of Cache Valley. The samples were taken from medium to fine-textured, moderately deep-water lake sediments positioned on a former low lake terrace of lake Bonneville (Web Soil Survey 2015; Williams 1962). They likely date to around the time of the Bonneville highstand. These sediments are dominated by medium-to-coarse silt with very little sand present (~1 to 4%) (Figure 48; b). These sediments also contain the highest clay fractions among all of the control samples, ranging from 9% to 14%.

The higher energy alluvial control samples (#s HEA-AWT-24, HEA-AWT-70, HEA-AWT-89, and HEA-AWT-141) (Figure 49, a) were collected about 3.3 km

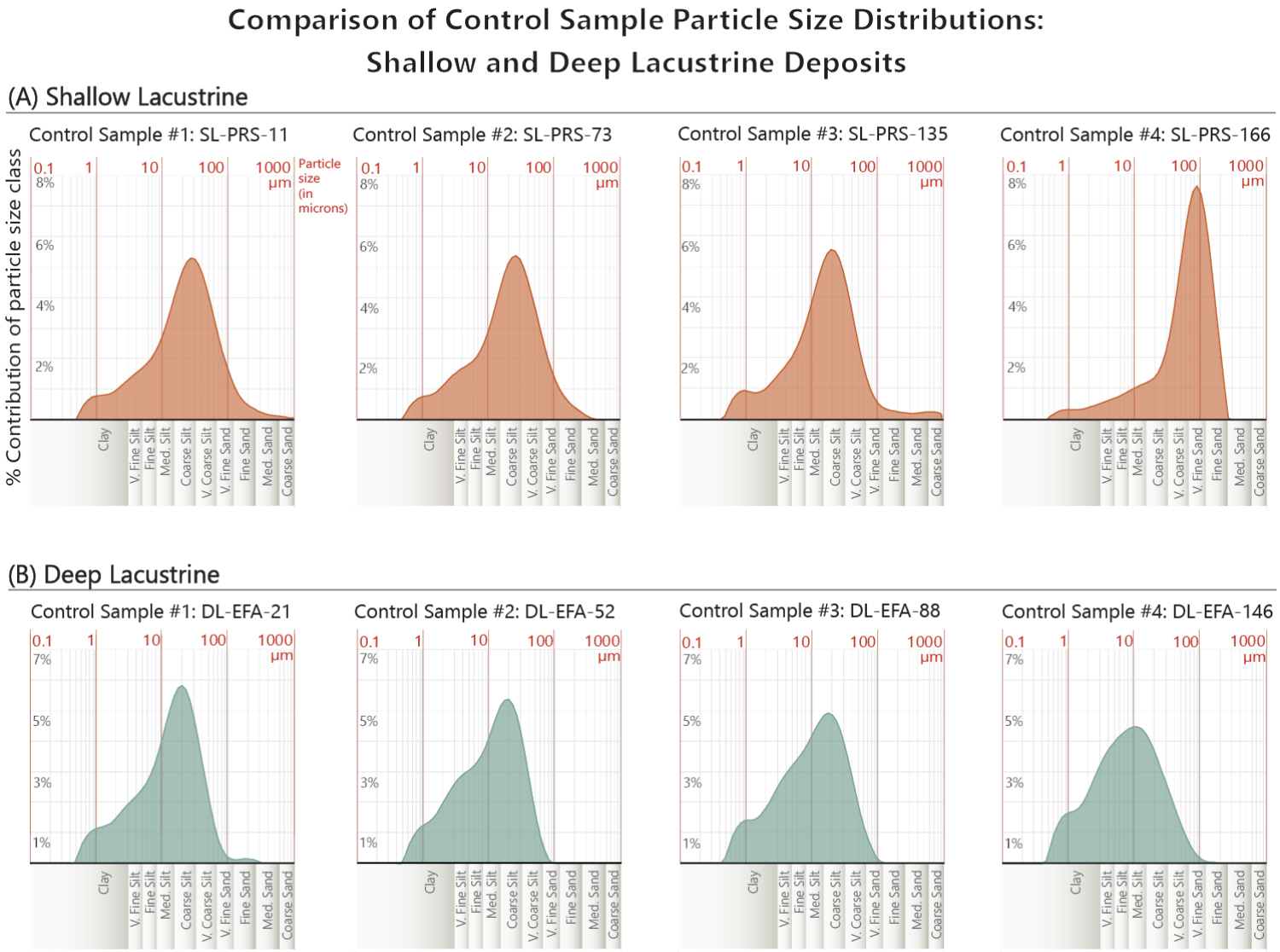

Figure 48. Lacustrine (shallow and deep) control sample comparisons.

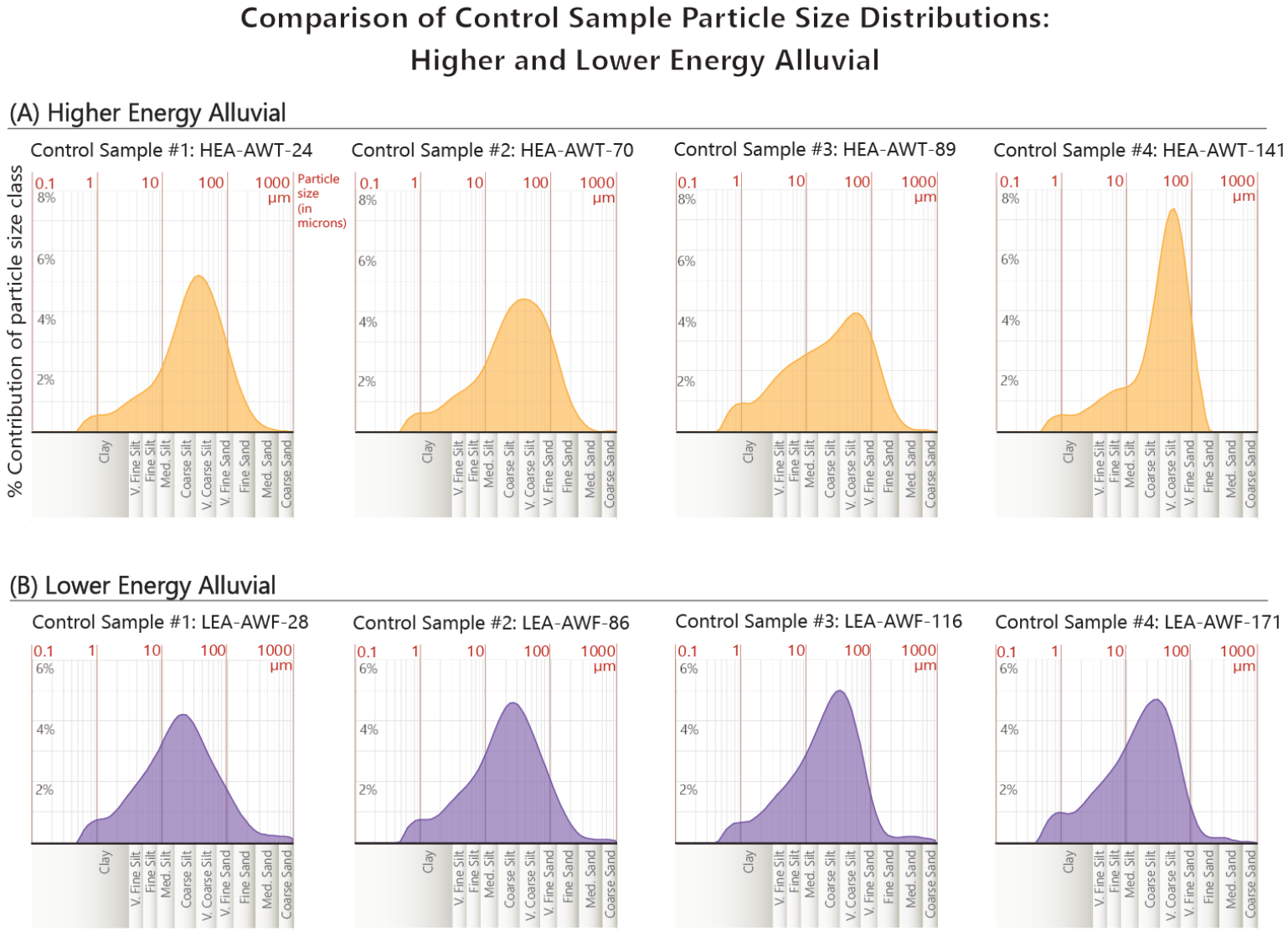

Figure 49. Alluvial (higher and lower energy) control sample comparisons.

northeast of Wellsville, Utah from a Little Bear River T2 terrace situated approximately 8 m above the modern channel (Google Earth 2017). The river terrace sediments were laid down some time after the Bonneville flood during late Pleistocene glacial retreat (Barker and Barker 1993; Janis Boettinger, personal communication April 11, 2017; Williams 1962). The deposits likely derive from overbank flood events when the ancestral Little Bear River was a steeper, higher energy stream with greater competency and coarser available sediment load than present. These factors resulted in somewhat sandier deposits than present in the modern floodplain.

I collected the lower energy alluvial control samples (#s LEA-AWF-28, LEA-AWF-86, LEA-AWF-116, and LEA-AWF-171) (Figure 49, b) from Holocene Little Bear River floodplain deposits about 1 m above the modern channel. The sampling site is approximately 3 km northeast of Wellsville and 0.5 km west of the higher energy alluvial terrace collection location noted above. Based on discernable buried epipedons, the floodplain samples derive from at least three separate sediment packages. The lower energy alluvial samples exhibit more uniform grain size distributions with somewhat finer central tendencies than the nearby higher energy alluvial terrace deposits (Figure 49, Appendix B). The Wellsville floodplain samples may have finer textures than terrace samples for two reasons (Barker and Barker 1993; Evans et al. 1996; Janis Boettinger, personal communication April 11, 2017). First, the modern river is likely a lower energy, lower competency stream than the ancestral Little Bear River as it is no longer fed by melting alpine glaciers and carrying glacial outwash load. Second, the modern channel is incised into lower, deeper water Lake Bonneville sediments so floodplain deposits include reworked deep-lake muds. Conversely, geologic mapping and excavated soil pits

in the vicinity (Janis Boettinger, personal communication April 11, 2017) show that sampled terrace sediments overlie older alluvium rather than lacustrine sediments meaning that the terrace deposits likely don't include much reworked lake mud.

Statistical Comparison Between Control and Study Area Sediments

Quantifying the particle size distributions of eolian, lacustrine and alluvial control samples helped me establish baseline textural expectations for sediments deposited in those environments. However, I must be able to differentiate among control samples in order to use them for study area sediment comparison (Figure 50). Unfortunately, there is substantial overlap between attributes of some control samples and internal variation among samples from the same environment complicates differentiation between environments (i.e. Figure 50; c and e). The small size of my control sample group is partly responsible for these issues. I therefore attempted to bootstrap my control data by using nine aliquots of each sample in order to create a bivariate plot of sample attribute spread. I explored combinations of various GSD attributes (including median, D_{10} and D_{90} cumulative percentages, mean diameter volume, and mean diameter surface area) to determine which parameters produced the tightest sample clustering. I determined that comparing samples' uniformity (absolute deviation from mean) against specific surface area (total surface area of a material per unit of mass) produced the greatest level of differentiation within a scatterplot (Figure 51). The control sample scatterplot illustrates that the dune sand, proximal loess, and deep lacustrine control samples can be differentiated from other environment types and do not overlap with other deposits' uniformity or specific surface area attributes. However, higher and lower energy alluvial

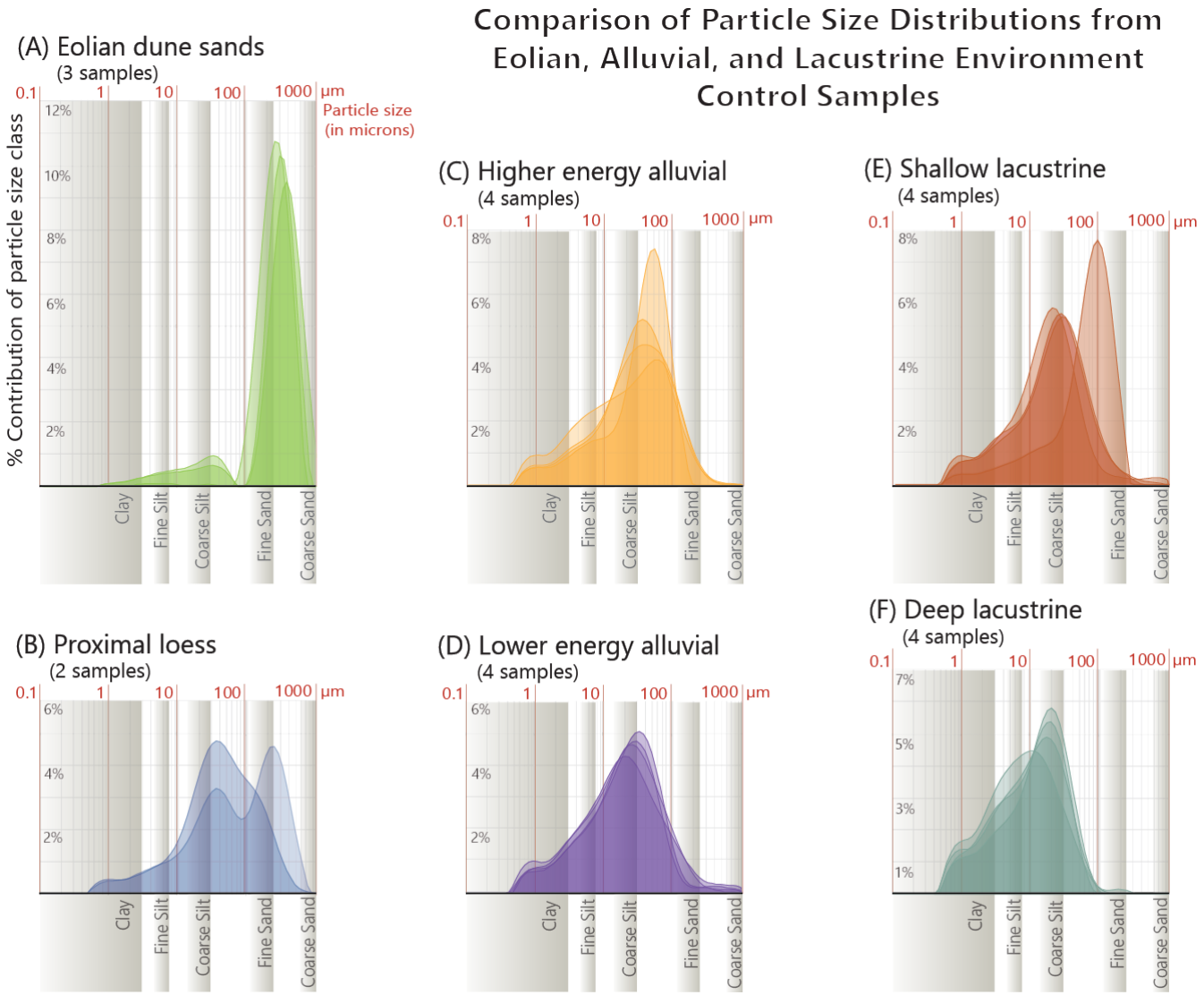

Figure 50. Stacked distribution curves for the six sub-environment control samples, ordered coarsest to finest.

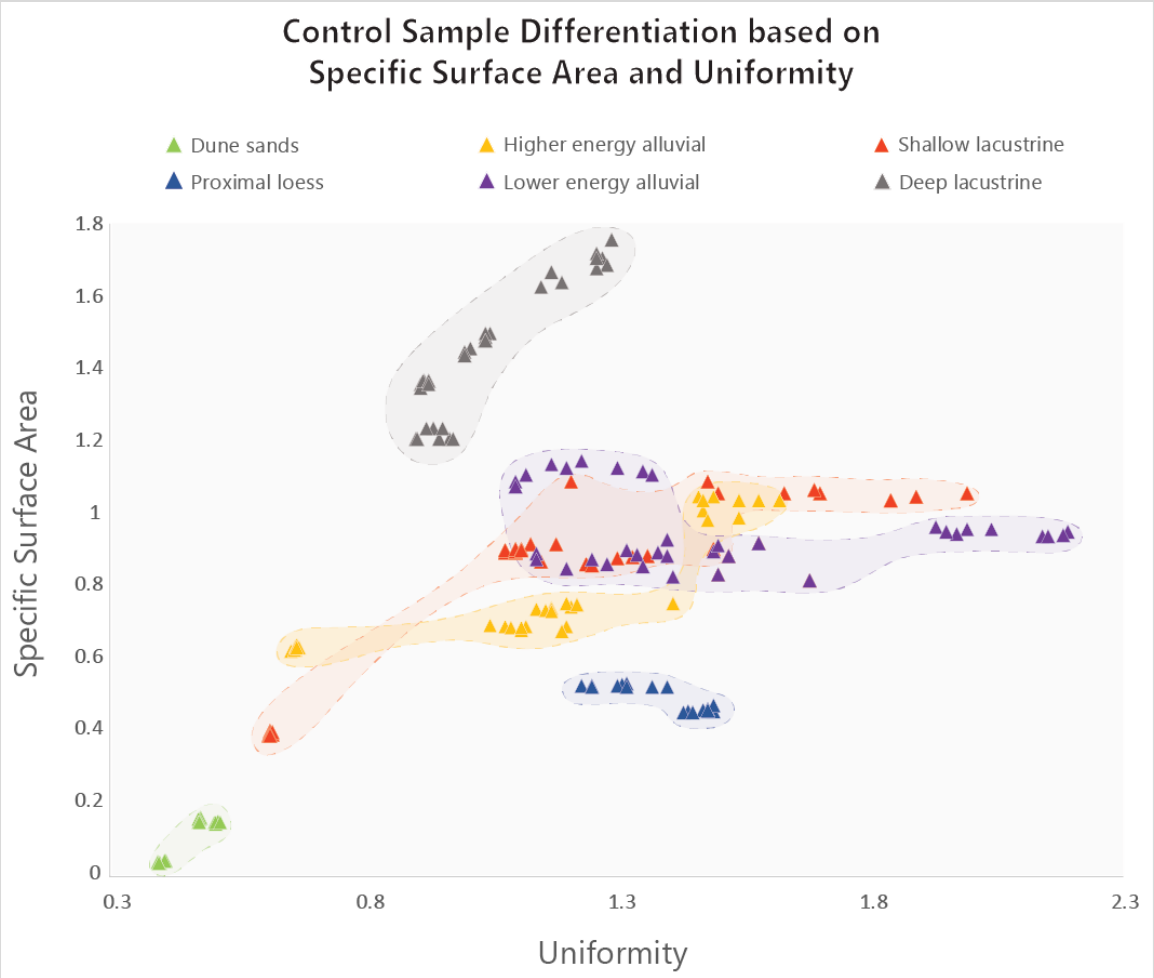

Figure 51. Scatterplot of control sample aliquots based on specific surface area and uniformity.

and shallow lacustrine samples show substantial overlap. Still, the samples are distinguishable, particularly at the scatter extremes. This analysis illustrates that control samples are discernable enough to be of some utility for study area sample correlation in order to determine depositional environment.

In order to determine associations between study area and control sample GSDs, I conducted a hierarchical cluster analysis comparing nine GSD metrics (span, residuals, volume and surface weighted mean, specific surface area, uniformity, and D_{90}, D_{50}, and D_{90} cumulative percents) of the samples in IBM SPSS v.20. I chose Ward's clustering

method and Euclidean distance measure, appropriate for interval level data (Field 2013). Given wide ranges in variance, I also chose to standardize the cases using Z-scores. The resulting dendrogram illustrates the degree of similarity among control and study area samples. It shows a close association between deep lacustrine sediments and many strata in west-end Profiles 9, 6, and 1 (Figure 52). Other strata, including many from Profiles 2 and 5 do not correlate strongly with any control samples. In the following Discussion chapter, I use these associations to help infer profile stratigraphic sequences and build a sequence of geomorphic events in the study area.

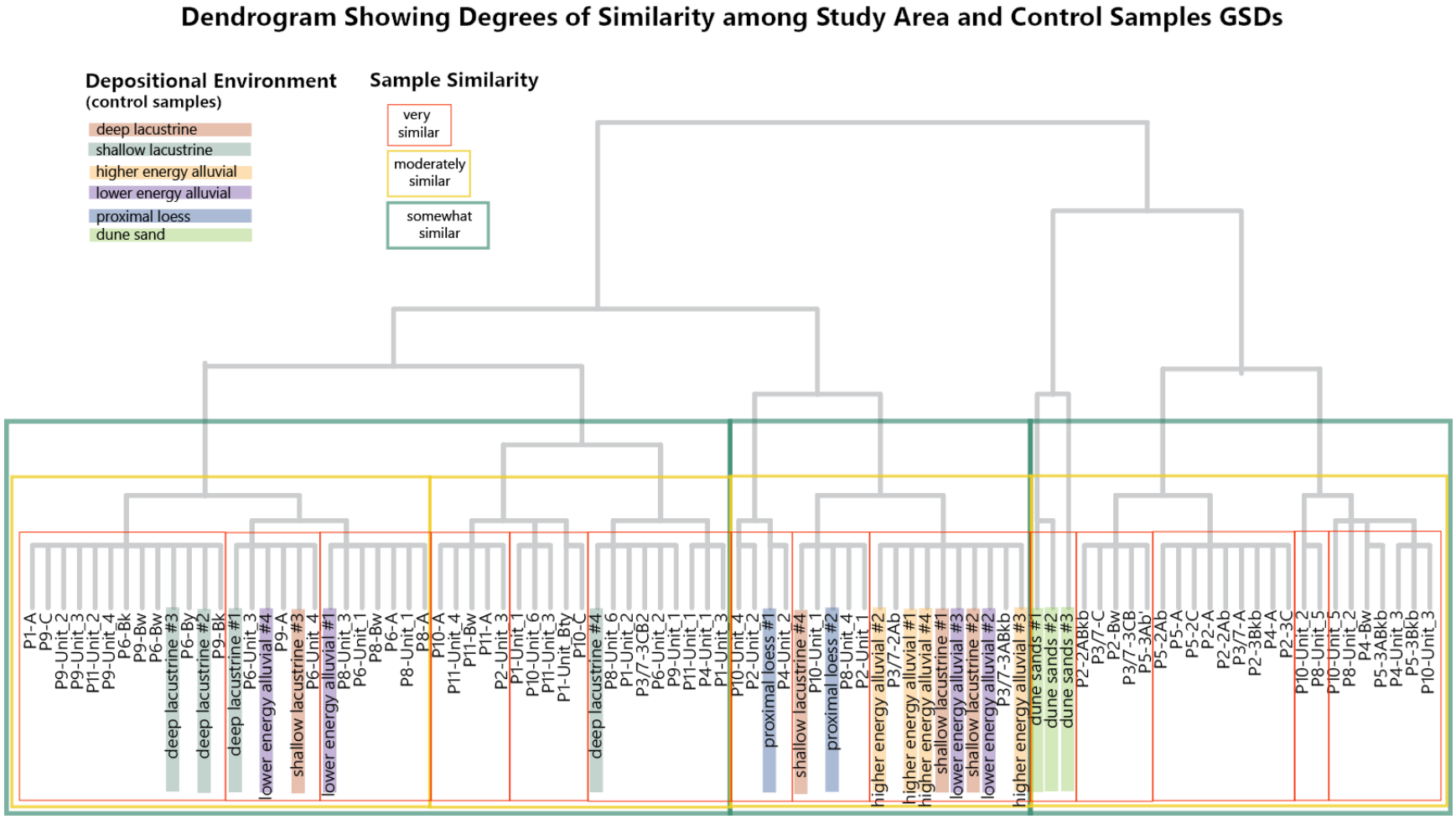

Figure 52. Dendrogram of control and study area sediment sample associations.

CHAPTER FIVE:

DISCUSSION

The final step for determining criteria of regional cultural age and pre-cultural sediment packages is to synthesize stratigraphic, OSL, and granulometry results into a late Quaternary geomorphic sequence of events for the study area. Based on dated sediments, the geomorphic event sequence spans roughly the last 60,000 years, but my data and analysis emphasize late Pleistocene and Holocene deposits with archeological potential. This chapter integrates trends and age relationships across the west, central, and east sub-regions, first detailing pre-occupation age (> 14,000 cal BP) and then cultural age (≤ 14,000) events and deposits. I used chronometrically dated sediments, relative age relationships, and, to a lesser extent, GSD correlations to infer age relationships and associations between strata in different profiles (Figure 53). For simplicity, Figure 53 shows age associations color-coded according to three broad age classes: Occupation Age (≤ 14 ka), Late Wisconsin Pre-Occupation (ca. 28 - 14 ka), and Middle Wisconsin Pre-Occupation (ca. 71 - 28 ka) (Schoeneberger et al. 2012). Note that packages with uncertain but inferred ages are shown with hash lines over the age-coded color. In the following discussion, I center on chronometrically age-controlled strata and then extrapolate the relative timing of undated deposits while evaluating possible sources of error for my interpretations. Simultaneously, I examine likely depositional environments of these packages based on field observations and granulometry results (Figure 52) in order to reconstruct a possible landscape evolution scenario for the late Quaternary Centennial Valley.

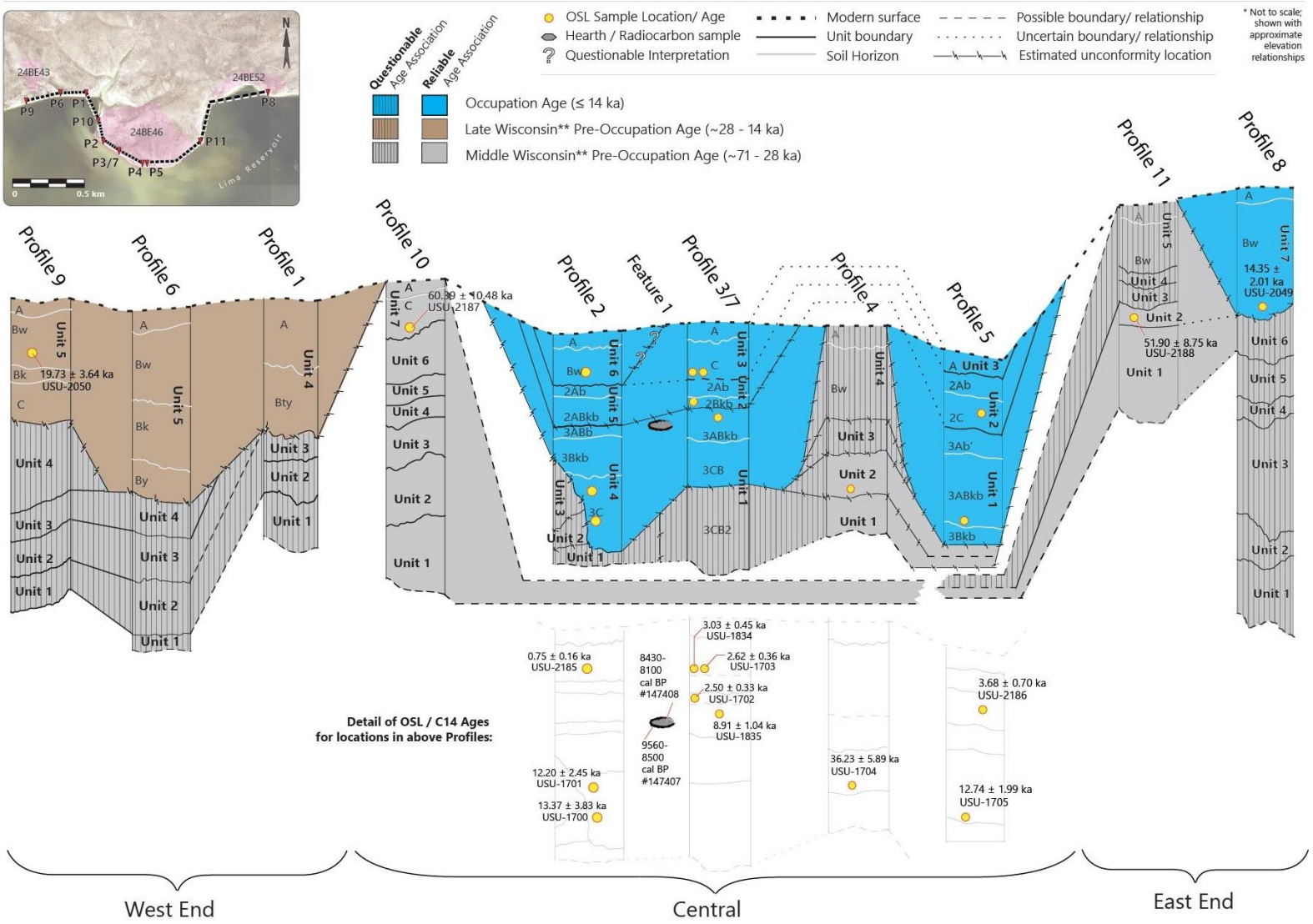

Figure 53. Fence diagram showing schematic age relationships of study area strata inferred from stratigraphic profiles.

Middle Wisconsin Pre-Occupation Age Deposits: ca. 71,000 to 28,000 cal BP

The west, central and east sub-regions all contain near-surface strata (60-95 cmbs) pre-dating a cultural time-frame. The oldest dated stratum in the study area is in the uppermost package of Profile 10 (C horizon of Unit 7). Unit 7 in Profile 10 (P10-U7) dates within the Middle Wisconsin at 60.39 ± 10.48 ka (USU-2187, elevation 2001.3 m AMSL). The unit consists of medium silt with a bimodal distribution and relates moderately with the Deep Lacustrine #4 control sample (the most clay-rich), though not closely with any control. No sedimentary structures were visible in P10-U7 to help infer depositional environment. Unit 7 caps six older packages that exhibit a heterogenous array of facies, generally coarser and more poorly sorted than sediments in other mapped exposures. Based on granulometry, lower units are a succession of (from bottom to top) fairly well-sorted proximal loess and/or near-shore very fine sands (unit 1), bimodal sandy deposits, which may represent eolian dunes (units 2 and 3), more well-sorted sands that correlate closely with eolian dunes (unit 4 with 82% sand), gravel-dominated braided stream or delta deposits (polymodal unit 5 with 36% gravel, 31% sand, and 33% mud), and deep lacustrine clay and fine silts (unit 6) (Appendix B, Figures 28 and 52). Finally, in addition to lacustrine-like facies in units 6 and 7, previous inundation is indicated by soft sediment deformation structures in a stratum that correlates with unit 2 about 50 m to the east-southeast (at OP-C) (Bridge and Demicco 2008:471) and redoximorphic color alteration of the lowest units 1 and 2.

Unit 2 of Profile 11 (P11-U2) in the study area east end produced another Middle Wisconsin age, which overlaps that of P10-U7, but with a somewhat younger range. P11-

U2 dates to 51.90 ± 8.75 ka (USU-2188, elevation ~2004.7 m AMSL). Profile 11 strata all appear to be lacustrine in origin. The units are flat-lying with consistent thicknesses, traceable on the high east-side wall for over 300 m to the north-northeast. All packages exhibit some degree of redoximorphic color effect, changing at regular vertical intervals between reddish fine silt-dominated units and light-colored medium silt packages. Alternating fine and medium silt textures could possibly indicate changing lake depths through time (Bridge and Demicco 2008:468). Furthermore, the parallel, repeating sequence of Profile 11 strata indicates that they are conformable. Finally, granulometry indicates that units 1, 3, 4, and 5 (from bottom to top) are all unimodally distributed and align moderately with the most clay-rich control sample; Deep Lacustrine #4. The dated package, P11-U2, is one of the buff-colored medium silt packages and correlates closely with slightly coarser control samples Deep Lacustrine #2 and #3.

Though the oldest possible age of P10-U7 (ranging from 70.87 to 20.96 ka) is about 10,000 years older than the oldest possible age of P11-U2 (ranging from 60.65 to 43.15 ka), their wide error margins overlap by 10.74 ka, making them analytically indistinguishable. Indeed, the upper two (clay- and silt-dominated) units of Profile 10 correlate closely with unit 3 and moderately with units 1, 4, and 5 of Profile 11. Furthermore, Observation Point E, just northwest of Profile 11 shows that strata in that profile lie about one meter above much coarser, crossbedded sand packages that may have a relationship to the sandy lower units of Profile 10. As noted in Chapter Two, paleolakeshores and other evidence suggest that multiple lakes occupied Centennial Valley during the Pleistocene, but their lateral extent and the timing of their creation and withdrawal are not precisely understood (Honkala 1949; Sonderegger et al. 1982). While

the exact stratigraphic relationship between P11-U2 and P10-U7 is unknown, these units appear to represent the early stages of lake body formation extending at least across most of the study area and capping earlier coarse alluvial and possibly eolian-derived packages. Deepening lake waters, likely indicating increased effective moisture in the region (Thompson et al. 1993), appear to have covered terrestrial sediments in the study area between ca. 70,870 and 43,150 years ago. The exact timing of Pinedale advances and retreats (and concomitant changes in temperature and effective moisture) appears asynchronous in the northern Rockies (Licciardi and Pierce 2008). However, dated loess deposits near Porcupine Creek (about 100 km southeast of the study area) indicate the age range of early lacustrine deposits in the study area (70.87 - 43.15 ka) overlaps the transition between a cooler-than-present period of higher moisture and mollic soil formation (ca. 69 - 57 ka) and a following colder stage of mountain glacial advance and loess deposition (ca. 51 - 43 ka) (Pierce et al. 2011:137). The actual age of lake development most likely falls within the earlier, moister period. Alternatively, microclimatic variations may have produced conditions conducive to pluvial lake formation in Centennial Valley at the same time loess deposits record colder and drier conditions at Porcupine Creek to the southeast.

The third oldest dated sediment package is unit 2 at Profile 4 (P4-U2) in the central study area. P4-U2 dates to 36.23 ± 5.89 ka (USU-1704, elevation 1997.1 m AMSL). It is about 6.7 m lower in elevation and at least 1,030 years younger than deep lacustrine P11-U2 420 m to the northeast. It appears that sometime after deposition of P11-U2 (51.90 ± 8.75 ka) lake waters receded and several meters of incision took place. Although water associated with valley margin alluvial fans could have been the cause of

erosion (Honkala 1949), river downcutting by the ancestral Red Rock River seems more likely given topographic evidence. Google earth images (2014) show an apparent river meander bend in the central study area, separating higher elevation landforms encompassing Profiles 10 and 11 from the low-lying area surrounding Profile 4 (Figure 54).

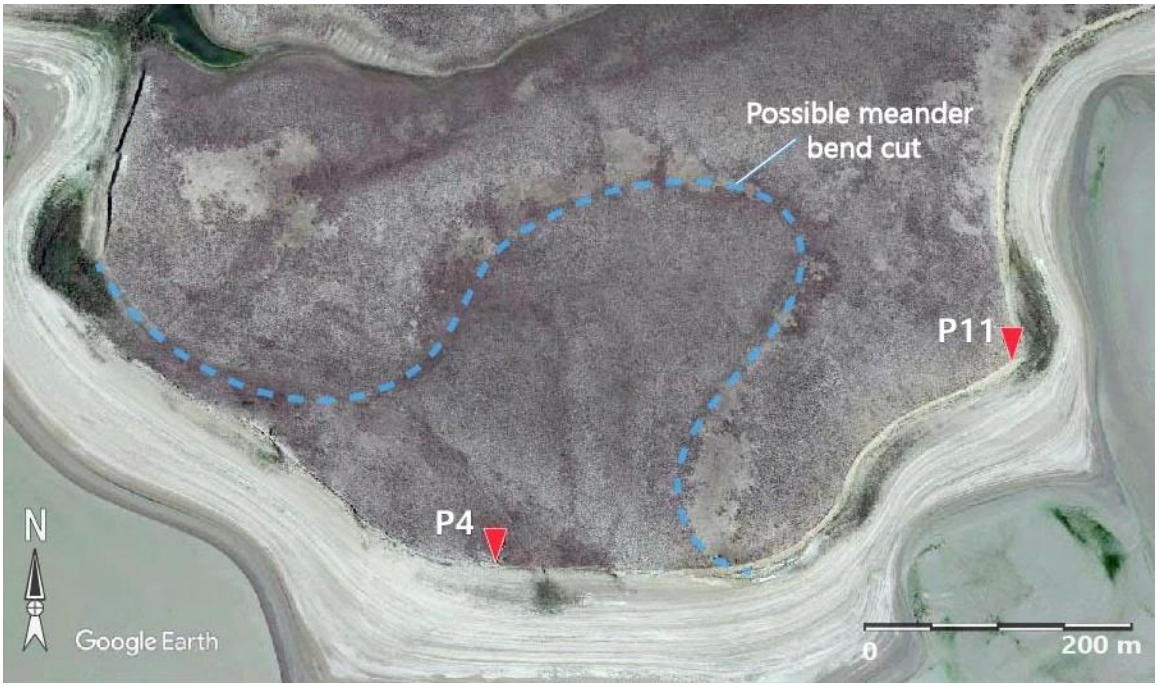

Figure 54. Aerial view of Profile 4 and 11 locations relative to abrupt elevation change (blue dotted line). (modified from Google Earth 2017)

Following incision of lacustrine and possibly underlying coarse sediments, P4-U2 was deposited ca. 36.23 ± 5.89 ka. There is an abrupt facies change and apparent unconformity between unit 1 (P4-U1) and the overlying P4-U2, apparently marking the cessation of downcutting into lacustrine silts and initiation of eolian reworking and deposition (Figure 53). Unit 1 (P4-U1) is structureless (massive) with a unimodal distribution dominated by fine silt. Cluster analysis shows that the texture of P4-U1 correlates closely with the finest control sample; Deep Lacustrine #4, much like strata in

Profile 11. Conversely, the overlying P4-U2 layer is finely horizontal laminated with a bimodal distribution of both fine sand and fine silt (Figure 37).

Grain size distribution of the P4-U2 package closely correlates with the Proximal Loess #1 control (Figure 52). Proximal Loess #1 is the more poorly sorted of the two loess control samples. It exhibits a pronounced bimodal distribution (with modes at 37µm: very coarse silt and 257µm: border of fine and medium sand). Unlike more distal loess deposits, eolian sediments deposited close to their source (such as Proximal Loess #1) are often poorly sorted and bimodal (Pye 1987). The Proximal Loess #1 sample consists of eolian transported silt and sand derived from deflated Snake River Plain sediments dating to between 8,000 and 3,000 cal B.P. (Rich et al. 2015; Tammy Rittenour personal communication April 12, 2017). While this is much younger than the P4-U2 package, given their close correlations it appears that similar eolian processes were acting on a nearby sediment source in Centennial Valley around 36.23 ± 5.89 ka. Forman et al. (1993) determined a correlating period of Snake River Plain loess deposition began between 40,000 and 30,000 and ended ca. 10,000 years ago.

Facies observations and GSD correlations provide some clues as to how lower Profile 4 units may relate to other packages to the east and west. Strong similarities are apparent between the OSL dated P4-U2 and unit 2 of Profile 2 (P2-U2) about 330 m to the northwest. Strata P4-U2 and P4-U2 exhibit remarkably similar depositional structures (both finely horizontal parallel laminated), textures (coarse silty fine sand and fine silty fine sand, respectively), and colors (2.5Y7/2 and 2.5Y 6/3). Regarding color similarities, neither unit seems to have been affected by redoximorphic alteration or pedogenesis, and color appears to represent parent material lithology. Finally, the grain size distributions of

the two packages group very closely with each other (as well as with the Proximal Loess #1 control sample). The east edge of P2-U2 is bounded by a vertical buttress unconformity (Figure 32). No sediment units resembling P2-U2 are present at Profile 3/7, the next exposure 130 m to the southeast. The apparently homologous P4-U2 strata picks up again at Profile 4. It seems that P2-U2 and P4-U2 were once a contiguous stratum that was incised sometime after ca. 36.23 ± 5.89 ka, leaving remnants at P2-U2 to the west and P4-U2 to the east. The resulting accommodation space was filled with sediments that are the upper packages (units 4, 5, and 6) of Profile 2, all or part of packages at Profile 3/7, and possibly the upper units (3 and 4) of Profile 4.

Given that a parallel laminated fine sand unit similar to P2-U2 and P4-U2 is absent in Profile 3/7, all sediments exposed at P3/7 may be younger than those units (< 36.23 ± 5.89 ka). Alternatively, an unconformity may be present in the P3/7 exposure, but was undetected in the field. The Profile 3/7 unconformity argument is supported by first, similarity between the lowest P3/7 horizon (P3/7-3CB2) and the lowest unit of Profile 4 (P4-U1), and second, by marked dissimilarity between the two lowest soil horizons of unit 1 in Profile 3/7; overlying P3/7-3CB and underlying horizon P3/7-3CB2. First, the lowest 10 cm of horizon P3/7-3CB2 exhibits redoximorphic alteration much like the concentrations present in P4-U1, to the east. Staining in both strata is similar to that seen in units interpreted as lacustrine at Profiles 10 and 11. While the evidence of post-depositional inundation does not necessitate that the strata were deposited by the same mechanism, the comparable alteration suggests they are of similar ages. Moreover, the grain size distribution of P4-U1 clusters tightly with P3/7-3CB2, and both align closely with the most clay-rich control sample; Deep Lacustrine #4. These apparent

correlations suggest that horizon P3/7-3CB2 and P4-U1 are homologous strata. This explanation would indicate that I had misinterpreted a sediment package boundary (between P3/7-3CB and P3/7-3CB2) as a soil horizon transition in the field, possibly due to the masking effect of structural B horizon development. In support of this interpretation, GSD cluster analysis shows that adjacent horizons P3/7-3CB and P3/7-3CB2 do not correlate, even remotely (Figure 52). Rather, the overlying P3/7-3CB correlates moderately with the coarser control samples; Dune Sands #1, #2, and #3, while the underlying P3/7-3CB2 correlates closely with the finest control sample; Deep Lacustrine #4. Grain-size correlation between P3/7-3CB2 and P4-U1 (and disassociation between P3/7-3CB and P3/7-3CB2) may be explained by pedogenic clay enrichment of the lower P3/7-3CB2 horizon. The 'weak medium prismatic structure' of 3CB2 indicates some level of clay illuviation in this horizon. However, the overlying 3CB horizon exhibits smaller peds with more resistant 'moderate fine prismatic' structure, indicating it has undergone a higher degree of illuvial clay enrichment than 3CB2 (Bilzi and Ciolkosz 1977). This means that the texture divergence between the two horizons was, if anything, more pronounced *prior* to soil formation. It therefore seems most likely that 'horizon' 3CB2 actually represents a pedogenically affected fourth sediment package in the lowest ~66 cm of P3/7, with an unconformity between it and the overlying 3CB horizon. If this is correct, and stratum P3/7-3CB2 correlates with P4-U1, it would mean that the lowest 66 cm of P3/7 ('3CB2') is a sediment package predating the 36.23 ± 5.89 ka age of P4-U2, which likely formed in a lacustrine setting. The relationship of occupation age upper sediment packages in Profiles 4, 3/7 and 2 will be discussed in detail below, following an examination of the most recent pre-occupation units at the study area west end.

Late Wisconsin Pre-Occupation Age Deposits ca. 28,000 to 14,000 cal BP

The uppermost unit 5/ Bw horizon of Profile 9 (P9-Bw / P9-U5) in the western sub-region is the youngest pre-occupation dated package in the study area. At an elevation of 2001.3 m AMSL (level with USU-2187 at Profile 10), USU-2050 dates to 19.73 ± 3.64. The upper unit of Profile 9 shares similarities and appears conformable with the uppermost unit 5 of Profile 6 (P6-U5), 210 m to the east, and uppermost unit 4 of Profile 1 (P1-U4), 405 m to the east. The primary difference between P9-U5 and P6-U5 is the presence of a By gypsum-rich soil horizon present in Profile 6, which is absent at Profile 9. Otherwise, the upper soil sequences are the same (A-Bw-Bk). The lack of a By at Profile 9 indicates nothing about sediment ages, only that following deposition of the uppermost package (Unit 5), the Profile 6 location experienced saturated conditions conducive to gypsum precipitation (such as pluvial marsh inundation; Nettleton 1991) but Profile 9 did not.

All horizons but the A of Profile 9, unit 5 (P9-U5), align closely with control samples Deep Lacustrine #2 and #3. These are the moderately fine deep lacustrine samples, each is coarse silt dominated with very little sand. Most horizons (Bw, Bk, and C) of P9-U5 also correlate moderately with control samples Deep Lacustrine #1 (the coarsest deep lacustrine), Lower Energy Alluvial #4 (finest alluvial), and Shallow Lacustrine #3 (the only bimodal clay and coarse silt-dominated shallow lacustrine). These correlation trends are repeated roughly with the upper units of Profile 6 (P6-U5) and Profile 9 (P1-U4). Like P9-U5, P6-U5 horizons tend to be coarse silt-dominated and unimodal.

As depositional structures are not discernable in the P9-U5, P6-U5, or P1-U4

packages, my depositional environment interpretations are based primarily on texture properties. Generally, the package textures are coarse silt-dominated and unimodally distributed, aligning most closely with coarser lacustrine and very fine alluvial control samples. Reineck and Singh (1980:242) illustrate the concentric 'belt-like' distribution of sediments of an idealized lake basin. The outer high-energy breaker zone is characterized by beach pebbles, the second above-wave-base zone, by sand, and the below-wave-base zone first by sandy marly mud and finally mud in the lowest depths. Based on this simplified schematic, as well as control sample correlations, it appears that the upper units of Profiles 9, 6, and 1 were deposited in a below-wave-base zone of marly mud, likely shallower than the deep lacustrine packages found in Profiles 10 and 11. Based on the OSL date at Profile 9, and if the units are indeed conformable, deposition of upper units in the study area west end occurred about 19.73 ± 3.64 ka. This age overlaps varying Pinedale LGM dates in the greater Yellowstone-Teton glacial system ranging from ca. 18.8 to 16.5 ka (Licciardi and Pierce 2008). To understand how shallow lake deposition just prior to human occupation fits into a broader chronology of late Pleistocene climate change and local geomorphic response, I examine evidence of preceding conditions recorded in strata underlying P9-U5.

The dated P9-U5 overlies three parallel, fine silt-dominated packages (units 1-4) that are visually distinct but appear conformable based on internal bedding structures and boundary orientation. All four units appear to be lacustrine in origin. P9-U2, the distinct bright white silt bed, exhibits finely parallel-laminated facies. These are possibly consistent with littoral zone 'lake chalk' deposits found in shallow standing water bodies (Reading 1986:76). The lowest three packages of Profile 9 (units 1, 2, and 3) correlate

with units 2, 3, and 4, respectively, at Profile 6 (Figure 53). Unit 4 in Profile 9 apparently pinches out or is eroded to the east and is not visible at Profile 6.

P9-U2 (the bright white silt bed) is easily traceable and conformable with P6-U3, and I interpret it as the same shallow lake littoral zone deposit. Interestingly, however, apparent bed dip of the unit at Profile 9 (as well as units directly above and below) is to the west while the beds have a slight east-facing aspect at Profile 6. Fault movement effects are present in the study area west end (i.e., observation points OP-A and OP-B), and it is conceivable that varying dip angles result from tectonic action. However, the lower units in both profiles maintain consistent bed thickness, relative position, and follow the same gently undulating dips without apparent bed fracturing like that present in OP-A and OP-B. Therefore, it seems more likely that the lower four packages in Profiles 9 and 6 represent subaqueous deposition over paleotopographic features, rather than post-depositional deformation.

Based on the shape and distinctness of package boundaries, as well as structure and texture comparisons, I interpret that there is an erosional unconformity underlying (from west to east) uppermost units P9-U5, P6-U5, and P1-U4, discussed earlier (Figure 53). For instance, the transition between units 3 and 4 at Profile 1 (Figure 23) shows an abrupt, wavy, boundary that clearly represents an erosional surface. Structurally and texturally, the lowest unit of Profile 9 (P9-U1) appears to conform with P6-U2 and both P1-U2 and P1-U3. Furthermore, these packages all correlate closely with the finest control sample; Deep Lacustrine #4. However, the white silt bed and overlying conformable strata present in Profiles 9 and 6 are not present at Profile 9 and apparently pinch out or were eroded.

The west-end late Pleistocene history appears to indicate periods of deep and shallow lake deposition interrupted by incision events. Clay-rich, apparently deep lacustrine sediments were laid down in a conformable layer between Profiles 9, 6, and 1. Slightly coarser silt beds (including the prominent white bed) were deposited next. Though textures don't correlate closely with the underlying stratum, bed thickness, orientation, and internal parallel structures indicate they are conformable. This represents a local transition to a shallower lake environment and thus regressive sequence. Interestingly, the prominent white silt bed and overlying paired bed, while easily traceable between Profiles 9 and 6, do not exhibit close GSD correlation, but are coarser in Profile 6 than in Profile 9. This could indicate a lateral facies transition as the same age beds are formed in deeper water to the west and shallower water to the east (e.g. Walther's Law, Middleton 1973). Neither of the two beds are visible in farthest eastern Profile 1, and they appear to have either pinched out or been eroded. Both scenarios are plausible given evidence of erosional unconformities between each unit in Profile 1. Either an erosional period occurred then (represented by the unconformity shown below units P9-U5, P6-U5, and P1-U4 in Figure 53) or possibly the shallow lake(s) continued to decrease in extent and caused a lack of correlation between second-from-the-top units P9-U4, P6-U4, and P1-U3. As the Profile 9 OSL sample (USU-2050) is approximately the same elevation as the 29,000 years older Profile 10 OSL sample (USU-2187), an accommodation space must first have been incised into underlying deep lake sediments. It is unknown whether this occurred just prior to deposition of P9-U5 and related units or before the deposition of lower P9 packages (units 1-4) and related strata. Therefore, Figure 53 shows strata below P9-U5 related units as being 'Questionable Middle

Wisconsin Pre-Occupation Age'. The lower units (especially P9-U1 and related strata) are possibly as old as units in Profiles 10 and 11 with which they correlate texturally, or possibly only slightly younger than P9-U5. Regardless, a single stratum representing the upper units of Profiles 9, 6, and 1 was deposited in a shallow lacustrine environment stretching at least from Profile 9 in the west to Profile 1 in the east. Deposition occurred about 19.73 ± 3.64 ka. Sometime after deposition, the area between Profiles 6 and 1 was apparently saturated for long enough (such as in a pluvial marsh setting; Nettleton 1991) to form a thick gypsum soil horizon. In summary, west end strata record an initial deep lake environment followed by a shallower lake with sediments coarsening to the east. The area between Profiles 9 and 1 was then incised, creating a low-lying area that was subsequently filled by wide extent, but shallow lake around 19.73 ± 3.64 ka. Finally lake waters were reduced to limited marshy areas about the same time, or just preceding, human arrival in the region.

Cultural Age Deposits: ≤ 14,000 cal BP

Deposits returning cultural ages were found in the central and eastern study areas. The central study area contains nine of the ten OSL samples dating within a cultural time frame, as well as both radiocarbon samples from the hearth feature (F1). All of the cultural-age OSL and radiocarbon samples come from strata within approximately 1.6 meters of elevation of each other (ranging from 1997.10 m to 1998.7 m AMSL). The outlying cultural-age sample (USU-2049) was collected in the eastern study area at an elevation of 2004.95 m AMSL, within a stratum over 6 meters higher in elevation than any other cultural-age strata. The high elevation (versus other cultural-age deposits) of

USU-2049 within the uppermost unit of Profile 8 make it an unexpected outlier in the study area. Understanding its context and origin is therefore critical to reconstructing late Pleistocene-early Holocene events that may have buried archeological materials.

Explaining High Elevation Cultural-Age Strata in Eastern Study Area

All but one dated cultural-age deposit occurs in the central study area at relatively low elevations ranging from 1997.10 m to 1998.75 m AMSL. However, the oldest dated occupation-age package in the study area is the uppermost unit 7 of Profile 8 (P8-U7) at the far eastern end of the research area. The Profile 8 OSL sample (USU-2049) was collected at an elevation of 2004.9 m AMSL and a below-surface depth of 136 cmbs, near the bottom of stratum P8-U7. It returned an age of 14.35 ± 2.01 ka. To piece together the relationship of Profile 8 with central area cultural-age deposits, I first determined possible depositional environments of Profile 8 strata.

While soil formation has obscured depositional bedding structure, P8-U7 may be alluvial in origin as GSDs of both horizons within it (A and Bw) correlate closely with control sample Lower Energy Alluvial #1 (Figure 52). Both horizons are dominantly coarse silt, but also contain 12% and 7% sand, respectively (ranging from very fine to very coarse). P8-U7 rests on unit 6 (P8-U6) which shows markedly different texture (less than 0.25% total sand) and structure. The units are separated by a clear wavy boundary that likely represents an erosional unconformity. P8-U6 is a structureless (single grain) package composed of tiny (~2-4 mm) rounded, flat, weakly cemented sediment aggregates which appear similar to small rip-up clasts. Rip-up clasts typically indicate fine sediments deposited underwater that become semiconsolidated either subaqueously

or subaerially and are disturbed prior to induration and subsequently redeposited near the original site (Boggs 2006:139). Cluster analysis indicates that P8-U6 texture correlates closely with the finest control sample; Deep Lacustrine #4. In light of both the unit's structure and textural correlations, it seems P8-U6 represents a partially cemented lake deposit reworked by high-energy near-shore or fluvial action. If this hypothesis is correct, it may help explain why the overlying cultural-age P8-U7 is so much higher in elevation than similar-age samples.

Pleistocene Lake Centennial appears to have formed rapidly following the end of the LGM, although it may have begun filling as early as 28,000 cal BP (Mumma 2010). However, the exact extent of the lake in the western Centennial Valley (encompassing the study area) is not known. It is possible that alluvial cutting-and-filling actions at higher elevations (equal with the top of Profile 8) in the eastern study area were re-working exposed ancient lake deposits (like those present at Profiles 10 and 11) at approximately the same time lake waters still occupied the western and central sub-regions (ca. 19.73 ± 3.64 based on shallow lake sediments at Profile 9 at the far west). Then, with the onset of drier conditions preceding a short Pinedale re-advance around 14,000 cal BP (Thompson et al 1993), lake levels may have begun to recede. Lake level drop may also have been precipitated by the cutting of a western outlet through previously dammed landslide deposits near the location of the modern Lima Dam (Anastasio et al. 2010). Assuming a relatively precipitous drop, the base level of the ancestral Red Rock River, already well above (by about 7 meters) the central and eastern study area, could have precipitated rapid down-cutting by the stream. This action would have exposed both younger alluvial deposits including cultural-age P8U7 and older reworked lake sediments such as P8-U6.

The possible existence of a major unconformity adjacent to the west of Profile 8 and separating it from Middle Wisconsin lake-deposit-exposing Profile 11 (~600 meters southeast), bolsters the likelihood of recent (latest Pleistocene) alluvial reworking and redeposit of ancient lacustrine sediments. Profile 8 is situated only 15 m east of a broad swale measuring about 290 m east-west (Figure 40). The broad swale obliterates otherwise vertical wall exposures in the study area east end. While wall elevations are the same east and west of the swale, the color and texture of upper packages are markedly different, with west side exposures redder, composed of thinner packages, and exhibiting finer textures. These beds correspond to upper units of Profile 11 and likely date to somewhat younger than 51.90 ± 8.75 ka (USU-2188). Conversely, east of the swale where Profile 8 is located, upper package sediments are in thicker units with much coarser textures and stratified bedding. Profile 8 strata exhibit only faint redoximorphic alteration, which tends toward yellow rather than red hues. It should be noted that lower Profile 8 packages (units 1-5, and especially cross-stratified unit 4) bear similarity to coarse sand deposits visible in Observation Point E, stratigraphically beneath Profile 11 lake beds. Given stark color, texture, and bed thickness differences on either side of the swale, the topography of the swale itself, as well as age relationships between similar elevation strata, I infer that the swale marks the site of a stream-cut unconformity. It appears that ongoing slopewash erosion is taking advantage of this path of least resistance to create the broad swale.

Cultural-Age Deposits in the Central Study Area: Trends and Challenges

Few structural or facies clues that could help infer depositional environment have

survived pedogenic alteration in central area late Pleistocene and Holocene packages. Depositional environment interpretations are therefore largely dependent on grain-size analyses, which are overall less definitive for these recent units than for older packages in the study area. Central area strata generally exhibit more multi-modal GSDs and higher coarse fractions than the west and east sub-areas and may represent deposition by eolian and /or fluvial action (Figure 55). No cultural-age sediments appear to have been laid down in deep lacustrine environments, although some recent deposits do correlate with shallow lake sediments. As illustrated in the control sample X-Y cluster diagram (Figure 51), however, overlap exists between many individual control samples of shallow lacustrine, higher energy alluvial and lower energy alluvial origins. Correlation results involving these controls are therefore not conclusive. While close associations exist with many pre-occupation strata and control samples, few cultural-age units show correspondence with known sediment examples. It is telling that, with the exception of 2Ab and 3ABkb from Profile 3/7, all of the cultural age strata from Profiles 2, 3/7, 5, and potentially cultural-age units from Profile 4 correlate *moderately* with the three coarsest control samples (Dune Sands #1, #2, and #3), but not *closely* with any control. Therefore, one apparent deficiency in my control sample suite may be adequate representation of coarse, multimodal sediments. Unfortunately, the strata for which I most need definitive depositional environment evidence are the ones for which I lack adequately analogous control samples. Finally, while I have ample age control in the low elevation central

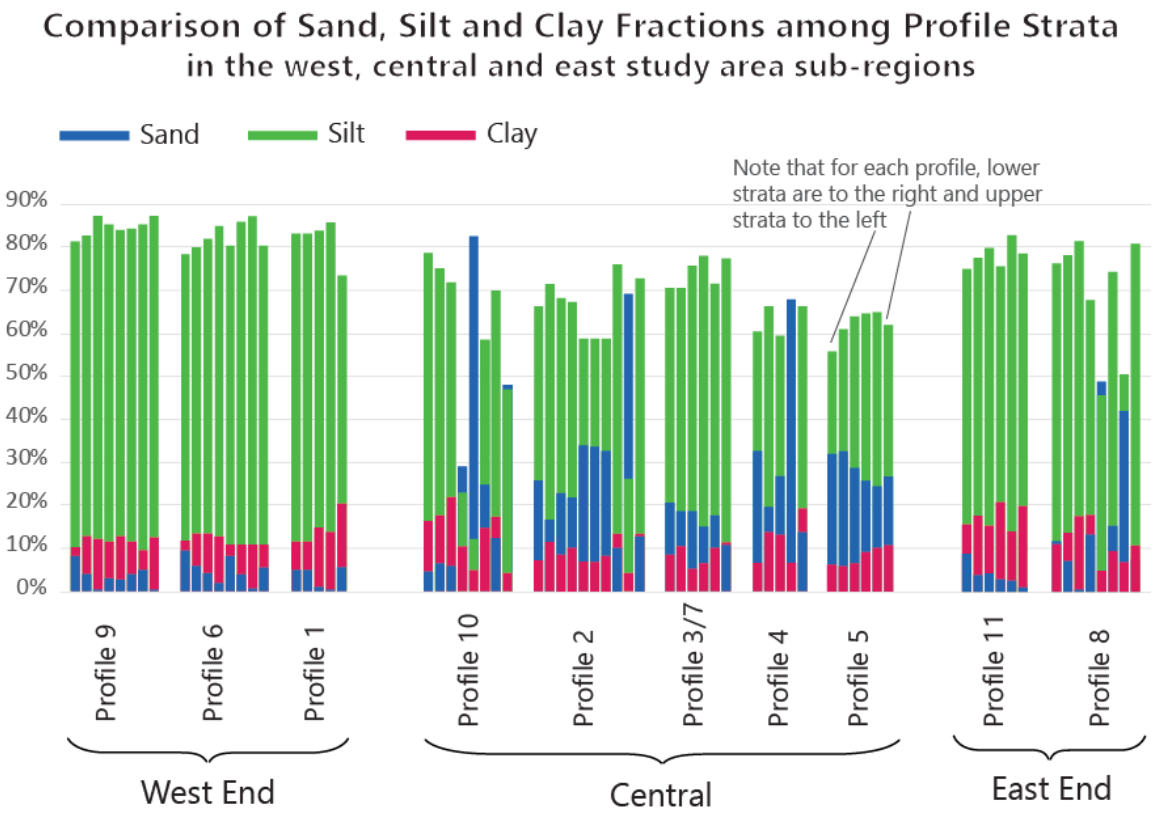

Figure 55. West, central, and east sub-region comparisons of sand, silt, and clay fractions.

study area (a total of 12 OSL and C^{14} samples within 360 m of shoreline), wide error margins and overlapping ages further complicate my interpretations of geomorphic sequence during a human time-frame. Though my conclusions are less definitive than ideal, a general event sequence can nevertheless still be distilled from these somewhat ambiguous data. The following section discusses the complex relationships among cultural-age and possibly cultural strata, roughly from oldest to youngest and west to east, using the complex Profile 2 exposure to anchor discussion of most likely geomorphic scenarios.

Profile 2 as Analog for Late Quaternary Central Area Event Interpretations

The complicated sequence of Profile 2, and its apparent relationship to other central area exposures, provides a useful vignette of the geomorphically eventful late Quaternary period in Centennial Valley. Gaps in the Profile 2 depositional record are represented by at least four erosional unconformities as well as two buried soils. Based on boundary shape, orientation, and distinctness, in conjunction with structure and texture differences, the contacts between units 1 and 2 as well as between units 2 and 3 are interpreted as unconformable. Unit 2 (P2-U2) and its likely correlation with P4-U2 was discussed previously. P2-U2 likely pre-dates a cultural timeframe by at least 16,000 years. The overlying unit 3 (P2-U3) is also most likely pre-cultural as the onlapping package (P2-U4) dates to the limit of possible occupation age.

P2-U4, the third unit below the surface, is nearly a meter thick and produced OSL ages of 13.37 ± 3.83 ka (USU-1700) at 130 cmbs and 12.20 ± 2.45 ka (USU-1701) at 100 cmbs. As the overlapping OSL ages cannot be statistically distinguished, it is unknown whether P2-U4 represents a rapid sedimentation event or accumulated slowly over time. P2-U4 onlaps a buttress unconformity with underlying units 1 - 3. The buttress unconformity is very abrupt and exhibits two sharp convex cuts into the underlying sediments (Figures 31 and 32). Given the sharp contact and distinct convex incisions at the base of P2-U4, as well as the unit's massive structure, it is possible the unit was deposited rapidly, likely simultaneously with the erosional event. Alternatively, the unit could be composed of indistinguishable, small influxes of sediment from periodic (possibly flood) events. If the unit was deposited slowly, the relatively thick paleosol

formed into it may represent a cumulic soil.

Non-pedogenically altered horizon 3C of P2-U4 is structureless (massive) with a fine sandy coarse silt texture and bimodal distribution peaking at 195 µm (fine sand) and 21 µm (coarse silt). Cluster analysis indicates P2-U4 GSD aligns moderately with the three sandy dune deposits (Dune Sands #1, #2, and #3) but not closely with any of the control samples. Despite moderate clustering with eolian sources, unit P2-U4 may result from fluvial action or represent fluvially reworked dune deposits (Vandenberghe 2013). It may also possibly represent a point bar deposit given that its texture is much coarser than the next youngest strata, and point bars tend to deposit the coarsest sediment available in a stream (Reineck and Singh 1980:268). Furthermore, highly sand-concentrated streams may entrain floodplain material and deposit massive sediment bodies associated with basal scour (Martin and Turner 1998). Given that my control sample catalog is limited, there may simply be no appropriate analog for the relatively coarse, bimodal, P4-U2 sediments. Overall, several factors point to some form of alluvial deposition for this package, and that interpretation is consistent with the unit's age and climate conditions at that time. The time of P2-U4 deposition (between ca. 17,200 and 9,540 ka) roughly coincides with cooler and moister environmental conditions from about 17,000 to 11,000 cal BP at Lower Red Rock Lake located about 35 km to the east (Mumma et al. 2012). The beginning of this period may have been marked by increased higher-energy fluvial action.

At the upper boundary of P2-U4 and overlying unit 5 (P2-U5), a short stone line is present, indicating a likely scoured surface and fourth erosional episode. Below the stone line, a paleosol is formed into the upper 37 cm of P2-U4. As the upper horizon of

P2-U4 (3ABb) exhibits both A (increased organics) and B (columnar structure) horizon properties, it is possible that erosion occurred following a depositional hiatus and ensuing soil formation, with incision cutting partially into the epipedon. Alternatively, 3ABb may exhibit both A and B horizon properties because soil formation in overlying strata has resulted in welded soil properties. P2-U5 is texturally similar to P2-U4, with a bimodal distribution peaking at fine sand, but medium versus coarse silt. Deposition of P2-U5 is bracketed by ages of upper and lower packages and so occurred within a wide time span between ca. 9,540 and 910 years before present. The boundary between P2-U5 and overlying uppermost unit 6 (P2-U6) does not show evidence of erosion, such as abrupt undulating contact or stone line. However, paleosol formation into P2-U5 indicates a depositional hiatus.

The uppermost unit, P2-U6, dates to 0.75 ± 0.16 ka (USU-2185) based on a sample taken near the base of the unit at 23 cmbs. Based on the unit's young age, it is unsurprising that soil formation consists of a weakly developed A-Bw sequence. Still, no depositional structures are discernible in the unit. Based on textural evidence of the (least pedogenically altered) Bw horizon, P2-U6 is again very similar to the P2-U4 bimodal distribution. However, the modal peaks are swapped in P2-U6 with major Mode 1 centered at 21 µm (coarse silt) and lesser Mode 2 peak at 195 µm (fine sand). Again, the unit does not correlate closely with any control sample but correlates moderately with the three sandiest and coarsest control samples: Dune Sand #1, #2, and #3. Again, pinpointing a likely depositional environment for the unit is problematic as it offers few clues, and correlations with control samples are relatively weak. It is notable however, that while the distribution is bimodal and 'very poorly sorted' (Folk and Ward 1957) like

the rest of Profile 2 strata, P2-Bw is more well-sorted than most, having a σ value of 2.32 (on a scale of σ < .350 = very well sorted to σ > 4.00 = extremely poorly sorted). Only the lowest three units of Profile 2 have comparable sorting values, with P2-U2 having the closest at 2.20. Control sample Proximal Loess #1 also has a sorting value of 2.20 σ, and falls closest to P2-Bw of any control. The high silt content of P2-Bw and its sorting similarity with Proximal Loess #1 and unit P2-U2 (established as proximal loess by several factors including depositional structure) indicates that P2-Bw is a loess package deposited ca. 910 - 590 years ago.

Correlations among Latest Pleistocene/ and Early Holocene Units

Although soil horizons, package thicknesses, and overlapping OSL ages suggest similarities and shared sedimentation histories, the relationships between Profile 2 and Profiles 3/7, 4, and 5 to the west are not readily apparent. The lowest cultural-age unit of Profile 2, P2-U4, dates to between ca. 17,200 and 9,540 ka. This range overlaps slightly with the oldest sample from Profile 3/7 (USU-1837) near the top of Unit 1, which has a maximum range of 9,950 to 7,870 years before present. While none of the P2-U4 horizon GSDs align closely with P3/7 unit 1 distributions of comparable age, overlapping OSL ages show that P2-U4 and the upper half of P3/7-U1 (above the misinterpreted unconformity overlying P3/7-3CB2) are homologous. It should also be noted that Feature 1 is situated between Profiles 2 and 3/7 and lies below the lower paleosol connecting the two exposures. Charcoal in the feature dates between 9560 and 8100 cal BP (UCIAMS#147407 and UCIAMS#147408). It therefore overlaps dates for both P2-U4 and P3/7-U1, bolstering their association. Farther to the east, the lowest unit 1 of Profile 5

(P5-U1) is separated into three soil horizons, of which the texture of the uppermost (P5-3Ab) correlates closely with 3CB in Profile 3/7. The OSL age of encompassing P5-U1 is 12.74 ± 1.99 ka (USU-1705), which does not overlap with the Profile 3/7 unit 1 age of 8.91 ± 1.04 ka. However, the P5-U1 age *does* overlap with the two dates obtained from unit 4 in Profile 2, with which P3/7-U1 is correlated by age.

The relationship of Profile 4 with Profiles 2 and 3/7 to the west and Profile 5 to the east is not clear. As only one OSL age was obtained from Profile 4 (at 95 cmbs, from P4-U2), I can't definitively associate the upper two units (3 and 4) of Profile 4 with any other strata and can't infer with any certainty whether they are cultural age or not. Although the upper two packages of Profile 4 are not dated, unit 3 (P4-U3) appears to rest unconformably on the ca. 36.23 ± 5.89 age P4-U2 and is conceivably much younger. Furthermore, P4-U3 shows close textural correlation with cultural-age horizons of P5-U1. Alternatively, P4-U3 may represent an older deposit, closer in age to the underlying P4-U2 and not related to P5-U3 despite textural similarities. P4-U3 may be exposed at a similar elevation as P2-U4, P3/7-U1, and P5-U1 only due to irregular alluvial erosion, which incised accommodation spaces into the Profile 2, 3/7, and 5 locations but may have left older deposits intact around Profile 4. In support of this possibility, P4-U3 exhibits yellow-hued redoximorphic staining throughout the package that is not expressed in the other units in question, including P5-U1 only 35 m to the east. The redoximorphic alteration in P4-U3 is developed to an extent that the P4-U3 package is partially cemented and horizontal fractures are visible between it and the overlying P4-U4 (Table 11). While redoximorphic alteration does not, of itself, indicate age or depositional environment the lack of such alterations in the other units indicates a lack of shared

history. It seems most likely that P4-U3 represents a pre-cultural age unit not associated with P2-U4, P3/7-U1, or P5-U1 which was left intact during erosion of adjacent areas.

Based on age associations, and to a lesser extent textural correlations, I conclude that units P2-U4, P3/7-U1 (upper half), and P5-U1, are homologous packages deposited around the same time during the latest Pleistocene and early Holocene. Deposition was likely asynchronous in different locations but possibly through related means, given textural correlations. Again, none of these packages align closely with control sample grain-size distributions, but they all align moderately with the three coarsest controls; Dune Sand #1, #2, and #3. Given the bimodal distributions and very poor sorting of the three Pleistocene/Holocene packages (with both fine silt and fine sand peaks), their similarity with dune sands seems to derive more from correspondingly high sand fractions than analogous modality or sorting. Based on previously discussed interpretations of P2-U4, I infer that these units were deposited in an alluvial setting. However, this interpretation does not preclude eolian re-working of alluvial sediments (similar to Proximal Loess #1 formation) or vice versa.

Central Area Middle-to-Late Holocene Deposits

While imprecise OSL ages complicate relationships of recent central area units, stratigraphic and pedogenic similarities help resolve correlations. Unit 2 of Profile 3/7 (P3/7-U2) produced an age of 2.50 ± 0.33 (USU-1702). This age is statistically identical to the two ages of 3.03 ± 0.45 (USU-1834) and 2.62 ± 0.36 (USU-1703) from the uppermost unit 3 (P37/-U3) that overlies it. It is possible that P3/7-U3 was deposited so soon after P3/7-U2 as to be indistinguishable in age. However, it is unlikely that pedogenesis would have time to form the 2Bkb horizon in P3/7-U2 if this were the case.

Alternatively, USU-1702 in the lower unit may have produced an artificially young age due to contamination by more recently bleached sediment. As noted previously, this sample was obtained from an exposure that later calved off due to an unseen vertical wall crack. The crack may have introduced surface sediments to the sample location. Conversely, either USU-1834 or USU-1703 may have produced artificially old ages due to partial bleaching and incomplete reset of luminescence signals prior to burial. Moreover, my placement of USU-1834 (the oldest sample) may have been inexact. This sample was taken from the exposure revealed after the original wall slump at the Profile 3 location. While I was aiming to sample the bottom of the uppermost unit just above the top paleosol, heavy rain made it difficult to discern the exact location of the horizon. It is possible I may have sampled too close to the underlying package and inadvertently captured older sediments.

Further complicating interpretation, the upper package of Profile 2 to the west (P2-U6) yielded an age of 0.75 ± 0.16 ka (USU-2185). While stratigraphically the uppermost units of P2 and P3/7 appear to correlate, this age indicates that P2-U6 was deposited at least 1,260 years before P3/7-U3. If so, it would indicate that erosion had occurred about 1,000 years ago in the Profile 2 vicinity, creating an accommodation space that was subsequently filled ca. 0.75 ± 0.16 ka leaving an unconformity (undetected in the field) between Profiles 2 and 3/7. The more parsimonious explanation is that lack of correlation is caused by imprecision in either the P3/7 or P2 OSL ages. Note that the surface soil and two paleosols visible in Profiles 2 and 3/7 are traceable between the exposures and also bracket two upper sediment units of very similar thickness. While similar soils may develop into sediments of different ages, which are exposed

simultaneously, the parallel boundaries and even thicknesses of the upper two packages suggest that the timing of deposition for P2-U5 / P3/7-U2 and P2-U6 / P3/7-U3 is analogous. Finally, as described earlier for P2-U6, depositional environment is inconclusive for the uppermost units, but sorting, modality peaks, and high silt fractions indicate possible proximal loess origin.

Farther east, the upper two Profile 5 units share more similarities with the P2 and P3/7 strata than to any in Profile 4. Again, the upper two units of Profile 4, though not dated, do not show stratigraphic or soil formation similarity with exposures to the east and west. It appears that this location represents an older, vestigial group of sediment units which were left intact when (possibly alluvial) actions incised areas to the east and west.

Similar to upper P2 and P3/7, Profile 5 is composed of three sediment units, each altered by a similar soil horizon sequence. Although previously discussed problems with my P3/7 OSL ages prevent positive association, the age of 3.68 ± 0.70 ka (USU-2168) in the middle package of Profile 5 (P5-U2) predates USU-1703 in the upper unit of P3/7 as well as USU-2185 in the upper unit of Profile 2. The upper three units of Profiles 2, 3/7, and 5 therefore appear to correspond respectively. Package thickness is overall greater at Profile 5, however. As noted previously, Profile 5 is situated on a gentle (~ 5°) side-slope of a shallow swale to the east. It appears that the location has been acting as a sediment trap, collecting material either from upslope or-more likely-eolian sediment drop into this leeward topographic low. The parallel, east-sloping aspects of all unit and soil horizon boundaries indicates that the Profile 5 location has been trapping sediment and accreting upward and eastward since at least 12.74 ± 1.99 ka (USU-1705). Correlating thick Profile

5 packages with thinner Profile 2 and 3/7 units is therefore not problematic as Profile 5 appears to have received deposits at the same time, but was better able to retain sediment input than the somewhat higher, flat paleotopography at Profiles 2 and 3/7. If sediment units do in fact correlate to Profiles 2 and 3/7, Profile 5 soil sequences could possibly indicate cumulic soil bodies in which pedogenesis kept pace with sediment accumulation coming from the west. As in the upper two units of Profiles 2 and 3/7, the grain-size distributions appear to fit with Proximal Loess #1 but with a greater medium silt fractions. Finally, it is interesting to note that the (fine sandy coarse silt) A horizon of Profile 5 clusters very closely with similarly textured A horizons from Profiles 2 and 3/7 and even with the seeming outlier, Profile 4. Again these four horizons do not show close alignment with any control samples but are moderately correlated with the three dune controls. The A horizons topping the four low-elevation profiles may therefore include an influx of sandy material. Alternatively, the higher sand fractions could simply be the result of pedogenic eluvial clay translocation into underlying B horizons.

Sediment packages and soil formation in study area exposures record a sweeping, though coarsely refined, record of erosion, deposition, and stasis in the western Centennial Valley. Analysis of stratigraphic mapping, chronometric dating, and granulometry results culminates in a roughly 70,000 year-long history of geomorphic change in the area. The following chapter distills how these interpretations address the original research questions of this study and can help archeologists differentiate likely cultural versus pre-cultural packages in the greater Centennial Valley.

CHAPTER SIX:

CONCLUSIONS

Neighboring Paleoindian surface and buried assemblages along Lima Reservoir beg the question of what geomorphic circumstances led to theses divergent taphonomic outcomes. Moreover, as burial is advantageous for data preservation, these sites also prompt the management question of what other landforms in the valley potentially contain buried archeological sites. The second question is especially pressing given the dilemma of ongoing erosion along the margins of Lima Reservoir and possible effects to as-of-yet unidentified buried sites. In order to deduce what caused burial versus non-burial for archeological sites within the study area and thereby identify locales with buried site potential, I accomplished two related objectives. First, given that geologic mapping in the vicinity is not produced at scales useful to archeologists, I used stratigraphic mapping, OSL dating and granulometry to reconstruct the geomorphic history of the study area. Second, I used the reconstructed history to outline defining characteristics of occupation-age versus pre-occupation sediment packages in the area.

Reinterpretations of Geomorphic Associations

Existing geologic maps of the study vary in interpretations and are mapped at spatial and temporal scales that are too coarse to be useful for archeological investigations (Figure 11). The reconstructed geomorphic history results of this research give a more nuanced picture of Late Quaternary geologic association in the study area (Figure 56).

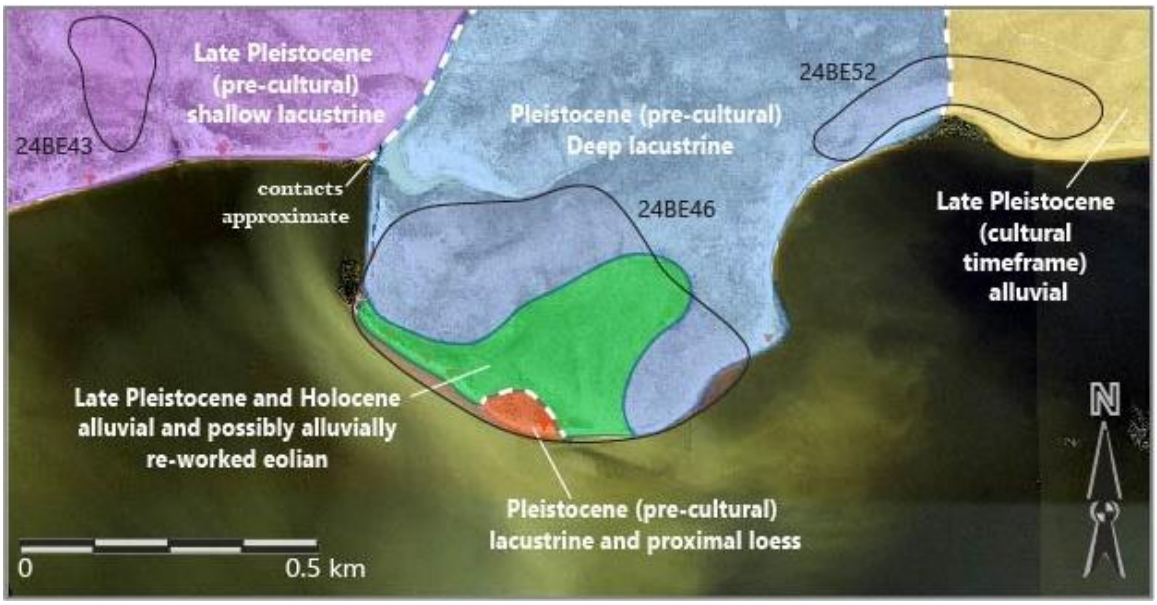

Figure 56. Revised interpretations of geologic associations based on results of this research.

The oldest packages in the study area are deep lacustrine and high energy alluvial sediments located in the central/northern study area (Figure 56; blue). These packages occupy relatively high elevation areas of the study location. The association dates from approximately 60.39 ± 10.48 ka (USU-2187) to 51.90 ± 8.75 ka (USU-2188). The second oldest dated association is a small island of apparent proximal loess overlying lacustrine sediments in the low elevation far south of the central study area (Figure 56; orange). This area dates to 36.23 ± 5.89 ka (USU-1704). The next oldest formation is in the mid-elevation western study area (Figure 56; purple). This area is primarily composed of shallow lacustrine or marsh sediments with upper packages dating to 19.73 ± 3.64 (USU-2050).

Cultural-age deposits are confined to two locales within the study area. In the highest elevation, far eastern study area, lies a thick surface stratum of cultural-age alluvially re-worked lacustrine material (Figure 56; yellow). Roughly the upper 1.3

meters of the landform dates to the latest Pleistocene, 14.35 ± 2.01 (USU-2049), and younger. This area is just east of a prominent swale (Figure 40; c and d), which may represent the edge of a former incision point where river water first incised, and then aggraded younger material onto older beds. Finally, the largest area of cultural age packages is within the low elevation southern central portion of the study area (Figure 56; green). Sediment packages in this association appear to be dominantly alluvial or possibly alluvially re-worked eolian materials. Sediment ages in this area range from the late Pleistocene; 13.37 ± 3.83 (USU-1700), to the late Holocene; 0.75 ± 0.16 (USU-2185). The area is bounded by what appears to be a former meander bend cut (Figure 54). These reconstructed geomorphic associations allowed me to accomplish my second objective. I used my results to outline criteria for identifying sediment packages beyond the study area with archeological burial potential, as well of those that are likely too old to contain cultural material.

Implications for Identifying Cultural-Age Deposits beyond the Study Area

Based on data from the ten Profile locations and five Observation Points, general trends among occupation-age and pre-occupation strata can be summarized (Table 15). The textures of occupation-age deposits may align with high- or low-energy alluvial, eolian dune, or proximal loess facies and textures. Some cultural-age deposits show similarity to shallow lacustrine sediments, although this apparent association may be a product of overlapping depositional energy regimes. Overall, sandy dune-like packages produced the most Holocene ages (Profiles 2, 3/7, and 5). Deposits displaying deep lacustrine facies such as at Profiles 10 and 11, are likely very old and considered low

Table 15. Generalized Occupation-Age and Pre-Occupation Strata Characteristics for Centennial Valley

Occupation-Age (14 - 0 ka)	Pre-Occupation (14 - 70 ka)
• Low elevation areas accessible by Holocene alluvial and eolian action may exhibit paired paleosol soil sequence. Sequence consists of a weakly developed modern soil forming into a thicker (~30 cm) sediment package, overlying an upper paleosol forming into a thinner (~15 cm) package, overlying a lower paleosol forming into a very thick (~70 cm) package. The lower paleosol may exhibit a truncated Bk horizon (as seen in Profiles 2 and 3/7). Package thickness may vary (as in Profile 5). • Bimodal grain size distributions dominated by silt (primary) and fine sand (secondary), very poorly sorted and may correlate with Proximal Loess control samples. • Depositional facies structures are not necessarily visible, these may be obscured by soil formation. Alternatively, the packages may have been massive to begin with (Profile 2:Unit 4). • Based on Google Earth or satellite imagery, landforms which appear onset and are relatively flat or rolling landforms. • High elevation (up to ca. 2006 m AMSL) does not preclude cultural association (Profile 8). Look for redoximorphic alteration visible from the ground if it is on a high wall. Saturated redoximorphic red colors are certainly too old, yellow is likely too old. • An epipedon sequence with a moderately thick A-Bw sequence may be cultural age (Profile 2:Unit 6; Profile 3/7: Unit 3; Profile 5: Unit 2). But if the stratum is thick (~70 cm) and includes a Bk, By, or Bty below the Bw, it is likely too old.	• Grain size distributions clustering with deep lacustrine control samples or other indications of deep lacustrine association such as: • Unimodal (more well-sorted) sediment textures dominated by clay and fine silts and: • Thinly bedded (~10 cm) banded redoximorphic red or alternating red and buff-colored clay or fine silt units (as in Profile 11). • Yellow and orange redoximorphic alteration may or may not be present in only pre-occupation packages. However, yellow and orange coloring are present in at least *some* strata inferred to be too old (Profile 4:Unit 3; Profile 3/7:Unit 1). • Pedogenic alteration featuring very thick By (gypsum) horizons of 50 cm or more. • No crossbedded sand units (flaser beds, OP-E), or gravel-dominated polymodal units (possibly deltaic, Profile 10:Unit 5) occur within a cultural time-frame. These examples even pre-date Pleistocene Lake Centennial deposits. • Associated with finely laminated white silt bed, as visible in west end of study area (Profile 9:unit 2; Profile 6:Unit 3). • Depositional structure consists of thin, parallel stratified, high clay content layers which may exhibit different colors on ped insides and outsides due to redoximorphic staining (deep or shallow lacustrine; Profile 1:Units 2 and 3, Profile 6:Unit 4, Profile 9:Unit 1).

priority for archeological testing. However, as with unit 6 in Profile 8, fine-textured packages that appear to be lacustrine may actually be younger, low-energy alluvial sediments, especially if fluvial action was reworking older lake sediments. Redoximorphic color alteration is one possible way to differentiate such deposits. Red and/or red and white banded units such as all of Profile 11 and units 1 and 2 of Profile 10 indicate apparent long-term inundation and signal ancient lake beds in the area.

Finally, one of the most notable markers of occupation-age packages in the low elevation cultural age units was a prominent paleosol sequence. Profiles 2, 3/7 and 5 all exhibit a distinct soil sequence of modern topsoil overlying a thinner paleosol (possibly with a truncated Bk horizon), and that package in turn caps a lower, much thicker paleosol with at least one and possibly two Bk horizons. While absolute soil thickness may vary (compare P5 and P3/7, for instance) the relative sequence of medium-thin-thick (top to bottom) remains constant.

Field reconnaissance and age control by OSL or other chronometric means will be required to test the predictions of this research. It is unknown, for instance, how far within Centennial Valley these expectations may prove useful given the unknown lateral extents of Pleistocene Lake Centennial and ensuing water bodies. It is also unknown whether these criteria may apply to sediment packages outside of Centennial Valley in adjacent valleys or other areas of the northwestern Rocky Mountains. However, the pedologic markers appear to align with similar sequences in high-order stream and loess-filled intermittent drainage settings on the Great Plains (Holliday et al. 2011; Mandel 2008). Specifically, the presence of possible cumulic soil sequences dating to a

Paleoindian time-frame is highly consistent with the findings of Holliday et al. (2011) and Mandel (2008).

The results of this research augment our understanding of Late Pleistocene through Holocene site formation processes and burial mechanisms in alluvial, eolian and lacustrine environments. These results should help orient management decisions regarding where to target testing for possible buried and erosion-threatened sites in Centennial Valley. Finally, the identification of Paleoindian-age soil sequences in alluvial settings within the study area dovetail with findings from other researchers on the Great Plains. These results may therefore have site burial prediction value beyond the confines of the Centennial Valley.

REFERENCES CITED

Aitken, Martin J.

1992 *Optical Dating*. Quaternary Science Reviews 11:127-131.

Aitken, Martin J.

1998 *An Introduction to Optical Dating: The Dating of Quaternary Sediments by the Use of Photon-Stimulated Luminescence*. Oxford University Press, New York.

Albanese, John P.

2005 A Field Reconnaissance Geologic Study. In T*he Merrell Locality (24BE1659) and Centennial Valley, Southwest Montana: Pleistocene Geology, Paleontology & Prehistoric Archaeology,* edited by Christopher L. Hill and Leslie B. Davis, pp. 15-22. Montana Bureau of Land Management, Billings.

Alden, William C.

1953 *Physiography and Glacial Geology of Western Montana and Adjacent Areas*. Geological Survey Professional Papers 231. United States Geological Survey, Washington, D.C.

Alley, Richard B.

2000 The Younger Dryas Cold Interval as Viewed from Central Greenland. *Quaternary Science Reviews* 19:213-226.

Anastasio, David J., Christina N. Majerowicz, Frank J. Pazzaglia, and Christine A. Regalla

2010 Late Pleistocene - Holocene Ruptures of the Lima Reservoir Fault, SW Montana. *Journal of Structural Geology* 32:1996-2008.

Avery, Brian W.

1980 *Soil Classification for England and Wales.* Soil Survey of England and Wales, Technical Monograph No. 14. Rothamsted Experimental Station, Lawes Agricultural Trust, Harpenden, United Kingdom.

Bagnold, Ralph A.

2005 [1954] *The Physics of Blown Sand and Desert Dunes.* Dover Publications, Inc. Mineola, New York.

Barker, Karl S. and Steven W. Barker

1993 *Interim Geologic Map of the Wellsville Quadrangle, Cache County, Utah*. Utah Geological Survey, Contract Report 93-2, Salt Lake City.

Bateman, Mark D., Charles D. Frederick, Manoj K. Jaiswal, and Ashok K. Singhvi

2003 Investigations into the Potential Effects of Pedoturbation on Luminescence Dating. *Quaternary Science Reviews* 22:1169-1176.

Benson L.V., S.P. Lund, J.P. Smoot, D.E. Rhode, R.J. Spencer, K.L. Verosub, L.A. Louderback, C.A. Johnson, R.O. Rye, and R.M. Negrini

2011 The rise and fall of Lake Bonneville between 45 and 10.5 ka. *Quaternary International* 235:57-69.

Bettis, E. A. III and Edwin R. Hajic

1995 Landscape Development and the Location of Evidence of Archaic Cultures in the Upper Midwest. In *Archaeoloical Geology of the Archaic Period in North America*, edited by E. Arthur Bettis III, pp. 87-113. Geological Society of America Special Paper No. 297, Geological Society of America, Boulder, Colorado.

Bilzi, A. F. and E.K. Ciolkosz

1977 Field Morphology Rating Scale for Evaluating Pedological Development. *Soil Science* 124:45-48.

Birkeland, Peter W.

1999 *Soils and Geomorphology.* 3rd ed. Oxford University Press, New York.

Boggs, Sam Jr.

1995 *Principles of Sedimentology and Stratigraphy.*2nd ed. Prentice Hall, Englewood Cliffs, New Jersey.

2006 *Principles of Sedimentology and Stratigraphy.*4th ed. Pearson Prentice Hall, Uper Saddle River, New Jersey.

Bridge, John S. and Robert V. Demicco

2008 *Earth Surface Processes, Landforms and Sediment Deposits.* Cambridge University Press, New York.

Bull, William B.

2008 *Geomorphic Responses to Climate Change.* Blackburn Press, Caldwell, New Jersey.

Buol, Stanley. W., Randal J. Southard, Robert C. Graham, and Paul A. McDaniel

2011 *Soil Genesis and Classification.* 6th ed. Wiley Blackwell, Hoboken, New Jersey.

Bureau of Reclamation, Great Plains Region, Montana Area Office (BOR)

2004 Draft Resource Management Plan Clark Canyon Reservoir and Barretts Diversion Dam. Electronic document, accessed at https://www.usbr.gov/gp/mtao/clarkcanyon/fea/ea_chap3.pdf on May 25, 2016.

Dyman, T.S., R. G. Tysdal, W. J. Perry Jr., D.J. Nichols, J.D. Obradovich

2008 Stratigraphy and Structural Setting of Upper Cretaceous Frontier Formation, Western Centennial Mountains, Southwestern Montana and Southeastern Idaho. *Cretaceous Research* 29:237-248.

Ebert, James I.

1992 *Distributional Archaeology.* University of New Mexico Press, Albuquerque.

Evans, James P., James P. McCalpin, and David C. Holmes

1996 *Geologic Map of the Logan Quadrangle, Cache County, Utah.* Utah Geological Survey Map 96-1, Washington, D. C.

Field, Andy

2013 *Discovering Statistics Using IBM SPSS Statistics.* 4th ed. Sage Publications, London.

Flemming, Burghard W.

2000 A Revised Textural Classification of Gravel-Free Muddy Sediments on the Basis of Ternary Diagrams. *Continental Shelf Research* 20:1125-1137.

Folk, Robert L. and William C. Ward

1957 Brazos River Bar: A Study in the Significance of Grain Size Parameters. *Journal of Sedimentary Petrology* 27:3-26.

Folk, Robert L.

1954 The Distinction between Grain Size and Mineral Composition in Sedimentary-Rock Nomenclature. *The Journal of Geology* 62:344-359.

Forman, Steven L., Richard P. Smith, William R. Hackett, Julie A. Talus, and Paul A. McDaniel

1993 Timing of Late Quaternary Glaciations in the Western United States Based on the Age of Loess on the Snake River Plain, Idaho. *Quaternary Research* 40:30-37.

Friedman, Gerald M.

1961 Distinction between Dune, Beach, and River Sands From their Textural Classifications. *Journal of Sedimentary Petrology* 31:514-529.

1979 Address of the retiring President of the International Association of Sedimentologists: Differences in size distributions of populations of particles among sands of various origins. *Sedimentology* 26:3-32.

Galbraith, R. F. and R. G. Roberts

2012 Statistical Aspects of Equivalent Dose and Error Calculation and Display in OSL Dating: An Overview and Some Recommendations. *Quaternary Geochronology* 11:1-27.

Galbraith, R. F., R. G. Roberts, and H. Yoshida

2005 Error Variation in OSL Palaeodose Estimates from Single Aliquots of Quartz. *Radiation Measurements* 39:289-307.

Galbraith, R. F., R. G. Roberts, G. M. Laslett, H. Yoshida and J. M. Olley

1999 Optical Dating of Single and Multiple Grains of Quartz from Jinmium Rock Shelter, Northern Australia: Part I, Experimental Design and Statistical Models. *Archaeometry* 41:339-364.

Gale, Stephen J. and Peter G. Hoare

1991 *Quaternary Sediments: Petrographic Methods for the Study of Unlithified Rocks.* Halsted Press, New York.

Godfrey-Smith, D. I., D. J. Huntley, and W. H. Chen

1988 Optical Dating Studies of Quartz and Feldspar Sediment Extracts. *Quaternary Science Reviews* 7:373-380.

Google Earth

2017 Lima Reservoir, Montana. Accessed online at https://earth.google.com/web on November 18, 2017.

Hill, Christopher L.

2005 Geology of Centennial Valley and Stratigraphy of Pleistocene Fossil-Bearing Sediments. In *The Merrell Locality (24BE1659) and Centennial Valley, Southwest Montana: Pleistocene Geology, Paleontology & Prehistoric Archaeology*, edited by Christopher L. Hill and Leslie B. Davis, pp. 39-78. Montana Bureau of Land Management, Billings.

Hill, Christopher L. and Leslie B. Davis (editors)

2005 The Merrell Locality (24BE1659) and Centennial Valley, Southwest Montana: Pleistocene Geology, Paleontology & Prehistoric Archaeology. Montana Bureau of Land Management, Billings.

Holliday, Vance T.

2004 *Soils in Archaeological Research*. Oxford University Press, New York.

Holliday, Vance T., David J. Meltzer and Rolfe Mandel

2011 Stratigraphy of the Younger Dryas Chronosequence and Paleoenvironmental Implications: Central and Southern Great Plains. *Quaternary International* 242:520-533.

Honkala, Fred S.

1949 *Geology of the Centennial Region, Beaverhead County, Montana.* Ph.D. Dissertation, University of Michigan, Ann Arbor.

James, Noel P. and Robert W. Dalrymple (editors)

2010 *Facies Models.*4th ed. Geological Association of Canada, Newfoundland.

Janecke, Susanne U. and Robert Q. Oaks

2011 Reinterpreted History of Latest Pleistocene Lake Bonneville: Geologic Setting of Threshold Failure, Bonneville Flood, Deltas of the Bear River, and Outlets for Two Provo Shorelines, Southeastern Idaho, USA. *Geological Society of America Field Guides* 21:195-222.

King, Thomas F.

2013 *Cultural Resource Laws and Practice.* AltaMira Press, Lanaham, Maryland.

Kornfeld, Marcel, George C. Frison, and Mary Lou Larson

2010 *Prehistoric Hunter-Gatherers of the High Plains and Rockies.* 3rd ed. Left Coast Press, Walnut Creek, California.

Krumbein, W. C. and F. J. Pettijohn

1938 *Manual of Sedimentary Petrography.* Appleton-Century-Crofts, New York.

Lemons, David R. and Marjorie A. Chan

1999 Facies Architecture and Sequence Stratigraphy of Fine-Grained Lacustrine Deltas along the Eastern Margin of Late Pleistocene Lake Bonneville, Northern Utah and Southern Idaho. *American Association of Petroleum Geologists Bulletin* 83:635-665.

Licciardi, Joseph M. and Kenneth L. Pierce

2008 Cosmogenic Exposure-Age Chronologies of Pinedale and Bull Lake Glaciations in Greater Yellowstone and the Teton Range, USA. *Quaternary Science Review* 27:814-831.

Lonn, J. D., B. Skipp, E. T. Ruppel, S. U. Janecke, W. J. Perry Jr, J. W. Sears, M. J. Bartholomew, M. C. Stickney, W. J. Fritz, H. A. Hurlow, and R. C. Thomas

2000 *Geologic Map of the Lima 30' x 60' Quadrangle, Southwest Montana.* Montana Bureau of Mines and Geology, Butte.

Mandel, Rolfe D. (editor).

2000 *Geoarchaeology in the Great Plains*. University of Oklahoma Press, Norman.

Mandel, Rolfe D.

2008 Buried Paleoindian-Age Landscapes in Stream Valleys of the Central Plains, USA. *Geomorphology* 101:342-361.

Mandel, Rolfe D. and E. Arthur Bettis III

2001 Use and Analysis of Soils by Archaeologists and Geoscientists: A North American Perspective. In *Earth Sciences and Archaeology*, edited by Paul Goldberg, Vance T. Holliday, and C. Reid Ferring, pp. 173-204. Kluwer Academic/Plenum Publishers, New York.

Majerowicz, Christina N. , Joanna K. Troy, David J. Anastasio, and Frank J. Pazzaglia

2010 *Bedrock and Surficial Geologic Map of the Lima Dam 7.5' Quadrangle, Beaverhead County, Southwest Montana.* Department of Earth and Environmental Sciences, Lehigh University, Bethlehem, PA.

McCave, I. N. and James P. Syvitski

1991 Principles and Methods of Geological Particle Size Analysis. In *Principles, Methods, and Application of Particle Size Analysis,* edited by James P. Syvitski, pp. 3-21. Cambridge University Press, New York.

McCave, I. N., R. J. Bryant, H. F. Cook, and C. A. Coughanowr

1986 Evaluation of a Laser-Diffraction-Size Analyzer for Use with Natural Sediments: Research Method Paper. *Journal of Sedimentary Research* 56:561-564.

McDonagh, Bryn

2011 The Principles of Laser Diffraction. Electronic document, accessed February 16, 2017 at http://www.atascientific.com.au/blog/2011/08/10/principles-laser-diffraction/.

Miall, Andrew D.

2000 *Principles of Sedimentary Basin Analysis,* 3rd ed. Springer, New York.

Midwest Geoscience Group (MGG)

2015 *Field Guide for Soil and Stratigraphic Analysis.* Midwest Geoscience Group Press, Carmel, Indiana.

Middleton, Gerard V.

1973 Johannes Walther's Law of the Correlation of Facies. *Geological Society of America Bulletin No. 84,* pp. 979-988.

Mumma, Stephanie A.

2010 *A 20,000-Yr-Old Record of Vegetation and Climate from Lower Red Rock Lake, Centennial Valley, Southwestern Montana.* Master's Thesis. Montana State University, Bozeman.

Mumma, Stephanie A., Cathy Whitlock, and Kenneth Pierce

2012 A 28,000 Year History of Vegetation and Climate from Lower Red Rock Lake, Centennial Valley, Southwestern Montana, USA. *Paleogeography, Paleoclimatology, Paleoecology* 326-328:30-41.

Murray, Andrew S. and Ann G. Wintle

2000 Luminescence Dating of Quartz Using an Improved Single-Aliquot Regenerative-Dose Protocol. *Radiation Measurements* 32:57-73.

Murry, Audrey L., James D. Keyser and Floyd W. Sharrock

1977 A Preliminary Shoreline Survey of Lima Reservoir: Archaeology in the Centennial Valley of Southwestern Montana. *Plains Anthropologist* 22:51-57.

Nelson, Michelle S., Harrison J. Gray, Jack A. Johnson, Tammy M. Rittenour, James K. Feathers, and Shannon A. Mahan

2015 User Guide for Luminescence Sampling in Archaeological and Geological Contexts. *Advances in Archaeological Practice* 3:166–177.

Nolan, Thomas B.

1964 Foreword. In *The Hebgen Lake, Montana Earthquake of August 17, 1959* pp. V-VI. Geological Survey Professional Paper No. 435. U.S. Department of the Interior, U.S. Government Printing Office, Washington, D.C.

North American Commission on Stratigraphic Nomenclature (NACSTRAT)

1983 North American Stratigraphic Code. *Bulletin of the American Association of Petroleum Geologists* 67:841–875.

Payne, Suzette J., Robert McCaffrey, and Robert W. King

2008 Strain Rates and Contemporary Deformation in the Snake River Plain and Surrounding Basin and Range from GPS and Seismicity. *Geology* 36:647-650.

Peart, Jonathan M, Jason M. Patten, and Paul Santarone

2011a Smithsonian Site No. 24BE43. Montana Cultural Resource Information System (CRIS) Form Update.

Peart, Jonathan M, Jason M. Patten, and Paul Santarone

2011b Smithsonian Site No. 24BE46. Montana Cultural Resource Information System (CRIS) Form Update.

Peart, Jonathan M, Jason M. Patten, and Paul Santarone

2011c Smithsonian Site No. 24BE52. Montana Cultural Resource Information System (CRIS) Form Update.

Peart, Jonathan M., Kenneth P. Cannon, Jason M. Patten, Paul Santarone, and Molly Boeka Cannon

2012 *Cultural Resource Inventory Along the North Shore of the Lima Reservoir, Beaverhead County, Montana*. USU Archeological Services, USUAS Technical Report Number 2011-016. Submitted to BLM Dillon Field Office, Montana. Copies available from USU Archeological Services, Inc. Logan, Utah.

Pierce, Kenneth L.

2003 Pleistocene Glaciations of the Rocky Mountains. *Developments in Quaternary Science* 1:63-76.

Pierce, Kenneth L. and Lisa A. Morgan

1992 The Track of the Yellowstone Hot Spot: Volcanism, Faulting, and Uplift. In *Regional geology of Eastern Idaho and Western Wyoming,* edited by Paul K. Link, Mel A. Kuntz, and Lucian B. Platt, pp. 1-52. Geological Society of America Memoirs 179.

Pierce, Kenneth L., Daniel R. Muhs, Maynard A. Fosberg, Shannon A. Mahan, Joseph G. Rosenbaum, Joseph M. Licciardi, Milan J. Pavich

2011 A Loess–Paleosol Record of Climate and Glacial History over the Past Two Glacial–Interglacial Cycles (~150 ka), Southern Jackson Hole, Wyoming. *Quaternary Research* 76:119-141.

Pye, Kenneth

1987 *Aeolian Dust and Dust Deposits.* Academic Press, San Diego.

Reading, H.G.

1986 *Introduction. In Sedimentary Environments and Facies.* 2nd ed. edited by H.G. Reading, pp.1-3. Blackwell Scientific Publications, Boston.

Reineck, Hans-Erich and Indra B.Singh

1980 *Depositional Sedimentary Environments: With Reference to Terrigenous Clastics.* 2nd ed. Springer-Verlag, New York.

Rich, J., Tammy Rittenour, Michelle S. Nelson, and J. Owen

2015 OSL Chronology of Middle to Late Holocene Aeolian Activity in the St. Anthony Dune Field, Southeastern Idaho, USA. *Quaternary International* 362:77-86.

Rittenour, Tammy R.

2012 OSL Sample Preparation Procedure. Manuscript on file, Utah State University Luminescence Laboratory, Logan, Utah.

Ritter, Dale F., R. C. Kochel, and Jerry R. Miller

2002 *Process Geomorphology.* 4th ed. McGraw-Hill Higher Education. San Fransisco.

Ryder, Robert T. and Robert Scholten

1973 Syntectonic Conglomerates in Southwestern Montana: Their Nature, Origin, and Tectonic Significance. *Geological Society of America Bulletin* 84:773-796.

Sahu, Basanta K.

1964 Depositional Mechanisms from the Size Analysis of Clastic Sediments. *Journal of Sedimentary Petrology* 34:73-83.

Schiffer, Michael B.

1987 *Formation Processes of the Archaeological Record.* University of Utah Press, Salt Lake.

Schoeneberger, Phillip J., D.A. Wysocki and E.C. Benham

2012 *Field Book for Describing and Sampling Soils.*3rd ed. USDA Natural Resources Conservation Service, National Soil Survey Center, Lincoln, Nebraska.

Scholten, Robert, K. A. Keenmon and W. O. Kupsch

1955 *Geology of the Lima Region, Southwestern Montana and Adjacent Idaho.* Geological Society of America Bulletin No. 4:345-404.

Schuster, LeAnn C.

2005 *The Tree Frog Site: A Protohistoric Large Game and Procurement and Processing Site in the Centennial Valley, Montana.* Master's Thesis. University of Montana, Missoula.

Simonson, Roy W.

1959 Outline of a Generalized Theory of Soil Genesis. *Soil Science Society of America Proceedings* 23:152-156.

Singh, Chander K., Pankaj Kumar, Alok Kumar and Saumitra Mukherjee

2015 Depositional Environment in Great Indian Desert using Grain Size Parameters and its Chemical Characterization. *Journal Geological Society of India* 86:412-420.

Sonderegger, J. L., J. D. Schofield, R. B. Berg, and M. L. Mannick

1982 *The Upper Centennial Valley, Beaverhead and Madison Counties, Montana.* Montana Bureau of Mines and Geology Memoir 50.

Stickney, Michael C. and Mervin J. Bartholomew

1987 Seismicity and Late Quaternary Faulting of the Northern Basin and Range Province, Montana and Idaho. *Bulletin of the Seismological Society of America* 77:1602-1625.

Tanner, William F.

1991 Suite Statistics: Evolution of the Sediment Pool. In *Principles, Methods, and Application of Particle Size Analysis,* edited by James P. Syvitski, pp. 225-236 Cambridge University Press, New York.

Thomas, D. G.

1987 Discrimination of Depositional Environments using Sedimentary Characteristics in the Mega Kalahari, Central Southern Africa. In *Desert Sediments: Ancient and Moder*n, edited by Lynne E. Frostick and Ian Reid, pp. 293-306. Geological Society Special Publication No. 35. Blackwell Scientific Publications, Boston.

Tucker, Maurice (editor)

1988 *Techniques in Sedimentology.* Blackwell Scientific Publications, Boston.

USDA (United States Department of Agriculture)

2008 Natural Resources Conservation Service: Soil Texture. Electronic document, accessed February 28, 2017 at https://www.nrcs.usda.gov/wps/portal/nrcs/detail/soils/survey/?cid=nrcs142p2_054167.

U.S. Geological Survey (USGS)

2006 FGDC Digital Cartographic Standard for Geologic Map Symbolization (PostScript Implementation). *U.S. Geological Survey Techniques and Methods* 11-A2. Electronic document, accessed on February 25, 2017 at: http://pubs.usgs.gov/tm/2006/11A02/.

Vandenberghe, Jef

2013 Grain Size of Fine-Grained Windblown Sediment: A Powerful Proxy for Process Identification. *Earth-Science Reviews* 121:18-30.

Waters, Michael R.

2000 Alluvial Stratigraphy and Geoarchaeology in the American Southwest. *Geoarchaeology: An International Journal* 15:537–557.

Wintle, Ann G. and Andrew S. Murray

2006 A Review of Quartz Optically Stimulated Luminescence Characteristics and their Relevance in Single-Aliquot Regeneration Dating Protocols. *Radiation Measurements* 41:369-391.

Witkind, Irving J.

1972 *Geologic Map of the Henrys Lake Quadrangle, Idaho and Montana.* United States Geological Survey Map I-781-A, Washington D. C.

Witkind, Irving J.

1975 *Geology of a Strip Along the Centennial fault, Southwestern Montana and Adjacent Idaho.* United States Geological Survey Miscellaneous Investigations Map 890, scale 1:62,500. U.S. Geological Survey, Reston, Virginia.

APPENDIX A:

OPTICALLY STIMULATED LUMINESCENCE DATA

Table 16. Optically Stimulated Luminescence (OSL) age information

Sample num.	USU num.	Depth (m)	Num. of aliquots[1]	Dose rate (Gy/ka)	D_E[2] ± 2σ (Gy)	OD[3] (%)	OSL age ± 2σ (ka)
SL2-1	USU-1700	1.3	17 (33)	2.18 ± 0.14	26.16 ± 7.79[4]	42.1 ± 8.1	13.37 ± 3.83
SL2-2	USU-1701	1	20 (40)	2.37 ± 0.12	28.96 ± 5.11[4]	37.7 ± 7.1	12.20 ± 2.45
SL3-1	USU-1702	0.5	12 (28)	2.99 ± 0.16	7.47 ± 0.67	0.0	2.50 ± 0.33
SL3-2	USU-1703	0.48	13 (27)	2.95 ± 0.16	7.75 ± 0.72	10.0 ± 5.0	2.62 ± 0.36
SL4-1	USU-1704	0.95	18 (31)	1.75 ± 0.10	63.37 ± 8.16	23.6 ± 5.2	36.23 ± 5.89
SL5-1	USU-1705	1.1	13 (29)	2.31 ± 0.16	29.44 ± 3.36	15.2 ± 5.1	12.74 ± 1.99
SL3-3	USU-1834	0.5	14 (32)	2.99 ± 0.16	9.06 ± 1.01	14.5 ± 5.2	3.03 ± 0.45
SL7-1	USU-1835	0.77	19 (28)	2.96 ± 0.16	26.33 ± 1.62	5.8 ± 4.5	8.91 ± 1.04
SL8-1	USU-2049	1.36	18 (29)	3.39 ± 0.19	48.67 ± 4.74	14.8 ± 4.6	14.35 ± 2.01
SL9-1	USU-2050	0.76	15 (27)	2.84 ± 0.16	55.98 ± 8.65	26.4 ± 6.1	19.73 ± 3.64
SL2-3	USU-2185	0.23	17 (51)	2.96 ± 0.15	2.23 ± 0.42	24.1 ± 8.6	0.75 ± 0.16
SL5-2	USU-2186	0.36	20 (57)	2.48 ± 0.14	9.13 ± 1.48	28.1 ± 6.9	3.68 ± 0.70
SL10-1	USU-2187	0.6	13 (30)	3.30 ± 0.26	199.56 ± 26.09	20.3 ± 5.3	60.39 ± 10.48
SL11-1	USU-2188	0.73	14 (20)	4.24 ± 0.32	220.23 ± 27.61	19.0 ± 5.2	51.90 ± 8.75

[1] Age analysis using the single-aliquot regenerative-dose procedure of Murray and Wintle (2000) on 1-mm small-aliquots of quartz sand. Number of aliquots used in age calculation and number of aliquots analyzed in parentheses.

[2] Equivalent dose (D_E) calculated using the Central Age Model (CAM) of Galbraith and Roberts (2012), unless otherwise noted.

[3] Overdispersion (OD) represents variance in D_E data beyond measurement uncertainties, OD >20% may indicate significant scatter due to depositional or post-depositional processes.

[4] Equivalent dose (D_E) calculated using the Minimum Age Model (MAM) of Galbraith and Roberts (2012).

Table 17. OSL dose rate information

Sample num.	USU num.	In-situ H_2O (%)[1]	Grain size (µm)	K (%)[2]	Rb (ppm)[2]	Th (ppm)[2]	U (ppm)[2]	Cosmic (Gy/ka)
SL2-1	USU-1700	13.5	125-250	1.25±0.03	58.7±2.3	6.7±0.6	2.2±0.2	0.26±0.03
SL2-2	USU-1701	7.6	125-250	1.25±0.03	63.6±2.5	7.2±0.7	2.3±0.2	0.27±0.03
SL3-1	USU-1702	4.5	125-250	1.78±0.04	82.5±3.3	9.5±0.9	2.5±0.2	0.29±0.03
SL3-2	USU-1703	2.8	125-250	1.73±0.04	86.5±3.5	9.9±0.9	2.4±0.2	0.29±0.03
SL4-1	USU-1704	3.5	180-250	0.76±0.02	36.8±1.5	4.9±0.4	2.4±0.2	0.28±0.03
SL5-1	USU-1705	14.8	180-250	1.32±0.03	65.6±2.6	7.8±0.7	2.4±0.2	0.27±0.03
SL3-3	USU-1834	5.3	90-180	1.76±0.04	80.5±3.2	9.4±0.9	2.4±0.2	0.29±0.03
SL7-1	USU-1835	3.9	90-150	1.70±0.04	79.7±3.2	9.6±0.9	2.4±0.2	0.28±0.03
SL8-1	USU-2049	8.2	75-150	1.47±0.04	88.5±3.5	10.8±1.0	4.8±0.3	0.26±0.03
SL9-1	USU-2050	8.0	75-150	1.14±0.03	67.4±2.7	8.3±0.8	4.3±0.3	0.28±0.03
SL2-3	USU-2185	9.1	90-180	1.68±0.04	79.5±3.2	9.1±0.8	2.5±0.2	0.30±0.03
SL5-2	USU-2186	10.3	125-212	1.42±0.04	64.2±2.6	7.6±0.7	2.1±0.2	0.30±0.03
SL10-1	USU-2187	18.3	63-150	1.70±0.04	86.4±3.5	9.2±0.8	5.3±0.4	0.29±0.03
SL11-1	USU-2188	16.8	63-150	1.82±0.05	101.0±4.0	11.7±1.1	8.5±0.6	0.28±0.03

[1] Average of all values >5% (10±3%) used as moisture content over burial history for in-situ values <5%.
[2] Radioelemental concentrations determined by ALS Chemex using ICP-MS and ICP-AES techniques; dose rate is derived from concentrations by conversion factors from Guerin et al. 2011.

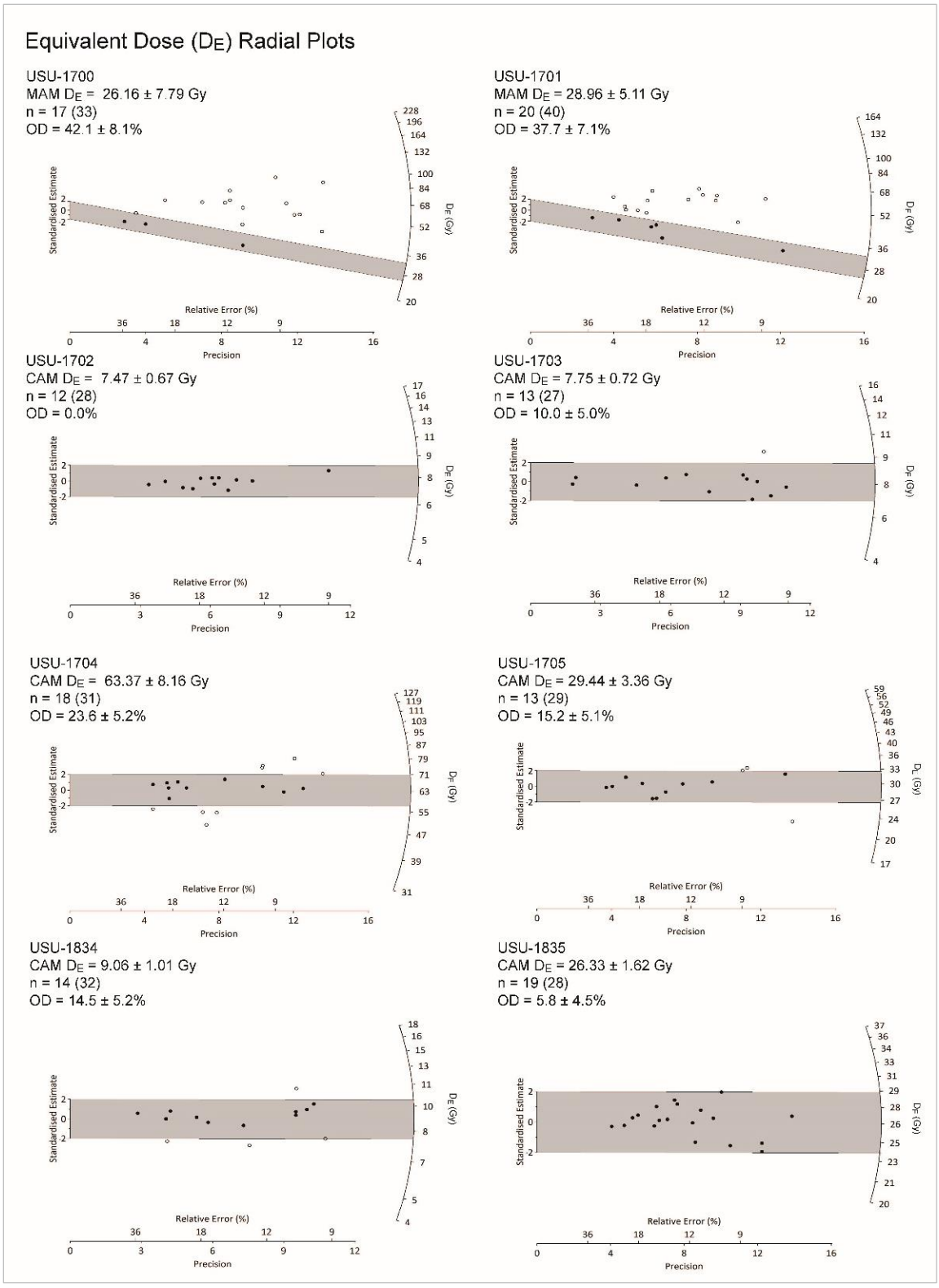

Figure 57. Equivalent Dose (D_E) radial plots for OSL samples USU-1700, USU-1701, USU-1702, USU-1703, USU-1704, USU-1705, USU-1834, and USU-1835.

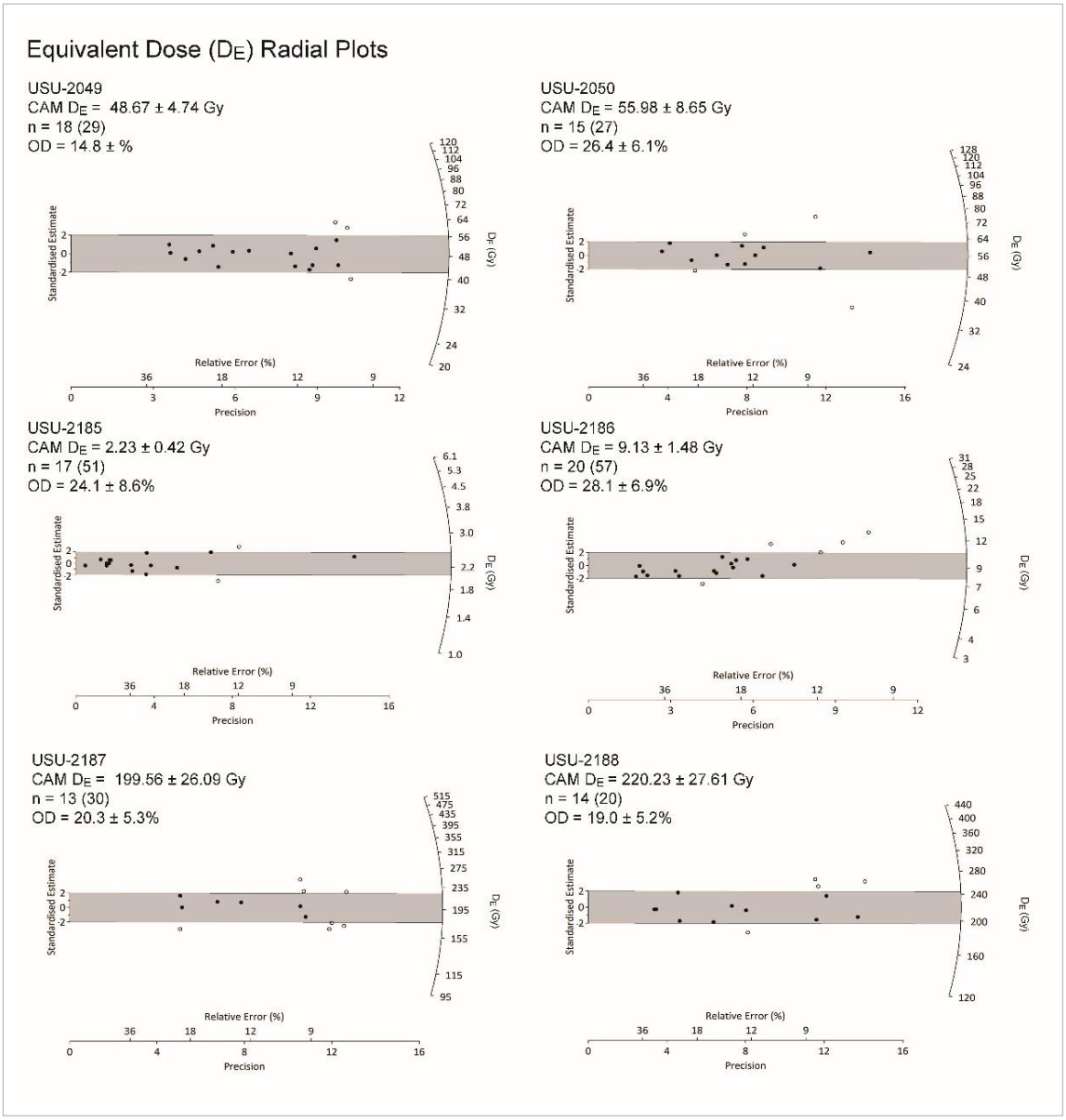

Figure 58. Equivalent Dose (D_E) radial plots for OSL samples USU-2049, USU-2050, USU-2185, USU-2186, USU-2187, and USU-2188.

APPENDIX B:

GRANULOMETRY DATA

Granulometry Descriptive Statistics

Formulas

I used formulas per Blott and Pye (2001:1241), based on their metric modifications of Folk and Ward (1957) measures for computing descriptive statistics (Table 18).

Texture Parameters

Texture data metrics include percentages of clay, silt, and sand, total fine and coarse fraction proportions, and ratios of sand to silt and clay combined (Tables 15-24). The USDA texture class is also provided.

Measures of Central Tendency

Central tendency data include median, mean, sorting (standard deviation), skewness and kurtosis values (Tables 25-34). Correspondent descriptions are provided per Folk and Ward (1957).

Cumulative Percentiles

Cumulative percentiles are useful for understanding the relative contributions of any grade of sediment size (Blott and Pye 2001) (Tables 35-44). Moreover, differences between these metrics provides useful measures of dispersion.

Modality of Particle Size Distribution

While suitable for understanding broad distinctions, common distribution measures such as mean, sorting, skewness, and kurtosis can mask important variations in natural sediment bodies (Schleyer 1986). Quantifying particle size mode is therefore important for identifying underlying differences among samples (Schleyer 1986:871) (Tables 45-54). This is especially true for mixed sediments and those affected by

pedogenesis (Yong et al. 2017).

Table 18. Granulometry formulas used for determining sediment descriptive statistics and categorical descriptions, per Blott and Pye's (2001) metric modification of Folk and Ward (1957).

Mean (M_G)	$M_G = \exp\frac{\ln P_{16} + \ln P_{50} + \ln P_{84}}{3}$
Standard Deviation/ Sorting (σ_G)	$\sigma_G = \exp\left(\frac{\ln P_{16} - \ln P_{84}}{4} + \frac{\ln P_5 - \ln P_{95}}{6 * 6}\right)$
Skewness (Sk_G)	$Sk_G = \frac{\ln P_{16} + P_{84} - 2(\ln P_{50})}{2(\ln P_{84} - P_{16})} + \frac{\ln P_5 + \ln P_{95} - 2(\ln P_{50})}{2(\ln P_{25} - P_5)}$
Kurtosis (K_G)	$K_G = \frac{\ln P_5 - \ln P_{95}}{2.44(\ln P_{25} - \ln P_{75})}$

Key: ln natural logarithm; exp exponential; P grain diameter in metric units; P_x grain diameter at cumulative percentile value of x

Sorting (σ_G) Categories		**Skewness (Sk_G) Categories**		**Kurtosis (K_G) Categories**	
v. well-sorted	<1.27	v. fine skewed	-0.3 to -1.0	v. platykurtic	<0.67
well-sorted	1.27-1.41	fine skewed	-1.0 to -0.3	platykurtic	0.67-0.90
mod. well-sorted	1.41-1.62	symmetrical	-0.1 to +0.1	mesokurtic	0.90-1.11
mod. sorted	1.62-2.00	coarse skewed	+0.1 to +0.3	leptokurtic	1.11-1.50
poorly sorted	2.00-4.00	v. coarse skewed	+0.3 to +1.0	v. leptokurtic	1.50-3.00
v. poorly sorted	4.00-16.00			ex. leptokurtic	>3.00
ex. poorly sorted	>16.00				

Table 19. Profile 1 texture data.

Strata / Sample Depth (cmbs)	**Texture Parameters**					**Sand/ Silt + Clay**	**USDA Texture Class**
	Clay (< 2 µm)	**Silt** (2 < 62.5 µm)	**Sand** (62.5 < 1000 µm)	**Fine Fraction Total** (<1mm)	**Coarse Fraction Total** (>1mm)		
A (0-70)	11.71%	83.30%	4.97%	99.98%	0.02%	0.06	silt
Bty (70-120)	11.71%	83.32%	4.98%	100.00%	0.00%	0.06	silt
Unit 3 (120-140)	14.90%	84.10%	1.01%	100.00%	0.00%	0.01	silt loam
Unit 2 (140-162)	13.95%	86.04%	0.01%	100.00%	0.00%	0.00	silt loam
Unit 1 (162-210)	20.61%	73.63%	5.76%	100.00%	0.00%	0.07	silt loam

Table 20. Profile 2 texture data.

Strata / Sample Depth (cmbs)	Texture Parameters					Sand/ Silt + Clay	USDA Texture Class
	Clay (< 2 µm)	**Silt** (2 < 62.5 µm)	**Sand** (62.5 < 1000 µm)	**Fine Fraction Total** (<1mm)	**Coarse Fraction Total** (>1mm)		
A (0-11) [a]	7.45%	64.40%	27.67%	99.51%	0.49%	0.43	silt loam
A (0-11) [b]	7.27%	66.89%	25.33%	99.49%	0.51%	0.38	silt loam
A (0-11) [c]	7.14%	67.99%	24.38%	99.51%	0.49%	0.36	silt loam
Bw (11-32)	11.54%	71.72%	16.72%	99.98%	0.02%	0.22	silt loam
2Ab (32-42)	8.66%	68.30%	23.02%	99.98%	0.02%	0.32	silt loam
2ABkb (42-62)	10.25%	67.58%	22.17%	100.00%	0.00%	0.30	silt loam
3ABb (62-74)	7.11%	58.84%	34.00%	99.95%	0.05%	0.54	silt loam
3Bkb (74-99)	7.10%	59.01%	33.85%	99.96%	0.04%	0.53	silt loam
3C (92-155)	8.24%	58.79%	32.92%	99.95%	0.05%	0.51	silt loam
Unit 3 (92-134)	13.48%	76.35%	10.15%	99.97%	0.03%	0.12	silt loam
Unit 2 (134-150)	4.23%	26.29%	69.49%	100.00%	0.00%	2.32	sandy loam
Unit 1 (155-160)	13.66%	73.04%	13.29%	100.00%	0.00%	0.17	silt loam

[a] Organic removal using only mechanical means

[b] Organic removal using mechanical means plus hydrogen peroxide (H2O2) treatment followed by desiccation (no liquid poured off so as to retain fine fraction)

[c] Organic removal using mechanical means plus water floating followed by desiccation (no liquid poured off so as to retain fine fraction)

Table 21. Profile 3/7 texture data.

Strata / Sample Depth (cmbs)	**Texture Parameters**					**Sand/ Silt + Clay**	**USDA Texture Class**
	Clay (< 2 µm)	**Silt** (2 < 62.5 µm)	**Sand** (62.5 < 1000 µm)	**Fine Fraction Total** (<1mm)	**Coarse Fraction Total** (>1mm)		
A (0-19)	8.68%	70.65%	20.67%	100.00%	0.00%	0.28	silt loam
C (19-43)	10.49%	70.85%	18.66%	100.00%	0.00%	0.25	silt loam
2Ab (43-58)	5.31%	75.81%	18.87%	100.00%	0.00%	0.28	silt loam
2Bkb (58-64)							
3ABkb (64-84)	6.83%	78.10%	15.06%	100.00%	0.00%	0.20	silt loam
3CB (84-119)	10.43%	71.69%	17.87%	99.99%	0.01%	0.23	silt loam
3CB2 (119-185)	11.32%	77.66%	11.01%	100.00%	0.00%	0.13	silt loam

Table 22. Profile 4 texture data.

Strata / Sample Depth (cmbs)	Texture Parameters					Sand/ Silt + Clay	USDA Texture Class
	Clay (< 2 µm)	**Silt** (2 < 62.5 µm)	**Sand** (62.5 < 1000 µm)	**Fine Fraction Total** (<1mm)	**Coarse Fraction Total** (>1mm)		
A (0-15)	6.59%	60.74%	32.68%	100.00%	0.00%	0.53	silt loam
Bw (15-59)	13.86%	66.43%	19.71%	100.00%	0.00%	0.26	silt loam
Unit 3 (59-80)	13.27%	59.69%	27.04%	100.00%	0.00%	0.38	silt loam
Unit 2 (80-101)	6.57%	25.45%	67.98%	100.00%	0.00%	2.13	sandy loam
Unit 1 (101-130)	19.59%	66.41%	14.00%	100.00%	0.00%	0.17	silt loam

Table 23. Profile 5 texture data.

Strata / Sample Depth (cmbs)	Texture Parameters					Sand/ Silt + Clay	USDA Texture Class
	Clay (< 2 µm)	**Silt** (2 < 62.5 µm)	**Sand** (62.5 < 1000 µm)	**Fine Fraction Total** (<1mm)	**Coarse Fraction Total** (>1mm)		
A (5-7)	7.08%	61.09%	31.82%	100.00%	0.00%	0.51	silt loam
A (9-11)	5.40%	50.92%	32.37%	87.25%	12.75%	0.82	silt loam
2Ab (19-21)	5.43%	59.78%	34.79%	100.00%	0.00%	0.59	silt loam
2Ab (28-30)	6.46%	62.97%	30.57%	100.00%	0.00%	0.48	silt loam
2C (39-41)	5.71%	64.73%	29.57%	100.00%	0.00%	0.47	silt loam
2C (49-51)	7.83%	63.72%	28.45%	100.00%	0.00%	0.42	silt loam
3Ab' (59-62)	9.40%	65.33%	25.27%	100.00%	0.00%	0.36	silt loam
3Ab' (68-70)	9.13%	64.35%	26.52%	100.00%	0.00%	0.38	silt loam
3ABkb (79-80)	10.11%	66.02%	23.86%	100.00%	0.00%	0.33	silt loam
3ABkb (89-91)	9.71%	65.12%	25.16%	100.00%	0.00%	0.35	silt loam
3ABkb (99-101)	10.99%	65.75%	23.26%	100.00%	0.00%	0.32	silt loam
3ABkb (109-111)	10.74%	63.31%	25.95%	100.00%	0.00%	0.36	silt loam
3Bkb (119-121)	11.01%	62.08%	26.92%	100.00%	0.00%	0.38	silt loam

Table 24. Profile 6 texture data.

Strata / Sample Depth (cmbs)	Texture Parameters					Sand/ Silt + Clay	USDA Texture Class
	Clay (< 2 µm)	**Silt** (2 < 62.5 µm)	**Sand** (62.5 < 1000 µm)	**Fine Fraction Total** (<1mm)	**Coarse Fraction Total** (>1mm)		
A (0-35)	11.86%	78.64%	9.50%	100.00%	0.00%	0.12	silt loam
Bw (35-105)	13.50%	80.30%	6.20%	100.00%	0.00%	0.07	silt loam
Bk (105-160)	13.47%	82.01%	4.52%	100.00%	0.00%	0.06	silt loam
By (160-195)	12.91%	85.12%	1.97%	100.00%	0.00%	0.03	silt loam
2By (195-200)							
2C (195-224)	10.89%	80.65%	8.46%	100.00%	0.00%	0.12	silt
Unit 3 (224-259)	10.89%	86.14%	4.02%	100.00%	0.00%	0.06	silt
Unit 2 (259-289)	10.89%	87.45%	0.92%	100.00%	0.00%	0.02	silt
Unit 1 (289-297)	10.89%	80.48%	5.74%	100.00%	0.00%	0.07	silt loam

Table 25. Profile 8 texture data.

Strata / Sample Depth (cmbs)	Texture Parameters					Sand/ Silt + Clay	USDA Texture Class
	Clay (< 2 µm)	**Silt** (2 < 62.5 µm)	**Sand** (62.5 < 1000 µm)	**Fine Fraction Total** (<1mm)	**Coarse Fraction Total** (>1mm)		
A (0-6)	11.32%	76.74%	11.86%	99.92%	0.08%	0.15	silt loam
Bw (6-153)	13.92%	78.66%	7.19%	99.76%	0.24%	0.09	silt loam
Unit 6 (153-192)	17.83%	81.93%	0.24%	100.00%	0.00%	0.00	silt loam
Unit 5 (192-237)	18.23%	68.09%	13.68%	100.00%	0.00%	0.16	silt loam
Unit 4 (237-261)	5.03%	45.95%	49.03%	100.00%	0.00%	1.09	sandy loam
Unit 3 (261-350)	9.67%	74.79%	15.44%	99.90%	0.10%	0.20	silt loam
Unit 2 (350-410)	7.02%	50.64%	42.34%	100.00%	0.00%	0.75	silt loam
Unit 1 (410-460)	11.01%	81.17%	7.82%	100.00%	0.00%	0.10	silt

Table 26. Profile 9 texture data.

Strata / Sample Depth (cmbs)	**Texture Parameters**					**Sand/ Silt + Clay**	**USDA Texture Class**
	Clay (< 2 µm)	**Silt** (2 < 62.5 µm)	**Sand** (62.5 < 1000 µm)	**Fine Fraction Total** (<1mm)	**Coarse Fraction Total** (>1mm)		
A (0-6)	10.20%	81.48%	8.32%	100.00%	0.00%	0.11	silt
Bw (6-71)	12.99%	82.82%	4.19%	100.00%	0.00%	0.06	silt loam
Bk (71-82)	12.13%	87.38%	0.48%	100.00%	0.00%	0.01	silt loam
C (82-109)	11.58%	85.35%	3.07%	100.00%	0.00%	0.04	silt
Unit 4 (109-190)	13.03%	84.26%	2.71%	100.00%	0.00%	0.04	silt loam
Unit 3 (190-213)	11.53%	84.27%	4.19%	100.00%	0.00%	0.06	silt
Unit 2 (213-240)	9.75%	85.26%	4.98%	100.00%	0.00%	0.06	silt
Unit 1 (240-257)	12.54%	87.36%	0.10%	100.00%	0.00%	0.00	silt loam

Table 27. Profile 10 texture data.

Strata / Sample Depth (cmbs)	Texture Parameters					Sand/ Silt + Clay	USDA Texture Class
	Clay (< 2 µm)	Silt (2 < 62.5 µm)	Sand (62.5 < 1000 µm)	Fine Fraction Total (<1mm)	Coarse Fraction Total (>1mm)		
A (0-15)	16.42%	78.82%	4.67%	99.91%	0.09%	0.06	silt loam
C (15-65)	17.94%	75.21%	6.85%	100.00%	0.00%	0.08	silt loam
Unit 6 (65-116)	22.01%	71.87%	6.12%	100.00%	0.00%	0.08	silt loam
Unit 5 (116-121)	10.50%	23.00%	29.10%	62.60%	37.40%	0.87	very gravelly loam
Unit 4 (121-148)	5.12%	12.10%	82.77%	100.00%	0.00%	4.81	loamy sand
Unit 3 (148-199)	14.76%	58.56%	24.89%	98.18%	1.82%	0.37	silt loam
Unit 2 (199-252)	17.37%	70.00%	12.63%	100.00%	0.00%	0.16	silt loam
Unit 1 (252-320)	4.22%	47.71%	48.07%	100.00%	0.00%	1.14	sandy loam

Table 28. Profile 11 texture data.

Strata / Sample Depth (cmbs)	Texture Parameters					Sand/ Silt + Clay	USDA Texture Class
	Clay (< 2 µm)	Silt (2 < 62.5 µm)	Sand (62.5 < 1000 µm)	Fine Fraction Total (<1mm)	Coarse Fraction Total (>1mm)		
A (0-11)	15.81%	75.33%	8.86%	100.00%	0.00%	0.11	silt loam
Bw (11-45)	17.98%	77.87%	4.15%	100.00%	0.00%	0.05	silt loam
Unit 4 (45-55)	15.55%	80.06%	4.38%	100.00%	0.00%	0.05	silt loam
Unit 3 (55-63)	20.98%	75.84%	3.19%	100.00%	0.00%	0.04	silt loam
Unit 2 (63-73)	14.19%	83.17%	2.65%	100.00%	0.00%	0.03	silt loam
Unit 1 (73-150)	20.15%	78.78%	1.07%	100.00%	0.00%	0.01	silt loam

Table 29. Profile 11 texture data.

Sample Number	Texture Parameters					Sand/ Silt + Clay	USDA Texture Class
	Clay (< 2 µm)	**Silt** (2 < 62.5 µm)	**Sand** (62.5 < 1000 µm)	**Fine Fraction Total** (<1mm)	**Coarse Fraction Total** (>1mm)		
PL-RF7-60	3.57%	44.05%	52.39 %	100.00%	0.00%	1.19	sandy loam
PL-MO4-100	3.84%	61.56%	34.59 %	100.00%	0.00%	0.60	silt loam
DS-RF6-200	0.97%	14.12%	84.92 %	100.00%	0.00%	5.68	loamy sand
DS-RF7-250	1.02%	11.34%	87.62 %	100.00%	0.00%	7.18	sand
DS-KNB-260	0.00%	1.21%	98.80 %	100.00%	0.00%	82.67	sand
SL-PRS-11	7.17%	79.42%	13.44 %	100.00%	0.00%	0.19	silt loam
SL-PRS-73	7.10%	81.39%	11.51 %	100.00%	0.00%	0.16	silt
SL-PRS-135	8.53%	83.86%	7.61%	100.00%	0.00%	0.10	silt
SL-PRS-166	2.89%	42.46%	54.64 %	100.00%	0.00%	1.46	sandy loam
DL-EFA-21	10.42%	87.12%	2.47%	100.00%	0.00%	0.04	silt
DL-EFA-52	11.83%	87.57%	0.60%	100.00%	0.00%	0.01	silt
DL-EFA-88	12.94%	85.64%	1.43%	100.00%	0.00%	0.02	silt loam
DL-EFA-146	15.35%	83.02%	1.61%	100.00%	0.00%	0.02	silt loam
HEA-AWT-24	5.10%	73.21%	21.66 %	100.00%	0.00%	0.33	silt loam
HEA-AWT-70	5.80%	69.69%	24.52 %	100.00%	0.00%	0.38	silt loam
HEA-AWT-89	8.85%	67.87%	23.29 %	100.00%	0.00%	0.36	silt loam
HEA-AWT-141	4.90%	71.99%	23.09 %	100.00%	0.00%	0.39	silt loam
LEA-AWF-28	7.42%	75.99%	16.59 %	100.00%	0.00%	0.23	silt loam
LEA-AWF-86	7.09%	76.72%	16.20 %	100.00%	0.00%	0.23	silt loam
LEA-AWF-116	6.46%	79.48%	14.06 %	100.00%	0.00%	0.20	silt loam
LEA-AWF-171	9.38%	81.26%	9.35%	100.00%	0.00%	0.13	silt

Table 30. Profile 1 measures of clast size central tendency

Strata / sample depth	Median value (D_{50})	Mean value	Mean description	Sorting value	Sorting description	Skewness value	Skewness description	Kurtosis value	Kurtosis description
A (0-70)	13.15	11.111	Medium Silt	3.487	Poorly Sorted	-0.189	Fine Skewed	0.923	Mesokurtic
Bty (70-120)	13.14	11.107	Medium Silt	3.485	Poorly Sorted	-0.189	Fine Skewed	0.922	Mesokurtic
C (120-140)	7.041	6.947	Fine Silt	2.922	Poorly Sorted	-0.039	Symmetrical	0.914	Mesokurtic
Unit 2 (140-162)	10.08	8.465	Medium Silt	3.024	Poorly Sorted	-0.261	Fine Skewed	0.919	Mesokurtic
Unit 1 (162-210)	6.693	6.554	Fine Silt	3.857	Poorly Sorted	0.038	Symmetrical	1.028	Mesokurtic

181

Table 31. Profile 2 measures of clast size central tendency

Strata / sample depth	Median value (D_{50})	Mean value	Mean description	Sorting value	Sorting description	Skewness value	Skewness description	Kurtosis value	Kurtosis description
A (0-11) [a]	28.58	26.722	Coarse Silt	5.065	Very Poorly Sorted	-0.094	Symmetrical	0.961	Mesokurtic
A (0-11) [b]	25.35	25.204	Coarse Silt	4.914	Very Poorly Sorted	-0.045	Symmetrical	0.997	Mesokurtic
A (0-11) [c]	25.46	25.025	Coarse Silt	4.784	Very Poorly Sorted	-0.055	Symmetrical	1.029	Mesokurtic
Bw (11-32)	15.61	15.222	Medium Silt	4.993	Very Poorly Sorted	-0.002	Symmetrical	1.059	Mesokurtic
2Ab (32-42)	21.48	22.461	Coarse Silt	5.225	Very Poorly Sorted	-0.006	Symmetrical	1.024	Mesokurtic
2ABkb (42-62)	18.16	19.828	Coarse Silt	5.528	Very Poorly Sorted	0.033	Symmetrical	0.986	Mesokurtic
3ABb (62-74)	28.05	30.141	Coarse Silt	5.473	Very Poorly Sorted	-0.018	Symmetrical	0.801	Platykurtic
3Bkb (74-99)	26.72	29.211	Coarse Silt	5.473	Very Poorly Sorted	-0.003	Symmetrical	0.783	Platykurtic
3C (92-155)	23.82	26.532	Coarse Silt	5.751	Very Poorly Sorted	0.014	Symmetrical	0.760	Platykurtic
Unit 3 (92-134)	10.42	10.236	Medium Silt	4.169	Very Poorly Sorted	0.026	Symmetrical	1.093	Mesokurtic
Unit 2 (134-150)	140.0	71.118	Very Fine Sand	4.615	Very Poorly Sorted	-0.647	Very Fine Skewed	0.917	Mesokurtic
Unit 1 (155-160)	8.769	10.666	Medium Silt	4.443	Very Poorly Sorted	0.159	Coarse Skewed	1.036	Mesokurtic

a Organic removal using only mechanical means
b Organic removal using mechanical means plus hydrogen peroxide (H2O2) treatment followed by desiccation (no liquid poured off so as to retain fine fraction)
c Organic removal using mechanical means plus water floating followed by desiccation (no liquid poured off so as to retain fine fraction)

182

Table 32. Profile 3/7 measures of clast size central tendency

Strata / sample depth	Median value (D_{50})	Mean value	Mean description	Sorting value	Sorting description	Skewness value	Skewness description	Kurtosis value	Kurtosis description
A (0-19)	20.27	20.424	Coarse Silt	4.980	Very Poorly Sorted	-0.013	Symmetrical	1.055	Mesokurtic
C (19-43)	17.64	17.734	Coarse Silt	5.218	Very Poorly Sorted	0.004	Symmetrical	1.064	Mesokurtic
2Ab (43-58)	31.34	25.978	Coarse Silt	3.657	Poorly Sorted	-0.207	Fine Skewed	1.309	Leptokurtic
2Bkb (58-64)									
3ABkb (64-84)	22.35	19.279	Coarse Silt	3.903	Poorly Sorted	-0.134	Fine Skewed	1.168	Leptokurtic
3CB (84-119)	15.55	16.116	Coarse Silt	5.044	Very Poorly Sorted	0.043	Symmetrical	1.062	Mesokurtic
3CB2 (119-185)	11.78	11.291	Medium Silt	3.923	Poorly Sorted	-0.011	Symmetrical	1.122	Leptokurtic

183

Table 33. Profile 4 measures of clast size central tendency.

Strata / sample depth	Median value (D_{50})	Mean value	Mean description	Sorting value	Sorting description	Skewness value	Skewness description	Kurtosis value	Kurtosis description
A (0-15)	30.92	31.178	Coarse Silt	5.232	Very Poorly Sorted	-0.049	Symmetrical	0.912	Mesokurtic
Bw (15-59)	13.19	16.015	Coarse Silt	6.267	Very Poorly Sorted	0.129	Coarse Skewed	1.027	Mesokurtic
Unit 3 (59-80)	12.23	17.773	Coarse Silt	6.706	Very Poorly Sorted	0.203	Coarse Skewed	0.714	Platykurtic
Unit 2 (80-101)	149.3	60.705	Very Coarse Silt	5.775	Very Poorly Sorted	-0.697	Very Fine Skewed	0.814	Platykurtic
Unit 1 (101-130)	7.554	8.967	Medium Silt	5.384	Very Poorly Sorted	0.185	Coarse Skewed	1.091	Mesokurtic

184

Table 34. Profile 5 measures of clast size central tendency.

Strata / sample depth	Median value (D_{50})	Mean value	Mean description	Sorting value	Sorting description	Skewness value	Skewness description	Kurtosis value	Kurtosis description
A (5-7)	30.28	30.090	Coarse Silt	5.338	Very Poorly Sorted	-0.060	Symmetrical	0.909	Mesokurtic
A (9-11)	47.11	48.078	Very Coarse Silt	6.847	Very Poorly Sorted	0.031	Symmetrical	1.041	Mesokurtic
2Ab (19-21)	38.49	37.528	Very Coarse Silt	4.813	Very Poorly Sorted	-0.097	Symmetrical	0.969	Mesokurtic
2Ab (28-30)	31.80	31.485	Very Coarse Silt	5.026	Very Poorly Sorted	-0.072	Symmetrical	0.967	Mesokurtic
2C (39-41)	33.74	33.154	Very Coarse Silt	4.688	Very Poorly Sorted	-0.079	Symmetrical	1.067	Mesokurtic
2C (49-51)	24.35	26.233	Coarse Silt	5.511	Very Poorly Sorted	0.006	Symmetrical	0.883	Platykurtic
3Ab' (59-62)	19.92	22.030	Coarse Silt	5.699	Very Poorly Sorted	0.037	Symmetrical	0.900	Mesokurtic
3Ab' (68-70)	18.57	22.192	Coarse Silt	5.788	Very Poorly Sorted	0.086	Symmetrical	0.852	Platykurtic
3ABkb (79-80)	16.19	19.966	Coarse Silt	5.884	Very Poorly Sorted	0.118	Coarse Skewed	0.925	Mesokurtic
3ABkb (89-91)	15.45	20.143	Coarse Silt	5.926	Very Poorly Sorted	0.152	Coarse Skewed	0.854	Platykurtic
3ABkb (99-101)	13.25	17.649	Coarse Silt	5.907	Very Poorly Sorted	0.177	Coarse Skewed	0.895	Platykurtic
3ABkb (109-111)	14.17	19.239	Coarse Silt	6.179	Very Poorly Sorted	0.175	Coarse Skewed	0.811	Platykurtic
3Bkb (119-121)	15.21	20.306	Coarse Silt	6.462	Very Poorly Sorted	0.157	Coarse Skewed	0.797	Platykurtic

185

Table 35. Profile 6 measures of clast size central tendency.

Strata / sample depth	Median value (D_{50})	Mean value	Mean description	Sorting value	Sorting description	Skewness value	Skewness description	Kurtosis value	Kurtosis description
A (0-35)	15.79	12.933	Medium Silt	4.115	Very Poorly Sorted	-0.160	Fine Skewed	1.030	Mesokurtic
Bw (35-105)	11.80	10.137	Medium Silt	3.725	Poorly Sorted	-0.131	Fine Skewed	0.987	Mesokurtic
Bk (105-160)	11.74	10.097	Medium Silt	3.556	Poorly Sorted	-0.167	Fine Skewed	0.916	Mesokurtic
By (160-195)	11.29	9.776	Medium Silt	3.312	Poorly Sorted	-0.191	Fine Skewed	0.892	Platykurtic
2By (195-200)									
2C (195-224)	19.85	14.787	Medium Silt	3.917	Poorly Sorted	-0.292	Fine Skewed	0.972	Mesokurtic
Unit 3 (224-259)	15.55	12.714	Medium Silt	3.315	Poorly Sorted	-0.263	Fine Skewed	0.966	Mesokurtic
Unit 2 (259-289)	11.47	10.139	Medium Silt	3.208	Poorly Sorted	-0.186	Fine Skewed	0.882	Platykurtic
Unit 1 (289-297)	11.79	10.186	Medium Silt	3.746	Poorly Sorted	-0.138	Fine Skewed	0.936	Mesokurtic

186

Table 36. Profile 8 measures of clast size central tendency.

Strata / sample depth	Median value (D_{50})	Mean value	Mean description	Sorting value	Sorting description	Skewness value	Skewness description	Kurtosis value	Kurtosis description
A (0-6)	16.75	13.929	Medium Silt	4.325	Very Poorly Sorted	-0.131	Fine Skewed	1.059	Mesokurtic
Bw (6-153)	11.16	9.916	Medium Silt	3.960	Poorly Sorted	-0.063	Symmetrical	1.044	Mesokurtic
Unit 6 (153-192)	8.130	7.318	Fine Silt	3.287	Poorly Sorted	-0.145	Fine Skewed	0.844	Platykurtic
Unit 5 (192-237)	9.789	9.505	Medium Silt	5.077	Very Poorly Sorted	0.048	Symmetrical	1.077	Mesokurtic
Unit 4 (237-261)	66.99	45.437	Very Coarse Silt	4.318	Very Poorly Sorted	-0.413	Very Fine Skewed	0.971	Mesokurtic
Unit 3 (261-350)	16.28	15.676	Coarse Silt	4.389	Very Poorly Sorted	-0.033	Symmetrical	1.101	Mesokurtic
Unit 2 (350-410)	31.03	35.180	Very Coarse Silt	6.363	Very Poorly Sorted	0.018	Symmetrical	0.720	Platykurtic
Unit 1 (410-460)	12.85	11.433	Medium Silt	3.663	Poorly Sorted	-0.102	Fine Skewed	1.088	Mesokurtic

187

Table 37. Profile 9 measures of clast size central tendency.

Strata / sample depth	Median value (D_{50})	Mean value	Mean description	Sorting value	Sorting description	Skewness value	Skewness description	Kurtosis value	Kurtosis description
A (0-6)	18.44	14.585	Medium Silt	3.721	Poorly Sorted	-0.260	Fine Skewed	0.983	Mesokurtic
Bw (6-71)	12.63	10.687	Medium Silt	3.558	Poorly Sorted	-0.195	Fine Skewed	0.901	Mesokurtic
Bk (71-82)	10.71	9.185	Medium Silt	2.998	Poorly Sorted	-0.227	Fine Skewed	0.931	Mesokurtic
C (82-109)	11.98	10.247	Medium Silt	3.217	Poorly Sorted	-0.206	Fine Skewed	0.950	Mesokurtic
Unit 4 (109-190)	9.043	8.721	Medium Silt	3.258	Poorly Sorted	-0.063	Symmetrical	0.953	Mesokurtic
Unit 3 (190-213)	14.98	12.340	Medium Silt	3.584	Poorly Sorted	-0.244	Fine Skewed	0.879	Platykurtic
Unit 2 (213-240)	12.27	11.307	Medium Silt	3.285	Poorly Sorted	-0.117	Fine Skewed	1.026	Mesokurtic
Unit 1 (240-257)	7.720	7.466	Fine Silt	2.781	Poorly Sorted	-0.080	Symmetrical	0.937	Mesokurtic

188

Table 38. Profile 10 measures of clast size central tendency.

Strata / sample depth	Median value (D_{50})	Mean value	Mean description	Sorting value	Sorting description	Skewness value	Skewness description	Kurtosis value	Kurtosis description
A (0-15)	8.894	8.411	Medium Silt	3.698	Poorly Sorted	-0.051	Symmetrical	0.903	Mesokurtic
C (15-65)	7.693	7.559	Fine Silt	4.223	Very Poorly Sorted	0.079	Symmetrical	1.137	Leptokurtic
Unit 6 (65-116)	7.407	7.415	Fine Silt	4.350	Very Poorly Sorted	0.014	Symmetrical	0.871	Platykurtic
Unit 5 (116-121)	222.209	208.948	Fine Sand	12.49	Extremely Poorly Sorted	-0.068	Symmetrical	0.610	Very Platykurtic
Unit 4 (121-148)	182.5	109.437	Very Fine Sand	3.788	Poorly Sorted	-0.722	Very Fine Skewed	3.441	Extremely Leptokurtic
Unit 3 (148-199)	11.33	208.948	Fine Sand	6.834	Very Poorly Sorted	0.215	Coarse Skewed	0.732	Platykurtic
Unit 2 (199-252)	7.491	9.393	Medium Silt	4.700	Very Poorly Sorted	0.186	Coarse Skewed	0.920	Mesokurtic
Unit 1 (252-320)	66.58	45.715	Very Coarse Silt	3.332	Poorly Sorted	-0.532	Very Fine Skewed	1.239	Leptokurtic

189

Table 39. Profile 11 measures of clast size central tendency.

Strata / sample depth	Median value (D_{50})	Mean value	Mean description	Sorting value	Sorting description	Skewness value	Skewness description	Kurtosis value	Kurtosis description
A (0-11)	8.964	9.059	Medium Silt	4.273	Very Poorly Sorted	0.068	Symmetrical	1.026	Mesokurtic
Bw (11-45)	6.618	6.796	Fine Silt	3.455	Poorly Sorted	0.055	Symmetrical	0.992	Mesokurtic
Unit 4 (45-55)	7.517	7.482	Fine Silt	3.384	Poorly Sorted	0.020	Symmetrical	1.019	Mesokurtic
Unit 3 (55-63)	4.987	5.230	Fine Silt	3.117	Poorly Sorted	0.113	Coarse Skewed	1.115	Leptokurtic
Unit 2 (63-73)	8.168	7.742	Fine Silt	3.136	Poorly Sorted	-0.062	Symmetrical	0.990	Mesokurtic
Unit 1 (73-150)	5.119	5.112	Fine Silt	2.828	Poorly Sorted	0.026	Symmetrical	1.053	Mesokurtic

190

Table 40. Control sample measures of clast size central tendency.

Sample Number	Median value (D_{50})	Mean value	Mean description	Sorting value	Sorting description	Skewness value	Skewness description	Kurtosis value	Kurtosis description
PL-RF7-60	79.230	69.277	Very Fine Sand	4.614	Very Poorly Sorted	-0.213	Fine Skewed	0.925	Mesokurtic
PL-MO4-100	42.833	42.041	Very Coarse Silt	3.631	Poorly Sorted	-0.110	Fine Skewed	1.132	Leptokurtic
DS-RF6-200	279.792	250.510	Medium Sand	2.597	Poorly Sorted	-0.449	Very Fine Skewed	2.258	Very Leptokurtic
DS-RF7-250	345.508	323.788	Medium Sand	2.652	Poorly Sorted	-0.389	Very Fine Skewed	2.225	Very Leptokurtic
DS-KNB-260	260.612	257.300	Medium Sand	1.629	Moderately Sorted	-0.060	Symmetrical	0.953	Mesokurtic
SL-PRS-11	23.426	19.782	Coarse Silt	3.582	Poorly Sorted	-0.222	Fine Skewed	1.151	Leptokurtic
SL-PRS-73	21.938	18.380	Coarse Silt	3.476	Poorly Sorted	-0.228	Fine Skewed	1.112	Leptokurtic
SL-PRS-135	17.643	15.226	Medium Silt	3.394	Poorly Sorted	-0.205	Fine Skewed	1.216	Leptokurtic
SL-PRS-166	75.727	60.067	Very Coarse Silt	2.959	Poorly Sorted	-0.432	Very Fine Skewed	1.414	Leptokurtic
DL-EFA-21	14.758	12.004	Medium Silt	3.182	Poorly Sorted	-0.287	Fine Skewed	1.020	Mesokurtic
DL-EFA-52	11.982	10.067	Medium Silt	3.131	Poorly Sorted	-0.242	Fine Skewed	0.897	Platykurtic

191

Table 40. Control sample measures of clast size central tendency.

DL-EFA-88	11.375	9.829	Medium Silt	3.310	Poorly Sorted	-0.205	Fine Skewed	0.938	Mesokurtic
DL-EFA-146	8.377	7.866	Medium Silt	3.283	Poorly Sorted	-0.090	Symmetrical	0.949	Mesokurtic
HEA-AWT-24	31.417	27.456	Coarse Silt	3.472	Poorly Sorted	-0.213	Fine Skewed	1.155	Leptokurtic
HEA-AWT-70	31.244	27.027	Coarse Silt	3.789	Poorly Sorted	-0.211	Fine Skewed	1.065	Mesokurtic
HEA-AWT-89	25.325	21.023	Coarse Silt	4.492	Very Poorly Sorted	-0.208	Fine Skewed	0.892	Platykurtic
HEA-AWT-141	41.204	31.074	Coarse Silt	3.143	Poorly Sorted	-0.434	Very Fine Skewed	1.272	Leptokurtic
LEA-AWF-28	19.666	18.574	Coarse Silt	4.070	Very Poorly Sorted	-0.067	Symmetrical	1.071	Mesokurtic
LEA-AWF-86	22.732	20.138	Coarse Silt	3.782	Poorly Sorted	-0.166	Fine Skewed	1.081	Mesokurtic
LEA-AWF-116	24.363	20.456	Coarse Silt	3.506	Poorly Sorted	-0.236	Fine Skewed	1.043	Mesokurtic
LEA-AWF-171	19.037	15.845	Coarse Silt	3.674	Poorly Sorted	-0.245	Fine Skewed	1.013	Mesokurtic

192

Table 41. Profile 1 cumulative percentile measures and spans between measures.

Strata / sample depth	**D_{10}** (µm)	**D_{50}** (µm)	**D_{90}** (µm)	**(D_{90} / D_{10})** (µm)	**(D_{90} - D_{10})** (µm)	**(D_{75} / D_{25})** (µm)	**(D_{75} - D_{25})** (µm)
A (0-70)	1.926	13.15	46.97	24.39	45.05	6.034	22.85
Bty (70-120)	1.926	13.14	46.93	24.37	45.00	6.033	22.84
C (120-140)	1.663	7.041	26.47	15.92	24.81	4.694	12.03
Unit 2 (140-162)	1.599	10.08	28.95	18.11	27.35	4.888	15.25
Unit 1 (162-210)	1.202	6.693	38.34	31.91	37.14	6.062	13.51

Table 42. Profile 2 cumulative percentile measures and spans between measures.

Strata / sample depth	D_{10} (µm)	D_{50} (µm)	D_{90} (µm)	(D_{90} / D_{10}) (µm)	(D_{90} - D_{10}) (µm)	(D_{75} / D_{25}) (µm)	(D_{75} - D_{25}) (µm)
A (0-11) [a]	2.894	28.58	195.2	67.45	192.3	9.075	73.04
A (0-11) [b]	2.956	25.35	186.0	62.94	183.1	8.207	63.90
A (0-11) [c]	3.008	25.46	178.5	59.33	175.5	7.508	59.55
Bw (11-32)	1.919	15.61	148.4	77.37	146.5	7.793	34.51
2Ab (32-42)	2.505	21.48	187.6	74.91	185.1	8.066	52.02
2ABkb (42-62)	2.136	18.16	186.2	87.16	184.0	9.140	48.07
3ABb (62-74)	3.012	28.05	238.8	79.30	235.8	14.43	127.2
3Bkb (74-99)	2.982	26.72	235.3	78.92	232.3	15.10	125.7
3C (92-155)	2.605	23.82	232.2	89.11	229.6	17.34	122.2
Unit 3 (92-134)	1.688	10.42	70.80	41.94	69.11	6.234	21.10
Unit 2 (134-150)	5.141	140.0	281.7	54.79	276.5	8.759	187.0
Unit 1 (155-160)	1.705	8.769	87.75	51.47	86.04	6.501	20.67

a Organic removal using only mechanical means
b Organic removal using mechanical means plus hydrogen peroxide (H2O2) treatment followed by
desiccation (no liquid poured off so as to retain fine fraction)
c Organic removal using mechanical means plus water floating followed by desiccation (no liquid
poured off so as to retain fine fraction)

Table 43. Profile 3/7 cumulative percentile measures and spans between measures.

Strata / sample depth	**D_{10}** (µm)	**D_{50}** (µm)	**D_{90}** (µm)	**(D_{90} / D_{10})** (µm)	**(D_{90} - D_{10})** (µm)	**(D_{75} / D_{25})** (µm)	**(D_{75} - D_{25})** (µm)
A (0-19)	2.49	20.27	170.94	68.75	168.46	7.49	45.06
C (19-43)	2.09	17.64	173.47	82.93	171.37	7.81	38.50
2Ab (43-58)	4.09	31.34	118.57	29.01	114.48	4.24	43.55
2Bkb (58-64)							
3ABkb (64-84)	3.03	22.35	104.33	34.44	101.30	5.19	36.42
3CB (84-119)	2.11	15.55	153.90	73.02	151.79	7.73	35.56
3CB2 (119-185)	1.97	11.78	77.78	39.46	75.81	5.51	21.06

Table 44. Profile 4 cumulative percentile measures and spans between measures.

Strata / sample depth	**D_{10}** (µm)	**D_{50}** (µm)	**D_{90}** (µm)	**(D_{90} / D_{10})** (µm)	**(D_{90} - D_{10})** (µm)	**(D_{75} / D_{25})** (µm)	**(D_{75} - D_{25})** (µm)
A (0-15)	3.30	30.92	236.89	71.85	233.59	10.57	98.56
Bw (15-59)	1.64	13.19	208.37	127.43	206.74	9.65	35.48
Unit 3 (59-80)	1.72	12.23	230.07	133.85	228.35	24.66	96.53
Unit 2 (80-101)	3.23	149.33	296.29	91.75	293.06	14.24	207.50
Unit 1 (101-130)	1.23	7.55	114.18	93.08	112.95	7.90	19.64

Table 45. Profile 5 cumulative percentile measures and spans between measures.

Strata / sample depth	**D_{10}** (µm)	**D_{50}** (µm)	**D_{90}** (µm)	**(D_{90} / D_{10})** (µm)	**(D_{90} - D_{10})** (µm)	**(D_{75} / D_{25})** (µm)	**(D_{75} - D_{25})** (µm)
A (5-7)	3.06	30.28	232.45	76.07	229.39	10.76	96.95
A (9-11)	4.11	47.11	1083.06	263.28	1078.94	13.36	184.07
2Ab (19-21)	4.04	38.49	241.07	59.69	237.03	8.40	108.01
2Ab (28-30)	3.36	31.80	223.18	66.38	219.82	8.78	88.34
2C (39-41)	3.84	33.74	217.51	56.63	213.67	6.86	76.55
2C (49-51)	2.73	24.35	225.16	82.63	222.43	11.61	85.61
3Ab' (59-62)	2.30	19.92	209.85	91.07	207.55	11.42	64.75
3Ab' (68-70)	2.36	18.57	219.78	93.18	217.42	13.14	75.51
3ABkb (79-80)	2.17	16.19	214.92	99.24	212.75	11.08	55.11
3ABkb (89-91)	2.24	15.45	219.59	98.22	217.35	13.18	65.49
3ABkb (99-101)	2.03	13.25	202.63	99.97	200.60	11.85	51.08
3ABkb (109-111)	2.06	14.17	225.28	109.34	223.22	15.96	73.67
3Bkb (119-121)	2.01	15.21	247.27	122.91	245.26	17.85	84.20

Table 46. Profile 6 cumulative percentile measures and spans between measures.

Strata / sample depth	**D_{10}** (µm)	**D_{50}** (µm)	**D_{90}** (µm)	**(D_{90} / D_{10})** (µm)	**(D_{90} - D_{10})** (µm)	**(D_{75} / D_{25})** (µm)	**(D_{75} - D_{25})** (µm)
A (0-35)	1.87	15.79	66.47	35.60	64.61	6.71	28.56
Bw (35-105)	1.69	11.80	47.22	27.90	45.53	6.18	21.18
Bk (105-160)	1.70	11.74	44.82	26.36	43.12	6.23	21.32
By (160-195)	1.77	11.29	39.18	22.19	37.41	5.78	19.74
2By (195-200)							
2C (195-224)	2.01	19.85	63.71	31.71	61.70	6.68	32.78
Unit 3 (224-259)	2.22	15.55	48.32	21.80	46.11	5.25	24.13
Unit 2 (259-289)	1.93	11.47	38.97	20.17	37.04	5.63	20.12
Unit 1 (289-297)	1.66	11.79	47.23	28.48	45.57	6.66	22.44

Table 47. Profile 8 cumulative percentile measures and spans between measures.

Strata / sample depth	**D_{10}** (µm)	**D_{50}** (µm)	**D_{90}** (µm)	**(D_{90} / D_{10})** (µm)	**(D_{90} - D_{10})** (µm)	**(D_{75} / D_{25})** (µm)	**(D_{75} - D_{25})** (µm)
A (0-6)	1.95	16.75	84.65	43.37	82.69	6.87	30.95
Bw (6-153)	1.66	11.16	51.04	30.77	49.38	6.34	21.00
Unit 6 (153-192)	1.34	8.13	30.13	22.44	28.79	6.03	15.45
Unit 5 (192-237)	1.27	9.79	124.84	98.11	123.56	8.02	22.06
Unit 4 (237-261)	4.48	66.99	201.53	45.03	197.06	7.55	111.00
Unit 3 (261-350)	2.25	16.28	110.09	48.88	107.84	6.25	31.76
Unit 2 (350-410)	3.01	31.03	344.35	114.55	341.34	23.51	205.87
Unit 1 (410-460)	2.01	12.85	55.50	27.61	53.49	5.31	21.54

Table 48. Profile 9 cumulative percentile measures and spans between measures.

Strata / sample depth	**D_{10}** (µm)	**D_{50}** (µm)	**D_{90}** (µm)	**(D_{90} / D_{10})** (µm)	**(D_{90} - D_{10})** (µm)	**(D_{75} / D_{25})** (µm)	**(D_{75} - D_{25})** (µm)
A (0-6)	2.15	18.44	62.99	29.36	60.84	6.02	30.61
Bw (6-71)	1.74	12.63	46.46	26.66	44.71	6.33	22.94
Bk (71-82)	1.87	10.71	32.07	17.16	30.21	4.75	16.15
C (82-109)	1.93	11.98	39.05	20.19	37.12	5.17	19.09
Unit 4 (109-190)	1.77	9.04	37.68	21.29	35.91	5.23	16.33
Unit 3 (190-213)	1.92	14.98	51.84	27.00	49.92	6.63	27.38
Unit 2 (213-240)	2.23	12.27	47.25	21.18	45.02	4.89	20.17
Unit 1 (240-257)	1.87	7.72	26.04	13.94	24.17	4.27	11.99

Table 49. Profile 10 cumulative percentile measures and spans between measures.

Strata / sample depth	**D_{10}** (µm)	**D_{50}** (µm)	**D_{90}** (µm)	**(D_{90} / D_{10})** (µm)	**(D_{90} - D_{10})** (µm)	**(D_{75} / D_{25})** (µm)	**(D_{75} - D_{25})** (µm)
A (0-15)	1.46	8.89	42.27	28.99	40.81	6.72	18.88
C (15-65)	1.35	7.69	42.92	31.87	41.57	6.27	16.03
Unit 6 (65-116)	1.09	7.41	52.36	47.93	51.27	8.45	19.01
Unit 5 (116-121)	1.84	222.21	14358.79	7817.24	14356.95	685.43	7159.35
Unit 4 (121-148)	6.31	182.47	291.58	46.18	285.26	1.82	106.43
Unit 3 (148-199)	1.60	11.33	222.71	139.00	221.11	24.25	85.19
Unit 2 (199-252)	1.44	7.49	83.08	57.60	81.63	8.49	22.73
Unit 1 (252-320)	5.97	66.58	137.70	23.06	131.73	3.91	76.21

Table 50. Profile 11 cumulative percentile measures and spans between measures.

Strata / sample depth	**D_{10}** (µm)	**D_{50}** (µm)	**D_{90}** (µm)	**(D_{90} / D_{10})** (µm)	**(D_{90} - D_{10})** (µm)	**(D_{75} / D_{25})** (µm)	**(D_{75} - D_{25})** (µm)
A (0-11)	1.527	8.964	60.23	39.43	58.70	7.107	20.57
Bw (11-45)	1.423	6.618	35.08	24.65	33.66	5.404	12.83
Unit 4 (45-55)	1.578	7.517	36.67	23.24	35.09	5.133	13.60
Unit 3 (55-63)	1.330	4.987	25.43	19.12	24.10	4.171	7.968
Unit 2 (63-73)	1.683	8.168	32.10	19.07	30.42	4.770	13.45
Unit 1 (73-150)	1.350	5.119	19.75	14.63	18.40	3.889	7.491

Table 51. Control sample cumulative percentile measures and spans between measures.

Sample Number	D_{10} (µm)	D_{50} (µm)	D_{90} (µm)	(D_{90} / D_{10}) (µm)	(D_{90} - D_{10}) (µm)	(D_{75} / D_{25}) (µm)	(D_{75} - D_{25}) (µm)
PL-RF7-60	7.09	79.23	370.43	52.24	363.34	9.24	204.02
PL-MO4-100	6.95	42.83	188.35	27.09	181.40	5.05	78.61
DS-RF6-200	25.65	279.79	512.67	19.98	487.02	2.13	207.83
DS-RF7-250	34.02	345.51	673.75	19.80	639.73	2.23	276.18
DS-KNB-260	134.10	260.61	472.70	3.53	338.60	1.98	179.36
SL-PRS-11	3.07	23.43	82.74	26.96	79.67	4.73	36.02
SL-PRS-73	2.98	21.94	75.13	25.18	72.15	4.69	33.25
SL-PRS-135	2.62	17.64	58.60	22.39	55.98	4.26	25.35
SL-PRS-166	9.69	75.73	166.40	17.18	156.71	3.10	80.79
DL-EFA-21	2.10	14.76	42.72	20.33	40.62	4.62	21.22
DL-EFA-52	1.91	11.98	36.73	19.21	34.82	5.26	19.04
DL-EFA-88	1.71	11.38	38.87	22.69	37.16	5.41	19.15
DL-EFA-146	1.51	8.38	33.95	22.44	32.44	5.26	14.86
HEA-AWT-24	4.32	31.42	110.70	25.61	106.38	4.55	48.64
HEA-AWT-70	3.80	31.24	120.87	31.82	117.07	5.56	55.85
HEA-AWT-89	2.47	25.33	117.20	47.40	114.73	9.07	58.01
HEA-AWT-141	4.81	41.20	95.08	19.75	90.26	3.55	47.90
LEA-AWF-28	2.86	19.67	105.40	36.83	102.54	6.08	38.81
LEA-AWF-86	3.07	22.73	95.24	30.97	92.16	5.46	40.06
LEA-AWF-116	3.31	24.36	82.43	24.87	79.11	5.20	39.39
LEA-AWF-171	2.34	19.04	67.25	28.75	64.91	5.71	32.74

Table 52. Profile 1 modality.

Strata / sample depth	Modality description	Mode 1 (μm)	Mode 2 (μm)	Mode 3 (μm)
A (0-70)	Unimodal	21.43	N/A	N/A
Bty (70-120)	Unimodal	21.43	N/A	N/A
Unit 3 (120-140)	Unimodal	5.38	N/A	N/A
Unit 2 (140-162)	Bimodal	18.67	1.03	N/A
Unit 1 (162-210)	Unimodal	8.15	N/A	N/A

Table 53. Profile 2 modality.

Strata / sample depth	Modality description	Mode 1 (μm)	Mode 2 (μm)	Mode 3 (μm)
A (0-11) [a]	Bimodal	32.44	148.26	N/A
A (0-11) [b]	Bimodal	24.61	148.26	N/A
A (0-11) [c]	Bimodal	28.25	170.23	N/A
Bw (11-32)	Bimodal	21.43	195.45	N/A
2Ab (32-42)	Bimodal	24.61	195.45	N/A
2ABkb (42-62)	Bimodal	21.43	195.45	N/A
3ABb (62-74)	Bimodal	195.45	24.61	N/A
3Bkb (74-99)	Bimodal	195.45	21.43	N/A
3C (92-155)	Bimodal	195.45	21.43	N/A
Unit 3 (92-134)	Bimodal	12.33	129.13	N/A
Unit 2 (134-150)	Bimodal	195.45	18.67	N/A
Unit 1 (155-160)	Bimodal	8.15	97.96	N/A

[a] Organic removal using only mechanical means

[b] Organic removal using mechanical means plus hydrogen peroxide (H2O2) treatment followed by desiccation (no liquid poured off so as to retain fine fraction)

[c] Organic removal using mechanical means plus water floating followed by desiccation (no liquid poured off so as to retain fine fraction)

Table 54. Profile 3/7 modality.

Strata / sample depth	Modality description	Mode 1 (μm)	Mode 2 (μm)	Mode 3 (μm)
A (0-19)	Bimodal	24.61	170.23	N/A
C (19-43)	Bimodal	21.43	195.45	N/A
2Ab (43-58)	Bimodal	37.24	195.45	N/A
2Bkb (58-64)				
3ABkb (64-84)	Unimodal	28.25	N/A	N/A
3CB (84-119)	Bimodal	18.67	170.23	N/A
3CB2 (119-185)	Bimodal	14.16	112.47	N/A

Table 55. Profile 4 modality.

Strata / sample depth	Modality description	Mode 1 (μm)	Mode 2 (μm)	Mode 3 (μm)
A (0-15)	Bimodal	28.25	170.23	N/A
Bw (15-59)	Bimodal	18.67	224.41	N/A
Unit 3 (59-80)	Bimodal	195.45	6.18	N/A
Unit 2 (80-101)	Bimodal	195.45	4.69	N/A
Unit 1 (101-130)	Bimodal	7.10	112.47	N/A

Table 56. Profile 5 modality.

Strata / sample depth	Modality description	Mode 1 (µm)	Mode 2 (µm)	Mode 3 (µm)
A (5-7)	Bimodal	28.25	195.45	N/A
A (9-11)	Trimodal	28.25	195.45	1500.00
2Ab (19-21)	Bimodal	37.24	195.45	N/A
2Ab (28-30)	Bimodal	32.44	195.45	N/A
2C (39-41)	Bimodal	32.44	195.45	N/A
2C (49-51)	Bimodal	24.61	195.45	N/A
3Ab' (59-62)	Bimodal	21.43	195.45	N/A
3Ab' (68-70)	Bimodal	18.67	195.45	N/A
3ABkb (79-80)	Bimodal	16.26	195.45	N/A
3ABkb (89-91)	Bimodal	16.26	195.45	N/A
3ABkb (99-101)	Bimodal	12.33	195.45	N/A
3ABkb (109-111)	Bimodal	12.33	195.45	N/A
3Bkb (119-121)	Bimodal	14.16	224.41	N/A

Table 57. Profile 6 modality.

Strata / sample depth	Modality description	Mode 1 (µm)	Mode 2 (µm)	Mode 3 (µm)
A (0-35)	Bimodal	24.61	148.26	N/A
Bw (35-105)	Unimodal	18.67	N/A	N/A
Bk (105-160)	Unimodal	21.43	N/A	N/A
By (160-195)	Unimodal	21.43	N/A	N/A
2By (195-200)				
2C (195-224)	Unimodal	32.44	N/A	N/A
Unit 3 (224-259)	Unimodal	24.61	N/A	N/A
Unit 2 (259-289)	Unimodal	24.61	N/A	N/A
Unit 1 (289-297)	Unimodal	21.43	N/A	N/A

Table 58. Profile 8 modality.

Strata / sample depth	Modality description	Mode 1 (µm)	Mode 2 (µm)	Mode 3 (µm)
A (0-6)	Bimodal	24.61	170.23	N/A
Bw (6-153)	Unimodal	18.67	N/A	N/A
Unit 6 (153-192)	Unimodal	18.67	N/A	N/A
Unit 5 (192-237)	Bimodal	16.26	170.23	N/A
Unit 4 (237-261)	Bimodal	112.47	18.67	N/A
Unit 3 (261-350)	Unimodal	18.67	N/A	N/A
Unit 2 (350-410)	Bimodal	257.65	18.67	N/A
Unit 1 (410-460)	Unimodal	18.67	N/A	N/A

Table 59. Profile 9 modality.

Strata / sample depth	Modality description	Mode 1 (µm)	Mode 2 (µm)	Mode 3 (µm)
A (0-6)	Unimodal	28.25	N/A	N/A
Bw (6-71)	Unimodal	21.43	N/A	N/A
Bk (71-82)	Unimodal	16.26	N/A	N/A
C (82-109)	Unimodal	18.67	N/A	N/A
Unit 4 (109-190)	Unimodal	10.74	N/A	N/A
Unit 3 (190-213)	Unimodal	28.25	N/A	N/A
Unit 2 (213-240)	Unimodal	16.26	N/A	N/A
Unit 1 (240-257)	Unimodal	10.74	N/A	N/A

Table 60. Profile 10 modality.

Strata / sample depth	Modality description	Mode 1 (µm)	Mode 2 (µm)	Mode 3 (µm)
A (0-15)	Bimodal	18.67	6.18	N/A
C (15-65)	Bimodal	8.15	977.50	N/A
Unit 6 (65-116)	Bimodal	6.18	1.03	N/A
Unit 5 (116-121)	Polymodal	15800.00	7925.00	195.45
Unit 4 (121-148)	Unimodal	195.45	N/A	N/A
Unit 3 (148-199)	Bimodal	4.69	170.23	N/A
Unit 2 (199-252)	Bimodal	4.69	74.31	N/A
Unit 1 (252-320)	Bimodal	85.32	16.26	N/A

Table 61. Profile 11 modality.

Strata / sample depth	Modality description	Mode 1 (μm)	Mode 2 (μm)	Mode 3 (μm)
A (0-11)	Trimodal	12.33	6.18	148.26
Bw (11-45)	Unimodal	5.38	N/A	N/A
Unit 4 (45-55)	Unimodal	8.15	N/A	N/A
Unit 3 (55-63)	Unimodal	4.69	N/A	N/A
Unit 2 (63-73)	Unimodal	10.74	N/A	N/A
Unit 1 (73-150)	Unimodal	5.38	N/A	N/A

Table 62. Control sample modality.

Sample Number	Modality description	Mode 1 (μm)	Mode 2 (μm)	Mode 3 (μm)
PL-RF7-60	Bimodal	257.65	37.24	N/A
PL-MO4-100	Unimodal	37.24	N/A	N/A
DS-RF6-200	Unimodal	295.83	N/A	N/A
DS-RF7-250	Bimodal	389.97	977.50	N/A
DS-KNB-260	Unimodal	257.65	N/A	N/A
SL-PRS-11	Unimodal	28.25	N/A	N/A
SL-PRS-73	Unimodal	28.25	N/A	N/A
SL-PRS-135	Bimodal	21.43	1.03	N/A
SL-PRS-166	Unimodal	97.96	N/A	N/A
DL-EFA-21	Unimodal	21.43	N/A	N/A
DL-EFA-52	Unimodal	21.43	N/A	N/A
DL-EFA-88	Bimodal	18.67	1.18	N/A
DL-EFA-146	Unimodal	10.74	N/A	N/A
HEA-AWT-24	Unimodal	37.24	N/A	N/A
HEA-AWT-70	Unimodal	37.24	N/A	N/A
HEA-AWT-89	Bimodal	64.72	1.18	N/A
HEA-AWT-141	Unimodal	56.37	N/A	N/A
LEA-AWF-28	Unimodal	21.43	N/A	N/A
LEA-AWF-86	Bimodal	28.25	1.18	N/A
LEA-AWF-116	Unimodal	37.24	N/A	N/A
LEA-AWF-171	Bimodal	32.44	1.03	N/A

APPENDIX C:

METHODOLOGICAL INSIGHTS FOR FUTURE STUDIES

Methodological Recommendations for Future Studies

This research project used a multi-pronged approach including stratigraphic mapping, OSL dating and granulometry to reconstruct geomorphic events and predict the location of cultural-age strata in western Centennial Valley. The research resulted in the production of a generalized geomorphic history for the late Quaternary Centennial Valley from ca. 60,000 to 500 cal BP, as well as criteria for differentiating possibly cultural-age versus pre-occupation units in the valley. In addition, this research was a long and multi-phased learning process, with a possibly over-broad scope. The takeaways from this process also provide useful information for geoarcheologists attempting future projects.

Stratigraphic Mapping and Depositional Unit Versus Soil Horizon Differentiation

Locating wall faces conducive to stratigraphic profiling in the project area relatively straightforward given the many options for tall, vertical exposures. In fact, narrowing down which exposures to make detailed maps of was one of my biggest challenges. To that end, I made a useful compromise to include simple explanations of 'Observation Points'. This allowed me to use information from a location (such as observed faulting or notable facies) and its relationship to a profiled exposure without undue redundancy of mapping similar strata. Despite overall good cutbank visibility, correlation between profiles was still hampered by apparent lateral discontinuity across drainage cuts, lack of (safe) access to higher wall sections and wall slump which obscured stratigraphic tracing between exposures and resulted in imprecise estimations of unconformity locations and relative age relationships. Additionally, and due in part to my initial lack of experience, I had trouble defining and differentiating between sediment

units and soil horizons. This was especially troublesome in Profiles such as 3/7 where deeply formed soils masked unit boundaries and resulted in welded soils. This is a common problem and the difficulties of soil/sediment unit differentiation are shared by many other archeologists (Mandel and Bettis 2001). While greater experience helps, it is good reminder to take a conservative approach and keep open to multiple working hypotheses to explain exposure characteristics.

OSL Sample Imprecision and Age Overlap

Three of the four OSL samples from Profile 3/7 have questionable age associations. As discussed previously, this may result from multiple factors, including contamination by overlying sediments through a previously undetected wall crack, possible contamination with older sediments by inexact placement too near a unit boundary, or partial bleaching of sediments prior to burial. With the exception of possibly contaminated OSL samples at Profile 3/7, dates generally aligned well with both stratigraphic relationships and the two radiocarbon ages. Error margins were high with many samples, however, and this may be due to sediment mixing, pedogenic alteration, bioturbation, or possibly shallow sample depth. Unfortunately, as archeological sites and potentially cultural-age strata are typically shallow in this region and often affected by soil formation, these problems may be unavoidable. Often I felt caught between either sampling soil-altered sediments or sampling too near the contact of an underlying unit. However, I could have taken measures to identify wall instability (such as rim-line parallel fissures) prior to selecting an area for sampling. Furthermore, I would avoid sampling narrow strata or too near stratigraphic boundaries where I could potentially gather sediments from non-target units. Alternatively, gathering OSL samples with a

smaller diameter metal pipe (for instance 1" versus 2") could help alleviate this issue with thin strata.

Effect of Organic Removal Technique on Sediment Particle Size Distribution

Granulometry samples with observable plant matter required organic removal before analysis, and the removal technique can potentially affect particle size distribution (PSD). Most (~90%) study area samples contained little or no observable organic fiber content. However, I was concerned that PSD could be affected by incomplete organic removal in samples that required such preparation. I therefore conducted a test of PSD variance for three different organic removal methods using subsamples of the richest organic strata: Profile 2/ Horizon A. Assuming organic removal technique would show the highest degree of variance where the most organics were present, I chose sediment samples from this strata to compare GSD result differences among samples processed using different techniques.

Using a sediment splitter box, I split the sediment Profile 2/Horizon A sample into three equal portions and treated each separately using: (a) mechanical removal only (i.e., mechanical control), (b) mechanical followed by H_2O_2 saturation (i.e., H_2O_2), and (c) mechanical followed by water float (i.e., water-float). Specific procedures are detailed in Chapter Four. I then conducted granulometric laser diffraction analysis and statistically compared PSD results among the subsamples (Figure 59; a-c). Results for the three aliquots are presented in Section 3 of this chapter. They indicate that significant differences are found in some measures of central tendency.

I used IBM SPSS Statistics, Version 20 to conduct an analysis of variance

(ANOVA) test among subsamples subjected to three different organic removal methods (Field 2013:193). Using nine aliquots each, I contrasted subsample cumulative particle size percentages at 10% (D_{10}), 50% (the median, D_{50}), and 90% (D_{90}). Results show that the D_{10} spread of the mechanical control is not significantly different than H_2O_2, although it is borderline at .095 (Figure 59; a). There is significant difference between mechanical and the water-float sample at D_{10}, however. For D_{50} and D_{90}, the mechanical subsample is significantly different than both H_2O_2 and water-float (Figure 59; b and c). Finally, no significant difference exists between D_{10} and D_{50} values of the H_2O_2 and water-float samples, although the D_{90} distributions differ significantly (Figure 59; a-c).

The results of this methodological comparison indicate that significant PSD differences exist among the three organic removal methods and that the H_2O_2 and water-float methods produce results more similar to each other than to the mechanical control sample. However, these results do not indicate which method produces a more *accurate* representation of sediments with high organic content, only that different removal methods have an influence on size distribution. It is possible that the H_2O_2 and water-float methods *introduce* error, for instance, by dissolving soluble clasts such as limestone. However, two out of three of the H_2O_2 and water-float samples are statistically similar, while differing from the mechanical control sample. Furthermore, the mechanical D_{50} and D_{90} percentiles exhibit coarser distributions than either H_2O_2 or water-float. This may indicate that by using mechanical removal only, surviving organic particles are regarded as coarse sediment grains during laser diffraction analysis. This finding casts doubt on the PSD accuracy of organic-rich sediments in the study area. However, it is unknown if PSD differences are substantial enough to change correlations between study area and control

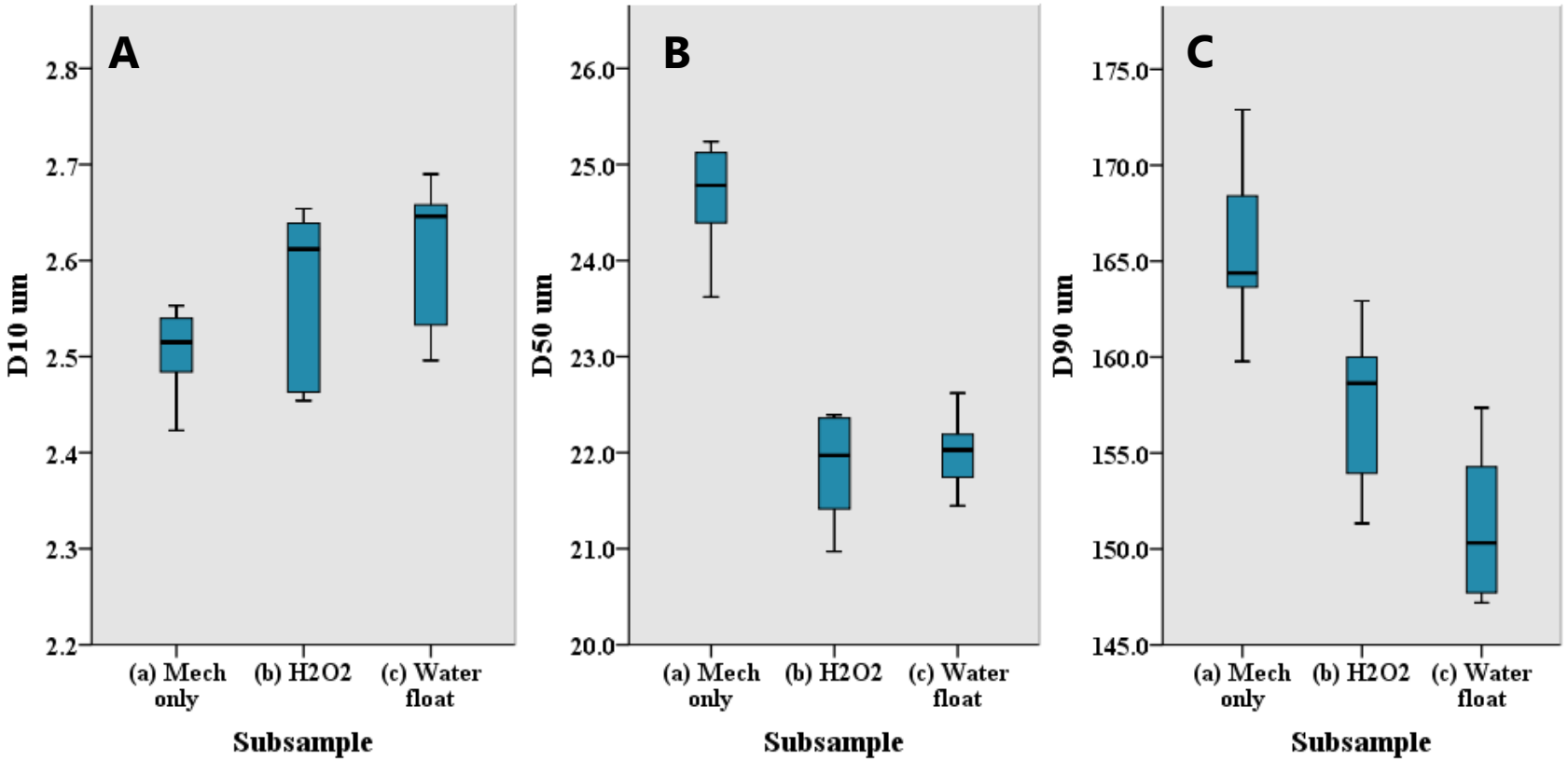

Figure 59. Particle size distribution effects for three methods of organic matter removal: (a) mechanical only, (b) mechanical and H_2O_2 treatment, and (c) mechanical followed by water float. Boxplot A compares D_{10} grain size cumulative percentiles (in microns), boxplot B compares D_{50}, and boxplot C compares D_{90}

samples. Fortunately, as only about 10% of samples contained significant observable organic content, these potential inaccuracies do not affect the majority of study area granulometry samples.

Utility and Limitations of Granulometric Analysis

I used granulometry for two related objectives; first to help infer the depositional environment of sediment packages through comparison to control samples and second to aid in correlating units between profiles. My results were variable, showing both the usefulness and complications of employing this technique. Using particle size distribution to discriminate among depositional mechanisms is well-established in sedimentology and assumes a relationship between clastic sediment particle size and energy regime and viscosity of the depositing medium (Gale and Hoare 1991; Krumbein and Pettijohn 1938; Sahu 1964). Overall, GSD cluster analysis worked very well to identify depositional environment when I had an analogous control sample example for the study area unknown. However, demarcations between sedimentary environments are fluid and factors such as available sediment type, post-depositional reworking, and pedogenic translocations and transformations complicate correlations between known environments and target deposits. Moreover, while I had a comprehensive (albeit small) control sample set based on previous research in the area, I lacked sufficient examples of polymodal, poorly sorted, and coarse-fraction dominated sediments. Sometimes, even apparently good analogs produced puzzling results (Figure 60). In any case, the cluster associations between sediment control samples and study area unknowns gave a starting point for differentiating complex and overlapping depositional environments, but cannot be relied upon wholly. Using GSD clustering to help correlate strata in different profiles had very

disparate results. Granulometric clustering failed to group some units which otherwise appeared homologous and in other cases granulometry confirmed traceable packages' equivalence. For instance, I traced the prominent white silt bed through much of the study area east end and it maintained a uniform thickness, consistent facies, and distinct color. Despite general consistency, however, my analysis categorized the bed as 'medium silt' in Profile 9 and 'coarse silt' in Profile 6 only about 210 m to the east. More concerning, my histogram classified samples from the two profiles as only 'moderately similar'. Granted, differences may be partly explained simply by lateral facies transitions which would be expected for similar-age strata deposited in different lake depths (Middleton 1973). Interestingly, samples from an apparently conformable strata directly underlying the white silt bed in Profiles 9 and 6 grouped very closely together and I was also able to trace this strata throughout the east end. It appears that using GSD to correlate packages between exposures may be at cross-purposes with inferring depositional context, at least where lateral (conformable) facies transitions within a package are possible. However, using this technique shows promise for interpreting variations in laterally continuous strata in the same depositional environment.

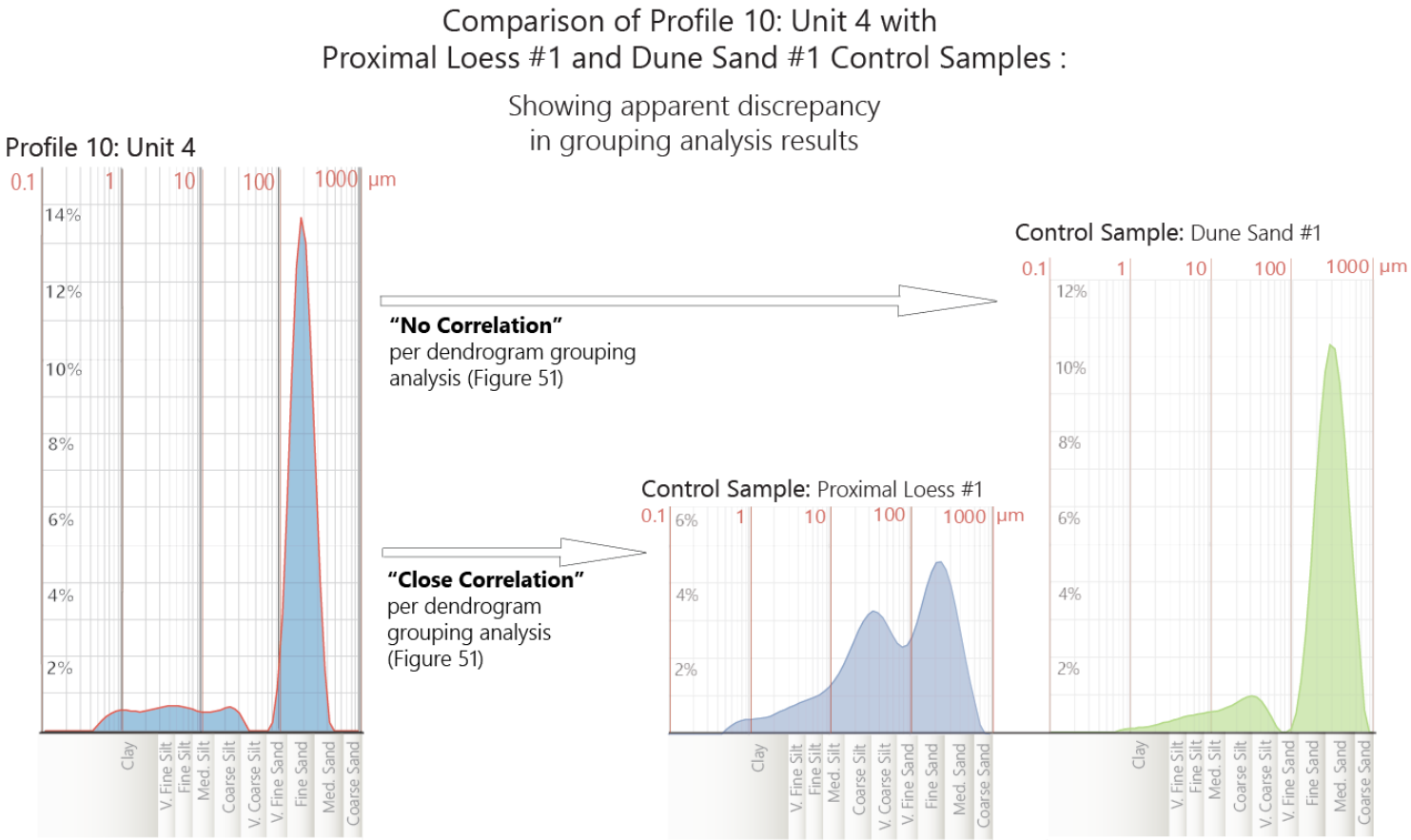

Figure 60. Example of possible grouping analysis discrepancy based on comparisons of Profile 10:Unit 4 (left) with Proximal Loess #1 (middle) and Dune Sand #1 (right) control samples.